Earth Observation:
Data, Processing and Applications

Volume 2D: Processing—Image Integration

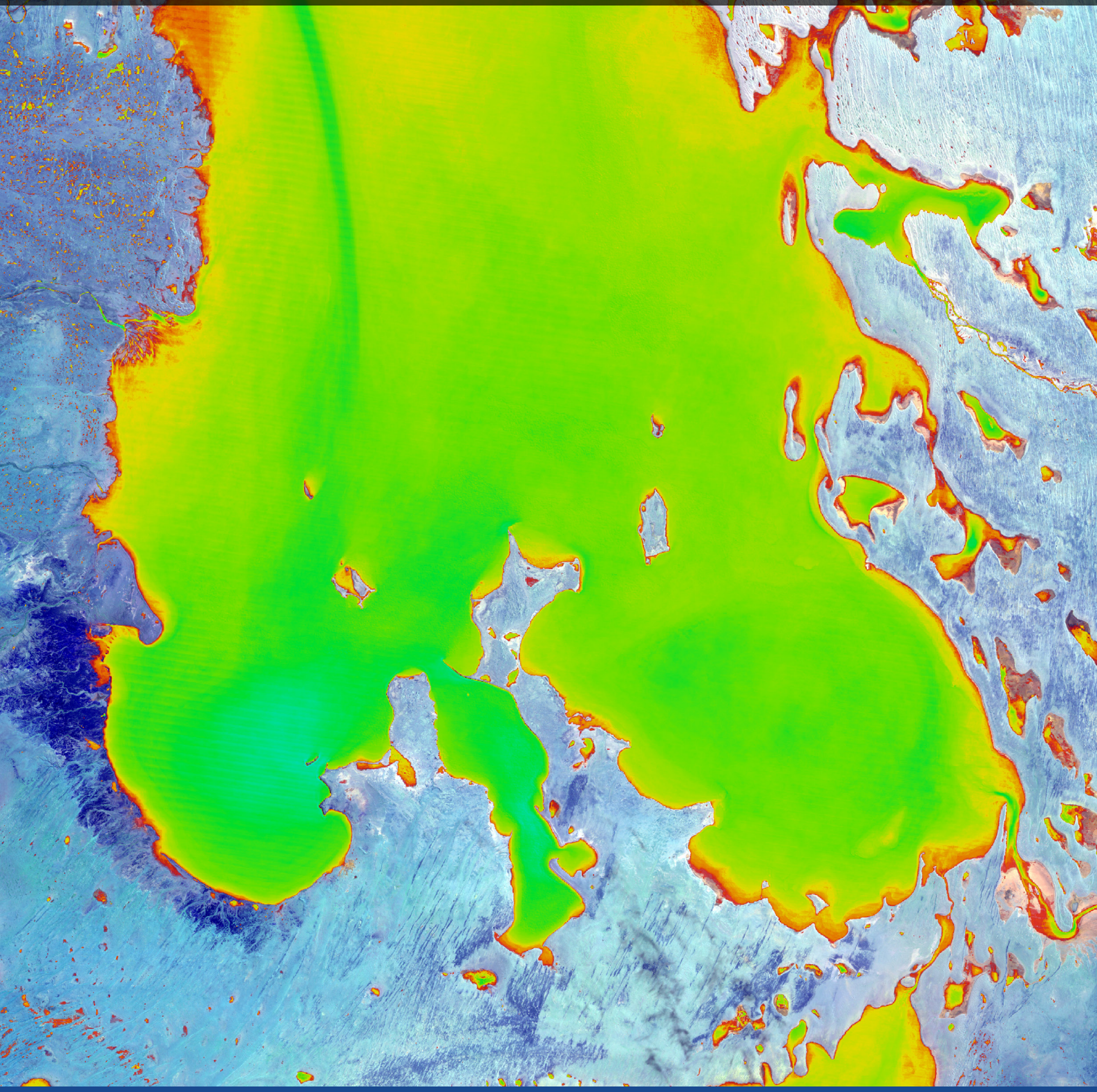

The report is available in PDF format at *http://www.crcsi.com.au/earth-observation-series*
We welcome your comments regarding the readability and usefulness of this report. To provide feedback, please contact us at *info@crcsi.com.au*.

Publisher:
Australia and New Zealand CRC for Spatial Information

ISBN [ONLINE]:
978-0-6482278-2-3

Recommended Citation for Volume 2D:
CRCSI (2019) *Earth Observation: Data, Processing and Applications. Volume 2D: Processing—Image Integration*. (Eds. Harrison, B.A., Jupp, D.L.B., Lewis, M.M., Mueller, N., Byrne, G., Hudson, D.A., Sparks, T.,) CRCSI, Melbourne.

Background image on previous page: The Water Observations from Space (WOfS; see Volume 1A—Excursus 5.1) for Lake Eyre in South Australia, overlaid on a false colour Landsat-5 image acquired on 9 May 2009. WOfS shows the percentage of time that surface water was present in a location since 1987, with red areas having very low occurrence transitioning through yellow and green to blue which has the highest occurrence.
Source: Norman Mueller, Geoscience Australia

Acknowledgements

Production of this series of texts would not have been possible without the financial support of CSIRO, CRCSI, GA and BNHCRC, input from members of the editorial panels and direction from members of the various advisory panels. Administrative support from FrontierSI is also gratefully acknowledged.

Volumes 1 and 2 of this series are based on text originally published in Harrison and Jupp (1989, 1990, 1992 and 1993)[1]. Many illustrations and some text from these publications have been reproduced with permission from CSIRO.

Other contributors are gratefully acknowledged:

- reviewers: Alfredo Huete and Laurie Chisholm for valuable feedback on Volumes 1 and 2; Irina Emelyanova (Excursus 6.1); Mark Grant, Matthew Stenson and Matthew Paget (Excursus 12.2 and Excursus 14.1); Matthew Brooks (Excursus 13.2);
- illustrations: Norman Mueller kindly supplied most of the lovely images; other contributors of graphical material include: Tony Sparks, Megan Lewis, David Jupp, Craig Shephard, Michael Caccetta, Jan Verbesselt, Glenn Newnham, Tim McVicar, Randall Donohue, Steven Sagar, Fuqin Li, Nearmap, and EagleView;
- excursus: David Hudson, Megan Lewis, Randall Donohue, Richard Thackway, Marian Wiltshire, Janet Anstee, Albert van Dijk, Tim Danaher, Dan Tindall, Mark Baird; and
- Carl Davies (CMDphotographics) for selected graphical illustrations.

We thank those owners of copyrighted illustrative material for permission to reproduce their work. Credits for individual illustrations are provided below the relevant graphic.

1 Harrison, B.A., and Jupp, D.L.B. (1989) Introduction to Remotely Sensed Data: Part ONE of the microBRIAN Resource Manual. CSIRO, Melbourne. 156pp.
Harrison, B.A., and Jupp, D.L.B. (1990) Introduction to Image Processing: Part TWO of the microBRIAN Resource Manual CSIRO, Melbourne. 256pp.
Harrison, B.A., and Jupp, D.L.B. (1992) Image Rectification and Registration: Part FOUR of the microBRIAN Resource Manual. MPA, Melbourne.
Harrison, B.A., and Jupp, D.L.B. (1993) Image Classification and Analysis: Part THREE of the microBRIAN Resource Manual. MPA, Melbourne.

Table of Contents

Volume 2D: Processing—Image Integration a

Acknowledgements i

Getting Started 1

1 EO Analysis Framework 3

1.1 Indirect Observations 3

1.2 Implicit Assumptions 4

1.3 Layers of Complexity 5

1.4 The Surface Mosaic 7

1.5 The Bigger Picture 10

1.6 Further Information 11

1.7 References 11

2 Multi-temporal EO Datasets 13

2.1 Bi-temporal and Multi-temporal Imagery 14

2.1.1 Conceptual structure 14

2.1.2 Satellite-acquired datasets 15

2.2 Appropriate Data 17

2.2.1 Timing 17

2.2.2 Scaling 18

2.2.3 Spectral and radiometric differentiation 18

2.3 Appropriate Processes 18

2.4 Processing Methodologies 19

2.4.1 Processing order 19

2.4.2 Processing workflows 19

2.5 Accuracy, Stability, Validation and Trust 21

2.6 Further Information 25

2.7 References 25

3 Data Standardisation 27

3.1 Image Calibration 27

3.1.1 Systematic effects 27

3.1.2 Local effects or 'noise' 30

3.2 Analysis Ready Data 30

3.3 Ancillary data 32

3.3.1 Provenance and caveats 32

3.3.2 Data formats 33

3.4 Further Information 34

3.5 References 34

4 Pre-processing **37**
4.1 Stratifying images 37
4.1.1 Spectral 37
4.1.2 Spatial 38
4.2 Reducing data volume 38
4.2.1 Spectral indices 38
4.2.2 Linear Transformations 39
4.3 Upscaling and Downscaling 40
4.3.1 Upscaling to a larger pixel size 40
4.3.2 Downscaling to a smaller pixel size 43
4.3.3 Resampling to a common pixel size 43
4.4 Further Information 44
4.5 References 44

Processing Image Pairs 45

5 Basic Comparisons **47**
5.1 Multi-date Colour Composites 47
5.2 Differencing and Addition 49
5.3 Manipulating Segmentation Masks 52
5.4 Transferring Category Statistics 54
5.5 Colour Balancing for Image Mosaicking 54
5.6 Further Information 56
5.7 References 56

6 Fusion Methods **57**
6.1 Spatial and Spectral Blending 58
6.2 Spatial and Temporal Blending 60
6.3 Further Information 66
6.4 References 66

7 Change Detection Methods **69**
7.1 Algebraic Operations 71
7.1.1 Channel subtraction 71
7.1.2 Channel ratioing 72
7.1.3 Channel regression 73
7.1.4 Change Vector Analysis 74
7.2 Linear Transformations 76
7.3 Classification Approaches 78
7.3.1 Comparing classifications 78
7.3.2 Classifying merged imagery 79
7.4 Post-processing 80
7.4.1 Thresholding and labelling 80
7.4.2 Filtering 80
7.4.3 Autocorrelation analysis 80
7.5 Accuracy Assessment 80
7.6 Further Information 81
7.7 References 81

Processing Time Series Datasets 85

8 Time Series Analysis **87**
- **8.1** Time Series Components and Processing 88
- **8.2** Understanding the Data 91
- **8.3** Creating a Data Cube 92
- **8.4** Detecting Anomalies 97
- **8.5** Further Information 98
- **8.6** References 98

9 Characterising Temporal Trends **101**
- **9.1** The Time Series Trajectory 101
- **9.2** Analysing Trends 104
- **9.3** Comparing Trajectories 105
- **9.4** Analytical Methods 106
- **9.5** Further Information 107
- **9.6** References 107

10 Pixel-based Composites **111**
- **10.1** Single Sensor Datasets 112
  - **10.1.1** Time period 112
  - **10.1.2** Composite values 114
- **10.2** Multiple Sensor Datasets 117
- **10.3** Further Information 119
- **10.4** References 119

11 Digital Earth **123**
- **11.1** The Concept 123
- **11.2** Digital Earth Australia 125
- **11.3** Further Information 129
- **11.4** References 129

Merging EO and Other Datasets 133

12 Sample-based Datasets **135**
- **12.1** Manually-Collected Field Site Data 135
- **12.2** Automatic Sensors 137
- **12.3** Spectroscopy datasets 141
- **12.4** Volunteered data 142
- **12.5** Further Information 144
- **12.6** References 144

13 Gridded Datasets **149**
- **13.1** Geographic Information Systems 149
- **13.2** Digital Elevation Models 150
- **13.3** Meteorological Records 154
- **13.4** Further Information 156
- **13.5** References 157

Integrated Solutions 159

14 Mapping, Monitoring and Modelling 161

14.1 Mapping 161

14.2 Monitoring 163

14.2.1 Environmental Accounting 163

14.2.2 Compliance Monitoring 169

14.3 Modelling 175

14.4 Further Information 179

14.5 References 180

List of Figures

Figure 1.1 Measurement and analysis of image features 4

Figure 1.2 Complexity levels in EO imagery 6

Figure 1.3 Upscaling and downscaling of soil data 7

Figure 1.4 Scales of EO 8

Figure 1.5 Mapping, monitoring and modelling for natural resource management 10

Figure 2.1 Structure of an EO image 14

Figure 2.2 Bi-temporal and multi-temporal image sets 15

Figure 2.3 Workflow for fractional cover product 20

Figure 2.4 Process flow chart example 20

Figure 2.5 Lifecycle model for a sensor data product 22

Figure 3.1 Five basic types of patches 33

Figure 4.1 Principal Component Analysis 39

Figure 4.2 Upscaling operations 40

Figure 4.3 Upscaling by picking and binning approach 41

Figure 4.4 Vector to raster conversion 41

Figure 4.5 Bilinear interpolation 42

Figure 4.6 Cubic convolution interpolation 42

Figure 4.7 Downscaling by duplicating pixels 43

Figure 5.1 Multi-date NDVI composite 48

Figure 5.2 Image differencing 49

Figure 5.3 Colour composite difference image 50

Figure 5.4 Residual image 51

Figure 5.5 Examples of Euclidean distance images 52

Figure 5.6 Recombining images 53

Figure 5.7 Colour balancing 55

Figure 6.1 STARFM approach 61

Figure 6.2 Temporal profiles of blending algorithms 62

Figure 6.3 Image blending algorithms 62

Figure 6.4 Generic overview of Landsat-MODIS blending. 65

Figure 7.1 Difference channel histogram 71

Figure 7.2 Change detection based on differencing 71

Figure 7.3 Ratio channel histogram 72

Figure 7.4 Change detection based on ratioing 73
Figure 7.5 Automatic Scattergram-Controlled Regression 73
Figure 7.6 Change Vector Analysis (CVA) 74
Figure 7.7 Direction of change 75
Figure 7.8 Magnitude of change 75
Figure 7.9 Original images 77
Figure 7.10 Principal components 78
Figure 8.1 Time series imagery of Australia 88
Figure 8.2 Components of time series variations 89
Figure 8.3 fPAR time series examples 90
Figure 8.4 Vegetation cover triangle 93
Figure 8.5 Land cover reflectances 94
Figure 8.6 Seasonal trends 1981–2006 95
Figure 8.7 fPAR decomposition 96
Figure 8.8 Dynamic Time Warping (DTW) 96
Figure 9.1 Temporal trajectory attributes 102
Figure 9.2 Time series distance measures 105
Figure 10.1 Brightness Temperature Composites from SSM/I 115
Figure 10.2 Workflow for Australian Landsat composite images 116
Figure 10.3 Flow chart for multisensor composites 118
Figure 11.1 Technological and cultural advances enabling Digital Earth 124
Figure 11.2 Global network of data cubes 124
Figure 11.3 DEA concept 125
Figure 11.4 National Intertidal Digital Elevation Model 126
Figure 11.5 Radiometric correction of LSR25 128
Figure 12.1 TERN sites 138
Figure 12.2 IMOS National mooring network 140
Figure 12.3 Inadvertent map of distance to earthquake epicentre 142
Figure 12.4 Using the EyeonWater Australia app 143
Figure 12.5 EyeonWater Australian observations 2017–2018 143
Figure 13.1 DTM versus DSM 150
Figure 13.2 Elevation data formats 151
Figure 13.3 Geofabric datasets 153
Figure 13.4 GPCC average precipitation 1982–2010 154
Figure 13.5 GPCC buffer mask 155

Figure 14.1 Australian environmental-economic account for agriculture 164

Figure 14.2 Australia's Environment Explorer 167

Figure 14.3 2018 OzWALD summary for ACT 168

Figure 14.4 Schematic representation of SLATS processing steps 171

Figure 14.5 Example of SLATS change index and likelihood images 172

Figure 14.6 Example of SLATS reporting outcome 173

Figure 14.7 eReefs modelling framework 177

Figure 14.8 Temporal and spatial scales of GBR processes and observations 177

Figure 14.9 eReefs model interactions 178

List of Tables

Table 1.1 Logical stages in EO data use 3

Table 1.2 Assumptions implicit in the analysis of EO data 5

Table 1.3 Scale hierarchy for soil and landscape data 8

Table 1.4 Landform models relating to mapping scales 9

Table 1.5 Complementary benefits of mapping, monitoring and modelling 11

Table 2.1 Sampling dimensions in EO imagery 14

Table 2.2 Global EO time series datasets 16

Table 2.3 CEOS WGCV validation hierarchy for moderate resolution global products 21

Table 2.4 Factors impacting the uptake of EO products 23

Table 2.5 EOPU framework for emergency management 24

Table 3.1 HLS processing overview 32

Table 5.1 Example histogram percentage points 55

Table 6.1 Terminology associated with data fusion 58

Table 6.2 Pan-sharpening methods 59

Table 6.3 Landsat and Terra/MODIS characteristics 60

Table 6.4 Notation for blending framework 63

Table 7.1 Bi-temporal change detection stages 70

Table 7.2 PC transformation matrix 77

Table 8.1 Time series processing sequence 89

Table 9.1 Time series sub-sequence differences 103

Table 9.2 Time series analysis methods 104

Table 9.3 Time series similarity measures 106

Table 9.4 Landsat-based change detection approaches 106

Table 10.1 MODIS land products 113

Table 10.2 Popular criteria for selecting 'best' pixel 114

Table 11.1 Foundations of DEA 126

Table 12.1 Information Hierarchy 136

Table 12.2 Spectral database processing levels 141

Table 13.1 Terrain variables 151

Table 13.2 Australian DEM 152

Table 14.1 TERN EO-based continental products 162

Table 14.2 OzWALD model components 166

List of Excurses

Excursus 1.1—Landform models 9

Excursus 2.1—Why is an EO Product Trusted? 22

Excursus 6.1—Theoretical Framework for Image Blending 63

Excursus 7.1—Change Detection using PCA 77

Excursus 8.1—Relative Calibration of Time Series Datasets 93

Excursus 10.1—MODIS Composites 113

Excursus 11.1—GA Analysis Ready Data 127

Excursus 12.1—National Vegetation Information System 136

Excursus 12.2—Terrestrial Ecosystem Research Network (TERN) 137

Excursus 12.3—Integrated Marine Observing System (IMOS) 139

Excursus 12.4—EyeonWater Australia 143

Excursus 13.1—NationalMap 150

Excursus 13.2—Australian Hydrological Geospatial Fabric 153

Excursus 14.1—TERN Continental Products 162

Excursus 14.2—OzWALD 165

Excursus 14.3—SLATS: Monitoring Woody Vegetation Clearing 170

Excursus 14.4—eReefs 176

Getting Started

In the context of Earth Observation (EO), data integration encompasses a range of image processing techniques that enable spatial datasets from different sources to be compared and combined. This sub-volume describes processing operations that are relevant to either:

- a pair of bi-temporal EO images—two images of the same ground area taken at different times (see Sections 5 to 7); or
- a multi-temporal EO image dataset—more than two images of the same ground area, each of which is acquired at different times (see Section 8 to 11).

Various transformations for merging or analysing data from multiple image channels are introduced in Volume 2C. While an awareness of the underlying EO framework is necessary for all image processing operations, as described in Section 1 it has particular significance when integrating EO image datasets acquired at different times. Similarly the constraints and complexities involved with analysing any EO image are multiplied when processing bi-temporal or multi-temporal EO datasets. Some of the factors that are relevant to selecting the most appropriate data and processes for multi-temporal analyses are discussed in Section 2.

One of the most valuable opportunities afforded by EO data is the regular monitoring of changes in features on the Earth's surface (see Volumes 1 and 3). When bi-temporal or multi-temporal datasets are involved in such analyses, appropriate radiometric and geometric calibration of the EO data is critical. Essential pre-processing operations for bi-temporal and multi-temporal EO datasets are reviewed in Section 3, and optional pre-processing operations are discussed in Section 4.

EO datasets can also be integrated with non-EO data sources. Some of the options and challenges involved with such integration are considered in Sections 12 and 13. Examples of some mapping, monitoring and modelling results based on EO analyses are given in Section 14 and further expanded in Volume 3.

Contents

1 EO Analysis Framework 3

2 Multi-temporal EO Datasets 13

3 Data Standardisation 27

Background image on previous page: Sentinel-2a image over the Kimberly region, northwest WA, acquired on 10 September 2018. Bands 4, 3 and 2 are shown as RGB. **Source:** Norman Mueller, Geoscience Australia

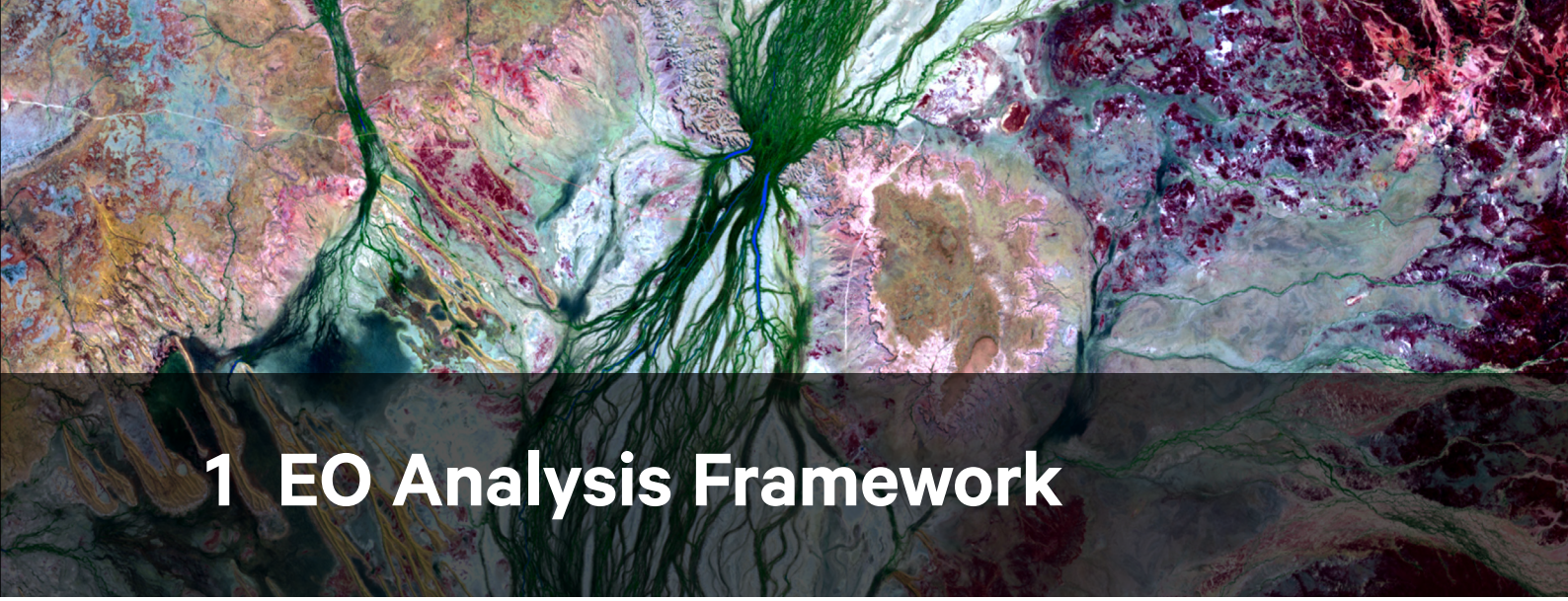

1 EO Analysis Framework

Interpretation of any Earth Observation (EO) image requires consideration of the way 'real world' objects generate, or contribute to, its colours, patterns, and textures. While the relationships between the image and the imaged target are important in the analysis of individual EO images, they carry even greater importance when two or more images are being processed and/or when other data sources are being integrated with EO imagery. In this section we will review some basic principles that underlie interpretation and analysis of all EO datasets, namely the:

- indirect nature of EO observations (see Section 1.1);
- implicit assumptions inherent to EO (see Section 1.2);
- layers of complexity in every EO image (see Section 1.3); and the
- 'mosaic' formed by features on the surface being imaged (see Section 1.4).

Finally we consider the bigger picture of data integration in Section 1.5.

1.1 Indirect Observations

Volume 1A—Section 1 introduced the concept that EO observations are implicitly indirect and that their interpretation necessarily involves at least one level of inference, or indirection. In Table 1.1, the generalised process of using EO data is summarised in terms of three logical stages: acquisition, processing and interpretation.

The indirect relationship between features in an EO image and quantifiable attributes of the Earth's surface is summarised in Figure 1.1 (see Volume 1A—Section 1 for details). In this diagram, image processing operates on the 'data space', or observation domain, and implicitly develops or utilises various assumptions which relate the image data back to selected parameters of the imaged ground scene (see Section 1.2).

Table 1.1 Logical stages in EO data use

Stage	Description	Domain
Acquisition	Observe object or surface using remote sensing	Observation
Processing	Convert remote sensing observation to measurable property of object or surface using pre-defined measurement model	Measurement
Interpretation	Interpret measured properties of object or surface (that is, the converted remote sensing observation) in terms of a specific application using pre-defined structure model	Attribute

Background image: Landsat-8 OLI image of Diamantina Gates, southwestern Queensland, acquired in winter 2013. Due to constraints imposed by the adjacent Goyder and Hamilton Ranges, the Diamantina River narrows to about 1 km wide at Hunters Gorge, which is located near the centre of this image.
Source: Craig Shephard, DSITI

Figure 1.1 Measurement and analysis of image features

Interpreting imagery from EO sensors is an indirect process, whereby a measurement model is used to transform EO observations to measurements of some measurable property, and a structure model is used to relate those measurements to application-specific attributes.

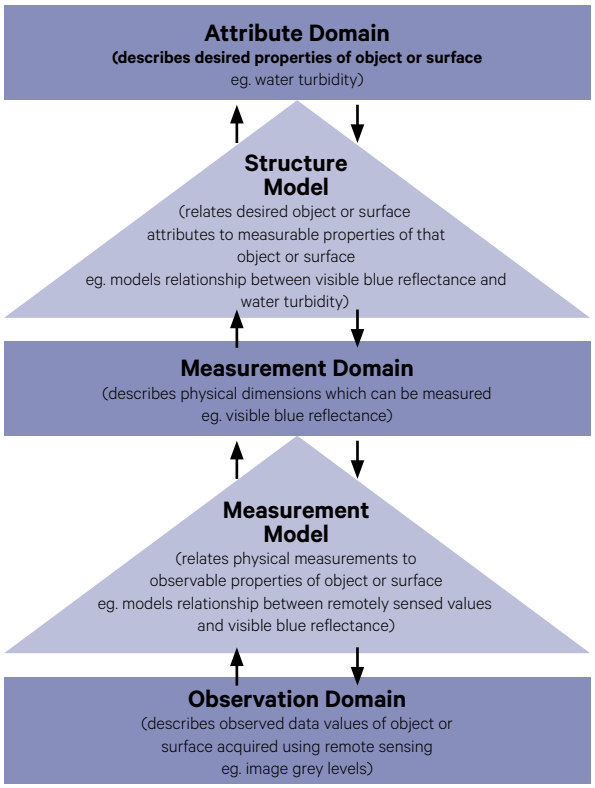

Adapted from: Harrison and Jupp (1989) Figure 33

In the context of Figure 1.1, the structure model defines how the properties that may be measured remotely, such as reflectance or emission, represent the physical parameters we want to analyse. For example, various studies have established that remote measurements of thermal infrared emission of a surface can be directly related to its temperature (see Volume 1B—Section 7). However, other variables such as atmospheric conditions (water vapour and aerosols) and surface emissivity, can modify this relationship, so need to be considered when deriving temperature information from thermal infrared images (see Volume 3).

Further approximation to the image representation of the original parameters, in both the spectral and spatial dimensions, is added by the measurement model. For example, when the quantisation levels for a thermal scanner measure thermal infrared emission in steps that are equivalent to 0.1°C then the finest interval for temperature categories from such an image is automatically defined. Similarly, if the spatial resolution of one sample measurement (that is, the pixel size) is 5 m, we cannot use the resulting image to precisely locate objects that are smaller than this size (even if their presence can be detected). Such characteristics of the measurement model are critical for reliable and repeatable mapping, monitoring or modelling of Earth features and attributes using EO datasets (see Section 2.2.3).

1.2 Implicit Assumptions

The major assumptions which are implicit in acquiring and analysing EO data are summarised in Table 1.2. Each of these factors affects the correlation between features in the ground scene and results derived by analysis of digital EO data, and thus affect the accuracy of any image analyses. The five stages listed in Table 1.2 fundamentally address the following questions:

- has the best available imagery been selected (see Section 2.2)?
- is the data quality adequate to the intended purpose(s) of the analysis (see Volume 1)?
- has the data been processed appropriately (see Volume 2A and Sections 2.3 and 2.4 below)?
- has the accuracy of results been assessed and can the results be reproduced precisely (see Volume 2E)?
- have results been reported to honestly state known limitations and assumptions and clearly represent the final interpretation?

The answers to these questions directly impact the use of EO data for monitoring land cover/use changes (see Volume 3A). For example, differences between two image classifications of a ground scene may be due to actual changes on the ground, or to differences in either the data acquisition mode or the data analysis and interpretation methods that were used (see Volume 2E). Thus, before conclusions are deduced from the results of such analyses, an interpreter should investigate all possible causes for the observed differences.

Image processes that are commonly used with EO datasets are described in Volumes 2A, 2B and 2C and methods that can be used to assess the accuracy of EO analyses are detailed in Volume 2E. A further consideration relating to analysis of multi-temporal EO data is the delivery of results. Examples of this delivery stage may involve a wide range of presentation styles, including monitoring of specific environmental attributes and biophysical models. Australian examples of such outcomes are presented in Section 14 below and in Volume 3.

Table 1.2 Assumptions implicit in the analysis of EO data

Stage	Factor	Assumptions
Selection	Spatial resolution	Adequate to indicate shape, size and texture of target objects
	Spectral resolution	Discriminates target from background in terms of bandwidths and quantization
	Radiometric resolution	Detects differences in reflectance and/or emission required to differentiate target features
	Temporal resolution	Observes target at appropriate times of day, season or climatic event
Acquisition	Reflected and/or emitted radiance	Target objects are characterised by upwelling radiance
	Atmosphere	Atmospheric attenuation of upwelling radiance is negligible or can be corrected
	Analogue-to-digital conversion	Negligible A/D converter noise and required radiometric quantization level available from sensor
	Image transmission and reception	Data encoding and compression/decompression activities do not increase radiometric or geometric errors
Processing	Image calibration	Geometric correction approach is relevant and accurate
		Radiometric correction approach accounts for atmospheric and sensor 'noise'
	Pre-processing	Transformations applied to enhance image features do not misrepresent the relationship between image values and target features
	Analysis	Processes selected are appropriate to image dimensions and target attributes
Interpretation	Provenance	Data provenance is understood and retained
	Constraints	Limitations of selected processes are understood and acknowledged
	Validation	Results are verified against independent datasets
Delivery	Reporting	Provenance and limitations are clearly documented
	Accuracy	Accuracy assessment is reported in terms of methods and results
	Presentation	Analysis results are presented in a transparent and unambiguous manner

Adapted from Duggin and Robinove (1990)

1.3 Layers of Complexity

Some of the characteristics of EO data that complicate its analysis can be seen in another example. Let us start with imaging a very simple scene, which could be compared with a thematic map. In the simplest case, the scene would be a flat surface with flat features, which are identified by distinct, solid colours (see Figure 1.2a). We will assume that the scene is imaged with sufficient spatial resolution to clearly represent the boundaries between features and sufficient spectral resolution to differentiate all feature colours. Classification of this image would be able to reliably use the colour values to identify each feature in the image as a different class. In this case, assuming constant atmospheric conditions, images recorded with different illumination and viewing angles would be virtually identical.

If the same 'scene' is folded and bent before imaging, we would have to consider the effect of a non-flat surface on the imaged values. If the surface had considerable undulation, distinctly different images could result when the illumination and viewing positions are varied due to changes in shadowing. Surface topography alone could result in different surface colours being imaged with the same image values and/or the same surface colours being imaged with different image values (see Figure 1.2b).

A further level of complexity could be introduced by giving the surface colours some three-dimensional form. For example, the dark green colour may comprise groups of tall, spheres (like trees) and the pale green patch may include boxes (like buildings). Variations in illumination and viewing will now be further complicated by shadowing within features as shown in Figure 1.2c.

Figure 1.2 Complexity levels in EO imagery

a. A simple scene would comprise a flat surface with flat features having distinct, constant colours.

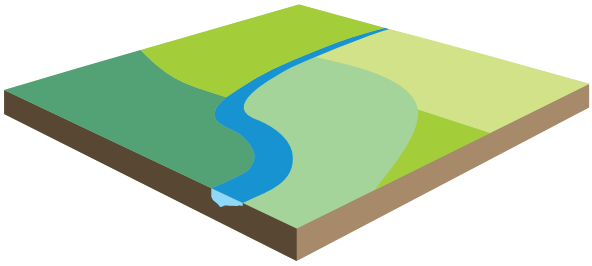

b. The simple scene with added topography introduces surface shading.

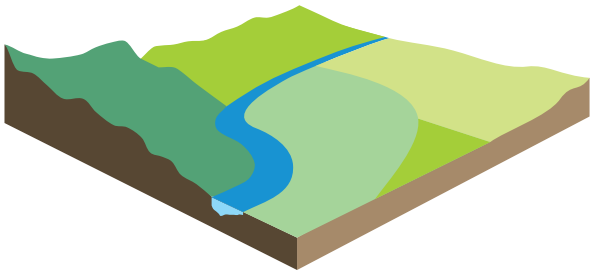

c. When three-dimensional features are imposed on the simple scene with topography shadowing between features is introduced.

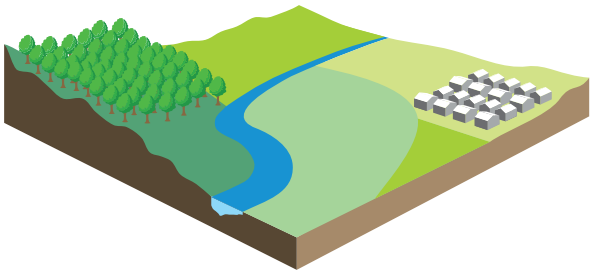

d. By varying the spacing within the three-dimensional features, the interactions between topography, surface colour and feature separation become more complex.

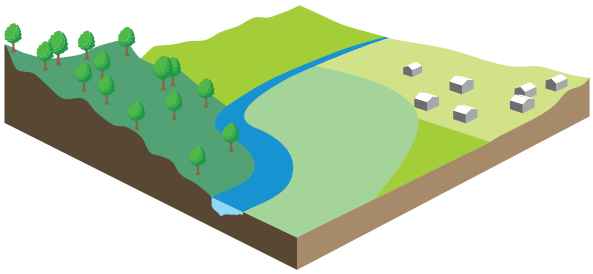

Source: Harrison and Jupp (1993) Figure 4

As well as a three-dimensional surface containing three-dimensional features, we can allow variations of structure and colour within each surface feature. For example, the trees might be spaced so that some are adjacent while some are separated against a background of differing colour, and the buildings could be dispersed unevenly (see Figure 1.2d). These structural factors will vary not only the average colour of each surface feature but also the variance of each surface colour. This variance will also differ when the scene is imaged using different pixel sizes, and different illumination and viewing angles. A finer resolution image, such as Landsat TM rather than MSS, will show more detail about smaller objects, but this additional information will necessarily increase the variance of the image (see Volume 2A—Section 8.1). For example, some composite features, like woodland areas, are resolved into trees and background patches in fine resolution images (such as Landsat TM) but may conveniently blend into a single, distinct patch when imaged at coarser resolutions (such as Landsat MSS; see Volume 2A—Section 8.2).

The Earth's surface is comparable to the final scene described above and illustrated in Figure 1.2d, having variable relief and a range of three-dimensional structures (such as vegetation and buildings) with variable spacing. Representation of these features in terms of mean and variance in an image can also vary widely with different spatial and spectral resolutions. Sensor design and calibration characteristics can mean that the same reflectance level can sometimes be recorded as different values in the image (see Volume 1A). Remote imaging will be affected by illumination differences, since the Sun position varies with time of day and time of year, as well as view angle differences for different sensors and platforms (see Volume 1B). A further variable affecting EO data is atmospheric attenuation, since the condition of the Earth's atmosphere will modify the surface reflectance measured by sensors on aircraft and satellite platforms (see Volume 2A). Reliable and repeatible analysis of EO datasets requires a comprehensive understanding of these layers of complexity and their interrelationships with processing methods.

1.4 The Surface Mosaic

In addition to the layers of complexity inherent to EO imagery discussed above, it is instructive to view each landscape being imaged as 'a mosaic of tiles of odd shapes and sizes' (Speight, 2009). A similar view can be taken for features of the 'waterscape' (see Volume 3B).

Relating features and patterns in the surface mosaic to pixel values in a EO dataset relies on the:

- ability of the type of measurements being recorded in the image to resolve the surface features and patterns; and the
- effectiveness of the models that implicitly or explicitly relate surface features or physical processes to these EO-based measurements.

While the intrinsic scale of selected features and patterns on the Earth's surface may appear to be discernible in EO imagery, each image only captures those features and patterns of the surface mosaic at a single spatial scale. Different features and patterns, however, occur at different spatial scales, and can vary from place to place and from time to time. As such it is not possible for any single EO image, at one spatial resolution, to capture all features and patterns that comprise the imaged surface mosaic.

In order to sensibly interpret the features and patterns in a given EO image we need to consider whether their representation in the image adequately mirrors their characteristics on the Earth's surface.

This is not just a matter of spatial resolution, as some features and patterns with a larger extent are more easily distinguished in lower resolution imagery. When classifying some vegetation types, for example, a larger pixel size usefully integrates the variation within a vegetation canopy, making it more spatially coherent. The concept of a mosaic model for image classification is introduced in Volume 2A and expanded in Volume 2E.

Traditional landscape mapping approaches have long grappled with mismatches between the scales of measurement, estimation and prediction in terms of specific landscape features (Gallant *et al.*, 2008). Many landscape mapping methodologies embrace a multi-scale approach (see Excursus 1.1 and McKenzie *et al.*, 2008b), including recommended scales for mapping different surface features (see Table 1.4 below). For example, a hierarchy of spatial scales describing soils and landscapes is shown in Table 1.3. Within this hierarchy, however, the spatial and temporal scales for various landscape processes may not be correlated (Blöschl and Sivapalan, 1995). Further, while most landscape attributes can be represented as a nested hierarchy, with the associated levels being sequenced in time and space, the processes of moving either up or down the scale hierarchy (upscaling and downscaling respectively) present significant technical challenges (see Figure 1.3).

Figure 1.3 Upscaling and downscaling of soil data

While some forms of upscaling and downscaling are trivial, others are technically challenging.

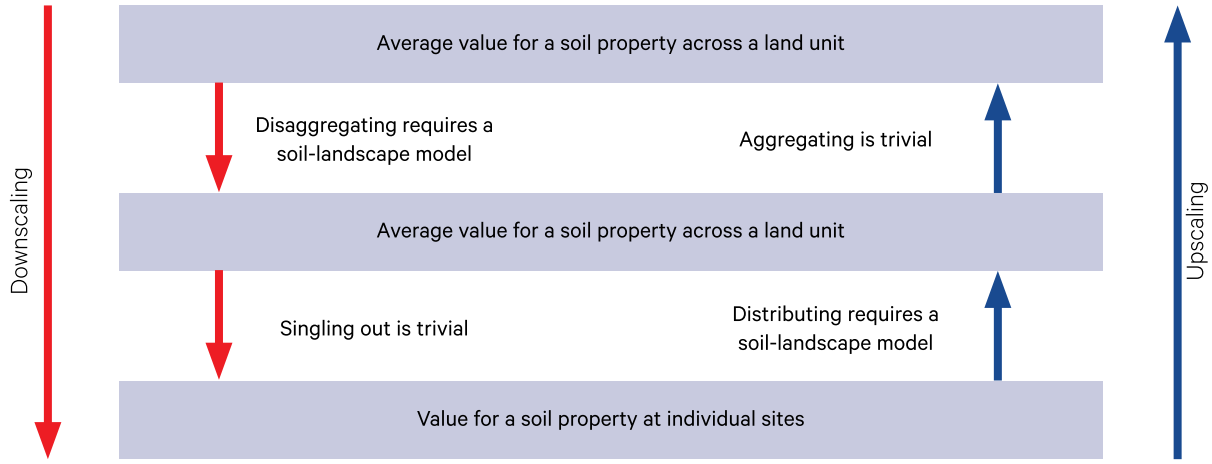

Adapted from Gallant *et al.* (2008) Figure 3.7

Similiarly, hierarchies of imagery over a range of scales may be appropriate to resolve relevant surface features and patterns and their spatial interrelationships (see Volume 1A—Section 1). Since the design of EO sensors traditionally imposes a choice between higher frequency of imagery at lower spatial resolution or vice versa (see Volume 1A—Section 13), multi-scale hierarchies of images can allow the detailed information acquired from field sites and higher resolution imagery to be extended over a larger area (see Figure 1.4).

Selection of appropriate imagery for EO analyses is further discussed in Section 2.2. The landscape mosaic has particular relevance to image integration when datasets with differing spatial resolutions are being merged. While technological solutions exist to resample imagery to a range of scales (see Volume 2B—Section 5), the critical consideration here is whether the resulting scale is appropriate to the spatial dimensions of the features and patterns that are being studied in the underlying surface mosaic. Implications of the surface mosaic, in the context of upscaling and downscaling of EO images, are explored in Section 4.3 (see also Volume 1B—Section 2.4).

Table 1.3 Scale hierarchy for soil and landscape data

Levels of organisation in this hierarchy can be ordered in both space and time, with lower levels being characterised by smaller areas and shorter times, and higher levels being characterised by larger areas and longer time intervals. Upscaling involves moving up the scale hierarchy, while downscaling moves down.

Level	Region	Significance
I+6	World	Provide context
I+5	Continent	
I+4	Region	
I+3	Catchment	
I+2	Catena/farm	
I+1	Field	
i	Site	Obtain field measurements
i-1	Soil horizon	
i-2	Soil structure	
i-3	Basic structure	Understand mechanisms
i-4	Molecular interaction	

Adapted from: Gallant *et al.* (2008) Figure 3.1

Figure 1.4 Scales of EO

Analysis of low and medium resolution imagery can be more easily related to ground data through high resolution imagery. Low resolution imagery tends to be acquired more quickly and cover a larger extent, so is most appropriate for large area surveys. Selected locations within the surveyed area would typically be checked using data with higher spatial resolution, such as aerial photography. Some of these locations would then be visited in the field to verify the image analysis. This scaled approach enables the results of expensive and time-consuming field work to be extended to a larger area.

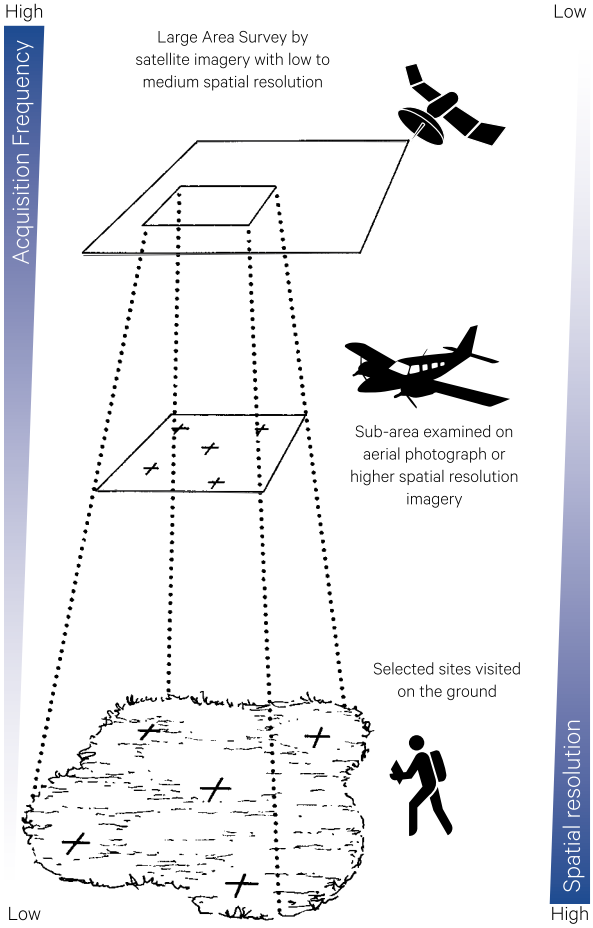

Adapted from: Harrison and Jupp (1989) Figure 39

Excursus 1.1—Landform Models

Source: Speight (2009)

The landform description methods recommended by Speight (2009) divide the landscape mosaic into two different scales, with the larger tiles comprising mosaics of the smaller tiles:

- landform patterns—larger tiles (>600 m across); and
- landform elements—smaller tiles (~40 m across).

The most appropriate scales for mapping these tiles as models of the landform are listed in Table 1.4. Thus, the landform pattern model is considered appropriate for parts of the landscape that span a complete toposequence, whereas the landform element model is more relevant to areas that contain only part of the toposequence.

Table 1.4 Landform models relating to mapping scales

Map scale	Minimum width of mapping units (m)	Appropriate landform model for mapping	Recommended uses
1:500,000	1500	Landform pattern	National/regional resource inventory
1:250,000	750	Landform pattern	Overview of land resources/status
1:100,000	300	Landform pattern	Land use suitability and strategic planning
1:50,000	150	Landform pattern	Major land uses and large catchment management
1:25,000	75	Landform pattern/ Landform element	Low intensity land use planning and medium catchment management
1:10,000	30	Landform element	Intensive land use developments and small catchment management
1:5,000	15	Landform element	Urban and farm planning

Source: Speight (2009) Table 1; Schoknecht *et al.* (2008) Table 14.1

In the Speight (2009) system, landform patterns are described in terms of around 40 predefined types. These types are based on the landform attributes that are observed within sample circles of radius of 300 m in the landform pattern. Examples of landform patterns include mountains, escarpment, hills, floodplains, dunefields and coral reefs. The attributes that determine landform patterns are:

- relief—difference in elevation between the highest and lowest points on the land surface;
- modal slope—most common slope class within the landform pattern;
- stream channel occurrence—described by spacing, development, depth-to-width proportions, pattern of streams, and integration and directionality of channel network;
- mode of geomorphological activity—gradational (eroded/aggragated) or anti-gradational (elevated/ excavated/subsided);
- geomorphological agent—gravity, precipitation, stream flow, wind, ice, standing water, internal forces, biological agents or extraterrestrial forces;
- status of geomorphological activity—whether agent is active, episodic or relict; and
- component landform elements—as observed.

Landform elements are defined by the following attributes within circles of 20 m radius:

- slope—in terms of eight categories based on inclination;
- morphological type—flat, crest, slope and depression (open and closed), plus position in toposequence and relative slope inclination for non-flat surfaces;
- dimensions—length, width and height;
- mode of geomorphological activity—as above; and
- geomorphological agent—as above.

Examples of landform elements include cliff, footslope, swamp, swale and valley flat.

1.5 The Bigger Picture

As introduced in Section 1.2, an implicit goal of any image interpretation exercise should be that its results can be verified and reproduced independently. More than for any single image processing task, however, the integration of bi-temporal and multi-temporal EO datasets demands that the interpreter retains awareness of the 'bigger picture'. This can be condensed into two questions:

- what is the goal of this analysis?; and
- how can 'success' be assessed?

These questions need to be answered before the most appropriate data, processes and methods can be selected for any particular study (see Section 2).

In the following sections we will consider established methods for calibrating and pre-processing multiple images (see Sections 3 and 4), processing bi-temporal EO image pairs (see Sections 5 to 7), and creating and analysing time series datasets (see Sections 8 to 11). The greater goal of most EO analyses involving bi-temporal and multi-temporal datasets, however, is to interpret measured properties of the target object (or surface) in terms of a specific application, using a pre-defined structure model (see Section 1.1). In this context the underlying EO framework must be explicitly acknowledged and considered in all stages of processing, interpretation and delivery.

It is also worth remembering at the outset of any EO-based study that mapping of Earth surface resources—whether derived directly from field observations or based on EO analyses—only describe biophysical attributes at one instance in time. To fully understand environmental change, however, mapping results must to be integrated with monitoring and modelling activites (see Figure 1.5). This integrated approach is required for competent land-use planning, assessing land management practices, understanding natural processes, forecasting future environmental conditions, and formulating appropriate policies for managing our natural resources (McKenzie *et al.*, 2008a).

Some of the current limitations with natural resource maps in Australia include incomplete and inconsistent coverage, inappropriate scaling, incompatible survey methods, insufficient rigour when measuring key attributes, lack of accuracy assessment, and lack of currency (McKenzie *et al.*, 2008a). Monitoring of natural resources requires a baseline from which observed changes over time can be measured (see Section 14.2 and Volume 3A), whereas modelling enables prediction of future conditions (see Section 14.3 and Volume 2A—Section 2.3). Modelling also provides an opportunity to explore the potential ramifications of changes in resource attributes, management regimes, land uses, or policies. The complementary relationships between mapping, monitoring and modelling are summarised in Table 1.5. Integrated mapping, monitoring and modelling systems that are based on EO datasets are introduced in Section 14, and further detailed in Volume 3.

Figure 1.5 Mapping, monitoring and modelling for natural resource management

To monitor environmental changes in a given landscape, these complementary activities need to focus on the key events and processes that drive those changes. The temporal scale for specific changes may span decades, centuries or millennia.

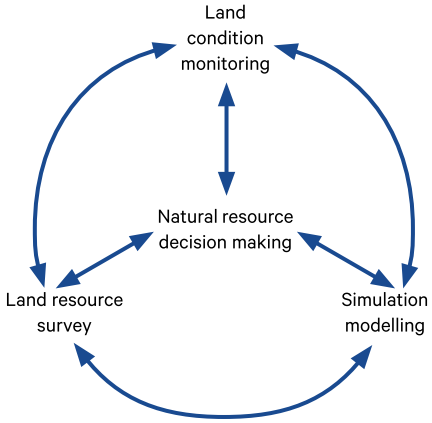

Adapted from: McKenzie *et al.* (2008a) Figure 1.1

Table 1.5 Complementary benefits of mapping, monitoring and modelling

Relationship	Benefits
Mapping → monitoring	Spatial framework for selecting representative sites; System for spatial extrapolation of monitoring results; and Broad assessment of resource condition.
Monitoring → mapping	Quantifies and defines important resource variables for mapping; and Assesses land suitability over time (including risk assessments for recommended land management).
Modelling → monitoring	Determines whether trends in specific land attributes can be successfully detected with monitoring; and Identifies key components of system behaviour that can be measured in a monitoring program.
Monitoring → modelling	Validates model results; and Provides data for modelling.
Modelling → mapping	Allows spatial and temporal prediction of landscape processes.
Mapping → modelling	Provides data for modelling; and Provides spatial association of input variables.

Source: McKenzie *et al.* (2008a) Table 1.1

1.6 Further Information

McKenzie *et al.* (2008b)

1.7 References

Blöschl, G., and Sivapalan, M. (1995). Scale issues in hydrological modelling: a review. *Hydrological Processes*, 9, 251–299.

Duggin, M.J., and Robinove, C.J. (1990). Assumptions implicit in remote sensing data acquisition and analysis. *International Journal of Remote Sensing*, 11, 1669–1694.

Gallant, J.C., McKenzie, N.J., and McBratney, A.B. (2008). Scale. Ch 3 in *Guidelines for Surveying Soil and Land Resources*. Australian Soil and Land Survey Handbook Series. (Eds: McKenzie, N.J., Grundy, M.J., Webster, R., and Ringrose-Voase, A.J.) CSIRO Publishing, Melbourne.

McKenzie, N.J., Ringrose-Voase, A.J., and Grundy, M.J. (2008a). Rationale. In *Guidelines for Surveying Soil and Land Resources*. Australian Soil and Land Survey Handbook Series. (Eds: McKenzie, N.J., Grundy, M.J., Webster, R., and Ringrose-Voase, A.J.) CSIRO Publishing, Melbourne.

McKenzie, N.J., Grundy, M.J., Webster, R., and Ringrose-Voase, A.J. (Eds) (2008b). *Guidelines for Surveying Soil and Land Resources*. Australian Soil and Land Survey Handbook Series. CSIRO Publishing, Melbourne.

Schoknecht, N., Wilson, P.R., and Heiner, I. (2008). Survey specification and planning. Ch 14 in *Guidelines for Surveying Soil and Land Resources*. Australian Soil and Land Survey Handbook Series. (Eds: McKenzie, N.J., Grundy, M.J., Webster, R., and Ringrose-Voase, A.J.) CSIRO Publishing, Melbourne.

Speight, J.G. (2009). Landform. In: *Australian Soil and Land Survey: Field Handbook* (3rd Edn). (Eds: National Committee on Soil and Terrain) pp. 15–72. CSIRO Publishing, Melbourne.

2 Multi-temporal EO Datasets

One of the strengths of EO is the provision of regularly updated imagery of the Earth, from which changes in surface features can be observed. While changes in surface features can occur for many reasons, most changes are driven by:

- climate variations, including seasonal cycles, short-term aberrations and long-term natural changes with consequent impact on soil moisture and phenology;
- landscape changes relating to erosion and deposition;
- natural disasters, including fire, floods, wild weather, tectonic activity and landslides;
- ecological succession in vegetation; and/or
- human activities, such as land cover changes, silviculture, agriculture, urban development and mining (see Volume 3).

All differences between bi-temporal and multi-temporal imagery, however, do not necessarily indicate real feature changes on the ground (see Section 1). As detailed in Volume 2A—Section 3, image differences can also result from changes in atmospheric condition, sensor characteristics, and viewing and illumination geometries. Accordingly, some form of image calibration is essential before surface changes can be reliably detected in bi-temporal or multi-temporal imagery (see Section 3).

When investigating changes in Earth surface features as viewed by EO sensors, it is tempting to think in terms of some 'equilibrium' state from which 'change' occurs. However, the Earth represents a dynamic system, and repeated observations of that system can vary for many reasons. Some of the temporal variations that can be observed in EO imagery derive from correlated changes—these image variations are correlated with natural environmental factors but do not necessarily indicate a change in the surface features. For example, terrain shading varies with Sun position and terrain characteristics, and is correlated with incident radiation. In EO imagery, variations in terrain shading may 'appear' as a change in land cover, but changes in shading are essentially ephemeral. Seasonally varying levels of solar radiation directly impact surface features but, on any given day, these are not necessarily represented by the current terrain shading. Rather, such seasonal patterns are inferred from a changing pattern that correlates with them. While imaging artefacts can be removed using physical models (see Section 3.1) and 'random noise' can be removed using statistical methods (see Volume 1B—Section 2), spuriously correlated interactions between the sensor 'view' and the Earth's surface are much harder to remove.

In this section we will firstly review some of the characteristics of multi-temporal imagery that directly impact its utility (see Sections 2.1 and 2.2), before considering appropriate processes (see Section 2.3) and methodologies (see Section 2.4) for such datasets.

Background image: ASTER image of Lake Mackay, Australia's fourth largest lake, acquired on 9 September 2010. This ephermal salt lake is located along the WA/NT border. **Source:** NASA ASTER gallery. Retrieved from *https://earthobservatory.nasa.gov/images/84984/australias-ephemeral-lake-mackay*

2.1 Bi-temporal and Multi-temporal Imagery

Time is but one dimension that is sampled by EO imagery. The four data dimensions inherent to EO datasets are introduced in Volume 1B—Section 1 and summarised in Table 2.1. Reliable processing of bi-temporal and multi-temporal image datasets requires that all images captured at different dates and/or times be comparable, that is, there is adequate consistency between their spectral, spatial and radiometric dimensions.

The time dimension, however, presents unique some unique challenges to an interpreter. As detailed in Section 1.3, each image represents a complex ground scene. While the spectral, spatial, radiometric and temporal characteristics of an EO sensor can be tailored to the idiosyncracies of particular ground features, the way those ground features change through time cannot be known or predicted with certainty. While the 'usual' range of spectral responses, for example, of a ground feature can be pre-determined, anomalies can occur. During extreme events, such as fires and floods, the designed sensitivity range of imaging sensors may be exceeded, to render saturated pixels in imagery at a time when reliable data is most needed (see Volume 1A—Section 13).

Table 2.1 Sampling dimensions in EO imagery

Dimension	Characteristic		
	Resolution	Density	Extent
Spectral	Width of each wavelength channel	Number of channels detected by sensor	Range of wavelengths covered by all channels
Spatial	Ground area imaged per optical pixel	Number of pixels and lines in image	Area covered by image
Radiometric	Smallest change in detected energy that would be represented as a different image brightness level	Number of gradations (grey levels) used to represent full range of radiances that could be detected by sensor	Actual range of radiances detected in each channel
Temporal	Time period over which each image is acquired	Frequency of successive image acquisitions	Total time period for which this imagery is available

Adapted from Emelyanova *et al.* (2013)

2.1.1 Conceptual structure

The conceptual structure of an EO image is introduced in Volume 2A—Section 1. For a single image, acquired on a particular date, this structure resembles a three-dimensional matrix as depicted in Figure 2.1. A bi-temporal image simply comprises two images acquired at different times (see Figure 2.2a). Sets of multi-temporal images can be considered as comprising multiple image matrices (see Figure 2.2b). The critical aspect of this structure is that any given pixel location in a set of multi-temporal images represents exactly the same ground area in all of the images in that set.

The number of images in a multi-temporal dataset can vary widely, potentially including tens of thousands of images. In terms of processing operations, it is convenient to distinguish between those that may be used to detect or highlight differences and similarities between two images and those that are relevant to a longer sequence of images.

Figure 2.1 Structure of an EO image

A multi-channel image comprises three data dimensions—pixels, lines and channels. Pixels (or 'elements' or 'samples') along the line can be considered as columns in a matrix. Lines in the image are like rows of a matrix, with each channel being an attribute layer in the matrix.

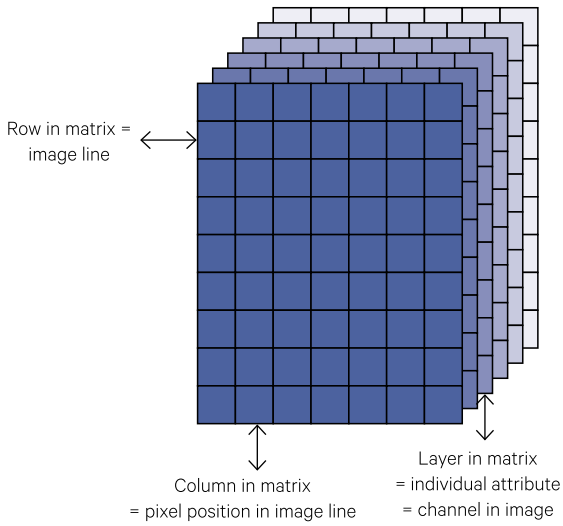

Figure 2.2 Bi-temporal and multi-temporal image sets

A given pixel location within a bi-temporal or multi-temporal image set (such as the red pixel below) is assumed to represent exactly the same target area on the ground.

a. A bi-temporal image set comprises two images acquired at different dates.

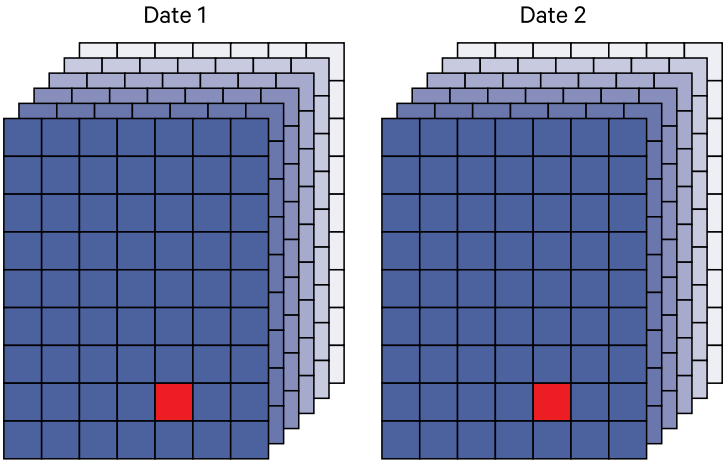

b. A multi-temporal image set comprises multiple images acquired at different dates, usually ordered chronologically.

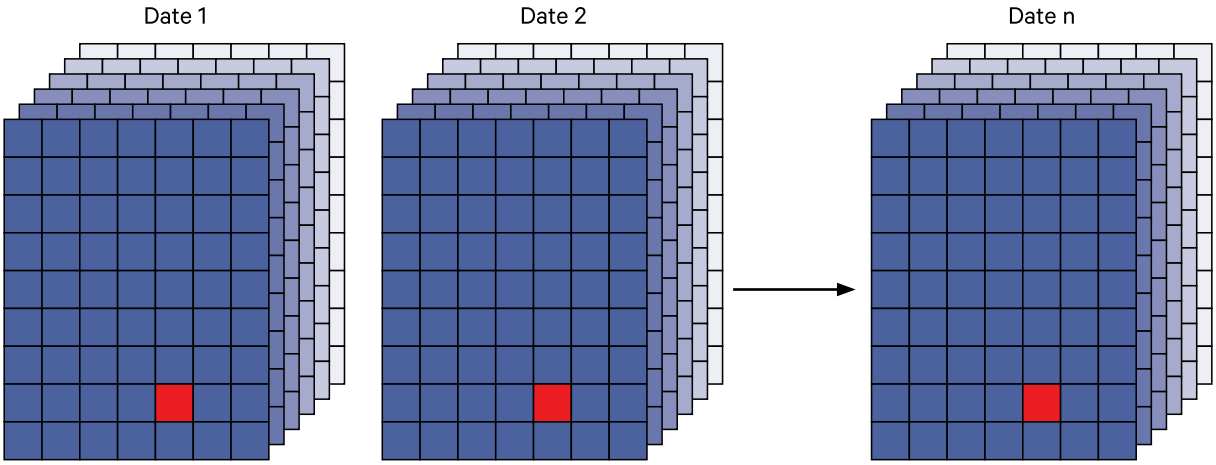

Operations that are commonly used for a calibrated, bi-temporal pair of EO images include:

- basic operations such as differencing, segmenting, colour balancing (see Section 5);
- fusion methods such as pan-sharpening (see Section 6.1) and temporal interpolation (see Section 6.2); and
- processes for detecting changes (see Section 7).

Longer sequences of EO images can be processed as time series data if their acquisition dates are evenly spaced (see Section 8). Many, but not all, multi-temporal datasets of EO images are acquired at regular time intervals, so can be treated as time series archives. Relevant processes for these datasets include characterising temporal trends (see Section 9) and creating composite images (see Section 10).

2.1.2 Satellite-acquired datasets

Satellite imagery has been acquired for several decades and some global EO datasets now span a substantial time series. Most satellite sensors acquire images at standard times of the day on a predefined acquisition schedule from a nadir viewing position (see Volume 1A). This ensures that the image archives for a particular sensor are imaged with the same sensor and illumination geometry. While solar illumination changes with the seasons, such variations can be modelled with sufficient accuracy (see Volume 2A—Section 3). However, when imagery acquired by different sensors is being compared or merged, differences in the diurnal acquisition times can become significant. Similar challenges result when some images are acquired from non-nadir viewing positions, as is possible for some satellite and most airborne sensors.

Table 2.2 Global EO time series datasets

Satellite (Agency)	Sensor	Spectral bands (in latest sensor)	Spectral range (in latest sensor)	Radiometric Quantisation (bits)	Spatial Resolution (m, at nadir, in latest sensor)	Swath Width (km, at nadir, in latest sensor)	Revisit Time (days)	Image Archive
ALOS (JAXA, Japan)	AVNIR-2	4	Optical	8	10	70	14–46	2006–2011
	PALSAR	1	L-band SAR in 3 modes	5	1–100	25–490	14–46	2006–2011; 2014–present
	PRISM	1	Panchromatic/ stereo	8	2.5	70 (35 in triplet mode)	14–46	2006–2011
TIROS/ AVHRR (NOAA, USA)	AVHRR	6	Optical/ thermal	10	1,100	~2700	daily	1978–present
Landsat (NASA/ USGS, USA)	MSS	4/ 1	Optical/ thermal (L-3)	8	68 x 83	185	16–18	1972–1997
	TM/ETM+	7	Optical/ thermal	8	30/ 120	185	16	1987–2011
	OLI/TIRS	11	Panchromatic/ optical/ thermal	12	15/ 30/ 100	185	16	2014–present
Terra (NASA, USA)	ASTER	9/ 5	Optical/ thermal	8/ 12	15/30/ 90	60	4–16	1999–present
Terra and Aqua (NASA, USA)	MODIS	36	Optical/ thermal	12	250/ 500/ 1,000	2330	1–2	2000–present
Quickbird (Digital Globe, USA)	Quickbird	5	Panchromatic/ optical	11	0.55/ 2.16 (at 400 km altitude)	14.9 (at 400 km altitude)	1–3.5	2001–2015
SPOT (Airbus DS, France)	SPOT PAN SPOT MS	5	Panchromatic/ optical/ stereo	8–12	1.56/ 6	60	1–3	1986–present
Geoimage (USA)	GeoEye	5	Panchromatic/ optical	11	0.41/ 1.65	15.2	£3	2008–present
MAXAR (formerly DigitalGlobe, USA)	WorldView	1/ 8–16	Panchromatic/ optical	11	0.31–0.46/ 1.24–2.0	17.6/ 13.1–16.4	<1	2007–present/ 2009–present

When using bi-temporal or multi-temporal imagery for change detection studies, it is clearly essential that the differences between images derive from changes in surface features rather than differences in their acquisition parameters (see Section 7). Accordingly, any imagery destined for such analyses need to be carefully calibrated to an absolute standard as described in Section 3.

Finally, some of the global EO archives available as time series datasets are listed in Table 2.2. Very high spatial resolution datasets with rapid revisit times, such as FORMOSAT-2 and IKONOS, can also be used to generate EO time series. Several EO data suppliers provide time series datasets for both the image reflectance (or albedo) data and for transformations, such as the Normalised Difference Vegetation Index (NDVI) or the Enhanced Vegetation Index (EVI), which have been derived from image reflectance (see Volume 2C). Examples of such composite products for the MODIS sensor are given in Excursus 10.1.

2.2 Appropriate Data

In Section 1 above, we reviewed some of the foundations of EO image datasets, including an appreciation for the underlying surface mosaic that was imaged. For any EO analysis exercise, a good understanding of the key features and patterns in this mosaic is a pre-requisite for reliable results. In this context, the following EO variables are particularly relevant to the selection of appropriate bi-temporal or multi-temporal imagery:

- acquisition dates and times (see Section 2.2.1);
- issues relating to image spatial scale (see Section 2.2.2); and
- spectral and radiometric differentiation (see Section 2.2.3).

2.2.1 Timing

Clearly, to detect a particular surface feature in an EO image, the timing of image acquisition must capture the differentiating characteristics of that feature in the surface mosaic. This requirement is just as, if not more, relevant when selecting bi-temporal or multi-temporal imagery, especially when monitoring multiple stages in some environmental process, such as crop phenology (see Volume 3A) or flooding (see Volume 3B). In this context, timing relates to both time of year (season) and time of day (see Volume 1B—Section 1).

The timing of image acquisition is of primary importance in change detection exercises. When comparing two images, familiarity with the 'initial state' image—insight that links its reflectance values to relevant properties of the surface features being imaged—is critical. Ideally, the timing of this image will maximise the contrast in surface features of interest and minimise 'contamination' from imaging artefacts (including atmospheric, illumination, and viewing angle effects). Similarly, the timing of the 'final state' image needs to highlight the anticipated changes in one or more particular surface feature(s). Anniversary dates are often recommended to highlight annual changes in surface features and minimise variations associated with the Sun and sensor geometries. For ecosystem studies, however, phenological cycles for different surface features can still vary intra-annually even when the features themselves have not changed (Coppin *et al.*, 2004). Variations in soil moisture levels can also significantly impact image radiance, especially in sparsely vegetated areas.

Thus, an understanding of the surface feature(s) being studied is essential for selecting appropriate image dates. This requires that the:

- spectral, spatial, radiometric and temporal resolution and extent of the images are suitable to observe and isolate the feature(s) of interest relative to other features in the surface mosaic (see Section 2.1); and the
- time interval between selected (set of) images is sufficient to allow the change(s) of interest to be detected.

In general, while vegetation differences will be highlighted during the growing season, the precise timing of this varies for different types of vegetation and between different geographic regions. When multiple features are being studied, it may be more relevant to select dates that maximise the contrast in their reflectance properties, rather than maximise the reflectance of any individual feature. Likewise, the interval between an 'initial state' image and the 'final state' image must allow sufficient time for the surface feature(s) to change, and this may vary from very short intervals (minutes or hours) for natural disasters, to longer intervals (days or months) for agricultural crops, to much longer intervals (years to decades) for forest vegetation or land rehabilitation studies.

The impact of changes in Sun position on EO radiances is detailed in Volume 2A—Section 3. Radiometric calibration attempts to correct for these seasonal and diurnal changes in bi-temporal and multi-temporal imagery (see Section 3.1.1.2), and renders reasonable success in datasets derived from a single sensor. However, when using processing methods that interpolate imagery from one sensor, based on the image values acquired from a different sensor (see Section 6.2), potential limitations of radiometric calibration need to be considered.

The optimal timing of images for bi-temporal or multi-temporal analyses will also be determined by climatic factors such as cloud cover and aerosol concentration. Unfortunately, however, EO imagery is not always available for the most appropriate dates. In many regions of the world, for example, cloud-free imagery are only available for limited seasons, which further restricts the selection of appropriate imagery for change detection studies. Similarly, available imagery may not coincide with maximum flood levels or peak fire activity. The final selection of image dates may become a compromise between the most suitable environmental time and the most convenient logistical time with respect to available and/or affordable imagery. Where sub-optimal pairs of images are used for change detection, their limitations need to be considered during the analysis, and acknowledged in reporting outcomes.

2.2.2 Scaling

A limiting factor for differentiating many surface features and processes is image scale (see Volume 1B—Section 2). Quite simply, does the pixel size allow the relevant feature(s)—or a representative characteristic thereof—to be discriminated? In some cases the size of surface features can change with time and that transition may be discernible in an appropriately-scaled sequence of images.

While image resampling methods are primarily used to correct geometric distortions in EO imagery, they can generate artefacts as well (see Volume 2B). Such potential problems may be more misleading when multi-resolution data from different sensors is processed to a common pixel size (see Section 4.3). Similarly, when fusion methods are used to interpolate a new temporal image from a lower spatial resolution dataset (see Section 6.2), the implications on the true scale of the resulting image need to be considered carefully. The importance of image scale in the classification process is further discussed in Volume 2E.

2.2.3 Spectral and radiometric differentiation

The importance of spectral and radiometric resolutions in EO imagery are introduced in Volume 1B—Section 1. Given the seasonality of changes in reflectance characteristics for many surface features, such as vegetation, selection of the most appropriate spectral bands across multiple image dates is important for any monitoring studies. While a particular spectral feature may be discernible in one season within a given radiometric range, it may not be discernible six months later. Likewise, in terms of diurnal changes in reflectance, different sensors that acquire imagery at different times of the day may not detect the same surface feature patterns. The interactions between spectral and spatial resolutions further complicate detection of some surface features when comparing imagery acquired by EO sensors that have different spatial resolutions (see Section 1.4).

Accordingly, when selecting image dates for a monitoring study, the likely discrimination of surface feature reflectance/emission across all dates needs to be determined. Pre-processing methods also need to consider the likely changes in all features across the dates of interest. For example, vegetation indices applied to sparse vegetation over wet soil may generate misleading results when compared with the same indices applied to vegetation over a dry soil background (see Volume 3A). Similarly, the limitations of all image processing algorithms need to be understood over the full temporal range of any bi-temporal or multi-temporal EO dataset (see Section 2.3).

2.3 Appropriate Processes

Just as a wide range of statistics can be computed for any set of numbers, a wide range of processes can be applied to EO images. The value of any particular process will depend on its relevance to the image being processed and the assumptions underlying both the data and the processing algorithm.

Unless supplied as Analysis Ready Data (ARD; see Section 3.2), all bi-temporal and multi-temporal EO image datasets require radiometric and geometric calibration (see Section 3.1 below; or Volume 2A—Section 3 and Volume 2B). This data preparation stage is essential to ensure that corresponding spectral radiance values are comparable across all image dates and that corresponding pixel locations reference the same ground positions.

A simple test for any image processing that involves image statistics is to ask the question: "Are the results reasonable?". For example, PCA of vegetation imagery tends to generate 'typical' statistics for which spectral bands are mostly likely to contribute to which PC (see Volume 2C—Section 9). Should the results of this analysis differ markedly from the usual situation then there is good reason suspect errors have been introduced which warrant investigation.

Occam's Razor: The more assumptions you have to make, the more unlikely the explanation.

The most appropriate processes to apply to a bi-temporal or multi-temporal image dataset will obviously depend on the purpose of the study. However, some simple guidelines are relevant to most image processing (see also Section 1.2):

- Is there a simpler way to do this? Simpler usually means more robust and repeatable, two characteristics that should underpin good science.
- How is the data provenance being maintained and updated through these processing operations (see Volume 2A—Section 2.1)?
- How can the results be validated? If you use all your data to create the model, how do you check it is correct? Approaches to validation in the context of image classification are detailed in Volume 2E.
- Do the results from this process acknowledge any known limitations in the input data?

Unfortunately, a nice-looking output image is rarely sufficient confirmation that the processing was appropriate.

2.4 Processing Methodologies

The concept of a processing methodology was introduced in Volume 2A—Section 2.2. Three broad stages of processing imagery are followed in many EO applications and involve:

- descriptive interpretation—delineating and identifying patterns in the image (such as identifying major land covers);
- exploratory data analysis—using statistical tools to detect and highlight features and patterns across the image (such as creating a land cover map); and
- modelling—relating images values for identified features with measured attributes of those features from another data source (such as characterising mapped land cover categories in terms of structural or spectral properties).

The following terms are used in these publications to distinguish between EO imagery that has been calibrated versus imagery that has been processed to deliver application-specific information (see Volume 2A—Section 2.1):

- data products—corrected image observations from EO sensors, such as surface reflectance products (see Section 3); and
- information products—derived from EO data products using defined processing methodologies for use in specific applications, such as vegetation greenness or land cover categories (see Section 14).

While some EO image processing exercises may not include all three processing stages, most EO information products include them as sequential steps required for product delivery. As well as selecting appropriate processes for a particular image dataset, those processes need to be applied in an appropriate sequence or order (see Section 2.4.1). The actual steps involved in processing are commonly standardised in a workflow (see Section 2.4.2).

2.4.1 Processing order

Just as computation in equations is governed by a pre-defined order of operations, the sequence of image processes applied to bi-temporal or multi-temporal datasets need to be ordered appropriately. General guidelines include:

- apply geometric corrections before radiometric corrections (see Section 3);
- segment irrelevant parts of the image before generating surface feature statistics;
- maintain consistency when processing each image in a large bi-temporal or multi-temporal dataset;
- apply data smoothing operations (such as for presentation purposes) after the primary processing; and
- document the details of all processing for future reference.

The processing steps for selected examples integrated systems are described in Section 14, and examples of EO information products are given in Section 14.1.

2.4.2 Processing workflows

Processing workflows (or process flows) are a convenient notation for defining the steps and conditions involved in a particular processing procedure. In a multi-step process, workflows are essential in some form to ensure that the overall method can be faithfully reproduced. Now that EO standard products are being used in a wide range of applications, including those involved with legislative monitoring such as compliance checking (see Section 14.2.2), their provenance and limitations must ensure scientific transparency and repeatability.

We have included examples of processing workflows in previous volumes (see Volume 2A—Sections 9 and 10), and will encounter several more in Volume 3. On example of a processing sequence is shown in Figure 2.3 for the Australian fractional cover product (see Volume 3A for details). This sequence summarises the major steps and cycles involved with generating this product.

Figure 2.3 Workflow for fractional cover product

This product Is shown as the banner image for Section 14 below and further described in Volume 3A.

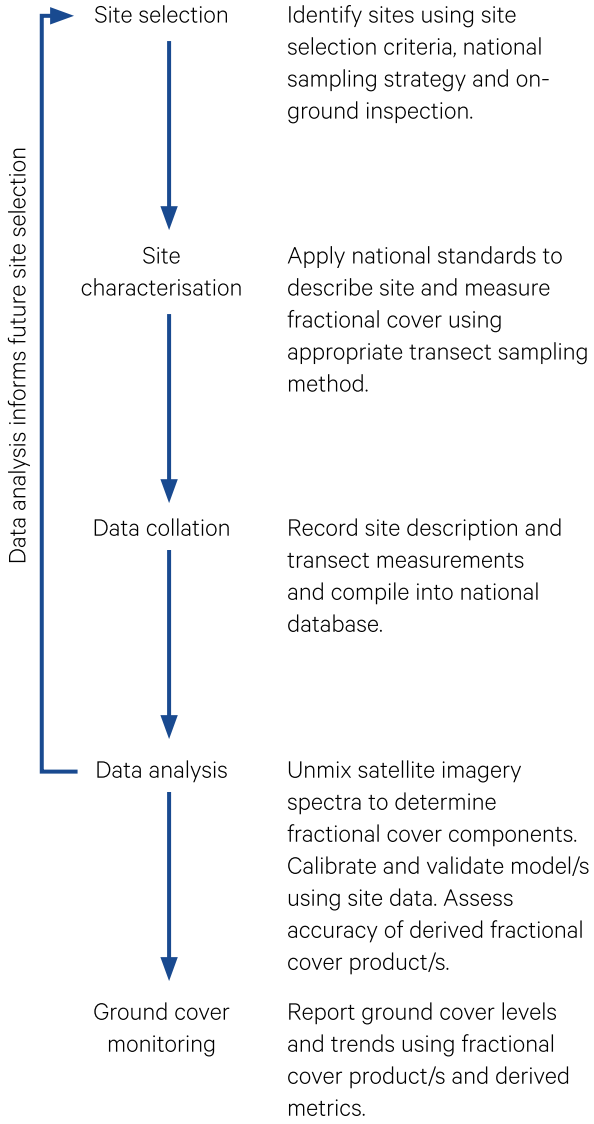

Adapted from: Stewart *et al.* (2014)

Standard symbols can be used in process flow charts to indicate the role of each segment, such as:

- oval—beginning or end of a process;
- rectangle—one step in the process;
- parallelogram—input or output data;
- diamond—decision points; and
- arrow—direction of connection between processes, data and decisions (see Figure 2.4).

Figure 2.4 Process flow chart example

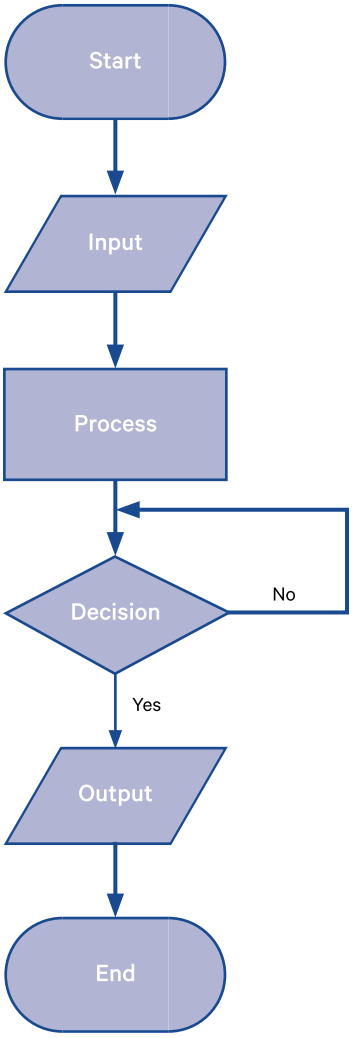

2.5 Accuracy, Stability, Validation and Trust

Given the expanding range and volume of EO data and information products, there is growing awareness of the need to ensure that they achieve dependable standards of accuracy and stability. For a given EO product, these desirables could be defined as:

- accuracy—'the closeness of agreement between product values and true or reference values'; and
- stability—'the systematic error over a long period of time, typically a decade or more' (GCOS, 2011; Soto-Berelov *et al*., 2018).

Validation, then can be defined as the process of determining the accuracy and stability of a product. For EO biophysical products, validation has been described as 'the process of assessing the uncertainty of higher level, satellite sensor derived products by analytical comparison to reference data, which is presumed to represent the true value of an attribute' (Soto-Berelov *et al*., 2018).

In the context of EO products, it is increasingly important that an objective set of validation standards exist, against which product accuracy and stability can be measured. To this end, the Committee on Earth Observing Satellites (CEOS) established the Working Group on Calibration and Validation (WGCV) to develop international standards for calibration and validation of EO activities, including missions and data (Dowman, 2004; see Section 2.6). For example, four stages of validation have been identified for moderate resolution global products (see Table 2.3). In this validation hierarchy, each successive stage is more comprehensive than the previous one. Such systems will allow the accuracy and stability of EO products to be compared consistently.

Both data and information products need to be 'trusted' by users, however, before they are integrated into their decision-making processes. For example, the use of EO data and information products for emergency management was reviewed by Hudson (2015). This review yielded interesting insights into the attitudes of potential users towards EO products, and recommended a design framework that would increase product uptake by encouraging greater interactions between product designers and users (see Excursus 2.1).

Table 2.3 CEOS WGCV validation hierarchy for moderate resolution global products

Validation Stage	Description
1	Product accuracy has been estimated using a small number of independent measurements (typically < 30) obtained from selected locations and time periods and ground-truth/field program effort.
4	Product accuracy has been assessed over a widely distributed set of locations and time periods via several ground-truth and validation efforts. The spatial and temporal consistency of the product has been evaluated over globally representative locations and time periods. Results are published in peer-reviewed literature.
3	Product accuracy has been assessed over a globally distributed set of locations and time periods via several ground-truth and validation efforts. Product uncertainties have been well-established via independent measurements made in a systematic and statistically robust way that represents global conditions. Results are published in peer-reviewed literature.
4	Validation results for Stage 3 are systematically updated when new product versions are released and as the time-series expands.

Source: Soto-Berelov *et al*. (2018) Table 2.1

If you torture the data long enough, it will confess to anything.
(Ronald Coase)

Excursus 2.1—Why is an EO Product Trusted?

Source: David Hudson
Further Information: Hudson (2015)

Earth Observation (EO) aims to improve decision making processes by providing objective evidence. However, like all data and information products, the potential utility of any EO product is impacted by its perceived 'flexibility', that is, whether the design choices made by its creator(s) can be tailored to the desired purpose(s) of its users. The acceptance of any product can be described in terms of four sequential stages:

- awareness—user familiarity with the product;
- usage—frequency of access or use;
- uptake—inclusion of the product as evidence within a decision; and
- adoption—extent of uptake.

As illustrated in Figure 2.5, these responses vary during the life cycle of a product (see also Volume 1B—Section 10).

A recent study analysed the use of EO products (both data and information products) in emergency management (Hudson, 2015). As well as compiling an Australian disaster inquiry database, the study delivered a wide range of findings relating to user perceptions of EO products. Those findings that were directly relevant to the uptake of EO products are summarised in Table 2.4.

Figure 2.5 Lifecycle model for a sensor data product

The 'hype' cycle of a new product, when visibility to users is high, occurs early in its lifetime (see Volume 1B—Figure 10.4), but usage, uptake and adoption take much longer to establish. The S-curve illustrates the increasing performance of a product over time, while the adoption curve shows market acceptance of the product.

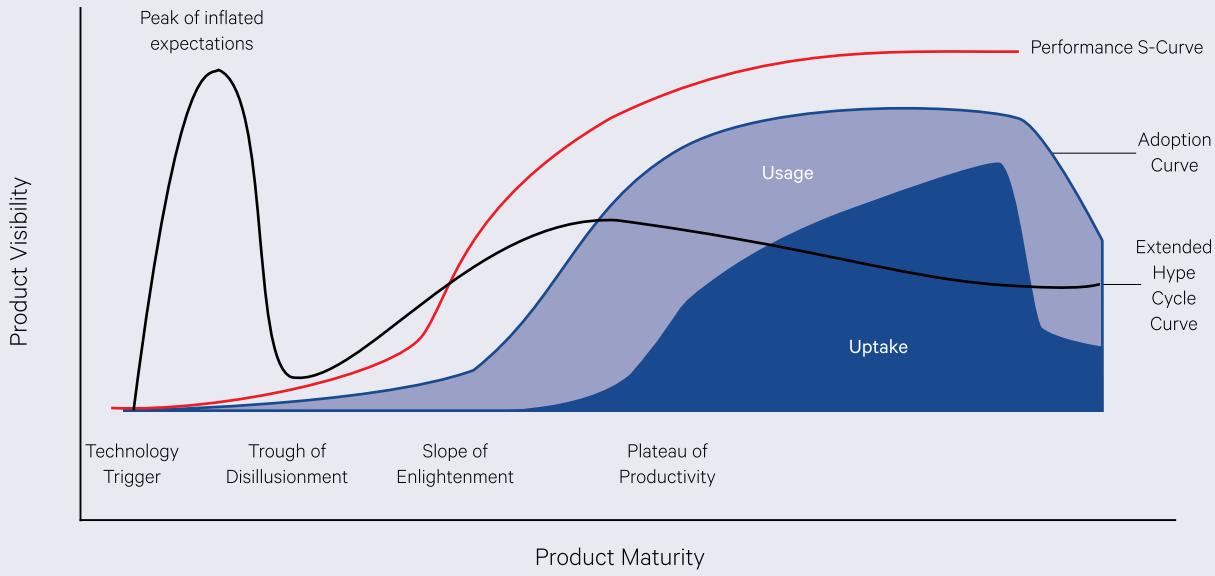

Source: Hudson (2015) Adapted from Linden and Fenn (2003)

Trust is a measure of the belief that someone or something can, has and will do something. More specifically, in the context of EO, trust is a collective measure of the design choices of a product.
Hudson (2015)

Table 2.4 Factors impacting the uptake of EO products

Finding number	Description
4	Not all data has sufficient quality to become an observation, variable or product (see Section 1.1 above)
10	The distinction between awareness, usage and uptake is critical in assessing the effectiveness of an EO product.
15	Open data and recent technological developments allow product creators to increasingly change and tailor EO products.
20	Data usage and/or uptake for Australian disaster enquiries are governed by at least 15 design choices (see Table 2.5).
22	EO products with greater maturity and integration have greater usage and uptake.
26	The most limiting factors for using EO products in the emergency management sector are availability of data, timeliness of data products, and skills to use the data.
28	Official data, or data from an organisation with an official mandate, is more trusted than data from an organisation without a mandate.
30	Emergency managers prefer EO products to be delivered to them by a public institution, even if the data was collected by the private sector.
31	Licence restrictions on the EO product or the original source data can decrease the trust in a dataset.
33	Australian emergency managers believe the most likely design choices to inform decision-making are accuracy, timeliness, reliability, simplicity, consistency and reputation.
40	The balance between accuracy and timeliness is complex and must be actively managed.
43	Reputation takes a long time to build but can be lost very quickly.
44	Trust is the overarching term to encompass all design choices.

Source: Hudson (2015)

Based on the findings of this study, an EO Product Uptake (EOPU) framework was defined to improve the uptake of sensor data products based on 'design choices' that data creators could consider during the product design and revision phases. The framework draws on the concept of a 'data adoption framework', which has been used in other fields (QA4EO Secretariat, 2007; Vanden Borre *et al.*, 2011). The EOPU framework has a hierarchical structure comprising four nested levels:

- the objective of the user for this data product;
- categories of design choices—such as quality, policy, reputation and maturity;
- design choices—specific features that the users want in this data product; and
- design levers—technical metrics and tools to help creators implement and track the design choices.

The EOPU framework is intended to be tailored to the requirements of specific outcomes or target user groups in order to encourage dialogue between the creators and users of sensor data products. The hierarchical structure of this framework enables traceability for designers to see the impact(s) of their design choices. The central proposition of this framework is that every aspect of a sensor data product involves a decision made by the creator of that product. These design choices are a mix of deliberate decisions, such as presentational choices, and inadvertent choices, such as the data policy or data delivery business model of the source dataset. Data product design choices cover many fields, including both traditional technical, scientific and engineering fields, as well as non-technical areas such as law, public policy and marketing. All of these fields must be considered to fully grasp the implications of uptake for a data product. Additionally, technological developments will inevitably create new design choices over time.

However, this framework can only be applied once certain technical criteria have been met. For example, EO datasets can only become products if the measurements used have sufficient accuracy and precision to resolve the desired surface attribute(s) and if the models being used to relate physical processes to the measurements are effective (see Section 1 above). It should also be noted that uptake takes longer and costs more to achieve than usage, which means that targeting design choices to improve uptake generally increases development costs and timeframes.

Gartner's Hype Cycle model adds another dimension to technology life cycle models: it characterizes the typical progression of an emerging technology from user and media overenthusiasm through a period of disillusionment to an eventual understanding of the technology's relevance and role in a market or domain. (Linden and Fenn, 2003)

Table 2.5 EOPU framework for emergency management

Objective	Design Choice Category	Design Choice	Design Lever
Trust	Maturity	Software readiness	Portability, numerical reproducibility, coding standards, code security
		Metadata	File level, collection level and standards
		Documentation	Algorithm Theoretical Basis Document, Operational Algorithm Description, Process Flow Chart, peer reviewed documents of algorithm and product
		Product validation	Independent validation, uncertainty, quality flag, operational monitoring
		Public access	Archive, updates to record, version control
		Utility	Data usage, Societal Sector Decision Support Systems, citations in peer-reviewed literature, user feedback
	Quality	Accuracy	Accuracy, consistency, completeness, errors of commission, omission, and human error
		Relevance	Tailored business model, coverage, frequency, specificity, absence of alternative resources, responsiveness, flexibility, level of value added
		Latency	Time from acquisition to delivery, efficiency of system
		Usability	Presentation, simplicity, consistency, accessibility, ease of use, consistency of terms, fitness for purpose
	Reputation	Credibility	Integrity, objectivity, provider familiarity, availability of experts, experience, user referrals, association with trusted resources, bias/perceived incentives
		Mandate	Officially recognised provider, absence of other alternative resources
		Reliability	Percentage uptime, availability of system, availability of communications, redundancy, scalability
		Security	Physical security, network security, authentication, authorisation
		Data source	Source, defence dual-use, third party source, sovereignty, ability to disclose source, confidentiality, privacy
		Popularity	Product visibility, user awareness
	Policy	Sensor data policy	Ownership, Intellectual property, pricing policy, archiving policy, licencing describing access to raw data, rights to distribute data, responsibilities, liabilities

Adapted from Hudson (2015)

Table 2.5 lists the design choices and levers that were identified as being most relevant to emergency managers. Design choices related to quality, data policy, reputation and maturity all contribute towards the likelihood of an emergency manager incorporating a data product in decision making. This likelihood can be summarised as a measure of *trust*. Thus, if a data product aligns all design choices with the requirements of a given user it is likely to be highly trusted, and therefore more likely to be considered when making decisions. Conversely, if a data product ignores some design choices, and does not tailor design choices to a given user, that user will be less likely to trust the product and unlikely to consider that product in decisions.

The EOPU framework can be implemented across two stages of the product cycle:

- before product launch—to ensure that the product will meet user requirements within the creator's funding and technical restrictions; and
- after product launch—to continuously improve the product based on its performance and feedback from users.

While products are traditionally launched as the hype cycle begins to recover and quality on the performance S-curve climbs (see Figure 2.5), this is not always the case as various studies have shown (Hudson, 2015). Uptake of sensor data products is not simply a function of the sensor, but is driven by a range of design choices. Quite simply, to maximise uptake of an EO product, the design choices and their levers are best determined by an ongoing dialogue between the product creators and its intended users.

2.6 Further Information

CEOS:

The Earth Observation Handbook: *http://www.eohandbook.com*

Committee on Earth Observation Satellites Working Group on Calibration and Validation Land Product Validation Subgroup: *https://lpvs.gsfc.nasa.gov/*

Global systems:

NASA Ocean Colour Web: *https://oceancolor.gsfc.nasa.gov/missions/*

Global Information and Early Warning System on Food and Agriculture (GIEWS, FAO): *http://www.fao.org/giews/earthobservation/index.jsp?lang=en*
http://www.fao.org/giews/earthobservation/asis/index_2.jsp?lang=en

2.7 References

Coppin, P., Jonckheere, I., Nackaerts, K., Muys, B., and Lambin, E. (2004). Digital change detection methods in ecosystem monitoring: A review. *International Journal of Remote Sensing*, 25(9), 1565–1596.

Dowman, I. (2004). Foreword. In *Post-Launch Calibration of Satellite Sensors*. International Society for Photogrammetry and Remote Sensing (ISPRS) Book Series Vol. 2 (Eds: Morain, S.A., and Budge, A.M.) A. A. Balkema Publishers, Leiden, The Netherlands.

Emelyanova I. V., McVicar, T. R., Van Niel, T. G., Li, L. T., and van Dijk, A. I. J. M. (2013). Assessing the accuracy of blending Landsat-MODIS surface reflectances in two landscapes with contrasting spatial and temporal dynamics: A framework for algorithm selection. *Remote Sensing of Environment*, 133, 193–209.

GCOS (2011). *Systematic Observation Requirements for Satellite-based Data Products for Climate. 2011 Update*. GCOS-154. WMO. *http://cci.esa.int/sites/default/files/gcos-154.pdf*

Hudson, D.A. (2015). *Uptake of sensor data in emergency management*. PhD thesis, ANU. *https://doi.org/10.25911/5d78d486abc4d*

Linden, A., and Fenn, J. (2003). *Understanding Gartner's Hype Cycles*. Strategic Analysis Report, Gartner. *http://www.ask-force.org/web/Discourse/Linden-HypeCycle-2003.pdf*.

QA4EO Secretariat (2007). *QA4EO. Quality Assurance Framework for Earth Observation*. *http://qa4eo.org/*.

Soto-Berelov, M., Jones, S., Farmer, E., and Woodgate, W. (2018). Review of validation standards of biophysical Earth Observation products. Ch 2 in *Effective Field Calibration and Validation Practices: A practical handbook for calibration and validation satellie and model-derived terrestrial environmental variables for research and management*. A TERN Landscape Assessment Initiative, NCRIS. ISBN: ISBN 978-0-646-94137-0. Retrieved from *https://www.tern.org.au/NEW-CalVal-handbook-for-remote-sensing-bgp4370.html*

Stewart, J.B., Rickards, J.E., Randall, L.A., McPhee, R.K., and Paplinska, J.Z. (2014). *Ground cover monitoring for Australia: Final report July 2012 to June 2013*, ABARES Technical report 14.1, Australian Bureau of Agricultural and Resource Economics and Sciences, Canberra, May 2014.

Vanden Borre, J., Paelinckx, D., Mücher, C., Kooistra, L., Haest, B., De Blust, G., and Schmidt, A. (2011). Integrating Remote Sensing in Natura 2000 Habitat Monitoring: Prospects on the Way Forward. *Journal for Nature Conservation*, 19 (2), 116–125. *https://doi.org/10.1016/j.jnc.2010.07.003*.

3 Data Standardisation

In addition to the three functional stages described in Section 2.4, all EO imagery needs to be calibrated before processing (see Volume 2A—Section 3). EO data providers routinely correct for radiometric (see Volume 2A—Section 8.3) and geometric distortions (see Volume 2B) in all distributed imagery. These corrections are essential for compiling and analysing time series datasets to ensure that pixels are accurately colocated and have values that are comparable.

In the context of bi-temporal and multi-temporal datasets, the following sub-sections review:

- calibrating EO imagery (see Section 3.1);
- using pre-calibrated image datasets known as analysis ready data (see Section 3.2); and
- incorporating ancillary data sources with EO datasets (see Section 3.3).

As an example of rigorous pre-processing procedures, the process flows used by Geoscience Australia (GA) to create the Land Surface Reflectance (LSR) dataset (previously called the Australian Reflectance Grid, ARG) are described in Excursus 11.1 below.

3.1 Image Calibration

Before two or more images can be compared they need to be registered in terms of all image dimensions (see Section 2.1), that is:

- spectrally—corresponding pairs of image channels from each image should measure comparable spectral ranges in terms of reflected or emitted wavelengths;
- spatially—each geometric pixel needs to represent the same ground position and area in both images;
- radiometric—image values in both images need to relate to the same numeric range for all measured reflectances/emissions. Also, pixel values generally need to be represented by the same number of bits in both images (although some image processing systems can convert on the fly); and
- temporal—image differences resulting from changes in the illumination or sensor position, or atmospheric conditions, also need to be corrected (see Volume 1B—Section 1 for more details).

3.1.1 Systematic effects

All forms of EO imagery contain systematic variations which modify the local values of image attributes and can complicate comparison of attributes from different parts of the image (see Volume 2A—Section 3). Most of these effects arise from the:

- interactions between a scanner's viewing geometry and Earth surface layer(s) (see Volume 1B—Section 3);
- physics of radiative transfer through a variable atmosphere (see Volume 1B—Sections 4 and 5); and/or
- physical process of imaging (see Volume 1A—Section 13).

Background image: ASTER L1B scenes across the Australian continent before cross-calibration to create a seamless mosaic (see Volume 2A—Excursus 8.3).
Source: Michael Caccetta, CSIRO

Examples of systematic effects include:

- vignetting in early aerial photography which cause pixels at the edges of a scanned photograph to be brighter than those in the centre.
- surface radiance recorded by an airborne scanner is modified by the atmosphere and the relative positions of the Sun and the scanner view direction to produce systematic 'limb brightening' across scan lines (see Volume 2C—Section 7.2).
- over water, near to the specular reflection point between the Sun, the water surface and a scanning sensor, there will be brightening due to 'sunglint', which depends on both the view direction and wind speed over the surface.
- in some images, around the point where the shadow of the platform for a scanner (such as an aircraft) would be located, there is a general brightening called the land surface 'hotspot' which creates very large differences across images when the Sun and sensor geometry bring it into the image field of view (see Volume 2X—Appendix 1).
- more commonly, the changing angle between the sensor, the Sun and the orientation of the land surface creates systematic topographic brightness variations, especially in satellite images (see Volume 1B—Section 3).

Such variations are best handled is through physical models, which either allow the data to be interpreted in the context of the pixel position, or 'correct' or compensate for the variations. When the purpose is simply to 'balance' the effects over the extent of an image, it is sometimes possible to use a transformation based on a reference channel to extract the systematic component (see Volume 2C—Section 7.3.1). Alternatively, image transformation such as ratioing can reduce the systematic effects. For example, both topographic shading and sunglint appear to be reduced in ratio channels (see Volume 2C—Section 10). However, since some systematic variation is additive and some multiplicative, each type of variation should be considered individually.

Systematic variation can also arise from engineering aspects of detector calibration and data collection (see Volume 1B—Section 2). For example, any imbalance between detectors in a pushbroom scanner (a scanning device uses multiple detectors to form each line of image data) will result in systematic 'lines' running vertically through an image (see Volume 1A—Section 14.2 for details). Similarly, if the sensitivities of multiple detectors in a whiskbroom scanner vary during scanning, there will be an apparent horizontal (or line) striping in the resulting image. For example, the Landsat TM/ETM+/OLI whiskbroom sensors use multiple detectors to image groups of 16 lines per scan. While the detectors in these line groups are calibrated and balanced prior to launch, variations between on-board calibration of different detectors and their interactions with different surface features can result in a residual 16 line striping effect, which typically makes analysis difficult over low contrast targets such as forests and water (see Volume 2A—Section 3.2.3 and Volume 2C—Section 2.4). Geophysical data, such as airborne magnetics data, which is interpolated to an image format from separately-flown flightlines, may also need considerable balancing between lines to avoid strong striping effects in the image (see Volume 1A—Sections 7 and 8).

The logical pre-processing steps required before bi-temporal or multi-temporal image analysis are generally considered in terms of geometric correction (see Section 3.1.1.1) and radiometric correction (see Section 3.1.1.2).

3.1.1.1 Geometric correction

As detailed in Volume 2B, the mechanism of EO image acquistion necessarily results in geometric distortion in the imagery. Many sources of distortion can be modelled using known characteristics of the sensors, platforms and their modes of operation (see Volume 2B—Section 2). Accurately associating each pixel in one image with its corresponding pixel in another image, or with precise locations on a map or on the ground, requires the development of specific registration models that associate different coordinate systems (see Volume 2B—Sections 1 and 3). Registration models are generally based on sets of ground control points from each image (see Volume 2B—Section 4).

A rectification procedure should allow model accuracy to be iteratively tested and improved before further processing (see Volume 2X—Appendices 7 and 8). Adequate coverage of accurately located control points is essential for precise registration of bi-temporal or multi-temporal images. Various algorithms are available for resampling an image to a different geometry (see Volume 2B—Section 5). This process involves estimating the expected value for some new pixel, with a known size and location, from the values of those original pixels that overlap and/or are adjacent to it. The two most commonly used resampling approaches are:

- nearest neighbour resampling—simply selects the values of the pixel in the original image which is closest to the resampled pixel location, so produces an image which only contains pixel values that exist in the original image. This method can lead to significant aliasing errors, however, so it is generally recommended that the nearest neighbour algorithm

be used to resample to a smaller pixel size than is finally required (such as half the final pixel size), then blocks of pixels in the resulting image can be combined to determine pixel values in the resampled image (see Volume 2B—Section 5.2).

- cubic convolution—assumes the original pixel values represent some underlying surface that can be modelled by a smooth, continuous function, and effectively uses this function to derive the new pixel value. Such assumptions may not be valid for EO data (especially when the image scale changes during resampling), and images produced by this method can appear to be smoothed relative to the original data (see Volume 2B—Section 5.4).

However, the image processing procedures used to correct geometric errors and create information products can also introduce image artefacts into the resampled image. For example, the term 'gridding' is used to define the process of allocating the original sensor observations to cells in a predefined image grid (Wolfe *et al*., 1998). The gridding algorithms used for MODIS products resample the acquired observations into a grid based on the Sinusoidal projection. Inevitably, to translate the original image pixels into the resampled grid cells introduces 'pixel shift', that is, each original pixel does not have the same spatial dimensions or alignment as its corresponding grid cell in the resampled image. The MODIS gridding algorithms have been shown to produce imagery in which the locations of the original imaged observations only overlap with the final grid cells by less than 30% (Tan *et al*., 2006). A metric called 'obscov' (Wolfe *et al*., 1998; Yang and Wolfe, 2001) was been developed to indicate the proportion of each observation that is derived from the area of its corresponding grid cell. Given the range of potential mismatches and misalignments between observations and grid cells, the obscov metric can vary significantly between adjacent grid cells. This metric is routinely included with the geolocation information in MODIS level 2 products and needs to be considered when MODIS pixels are being compared with field sites or other spatial datasets. Band-to-band registration of MODIS products can also be degraded by gridding algorithms, especially when comparing MODIS products acquired at different spatial resolutions (Tan *et al*., 2006).

3.1.1.2 Radiometric registration

As introduced in Volume 2A—Section 3.3.2, radiometric registration corrects for:

- known sensor errors;
- atmospheric conditions such as cloud, haze and rain;
- topographic shadowing; and
- variations caused by changing illumination and viewing positions (see Volume 2A—Section 3 and Volume 2X—Appendix 1; Paolini *et al*., 2006).

Absolute radiometric registation aims to create a set of images that appear to have been imaged by the same sensor with standardised illumination and atmospheric conditions (see Volume 2A). Such correction methods convert pixel digital values to radiance at the sensor before using atmospheric/bidirectional reflectance distribution function (BRDF) models to estimate surface reflectance(s) (see Volume 2X—Appendices 1 and 2 for model details). The presence of cloud, cloud shadow and snow in imagery is commonly detected and corrected using the Fmask algorithm (Zhu and Woodcock, 2012, 2014; Zhu *et al*., 2015).

Relative radiometric registration of bi-temporal image pairs can be achieved by matching recorded channel radiance values for common features. A simple approach cross-calibrates and rescales channel histograms using crossplots of paired channels in each image (see Volume 2A—Section 8.1.3). This effectively fits a regression line through the crossplot, which can be used to derive an equation to convert channel values from one image to equivalent values in the other (see Volume 2C—Section 7.2). All regression-based techniques effectively assume values in paired channels can be related via a linear, or affine, transformation (see Volume 2C—Section 7).

3.1.2 Local effects or 'noise'

In contrast to the low frequency systematic effects, which make it difficult to compare pixel attributes in different parts of the image, there are often very local effects (or image 'noise'), which can make it difficult to compare the attributes of a pixel with those of its neighbour. Some of these effects are due to scaling issues (see Volume 1B—Section 2.3) and represent variations introduced into the image by spatial variation at a sub-pixel level. Sub-pixel effects may be considered either as useful data or 'noise'. In image classification, sub-pixel effects are generally assumed to represent noise, although once classes are formed the sub-pixel effects within the class may be investigated for their data (see Volume 2E). Uncorrelated variance at the pixel scale can also be introduced by physical processes operating in the atmosphere and land surface system, or in the process of imaging.

Just as "one man's meat is another man's poison" however, it is worth asking the question "What is noise?" in the context of any given analysis. For example, seasonal variations in a dynamic system may be considered as noise when the purpose of an analysis is to detect longer term changes in the system, but as information when season-to-season changes are being observed (see Section 2).

Whether uncorrelated variation, or variation with a very local range of autocorrelation, should be 'removed' will depend on the purpose of the analysis. When the data are to be 'cleaned', spatial filtering, adaptive filtering and thresholded 'despiking' can be used to reduce or remove high frequency variance from an image (see Volume 2C). In image classification, if the data are not modified prior to the generation of image classes, the effect of noise is often to create variation from pixel to pixel in any derived classification resulting in heterogeneous classes or small 'noise' classes. The spatial variance can sometimes be removed (or reduced) after image classification by filtering as described in Volume 2E.

3.2 Analysis Ready Data

Analysis Ready Data (ARD) was introduced in Volume 2A—Section 7.4. CEOS (2016) defines ARD for land (CARD4L) as: "*... satellite data that have been processed to a minimum set of requirements and organized into a form that allows immediate analysis with a minimum of additional user effort and interoperability both through time and with other datasets*".

In parallel with the growing volumes of EO time series data, there is an urgent need for efficient mechanisms to access and process these datasets. The potential of these already enormous archives can only be realised by appropriate organisational structures and analytical tools, to identify spatial and temporal patterns embedded in the imagery, and extract correlations with other biophysical parameters. The first step in this process is to remove the need for traditional image-by-image calibration to correct for geometric and radiometric distortions.

The traditional approach to calibration of EO imagery is outlined in Section 3.1. ARD, however, allows users to analyse different data sources at different resolutions and in differerent projections without this laborious pre-processing. The essential elements of ARD include:

- efficient data storage structures—to organise data for easy and rapid access;
- high-performance computing—to analyse data remotely;
- grid-based data format where pixels and locations are directly comparable—data-agnostic approach to storage and analysis;
- resampling and reprojection of spatial data 'on the fly';
- pixel values calibrated to surface reflectance and directly comparable;
- remote storage of data to avoid downloading large volumes for analyses; and
- quality assessment and provenance tracking for each pixel (Lewis *et al.*, 2017).

A CEOS Virtual Constellation is a set of space and ground segment capabilities operating together in a coordinated manner, in effect a virtual system that overlaps in coverage in order to meet a combined and common set of Earth observation requirements.
(CEOS, 2013)

A natural progression of analytical tools will involve deep learning (machine learning) techniques and high-dimensional statistical analyis to manipulate EO datasets. For example, Digital Earth Australia (DEA—detailed in Section 11.2) is a 'big data' platform that integrates a range of Australian geospatial datasets, including Australian EO time series datasets. Preparation and management of these time series datasets involve many stages of data processing and verification. To guarantee the veracity of this product, sophisticated protocols are required in three key areas:

- accurate spatial alignment of pixels—to be certain that they can be 'stacked' as time series observations;
- pixel values presented as normalised surface reflectance measurements—to ensure that they are comparable across the continent and through time; and
- dependable assessment of quality for each pixel—delivered as pixel quality flags and dataset metadata, which traces the provenance of each pixel (see Volume 2A—Section 1), so that users can decide which observations are suitable for particular uses (Lewis *et al*., 2017).

These protocols are detailed for one DEA dataset, the Land Surface Reflectance[2] product suite, in Excursus 11.1.

An extension to ARD sourced from a single sensor series (such as Landsat TM/ETM+/OLI) is to integrate imagery from different sensors into a single, consistent time series. The major advantage of such integration is to create a seamless time series populated with more frequent imagery. In this context, 'seamless' implies a smooth time series, with minimal temporal noise resulting from sensor-to-sensor difference, which accurately measures surface conditions (Claverie *et al*., 2018). More frequent temporal coverage is important for many applications, especially disaster management, water quality and phenological studies (Li and Roy, 2017; see Volume 3).

The Harmonized Landsat and Sentinel-2 (HLS) surface reflectance dataset (Claverie *et al*., 2018) is the first, publicly-available, multisensor ARD product. Helder *et al*. (2018) define 'harmonised' in this context to mean "that sensor-specific radiometric and geometric differences are adjusted and removed, such that it should be transparent to end users which sensor originated any specific reflectance observation within an HLS time series". This NASA initiative is designed to create a Virtual Constellation (VC) of the surface reflectance data acquired by Landsat's Operational Land Imager (OLI) and Sentinel's Multi-Spectral Imager (MSI). Since Landsat OLI and Sentinel-2 MSI both observe the Earth from a sun-synchronous orbit at a similar time of day using similar spectral, spatial and angular dimensions, they present an ideal pair of datasets for a multisensor ARD product. A VC has been defined as '*a coordinated set of space and/or ground segment capabilities from different partners that focuses on observing a particular parameter or set of parameters of the Earth system*' (CEOS, 2019). Claverie *et al*. (2018) describe harmonised products in terms of the following characteristics:

- "gridded to a common pixel resolution, map projection and spatial extent;
- atmospherically corrected and cloud masked to surface reflectance using a common radiative transfer algorithm;
- normalised to a common nadir view geometry via BRDF estimation; and
- adjusted to represent the response from common spectral band passes".

The additional characteristic when integrating imagery acquired by different sensors, compared with a single sensor, is the need to account for any differences in the sensors' spectral resolutions, densities and extents (see processing step 4 in Table 3.1). In this case, for the spectral bands common to both sensors, the radiometry of the finer resolution MSI data is adjusted to match the bandpasses of OLI. Some of the challenges being faced to calibrate and validate this product are reviewed by Helder *et al*. (2018).

Applications of the HLS product thus far are many and varied, including monitoring aquatic systems (Pahlevan *et al*., 2019), crop type inventories and projections (Torbick *et al*., 2018), and crop and land cover mapping (Griffiths *et al*., 2019). Composite imagery derived from multisensor ARD sources is described in Section 10.2.

2 Formerly referenced as the Australian Reflectance Grid (ARG)

Table 3.1 HLS processing overview

Processing stage		Sentinel-2 processing		Landsat-8 processing
Input		Sentinel-2 MSI (L1C)	Sentinel-2 MSI (L1C)	Landsat-8 OLI (L1T)
Processing step	1. Atmospheric correction (based on Landsat-8 Surface Reflectance Code (LaSRC) approach; Vermote *et al.*, 2016) and cloud masking (LaSRC output with Fmask algorithm; Zhu and Woodcock, 2012, 2014; Zhu *et al.*, 2015)	✓	✓	✓
	2. Geometric resampling and geographic registration to Sentinel-2 UTM tiling system at 30 m spatial resolution (Helder *et al.*, 2018)	✓	✓	✓
	3. BRDF adjustment to nadir view angle and constant solar elevation (Roy *et al.*, 2016, 2017)	×	✓	✓
	4. Band pass adjustment using a spectral band adjustment factor (Chander *et al.*, 2010; Helder et al., 2018; Barsi *et al.*, 2018)	×	✓	×
Output		S10 (MSI SR 10 m)	S30 (MSI NBAR 30 m)	L30 (OLI NBAR 30 m)

Source: Claverie *et al.* (2018) Figure 1

3.3 Ancillary data

In this context, ancillary data refers to any datasets that are not derived from EO. While processing of EO imagery is primarily based on image data, it is often useful (and sometimes necessary) to integrate data from different sources with the image data prior to further processing. This is especially true for other information, such as soil type, which cannot necessarily be inferred from the EO image, or topographic information, which is unlikely to change over time. The process of integrating the different data types involves bringing the geometry and scale of the non-image data sources to the geometry and scale of the image, and potentially integrating the data as additional image channels.

3.3.1 Provenance and caveats

The inherent framework that encapsulates EO data analyses is particularly relevant when using other data sources in conjunction with EO datasets (see Section 1). Familiarity with both datasets—their provenance and goals, and their limitations—is an important prerequisite to their successful integration.

Firstly, EO datasets comprise indirect observations (see Section 1.1). With appropriate processing (see Section 2.3) these observations can be treated as measurements. This distinction is critical for selecting ancillary data to calibrate or validate EO products (see Section 3.1).

Secondly, the ancillary data needs to be relevant to the EO dataset in terms of representing similar surface target features. The extent to which ancillary data must represent similar intrinsic attributes of the target will depend the type of analysis being undertaken. For example, to assess the accuracy of an image classification exercise, the classes could be presented as a set of labels describing the expected land cover categories at specific locations (see Volume 2E), whereas to validate a spectral index derived from EO data would require more detailed biophysical information (see Volumes 2C and 3A).

Finally, the importance of scale in all four dimensions of EO datasets needs to be considered when ancillary data sources are being integrated (see Section 2.1):

- spectral—are the wavelengths observed in the EO dataset relevant to the ancillary data?
- spatial—can the ancillary data be accurately located in the EO dataset?
- radiometric—is the level of differentiation between image values appropriate for the ancillary data?
- temporal—does the timing of acquisition for the EO dataset correspond to the currency of the ancillary data?

Potential sources of ancillary data that can be integrated with EO datasets, and considerations about their suitability, are further addressed in Sections 12 and 13.

3.3.2 Data formats

Ancillary data sources may be available in either raster (grid-based) or vector (point-based) formats. While image datasets, by definiton, are stored and processed in raster format (albeit sometimes using compression algorithms for storage and processing efficency; see Volume 2A—Section 1.3), vector data is stored as coordinate strings. In both data formats, target features can be described in terms of:

- points—specific locations defined by coordinates;
- lines—a straight line between two points, or a series of straight lines interpolated between consecutive points to form a string; or
- areas—rectangular boxes or polygons (see Figure 3.1).

Algorithms to convert vector to raster format are commonly available in image processing and Geographic Information Systems (GIS; see Section 13.1).

Figure 3.1 Five basic types of patches

In image formats, the precison of data points is limited by the size of each pixel, whereas in vector formats, data points are defined as map coordinates (relative or absolute) so can be precisely represent a given ground location

a. Point

single pixel recorded by column and row (referred to as pixel and line) position in the image

b. Line

straight line interpolated between any two points

c. Box

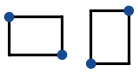

rectangle interpolated between two diagonally opposite corner points

d. String

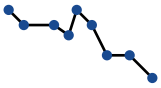

series of straight lines interpolated between pairs of adjacent, irregularly spaced points to form a ragged line

e. Polygon

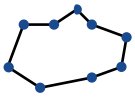

closed string which outlines a single region

Source: Harrison and Jupp (1995) Figure 45

Vector data can be used to spatially stratify an image to allow different parts of the image to be processed independently (see Section 4.1.2). Vector data from other sources, such as GIS, can be converted to a compatible format and rescaled to match the image coordinate system. Such data can then be used as patches, or referenced in categories, to stratify an image. Non-EO based spatial data, in vector or raster formats, can also be used to segment an image into multiple zones or classes. For example, patches or categories can be used to create a channel in which each pixel is given the value associated with the patch or category that it satisfies (see Volume 2E). This process allows vector data, derived independently of the image, to be represented in raster format and registered with the image. Ancillary data which is available in raster format can also be registered to the image geometry using a standard resampling process (see Section 3.1.1.1 and Volume 2B—Section 5).

A third data format, Triangular Irregular Networks (TIN), is sometimes used as an efficient method for recording elevations at defined locations. The density of surveying points can vary with relief so this approach means that the elevation at each location can be recorded precisely. To construct a Digital Elevation Model (DEM) from TIN data uses triangles between the each set of three closest points (or nodes), with the condition that the triangles do not intersect each other (see Section 13.2). Each triangle then represents a terrain surface (or facet) with uniform slope and aspect. An indexing system is required by the TIN data format to connect neighbouring points recursively (Bolstad, 2008).

3.4 Further Information

Analysis Ready Data:

Committee on Earth Observation Satellites (CEOS): *http://ceos.org/ard/*

Digital Earth Australia (DEA): *https://www.ga.gov.au/dea/products*

USGS:

US Analysis Ready Data (ARD): *https://www.usgs.gov/land-resources/nli/landsat/us-landsat-analysis-ready-data?qt-science_support_page_related_con=0#qt-science_support_page_related_con*

3.5 References

Barsi, J.A., Alhammoud, B., Czapla-Myers, J., Gascon, F., Haque, M.O., Kaewmanee, M., Leigh, L., and Markham, B.L. (2018). Sentinel-2A MSI and Landsat-8 OLI radiometric cross comparison over desert sites. *European Journal of Remote Sensing*, 51(1), 822–837. *https://doi.org/10.1080/22797254.2018.1507613*

Bolstad, P. (2008). *GIS Fundamentals: A First Text on Geographic Information Systems*. 3rd Edn. Elder Press, White Bear Lake, Minnesota. ISBN 978-0-9717647-2-9

CEOS (2016). *CEOS Analysis Ready Data* webpage, Committee on Earth Observation Satellites website: *http://ceos.org/ard/*

CEOS (2019). *Virtual Constellations* webpage, Committee on Earth Observation Satellites website: *http://ceos.org/ourwork/virtual-constellations/*

Chander, G., Mishra, N., Helder, D.L., Aaron, D., Choi, T., Angal, A., and Xiong, X. (2010). Use of EO-1 Hyperion data to calculate spectral band adjustment factors (SBAF) between the L7 ETM+ and Terra MODIS sensors. *Proceedings of the 2010 IEEE International Geoscience and Remote Sensing Symposium*, Honolulu, HI, USA, 25–30 July. IEEE, Piscataway, NJ, USA. pp. 1667–1670.

Claverie, M., Ju, J., Masek, J.G., Dungan, J.L., Vermote, E.F., Roger, J.-C., Skakun, S.V., and Justice, C. (2018). The Harmonised Landsat and Sentinel-2 surface reflectance data set. *Remote Sensing of Environment*, 219, 145–161. *https://doi.org/10.1016/j.rse.2018.09.002*

Griffiths, P., Nendel, C., and Hostert, P. (2019). Intra-annual reflectance composites from Sentinel-2 and Landsat for national-scale crop and land cover mapping. *Remote Sensing of Environment*, 220, 135–151. *https://doi.org/10.1016/j.rse.2018.10.031*

Harrison, B.A., and Jupp, D.L.B. (1995). *Image Classification and Analysis: Part THREE of the microBRIAN Resource Manual*. MPA, Melbourne.

Helder, D., Markham, B., Morfitt, R., Storey, J. Barsi, J., Gascon, F., Clerc, S., LaFrance, B., Masek, J., Roy, D. (2018). Observations and recommendations for the calibration of Landsat 8 OLI and Sentinel 2 MSI for improved data interoperability. *Remote Sensing*, 10, 1340. *https://doi.org/10.3390/rs10091340*

Lewis, A., Oliver, S., Lymburner, L., Evans, B., Wyborn, L., Mueller, N., Raevksi, G., Hooke, J., Woodcock, R., Sixsmith, J., Wu, W., Tan, P., Li, F., Killough, B., Minchin, S., Roberts, D., Ayers, D., Bala, B., Dwyer, J., Dekker, A., Dhu, T., Hicks, A., Ip, A., Purss, M., Richards, C., Sagar, S., Trenham, C., Wang, P., and Wang, L.-W. (2017). The Australian Geoscience Data Cube— Foundations and lessons learned. *Remote Sensing of Environment*, 202, 276–292. *https://doi.org/10.1016/j.rse.2017.03.015*

Li, J., and Roy, D.P. (2017). A Global Analysis of Sentinel-2A, Sentinel-2B and Landsat-8 Data Revisit Intervals and Implications for Terrestrial Monitoring. *Remote Sensing*, 9, 902. *https://doi.org/10.3390/rs9090902*

Paolini, L., Grings, F., Sobrino, J.A., Jiménez Muñoz, J.C., and Karszenbaum, H. (2006). Radiometric correction effects in Landsat multi-date/multi-sensor change detection studies. *International Journal of Remote Sensing*, 27(4), 684–704. *https://doi.org/10.1080/01431160500183057*

Pahlevan, N., Chittimalli, S.K., Balasubramanian, S.V., and Vellucci, V. (2019). Sentinel-2/Landsat-8 product consistency and implications for monitoring aquatic systems. *Remote Sensing of Environment*, 220, 19–29. *https://doi.org/10.1016/j.rse.2018.10.027*

Roy, D.P., Zhang, H.K., Ju, J., Gomez-Dans, J.L., Lewis, P.E., Schaaf, C.B., Sun, Q., Li, J., Huang, H., and Kovalskyy, V. (2016). A general method to normalize Landsat reflectance data to nadir BRDF adjusted reflectance. *Remote Sensing of Environment*, 176, 255–271.

Roy, D.P., Li, J., Zhang, H.K., Yan, L., Huang, H., and Li, Z. (2017). Examination of Sentinel-2A multi-spectral instrument (MSI) reflectance anisotropy and the suitability of a general method to normalize MSI reflectance to nadir BRDF adjusted reflectance. *Remote Sensing of Environment*, 199, 25–38.

Tan, B., Woodcock, C.E., Hu, J., Zhang, P., Ozdogan, M., Huang, D., Yang, W., Knyazikhin, Y., and Myneni, R.B. (2006). The impact of gridding artifacts on the local spatial properties of MODIS data: Implications for validation, compositing, and band-to-band registration across resolutions, *Remote Sensing Environment*, 105, 98–114.

Torbick, N., Huang, X., Ziniti, B., Johnson, D., Masek, J., and Reba, M. (2018). Fusion of Moderate Resolution Earth Observations for Operational Crop Type Mapping. *Remote Sensing*, 10, 1058. *https://doi.org/10.3390/rs10071058*

Vermote, E., Justice, C., Claverie, M., and Franch, B. (2016). Preliminary analysis of the performance of the Landsat 8/OLI land surface reflectance product. *Remote Sensing of Environment*, 185, 46–56.

Wolfe, R.E., Roy, D.P., and Vermote, E. (1998). MODIS land data storage, gridding, and compositing methodology: Level 2 grid. *IEEE Transactions on Geoscience and Remote Sensing*, 36, 1324–1338.

Yang, K., and Wolfe, R.E. (2001). MODIS level 2 grid with the ISIN map projection. *Proceedings of IGARSS 2001, 9–13 July, Sydney*, pp. 3291–3293. *https://doi.org/10.1109/IGARSS.2001.978332*

Zhu, Z., and Woodcock, C.E. (2012). Object-based cloud and cloud shadow detection in Landsat imagery. *Remote Sensing of Environment*, 118, 83–94. *https://doi.org/10.1016/j.rse.2011.10.028*

Zhu, Z., and Woodcock, C.E. (2014). Automated cloud, cloud shadow, and snow detection in multitemporal Landsat data: An algorithm designed specifically for monitoring land cover change. *Remote Sensing of Environment*, 152, 217–234. *https://doi.org/10.1016/j.rse.2014.06.012*

Zhu, Z., Wang, S., and Woodcock, C.E. (2015). Improvements and expansion of the Fmask algorithm: cloud, cloud shadow, and snow detection for Landsats 4–7, 8 and Sentinel 2 imags. *Remote Sensing of Environment*, 159, 269–277. *https://doi.org/10.1016/j.rse.2014.12.014*

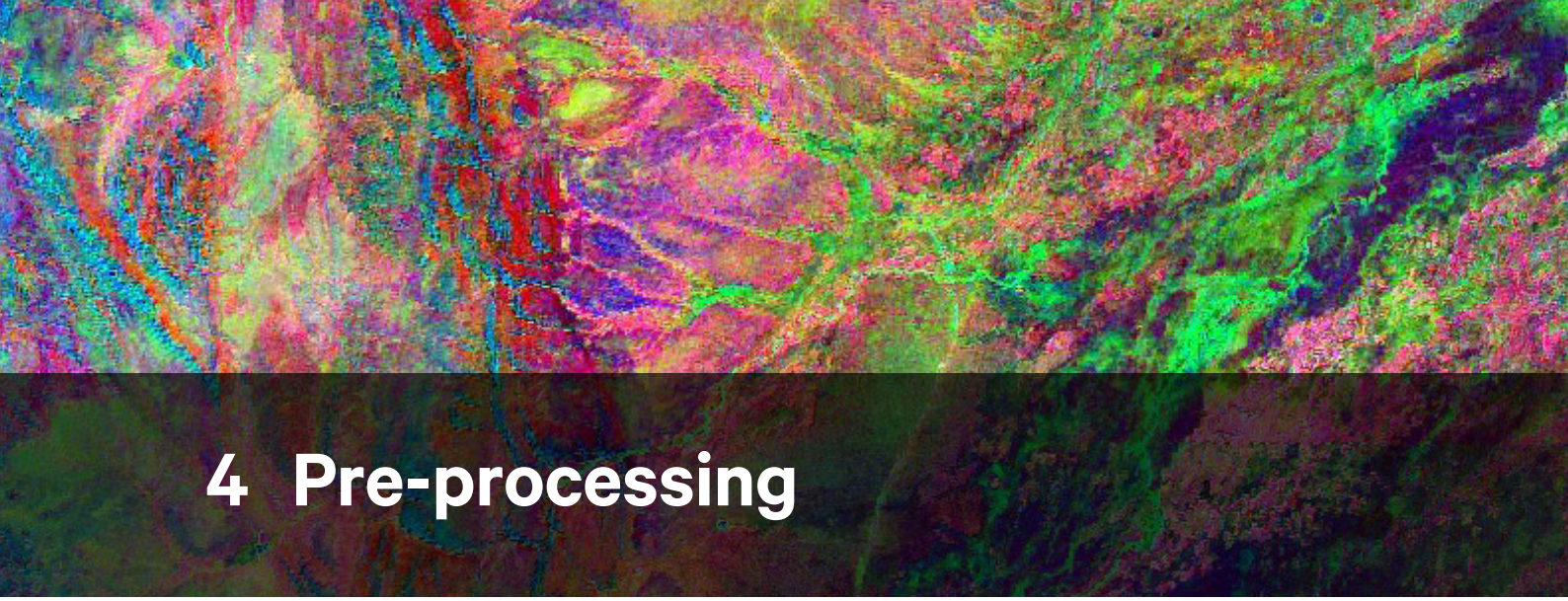

4 Pre-processing

In addition to the image calibration processes recommended in Section 3.1, selected pre-processing of input images may be beneficial for bi-temporal and multi-temporal analyses. In this context, pre-processing refers to operations that prepare or modify an image for integration with other EO imagery and/or ancillary data. These operations can enhance certain features, develop new channels for specific tasks, reduce data volume, reduce noise, or remove features that are not of direct interest to a particular analysis.

Where image integration involves either two or more images with different spatial resolutions, or ancillary data with differing spatial resolution to the EO image dataset(s), changes to the pixel resolution in one or both images may be required in addition to geometric correction (see Section 3.1.1.1). The spatial implications of these upscaling or downscaling operations are introduced in Volume 1B—Section 2.

In this section, we will consider potential pre-processing methods in terms of:

- stratifying images to remove unwanted pixels (see Section 4.1);
- reducing data volume (see Section 4.2); and
- upscaling and downscaling (see Section 4.3).

4.1 Stratifying images

An image may contain features or regions that are not of interest to, or may disturb the statistics for, a particular study. Any unnecessary components in an image can be 'removed' before data integration to save computational time or avoid inaccurate statistics. Pixels may be 'removed' by setting their values to the null value (often reserved as the highest or lowest value in the data range) in selected channels. An alternative to embedding the null value would be to create an additional channel, usually referred to as a mask channel, in which the 'removed' pixels are set to a pre-defined (often binary) value.

An image may be stratified into regions by using spatial boundaries (defined interactively on a displayed image or from registered ancillary data) or by using spectral characteristics of different image features. Here, stratification refers to a binary, or two-state, decision: pixels either do or do not belong to some pre-defined spatial layer, whereas segmentation generally involves sub-dividing an image into more than two segments, that is pixels can belong to one of several layers (see Volume 2A—Section 10).

4.1.1 Spectral

Different image features are considered to be spectrally separable when they have distinctly different values in one or more attributes. In this case, ranges of values, or spectral categories, may be used to identify all pixels belonging to a particular feature. Training patches which represent a particular feature may be used to define these ranges (see Volumes 2A and 2E). When the statistics of one or more patches satisfactorily map the feature of interest, their spectral ranges can be represented as one or more categories (see Volume 2A—Section 9). The spectral stratification process then involves identifying those pixels whose attribute values satisfy these categories. Spectral stratification has been used to successfully remove 'unwanted' pixels from an image prior to further processing, such as water from an analysis of land features, land from a water-oriented analysis, or clouds and possibly cloud shadows from a ground-based study.

Background image: Principal Components transformation of Landsat TM image over Fowlers Gap Research Station, NSW, acquired in January 1993. PC1, PC2 and PC3 are shown as RGB. **Source:** Megan Lewis, University of Adelaide

A procedure for developing logical categories to map specific features is outlined in Volume 2E. It is important that any categories being used for stratification should cleanly include or exclude the feature(s) to be removed, since it is usually preferable to leave some irrelevant data in the image rather than remove some relevant pixels. The image attributes used to develop the stratification mask need not be the same ones used for subsequent process (provided they register precisely, in terms of image geometry), since a category can be defined using one set of attributes or channels and then used to stratify a different set.

4.1.2 Spatial

The spatial stratification process involves identifying those pixels that are located in pre-defined regions in the image. Region boundaries can be defined by image patterns, or by registering vector format data from some other spatial data set, such as a GIS.

Boundaries that are clearly visible in an image may be delineated interactively on a displayed image using the screen cursor (see Volume 2E). Examples of such boundaries are irrigation channels, which define the limits of irrigated crops in a particular image, or major roads or rivers, which may define cadastral boundaries. If necessary, edge enhancement techniques (see Volume 2C—Section 5.2) may be applied to the image prior to screen digitising.

Ancillary data may also be used to stratify the image where the boundary of a study area is not sufficiently visible to allow screen digitising (see Section 3.3). For example, cadastral or other boundaries may define the limits of a study area. Using non-image boundaries may involve registering and integrating the ancillary data (usually in vector format) with the image before stratification (see Volume 2A—Section 10).

4.2 Reducing data volume

Some pre-processing operations have the advantage of representing essential image data in a smaller data volume. For example, spectral indices can condense relevant image data into fewer channels to simplify subsequent image processing tasks (see Section 4.2.1). Selected linear pre-processing operations (such as Principal Component Analysis, PCA; see Section 7.2 and Volume 2A) can re-orient the image data space to both distinguish specific features and reduce data volume (see Section 4.2.2).

While reducing data volume is often useful for simplifying image processing operations, when appropriately implemented it can introduce valuable focus into the overall image analysis methodology. Methods for 'feature selection', to highlight the most informative image bands for classification, are introduced in Volume 2A—Section 9.1.3.1. Such methods and their rationale are further detailed in the context of understanding data dimensionality in Volume 2E.

Where appropriate, image data volume can also be reduced by changing the pixel 'bit depth' (see Volume 2A—Section 1.2). For example, when is no advantage in storing data with the precision of floating point, integer format would result in a smaller file size.

4.2.1 Spectral indices

Ratios of selected channels are useful for enhancing particular features, such as those used for mineralogy, or removing atmospheric or topographic effects. Various transformations may be suitable for this purpose as detailed in Volumes 2C and 3A, although vegetation indices are the most commonly used (Thonfeld *et al.*, 2010).

Spectral indices may also simplify change detection exercises (see Section 7). When appropriate to the change being observed, such indices both highlight selected features and reduce data volume. They also allow images acquired by different sensors to be compared more easily when slightly different spectral wavelengths are measured by corresponding image channels. For example, it is more reliable to compare NDVI (Normalised Difference Vegetation Index) channels computed from imagery acquired by different sensors (such as MODIS and AVHRR) than to compare image values in their red and NIR channels. For hyperspectral images, a very wide range of indices has been developed (Roberts *et al.*, 2011; Sonobe and Wang, 2017; Thenkabail *et al.*, 2018). In these data-rich images, selection of the optimal indices, ratios or channels simplifies subsequent image processing steps.

4.2.2 Linear Transformations

Linear transformations allow rotation, rescaling, skewing and/or reflection of the image data space (see Volumes 2C and 2X). The original channel axes in an image can be rotated to align with some other direction in the data. Principal Component Analysis (PCA) is a special type of affine transformation that uses the image variance to define a rotation in which the first principal component (PC1) axis is aligned with the direction of greatest variance in the *n*-dimensional data space (where *n* is the number of channels in the image) and each higher numbered axis is orthogonal to (or uncorrelated with) the previous one (see Figure 4.1). The uncorrelated nature of the PC channels is often as (or more) important than their alignment. The PCA transformation is typically computed from the image covariance matrix, but the correlation matrix can also be used to derive 'standardised PCs' (Singh and Harrison, 1985; see Volume 2C for details).

Since the most 'significant' information contained in the image is summarised in the highest PCs, it is sometimes advantageous, in terms of reducing data volume, to compute a PCA transformation prior to integrating an image and use only the highest PCs for subsequent processing.

PCA transformations can be especially useful for comparing images of different dates as discussed in Section 7.2. However, since PCA is a scene-dependent transformation, significant misregistration errors between a pair of images would increase the variation between channel pairs from different images and consequently inflate the covariance statistics. This bias may result in misregistered features being isolated as an individual PC and could mask actual changes. Therefore image pairs should be carefully registered geometrically before applying PCA (see Section 3.1.1.1).

A PCA transformation can also be computed for specific features in the image. A training region encompassing the feature, or a logical category which spectrally describes it, can be used to derive a covariance matrix for a PCA. For example, if a study is particularly interested in forests, the covariance matrix from a forested area could be used to produce a PCA transformation which would optimally separate the variation contained in the forest vegetation type (see Volume 2C).

The value of using transformations which reduce the 'dimensionality' of an image (that is, the number of independent attributes used to describe a pixel) is further discussed in Volume 2E. Methods for optimum feature selection are also described in Volume 2E.

Figure 4.1 Principal Component Analysis

a. Image data values can be redefined relative to modified position and scaling of axes.

b. The PCA transformation defines a new primary data axis (PC1) in the direction of maximum image variance (over all image channels), then other axes are defined to be orthogonal to this direction.

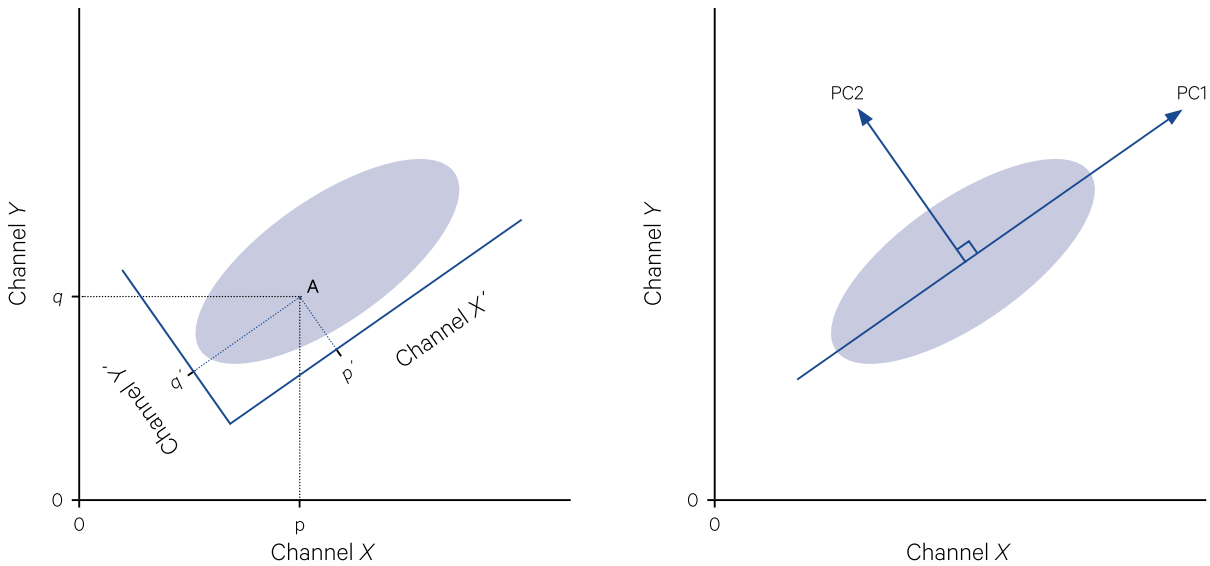

Source: Harrison and Jupp (1990) Figures 87 and 88

4.3 Upscaling and Downscaling

As introduced Volume 1B—Section 2.4, and reviewed in Section 1.4 above, the terms upscaling and downscaling derive from cartographical scale, to indicate the processes of changing from:

- a finer scale to a coarser scale—upscaling (such as from 1:10,000 to 1:100,000); and
- a coarser scale to a finer scale—downscaling (such as from 1:100,000 to 1:10,000).

When a higher resolution dataset (from EO or ancillary data source) is being integrated with a lower resolution dataset, there are essentially three options to reconcile their scales:

- upscale the higher resolution dataset to match the spatial scale (pixel size) of the lower resolution dataset (see Section 4.3.1);
- downscale the lower resolution dataset to match the spatial scale (pixel size) of the higher resolution dataset (see Section 4.3.2); or
- convert the spatial scale of both datasets to a common pixel size (see Section 4.3.3).

As introduced in Volume 2C, filtering techniques allow the values of each pixel to be modified by the values of its neighbouring pixels. These techniques are often used to remove spatial noise and undesirable spatial variation in an image, or enhance regions of contrast such as edges. Image smoothing produces a more spatially coherent image at the expense of 'blurring' spatially detailed image features. In this context, depending on the 'natural' scale of ground target features (see Section 1), image smoothing may be appropriate in conjunction with image upscaling or downscaling.

4.3.1 Upscaling to a larger pixel size

When applied to EO data, upscaling creates larger pixels, that is, ones that cover a larger ground area. This operation reduces the sample density in the higher resolution image to match the sample density in the lower resolution image. Computationally, upscaling typically involves:

- blocking or aggregation of the pixels in the higher resolution image to effectively create larger ones with a larger pixel size that matches those in the lower resolution image (see Figure 4.2a). This process may introduce blurring (see Volume 2A—Section 7.2);
- sub-sampling of pixels in the higher resolution so that the selected pixels in the input image are assumed to represent a larger ground area, and effectively matching the pixel size in the lower resolution image (see Figure 4.2b). This process may introduce aliasing (see Volume 1B—Section 2.2); or
- resampling pixels in the higher resolution image to match the pixel size in the lower resolution image (see Volume 2B—Section 5).

Figure 4.2 Upscaling operations

a. Blocking: a higher resolution image channel image is blocked using a 2x3 blocking factor to produce lower resolution image.

a	b	5	6	7	6	6	5	4	3
c	d	4	5	6	6	5	5	5	4
e	f	3	7	6	7	6	5	6	7
3	4	4	5	5	7	7	6	6	7
4	4	4	4	5	6	6	7	7	7
5	5	4	5	6	6	5	6	6	5
5	4	4	4	5	6	7	8	4	3
4	3	3	4	5	7	9	6	2	1
4	2	3	8	7	9	9	7	3	1
2	3	3	9	9	8	7	6	2	2

where (a+b+c+d+e+f)/6 = A

A	5	6	5	5
4	4	6	6	6
4	4	7	8	2

b. Sub-sampling: a higher resolution image is sub-sampled to simulate a lower resolution image by dropping alternate pixels and lines.

Input image pixel size = 20 m

a	b	c	d	e	f	g	h
i	j	k	l	m	n	o	p
q	r	s	t	u	v	w	x
y	z	A	B	C	D	E	F
G	H	I	J	K	L	M	N
O	P	Q	R	S	T	U	V
W	X	Y	Z	1	2	3	4
5	6	7	8	9	10	11	12

Output image pixel size = 40 m

a	c	e	g
q	s	u	w
G	I	K	M
W	Y	1	3

Source: Harrison and Jupp (1990) Figures 18 and 19

Figure 4.3 Upscaling by picking and binning approach

a. The underlying pixel grid of the lower resolution image is sub-divided to represent each pixel as four locations.

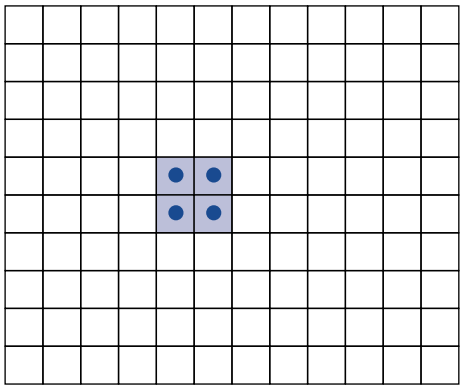

b. Higher resolution image grid showing location of the sub-divided pixel in the lower resolution image.

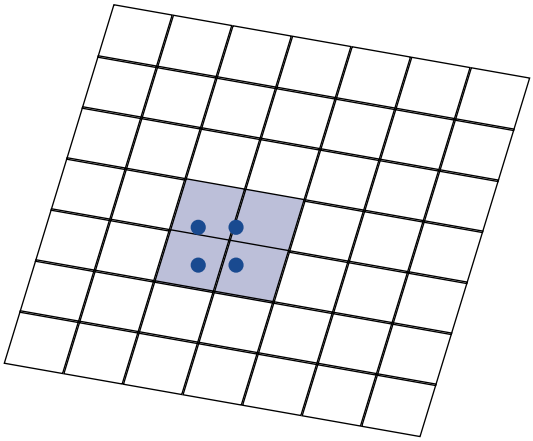

c. The pixel values in the higher resolution image at the four locations in Figure 4.3b are averaged to compute the upscaled pixel value.

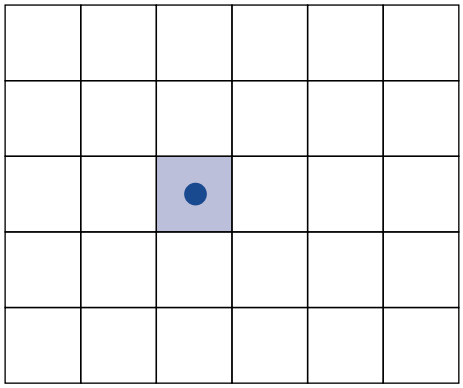

Source: Harrison and Jupp (1992) Figure 43

As illustrated in Figure 4.2, the blocking operation generally averages the relevant input image values to create a single output pixel in the upscaled image, whereas sub-sampling selects one of the relevant input image values as the output value (see Volume 2A—Section 7.2.1.3). Both of these operations compromise the spatial detail represented in the higher resolution image.

Image resampling algorithms are detailed in Volume 2B—Section 5. These methods interpolate the pixel values in the higher resolution image to simulate a pixel size that matches the lower resolution image. For example, the picking and binning approach to resampling (see Figure 4.3) provides better estimates of the upscaled pixel values than blocking alone. As detailed in Volume 2B, it also provides a better estimate for representing vector data in raster format (see Figure 4.4).

Figure 4.4 Vector to raster conversion

When vector data is represented in raster format, a finer pixel mesh renders better estimates of the original vector boundaries than a coarser mesh. Subpixels then allow the 'correct' pixel aggregate (or area average) solution.

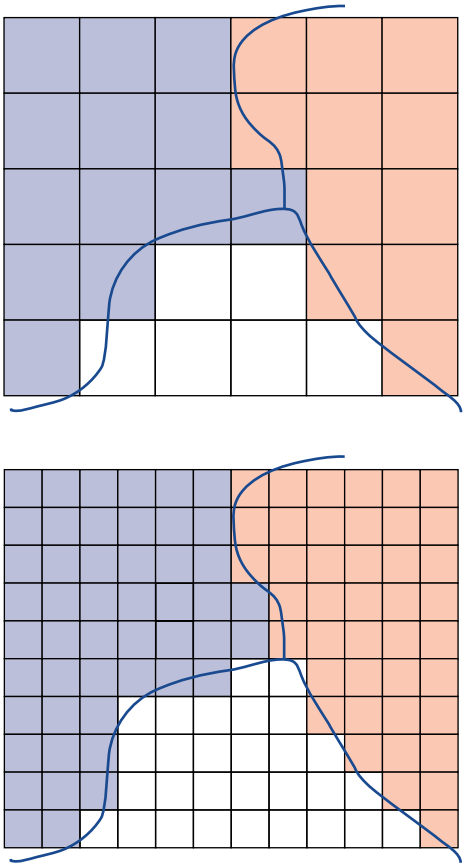

Figure 4.5 Bilinear interpolation

a. Example of unweighted interpolation, where the value of the output pixel is computed as the average value of the four closest input pixels: 135 = (200+150+90+100)/4

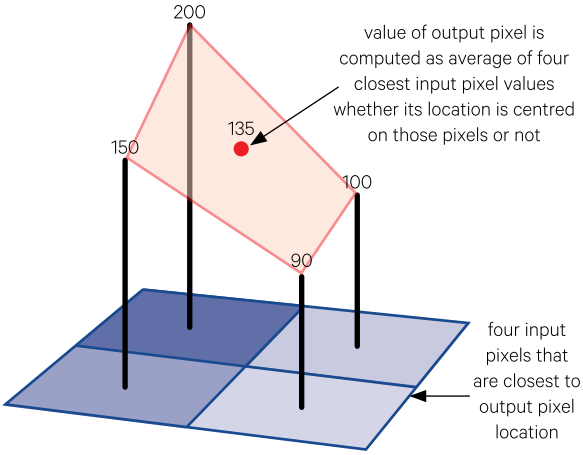

b. To determine the interpolation weights to use for each output pixel, bilinear interpolation computes the proportional spacing from the four input pixels that are its closest neighbours.

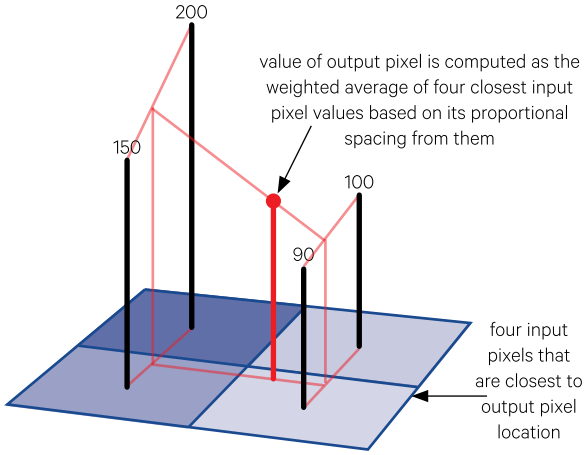

Bilinear and cubic convolution resampling can also be used to interpolate values from the spatial scale of the higher resolution image to the lower resolution image (see Figure 4.5 and Figure 4.6). Cubic convolution is the favoured resampling method for EO datasets (see Volume 2B—Section 5.4).

Image resampling attempts to consider the underlying spatial distribution of pixel values, so generally results in more continuous image values in the output image than blocking or sub-sampling. When the spatial detail of the original image values is retained (as occurs with selected compression and reconstruction algorithms), the upscaled image could be subsequently downscaled perfectly.

Figure 4.6 Cubic convolution interpolation

The method is commonly implemented by fitting four individual cubic polynomials to the four lines of pixels surrounding the output pixel. A fifth polynomial is then fitted across these four these four functions and through the output pixel location.

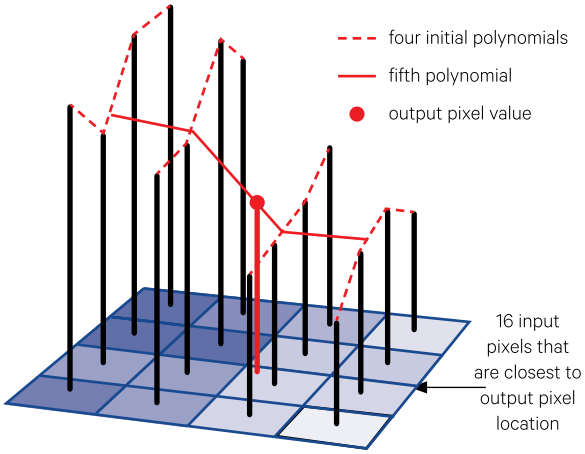

Scaling literally means to reduce or increase in size.
(Gallant et al., 2008)

4.3.2 Downscaling to a smaller pixel size

Since downscaling results in smaller pixels that cover a smaller ground area, the sample density of the image increases. This process can be likened to the display function of zooming in (see Volume 2A). Downscaling can be implemented by:

- enlarging the input image pixels, so that each input pixel becomes multiple pixels in the output image (see Figure 4.7); or
- interpolating the pixel values to create pseudo measurements positioned between the original ones using resampling methods (see Volume 2B—Section 5).

The process to enlarge input image pixels using pixel duplication is described in Volume 2A—Section 7.2.1.4. This process clearly misrepresents the spatial transitions between pixel values in the downscaled image, but offers an expedient method for representing the lower resolution image at the scale of the higher resolution image.

The resampling methods (described in Section 4.3.1 above and detailed in Volume 2B—Section 5) can also be used to downscale image data. However, unless care is taken with any of these methods, interpolation of EO data is ambiguous and can produce misleading information. The issues related to spatial resolution (see Section 1.2 above) and the underlying scale of the surface mosaic (see Section 1.4) are most relevant here.

Figure 4.7 Downscaling by duplicating pixels

Enlarging duplicate pixels in a lower resolution image to simulate a smaller pixel size.

a. Duplicate each pixel to represent a smaller pixel size

Input image pixel size = 40 m

a	b	c	d
e	f	g	h
i	j	k	l
m	n	o	p

Output image pixel size = 20 m

a	a	b	b	c	c	d	d
a	a	b	b	c	c	d	d
e	e	f	f	g	g	h	h
e	e	f	f	g	g	h	h
i	i	j	j	k	k	l	l
i	i	j	j	k	k	l	l
m	m	n	n	o	o	p	p
m	m	n	n	o	o	p	p

4.3.3 Resampling to a common pixel size

As introduced in Section 1.4, the surface of Earth, which is imaged in any EO dataset, can be considered as a mosaic of tiles. The tiles in this mosaic represent different surface features with varying dimensions and colours. Any single EO image, however, only captures these features and patterns at a single spatial scale. Given that the constituent tiles of the surface mosaic also vary in size spatially and temporally, it is not a simple matter to select the 'best' spatial resolution to suit all features and patterns being imaged. Rather, the resolution that is most appropriate for a particular application needs to be determined (see Section 2.2).

When resampling two (or more) EO images to a 'common grid' as defined by image pixel size and extent (spatial resolution and extent), both images generally need to be resampled (see Volume 2B—Section 5). Resampling will ensure that the original image data is more faithfully represented in the common grid compared with the simpler image rescaling methods of blocking, sub-sampling or duplicating pixels, as mentioned in Sections 4.3.1 and 4.3.2 above.

The most appropriate pixel size for this grid, however, will vary for different applications, and possibly at different acquisition times (see Section 2.2). There is no easy answer to this problem; it requires familarity with both the surface features and patterns of interest to a given study and the characteristics of available imagery. In many cases, the final selection of imagery may be governed by pragmatic factors, which will need to be addressed during analyses and reporting.

4.4 Further Information

Gonzalez and Woods (2018)

Jensen (2016) Chapter 8

4.5 References

Gallant, J.C., McKenzie, N.J., and McBratney, A.B. (2008). Scale. Ch 3 in *Guildelines for Surveying Soil and Land Resources*. Australian Soil and Land Survey Handbook Series. (Eds: McKenzie, N.J., Grundy, M.J., Webster, R., and Ringrose-Voase, A.J.) CSIRO Publishing, Melbourne.

Gonzalez, R.C., and Woods, R.E. (2018). *Digital Image Processing*. 4th Edn, Pearson Education, Hoboken, NJ.

Harrison, B.A., and Jupp, D.L.B. (1990). *Introduction to Image Processing: Part TWO of the microBRIAN Resource Manual*. CSIRO, Melbourne.

Jensen, J.R. (2016). *Introductory Digital Image Processing: A Remote Sensing Perspective*. 4th Edn. Pearson Education, Inc. ISBN 978-0-13-405816-0

Roberts, D.A., Roth, K.L., and Perroy, R.L. (2011). Hyperspectral Vegetation Indices. Ch 14 in *Hyperspectral Remote Sensing of Vegetation*. CRC Press. pp 309–328.

Singh, A., and Harrison, A. (1985). Standardised Principal Components. *International Journal of Remote Sensing*, 6, 883–896.

Sonobe, R., and Wang, Q. (2017). Hyperspectral indices for quantifying leaf chlorophyll concentrations performed differently with different leaf types in deciduous forests. *Ecological Informatics*, 37, 1–9. *https://doi.org/10.1016/j.ecoinf.2016.11.007*

Thenkabail, P.S., Lyon, J.G., and Huete, A. (2018). *Hyperspectral Indices and Image Classifications for Agriculture and Vegetation*. CRC Press. ISBN 9781138066038

Thonfeld, F., Hecheltjen, A., Braun, M., and Menz, G. (2010). From Algorithms to Processing Chains: A Review of Land Cover and Land Use Change Detection Methodologies. *Proceedings ESA Living Planet Symposium*. ESA SP-686. ESA, Bergen, Norway.

Processing Image Pairs

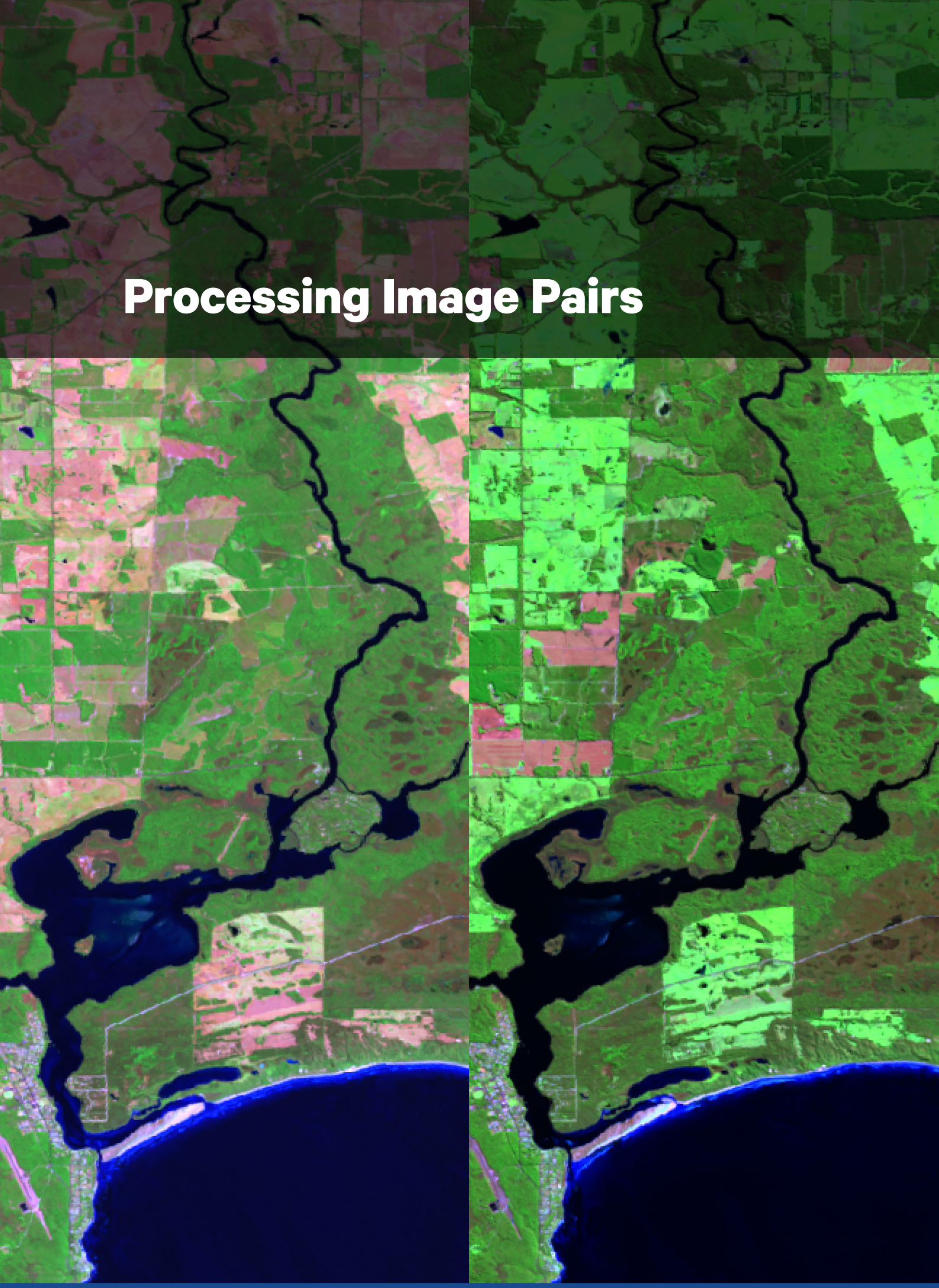

The following sections focus on image processing operations that can be used to analyse a pair of bi-temporal images. The processing procedures commonly used for comparing or combining image pairs are introduced in Section 5. Methods that merge and/or interpolate data from two different EO sources are considered in Section 6. Approaches to detecting changes between a pair of bi-temporal images are reviewed and evaluated in Section 7.

Contents

5 Basic Comparisons 47

6 Fusion Methods 57

7 Change Detection Methods 69

Background image on previous page: Landsat-8 images acquired over Augusta in summer (left) on 13 January 2015 and winter (right) on 25 August 2015. Both images are displayed as false colour composites, with band 6 as red, band 5 as green and band 3 as blue. **Source:** Norman Mueller, Geoscience Australia

5 Basic Comparisons

A simple method for comparing three EO images of the same ground area, which were acquired on three different dates, involves creating multi-date colour composites (see Section 5.1). The remainder of this section reviews some simple image processes for bi-temporal image pairs, namely:

- subtracting and adding images (see Section 5.2);
- manipulating image masks to separate, combine or complement images (see Section 5.3);
- transferring class statistics to another set of image channels (see Section 5.4); and
- balancing image colour for image mosaicking (see Section 5.5).

Other operations that can be used to merge multiple images include fusion techniques (see Section 6), affine transformations (see Volume 2C—Section 7); Principal Components Analysis (PCA; see Volume 2C—Section 9) and channel ratios (see Section 2C—Section 10). Specific processes for detecting changes in a pair of EO images are discussed in Section 7.

All operations described below assume that the bi-temporal pair of images has been registered to a common geometric grid (see Section 3.1.1.1). In particular, if the image pair was derived from different image sources, such as two different sensors or bi-temporal images from one sensor, the images must be well registered and radiometrically calibrated before they can be sensibly processed as a pair. This is also essential for the processes described in Section 7. The procedure for image registration is outlined in Volume 2B.

5.1 Multi-date Colour Composites

A simple way to compare registered, multi-date imagery of a given location is to display three channels representing three image dates as different primary colours in a colour composite. For example, in Figure 5.1 NDVI was derived for three contrasting seasons in 2018/19. When these greyscale images are combined into a colour composite, their combined colours highlight areas with consistently high or low vegetation cover. Similar composites could be generated using a wide range of spectral indices and other image transformations that summarise multispectral imagery into a single channel.

Background image: High resolution aerial image of Maroubra Beach, Sydney, acquired on 24 February 2016. **Source:** © Nearmap

Figure 5.1 Multi-date NDVI composite

In this colour composite, three NDVI composites derived from Sentinel-3 imagery are combined into a single colour image: December 2018 is shown as red, October 2018 is shown as green and June 2019 is shown as blue. These composite colours generate dark areas where vegetation greenness/cover was low for all three months and bright areas for 'greener' perennial vegetation. Interesting patterns are generated based on the seasonality of vegetation: vegetation resulting from early winter rainfall is highlighted as blue, monsoonal rains in summer invigorate vegetation in northern and central Australia (pink and red areas) whereas spring rains drive vegetation growth in temperate regions (brighter green patches). The less vegetated regions of Central and Western Australia show as darker colours. The NDVI channels in this composite have been enhanced using step-wise linear stretching to highlight lower values.

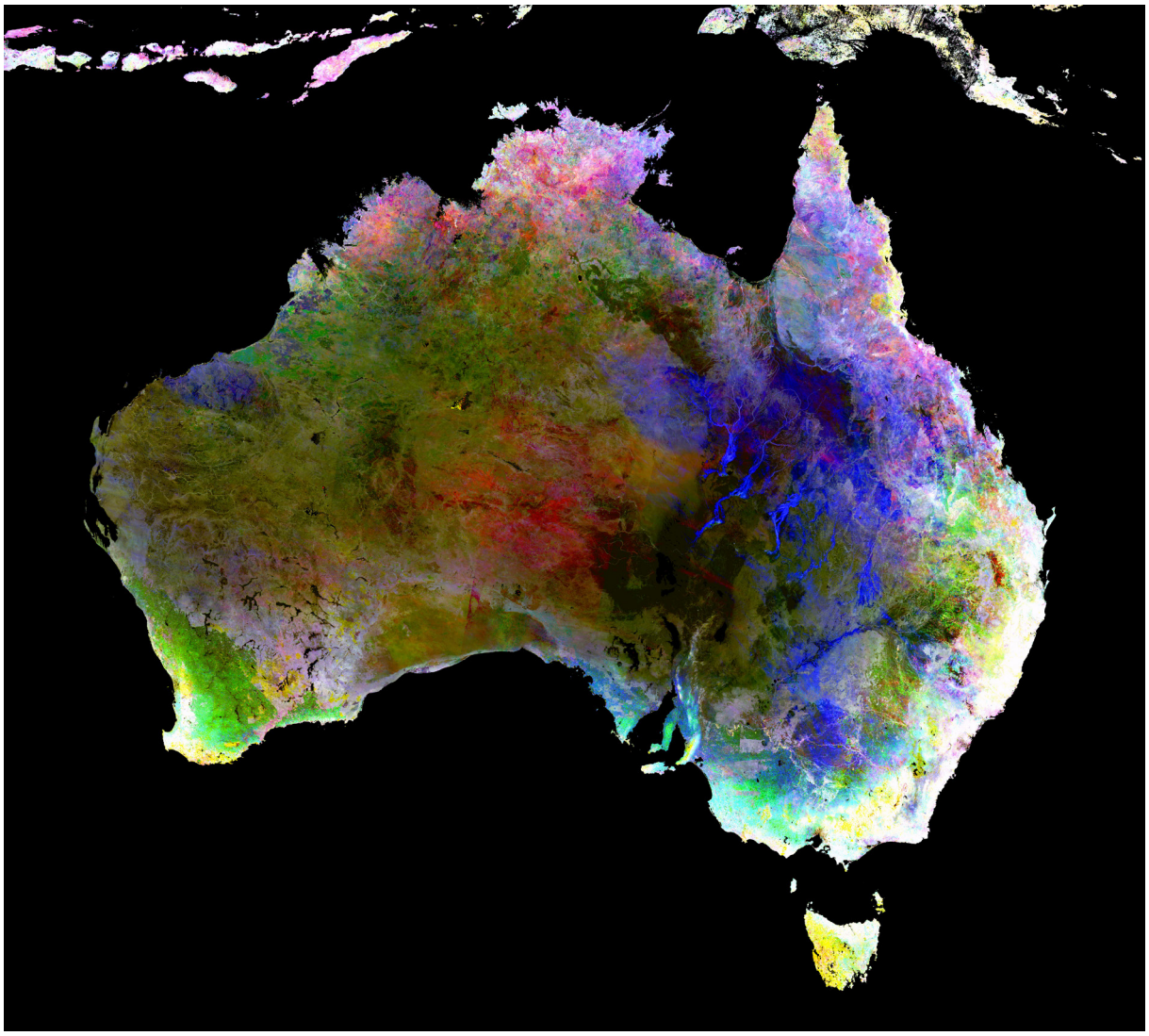

Source: Norman Mueller, Geoscience Australia

5.2 Differencing and Addition

Image differencing provides a simple assessment of the changes between two registered images. As illustrated in Figure 5.2, the process simply computes the difference between a co-registered pair of images on a pixel-by-pixel basis for each corresponding pair of channels. Naturally, for pixel values to be comparable between the two images, radiometric registration must be applied to the geometrically registered images before differencing (see Section 3.1). Also, for a difference image to consistently show the differences between an image pair, matching channels in the two images should have comparable data ranges. In the cases of bi-temporal or multi-source imagery, the channels should be rescaled to have matching data ranges before differencing. Methods for image colour 'balancing' are discussed in Section 5.5.

The differencing operation computes:

Channel i difference = Channel i in image A – Channel i in image B

The values in the difference channel, will be:

- < 0 when *channel i* values in *image A* are higher than in *image B*;
- = 0 when *channel i* values are the same in both images; and
- > 0 when *channel i* values in *image B* are higher than in *image A*.

Some image processing systems allow the difference result to be:

- compressed (divided by two);
- shifted (add an offset) to keep the output values within the image data range; or
- stretched within a defined output range.

An offset constant is usually added to the difference result to keep the output image values in the same range as the input image. For example, in a byte image (that is, with a data range from 0 to 255) a constant of 127 could be used to centre the range of difference values. If large differences (greater than half the data range) are expected between the images, the resulting difference values will also need to be rescaled (see Volume 2A). Unchanged pixels then have a value equal or close to the offset in the difference channel, and would appear as mid-grey when displayed as a greyscale.

An example of two NIR channels that have been differenced from two registered images is shown in Figure 7.2 in Section 7 below. As illustrated, changed pixels fall into the tails of the histogram of the difference image, so that pixels with higher values in *Image A* appear brighter in the difference channel, while those with higher values in *Image B* appear darker. A similar distribution results from image ratioing (see Section 7.1.2).

Figure 5.2 Image differencing

a. Process: two channels are differenced by subtracting the value of a pixel in one channel from the corresponding pixel value in the other channel. When differencing bi-temporal image pairs the two channels typically represent the same spectral data (such as NIR).

Channel i in image A

a	b	c
d	e	f
g	h	i

÷

Channel i in image B

1	2	3
4	5	6
7	8	9

=

Channel i differences

a-1	b-2	c-3
d-4	e-5	f-6
g-7	h-8	i-9

b. Numeric example. The resulting difference values are rescaled to the image data range. In this example, the computed value -6 is rescaled to 0 and the computed value 6 is rescaled to 12.

Channel i in image A

8	9	7	2
7	6	3	1

÷

Channel i in image B

8	3	7	5
6	4	6	7

=

Channel i differences

0	6	0	-3
1	2	-3	-6

or

Rescaled differences

6	12	6	3
7	9	3	0

Source: Harrison and Jupp (1990) Figure 60

This differencing operation can also be applied to all corresponding channels in a bi-temporal pair of images to create a colour composite difference image, although the colours in composite difference images can be harder to interpret (see Figure 5.3). They are, however, useful to assess particular image processing operations, such as image classification. For example, a residual image can be computed to highlight those pixels whose original image values are not close to the mean values of their allocated class (see Figure 5.4). In this case, the residual image indicates where additional classes may be required (see Volume 2E; Jupp and Mayo, 1982).

Channels can be processed before differencing, possibly to remove noisy pixels or to represent a land cover characteristic (such as vegetation greenness; see Volume 2C). When differencing pairs of transformed channels, rescaling may be required before differencing to ensure that channel values are comparable. Transformations that are scene-dependent, such as PCA (Principal Components Analysis) or MNF (Minimum Noise Fraction), are generally not recommended as a pre-processing operation before differencing images (see Volume 2E) although they are useful as tools to explore difference images. Differencing of ratioed or index channels offers the advantage of reducing any topographic, Sun angle and/or atmospheric differences between images. Ratios of two bands or indices can be more effective than differencing where terrain is significant as ratioing will subdue the effects of shadowing more than differencing (see Section 7.1.2 and Volume 2C—Section 10).

Multidimensional distance metrics that can be used to compute the 'direct' difference between multi-channel image values (such as the Euclidean distance) are discussed in Volume 2E. As illustrated in Figure 5.5, such metrics can be useful for comparing different image processes, such as filtering options or resampling methods, to show where the processed pixel values vary.

Figure 5.3 Colour composite difference image

This pair of Landsat MSS images of Adelaide have been differenced to show the impact of urban expansion between 1972 and 1989. In the difference image green indicates an increase in greenness and red indicates a decrease in greenness, white indicates an increase in cover and black indicates a decrease in cover.

a. 1972 b. 1989 c. Difference 1972-1989

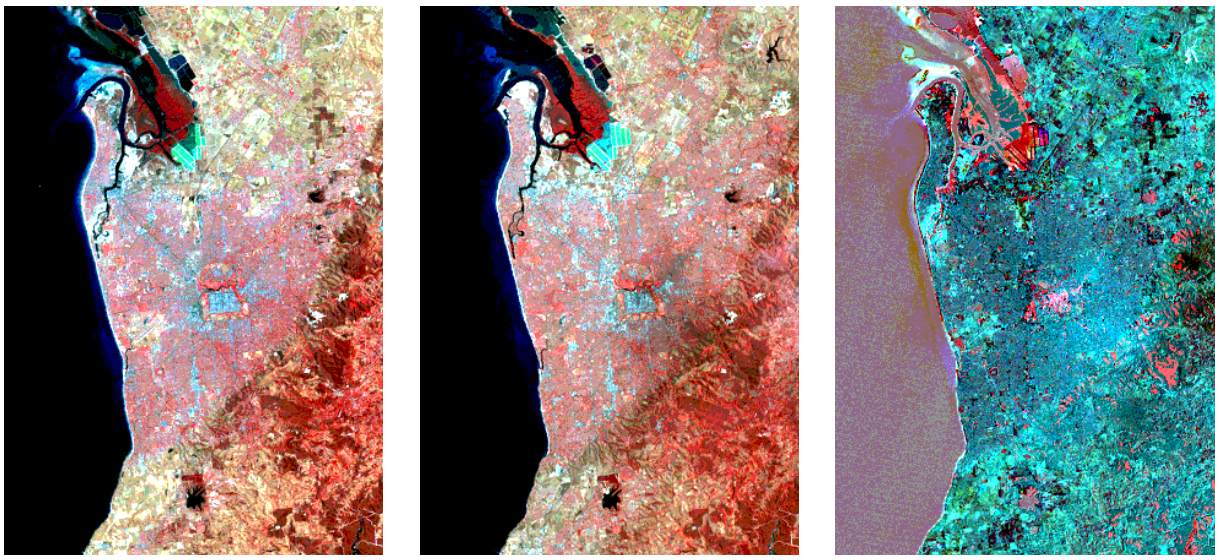

Source: Megan Lewis, University of Adelaide

Image addition effectively 'strengthens' any pixels that have positive spectral correlation between two images. This feature can be useful for crop identification, for example, where an individual image may not clearly differentiate between different ages or types of agricultural crop on the basis of spectral values, but the spectral correlation through a time series of images is able to separate such differences. The addition operation could also be weighted to compute the weighted average of the two images rather than each image contributing equally to the result. The weighting option could be useful for adding an additional channel after two images have been added together. For example, to produce an image that is equivalent to an unweighted average of three channels *A*, *B* and *C*, we could add pairs of images in the sequence:

$$temp = \frac{A}{2} + \frac{B}{2}$$

$$A + B + C = \frac{2 \times temp}{3} + \frac{C}{2}$$

Both addition and differencing of image pairs require that the two images be precisely registered, that is, the registration model is able to accurately relate each pixel in the first image to its corresponding position in the second image (see Volume 2B). When the image pair is formed from an original image and a spectrally transformed version of it (as in Figure 5.4 or Figure 5.5a), the geometries will already be exactly registered. Figure 5.5b highlights the variations in geometric registration that can result from different resampling methods (see Volume 2B for details).

If locational errors exist when a resampled image is differenced with its bi-temporal paired image, artificial edges can appear in the difference image. For example, Townshend *et al.* (1992) used simulated MODIS imagery to measure the effects of geometric misregistration in NDVI difference images. They concluded that misregistration by one pixel can result in up to 50% increase in the semi-variance of the difference image for densely vegetated images and a 10% increase for sparse vegetation. (Semi-variance is a measure of the scale of spatial pattern and is related to the variogram; see Volume 2A—Section 8.2.) Thus, in densely vegetated images, registration errors would need to be less than 20% of a pixel to ensure that the ensuing misregistration effects were less than 10%.

Figure 5.4 Residual image

This Landsat MSS image of Heron Island Reef, Queensland, was classified in terms of reef cover classes (Jupp *et al.*, 1985a; Jupp *et al.*, 1985b). The difference between the pixel values of the original image and the mean image (in which pixels are given the values of their class seeds) is shown as the residual image.

a. Original image

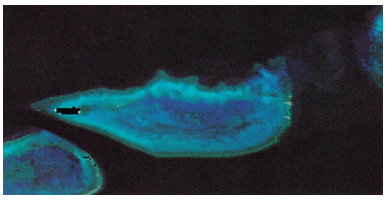

b. Mean image

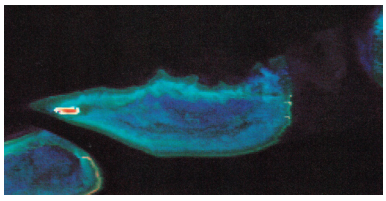

c. Residual image

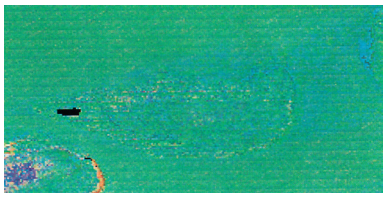

Source: Jupp *et al.* (1985a)

Figure 5.5 Examples of Euclidean distance images

The Euclidean difference between corresponding pixels in these image pairs highlights where the transformed image values differ in the two input images in each pair.

a. A Landsat-8 OLI image of Canberra, acquired on 10 August 2017, was processed using two different filtering operations with an active filter region of 3x3 pixels.

Full average filter

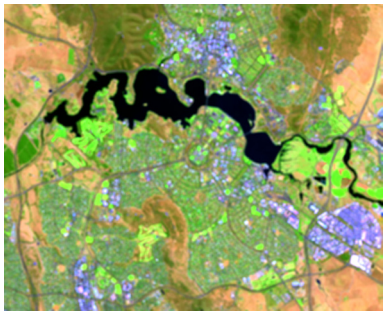

Edge-preserving filter

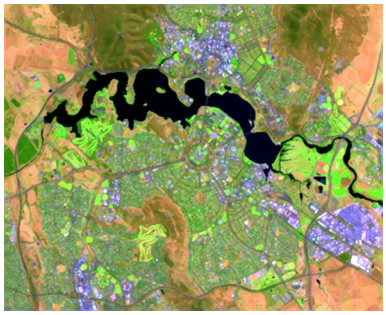

Euclidean difference

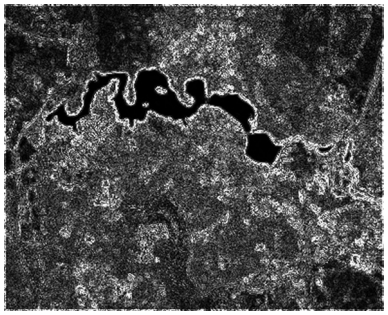

b. This pair of input images shows two resampling methods for a Landsat-8 OLI image of Brisbane airport, Queensland, acquired on 13 June 2018 and displayed using bands 6, 5, 3.

Bilinear resampling

Cubic Convolution resampling

Euclidean difference

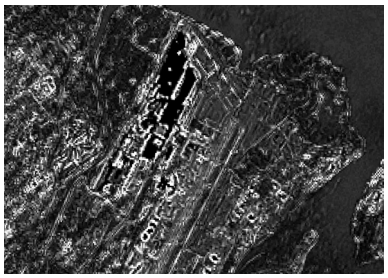

Source: Norman Mueller, Geoscience Australia

5.3 Manipulating Segmentation Masks

An ancillary operation to image segmentation (see Volume 2A—Section 10) involves transferring masked regions (defined by a specified value or the image null value) between registered images. This process can take a number of forms:

- paste a mask defined in one image into another image (see Figure 5.6a and Figure 5.6b);
- combine masks from two images (see Figure 5.6c);
- complement the masked and non-masked areas in an image (see Figure 5.6d); or
- recombine imagery to replace masked regions with data (see Figure 5.6e).

The complementing operation uses a mask to define the areas that will have non-null values in the output image but also sets all other values to the null value. The recombining function allows regions that have been masked out in one image can be given values from another image, possibly with any previously unmasked pixels becoming null (or masked) values. These operations may be useful during the classification process to extract unclassified pixels for further analyses (see Volume 2A—Section 9 and Volume 2E).

Figure 5.6 Recombining images

Masks can be transferred and combined between pairs of images in various ways.

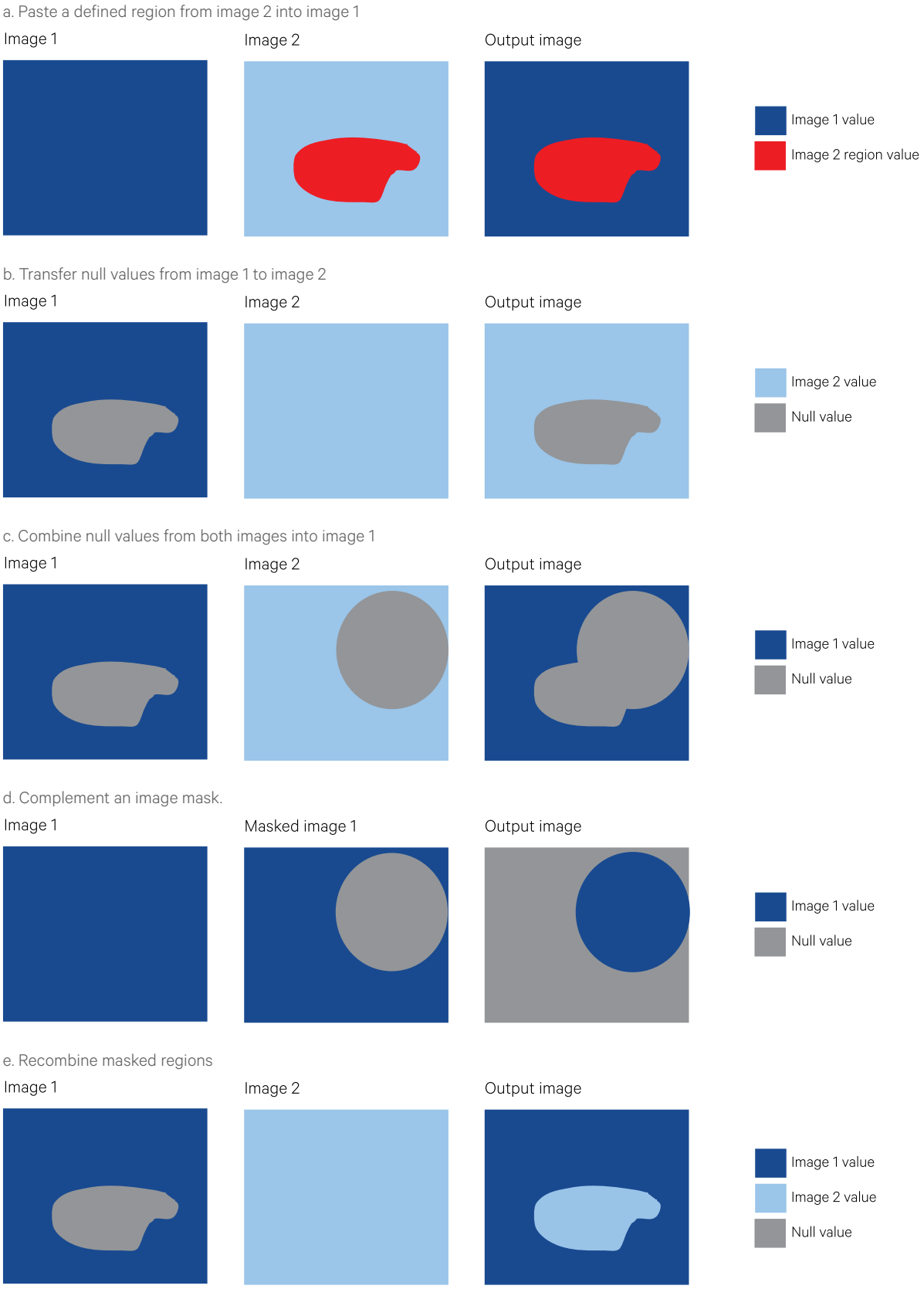

Source: Harrison and Jupp (1990) Figures 61 and 62

5.4 Transferring Category Statistics

A unique operation in some image processing systems involves generating spectral statistics for sets of pixels that are grouped by a reference channel or image. Statistics relating to the mean, standard deviation, number of pixels, and optionally the covariance matrix could be generated based on values from input image 1 for each category defined in input image 2. Typically this process is used during image classification (see Volume 2A—Section 9.3.2 or Volume 2E). Alternatively, the reference channel may be an ancillary data channel that defines regions of interest. For example, this technique could be used to analyse the relationship between crop yield (derived from EO data) and soil type regions.

In the classification context, the statistics indicate the variability of some particular set of categories (or classes) in terms of the input image(s). The categories may have been formed from the input image(s), in which case the operation will simply be one of mean migration (see Volume 2A—Section 9.2.3 or Volume 2E). The input images could also be a different set of channels in the image (either before or after processing) or a different, but registered, data source. For example, a classification based on transformed channels such as Principal Components can be transferred back to the original image data for subsequent processing with reference to a familiar colour composite image. Alternatively, a classification may be performed using visible and NIR channels then transferred to SWIR and TIR channels to assess the variability of the classes in terms of those channels, and hence possibly which classes need to be split using those additional channels. This technique has also been used to split a set of land cover classes into sunlit and shaded categories by gathering statistics for the classes from a topographicallyenhanced channel (Ahmad *et al*., 1989).

In a bi-temporal context, this spectral transfer process can be used to transfer a classification from an image at one date to a registered image at a different date. Major changes in image features will be highlighted in the 'residual' image (the difference between the original and classified images) of the second date (see Figure 5.4 and Volume 2E). Naturally, when different image sources are being used to transfer a classification, the two sources must be accurately registered (see Section 3.1 and Volume 2B).

5.5 Colour Balancing for Image Mosaicking

The geometric aspects of sewing and mosaicking multiple images are discussed in Volume 2A—Section 5.2.2 and Volume 2B. When the imagery being mosaicked is derived from different sources, a colour balancing or rescaling operation (see Volume 2C—Section 2) is usually required to ensure that the same features have similar values in the images being joined, so that the join position has low visual impact.

A number of methods may be used to rescale or 'balance' image colours. These usually involve matching the (normalised) histogram values of each image to obtain equivalent data ranges. A simple implementation of this is to use the channel histogram percentage points (see Volume 2A—Sections 4.1.1 and 8.1.1).

For example, histogram percentage points for a pair of channels A and B are shown in Table 5.1. These values can be compared graphically as shown in Figure 5.7. A regression line through the majority of points then defines a conversion scale from values in one image to the corresponding values in another image. The 1% and 99% points, and often the 5% and 95% points, are ignored for the regression if they depart significantly from a linear function. To rescale these channels, a good contrast stretch based on their actual histograms would have a minimum of 13 and a maximum of 56 in image B, which relate to the values 7 and 31 in image A. The selected scaling values should be checked visually, however, before rescaling images (Volume 2C—Section 2). However, if the mosaicked imagery is to be processed further, the maximum ranges should be used for rescaling to avoid truncation of values. In this example, to rescale channel A to match channel B, we would use a coefficient of 1/1.7 (= 0.588) with an offset of 2.

Table 5.1 Example histogram percentage points

Channel	Histogram percentage points												
	1%	5%	10%	20%	30%	40%	50%	60%	70%	80%	90%	95%	99%
A	11	11	13	14	14	16	16	17	18	20	21	23	32
B	17	20	22	24	26	28	29	30	32	35	39	44	86

In a mosaicked image, the join lines between different input images are often visible even when care is taken to achieve a good colour balance before mosaicking (see Section 5.5). If sufficient overlap occurs between the input images after they have been registered to a common base, the join boundary can be manually defined along a linear feature in the image, such as a road or river, in the overlap region. This process can be considered as the digital equivalent of photo-mosaicking.

Typically, this operation would require resampling of the images to a common base (see Volume 2B) then digitising along a feature using the screen cursor (see Volume 2A—Section 10.1) to remove part of the overlap region in one image. The digitised image can be used as a mask on the second image to remove the common overlap pixels (see Section 5.3). This results in two registered images with no overlapping pixels, but which abut along an image feature. These two images can then be recombined using image pasting (see Section 5.3) to produce the final mosaic.

Figure 5.7 Colour balancing

Histogram statistics can be used to match contrast ranges between different images.

a. Channel B = 1.7 x Channel A- 2

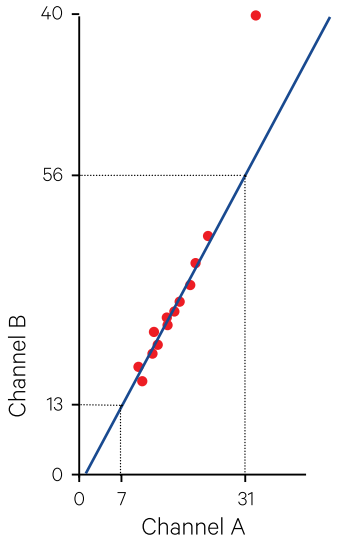

b. Channel A = 1/1.7 x Channel B + 2

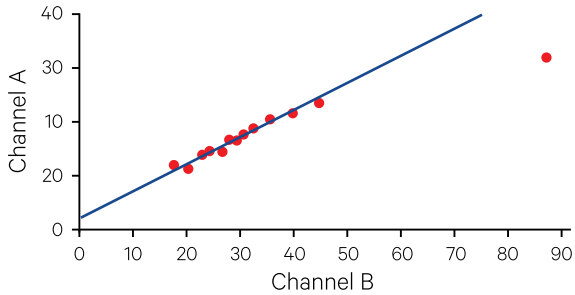

Source: Harrison and Jupp (1990) Figure 63

5.6 Further Information

Jensen (2016) Chapter 12

5.7 References

Ahmad, W., Jupp, D.L.B., and Nunez, M. (1989). Land cover mapping in a rugged terrain area using Landsat MSS data. *International Journal of Remote Sensing,* 13(4), 673–683. *https://doi.org/10.1080/01431169208904145*

Harrison, B.A., and Jupp, D.L.B. (1990). *Introduction to Image Processing: Part TWO of the microBRIAN Resource Manual*. CSIRO, Melbourne.

Jensen, J.R. (2016). *Introductory Digital Image Processing: A Remote Sensing Perspective*. 4th Edn. Pearson Education, Inc. ISBN 978-0-13-405816-0

Jupp, D. L. B., and Mayo, K. K. (1982). The use of residual images in Landsat image analysis. *Photogrammetric Engineering and Remote Sensing*, 48(4), pp. 595–604.

Jupp, D. L. B., Heggen, S. J., Mayo, K. K., Kendall, S. W., Bolton, J. R., and Harrison, B. A. (1985a). The BRIAN Handbook. *An Introduction to Landsat and the BRIAN (Barrier Reef Image Analysis) System for Users, CSIRO Division of Water and Land Resources, Natural Resources Series No.3*. CSIRO, Canberra, Australia.

Jupp, D. L. B., Mayo, K. K., Kuchler, D. A., Heggen, S. J., Kendall, S. W., Haywood, M. J., and Ayling, T. (1985b). *A Landsat-based interpretation of the Cairns Section of the Great Barrier Reef Marine Park. Interpretation of Landsat data by Computer-based Classification and Labelling, CSIRO Division of Water and Land Resources, Natural Resources Series No.4*. CSIRO, Melbourne, Australia.

Townshend, J.R.G., Justice, C.O., Gurney, C., and McManus, J. (1992). The impact of misregistration on change detection. *IEEE Geoscence and Remote Sensing*, 30, 1054–60.

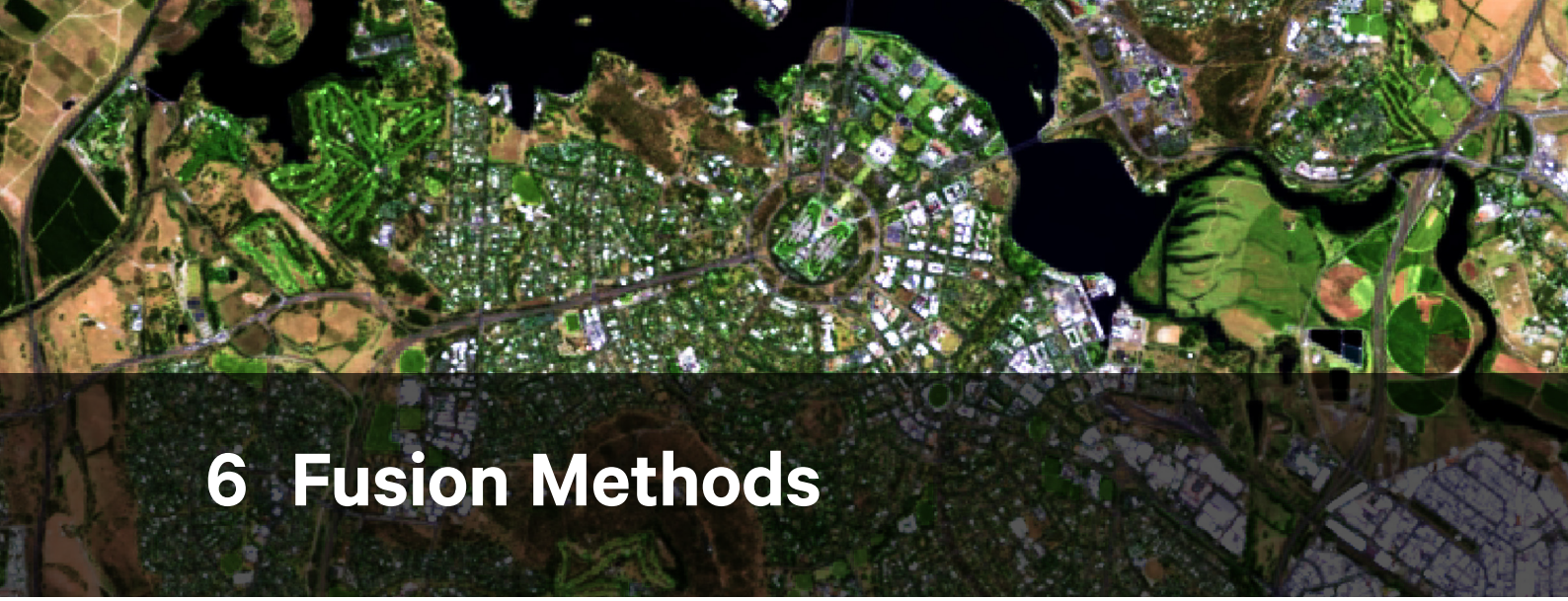

6 Fusion Methods

The four dimensions of EO dataset resolution, density and extent (namely spectral, spatial, radiometric and temporal) are introduced in Volume 1B—Section 1 and Volume 2C—Section 1, and summarised in Table 2.1 above. Sensor design constraints, such as detector efficiency in recording the incoming radiation and the data volume that can be be recorded or transmitted, make it difficult to deliver imagery with high resolution in more than one of these dimensions (see Volume 1A—Section 13).

A number of fusion methods have been proposed to combine different sources of EO imagery to achieve higher resolution in one dimension (Wald, 1999). Some of these methods use dynamic, physics-based models (Heinsch *et al*., 2006; Renzullo *et al*., 2008), while others rely on complementary EO-based datasets (Emelyanova *et al*., 2012, 2013). Methods solely relying on EO datasets are typically called fusion or blending algorithms and include:

- spatial and spectral blending, such as pan-sharpening—merging a higher spatial, but lower spectral, resolution image (generally panchromatic) with a compatible multispectral image that has lower spatial, but higher spectral, resolution to create a multispectral image with sharper spatial features (see Section 6.1); and
- spatial and temporal blending—merging imagery with higher temporal, but lower spatial, resolution with EO image datasets that have lower temporal, but higher spatial, resolutions to create a denser time series with higher spatial resolution (see Section 6.2).

Since terminology in this area can become confused, some working definitions of terms commonly used by the 'data fusion' research community are summarised in Table 6.1. Methods to create a composite image from time series datasets, in which the maximum number of pixels are unaffected by cloud, haze, smoke or sensor errors, are described in Section 10.

Data fusion is a formal framework in which are expressed means and tools for the alliance of data originating from different sources, in order to obtain information of greater quality.
Wald (1998)

Background image: Landsat-8 panchromatic and OLI images acquired over Canberra on 25 October 2018 have been merged to create a colour image with the spatial resolution of the panchromatic image. **Source:** Norman Mueller, Geoscience Australia.

Table 6.1 Terminology associated with data fusion

Term	Definition	Relevant Dimension(s)	Reference
Aggregating	Combining a scale of measurement		McVicar *et al.* (2002)
Blending	Merging images from different sources to generate information with high spatial and temporal resolution (see Section 6.2)	spectral spatial temporal	Hilker *et al.* (2009)
Compositing	Combining spatially overlapping images into a single image based on an aggregation function (see Volume 2B)	spatial temporal	Google Earth Engine
Disaggregation	Splitting a scale of measurement	spatial	McVicar *et al.* (2002)
Downscaling	Producing an image of finer resolution from an image of coarser resolution (see Section 4.3.2)	spatial	McVicar *et al.* (2002)
Prediction	Obtaining future image estimations in regular time step sequences by modelling future spatial-temporal states (behaviour) of an observed system (see Section 14.3 and Volume 3)	spatial temporal	Crespo *et al.* (2007)
Pan-sharpening	Integrating spatial detail in a higher resolution panchromatic image with the spectral information of a lower resolution multispectral image to produce a high resolution multispectral image (see Section 6.1)	spectral spatial	Du *et al.* (2007)
Reconstruction	Recovering detail in severely blurred images, the causes of whose imperfections are known a priori	spatial	Bates and McDonnel (1986)
Restoration	Recovering an image that has been recorded in the presence of one or more sources of degradation	spatial	Bates and McDonnel (1986)
Sharpening	Highlighting fine detail in an image or enhancing detail that has been blurred, either in error or as a consequence of the image acquisition method	spectral spatial	Gonzalez and Woods (1992)
Spectral unmixing	Classifying mixed pixels by deconvolving (unmixing) each pixel spectrum into fractional abundances of its surface constituents or endmember spectra (see Volume 2E)	spectral spatial	Rogge *et al.* (2006)
Upscaling	Producing an image of coarser resolution from an image of finer resolution (see Section 4.3.1)	Spatial	McVicar *et al.* (2002)

Adapted from Emelyanova *et al.* (2012)

6.1 Spatial and Spectral Blending

Some of the methods commonly used for panchromatic sharpening (or pan-sharpening)—blending the higher spatial resolution of a panchromatic image with the higher spectral resolution of a multispectral image—are introduced in Volume 2C. Pan-sharpening is most relevant for visual identification of detailed spatial features, such as intra-urban land cover and landslide scars (Fonseca *et al.*, 2011).

Prerequisites for quality results from image fusion methods include matching the panchromatic and multispectral images as closely as possible in terms of:

- acquisition date;
- spectral and radiometric extent;
- dynamic range within relevant spectral bands; and
- geometric registration (Fonseca *et al.*, 2011).

A wide range of methods has been proposed for pan-sharpening imagery (Amro *et al.*, 2011). All methods, and their numerous variations and hybrid versions, present different advantages and disadvantages (see Table 6.2).

Zhang (2004) lists the 'most popular and effective' pan-sharpening methods used for EO imagery as:

- HSI (Hue-Saturation-Intensity)-RGB (red-green-blue) conversion, where the intensity component of the MSS image is replaced with the panchromatic image (see Volume 2C—Section 8);
- PCA (Principal Components Analysis), where PC1 is replaced with the panchromatic image (see Volume 2C—Section 9);
- arithmetic combinations, such as the Brovey Transform (see Volume 2C—Section 8.3), Synthetic Variable Ratio (SVR) or Ratio Enhancement (RE) (see Volume 2C—Section 10); and
- wavelet fusion (Mallat, 1989), where the panchromatic image is decomposed into spatial details (wavelet coefficients), which are subsequently merged with each multispectral band by reverse wavelet transforms (Pajares and de la Cruz, 2004; Amolins *et al.*, 2007).

Table 6.2 Pan-sharpening methods

Category	Example methods	Advantages	Disadvantages	Reference
Substitute component derived from multispectral image with one derived from panchromatic image	Hue-Saturation-Intensity (HIS) Principal Components Analysis (PCA) Gram-Schmidt (GS)	Computationally simple	Colour distortions when substituted component does not contain same spectral information as original component	Dou *et al.* (2007)
Compute a linear combination of multispectral and panchromatic bands then replace relevant component in multispectral image	Brovey Transform	Computationally simple	Spectral distortion	Tu *et al.* (2005)
Inject high frequency information from panchromatic image into multispectral image	High pass filtering of panchromatic image then adding edge detail back into the multispectral image	Low spectral distortion	Can generate ripple effect	Ranchin and Wald (2000)
Exploit statistical characteristics of panchromatic and multispectral images	Price's method Spatially Adaptive Algorithm	Preserves low resolution radiometry Can use multiple panchromatic images for high frequency input	Can produce blocking artefact	Price (1999) Park and Kang (2004)
Use Bayesian framework to model images and estimate the pan-sharpened image	Markov Random Fields Stochastic Mixing Models	Defines pan-sharpening in clear probabilistic framework	Image noise is assumed to be modelled by Gaussian distribution	Fasbender *et al.* (2008)
Decompose multispectral and panchromatic images into different levels of spatial detail then merge higher frequency panchromatic detail into multispectral image	Laplacian pyramid Wavelet fusion	Good spectral representation	Quality of pan-sharpened image depends on the right number of decomposition levels	Burt and Adelson (1983) González-Audicána and Otazu (2005)

Source for data: Amro *et al.* (2011)

The first three methods listed above are sensitive to geometric registration errors (Jiang *et al.*, 2013) and are reliant on a skilled operator to minimise colour distortion and maximise fusion quality. This is particularly true for panchromatic imagery acquired by EO satellites launched after 1999 (Zhang, 2004), which have a wider spectral range to include both visible and IR wavelengths. These three methods also require prior upscaling of the multispectral image to match the spatial resolution of the panchromatic image (see Section 4.3).

By comparison, the wavelet transform reduces colour distortions and image noise (Thomas *et al.*, 2008; Jiang *et al.*, 2013). Variations of this fusion method include the Ridglet, Curvelet (Candès and Guo, 2002; Choi *et al.*, 2005) and Contourlet transforms (Donoho and Vetterli, 2002). Artificial neural networks (AAN; Shutao *et al.*, 2002) and the Dempster-Shafer theory of evidence (DS; Wu *et al.*, 2002; Le Hégarat-Mascle *et al.*, 2003) have also be used for image fusion of EO imagery.

Recommendations for assessing the spectral and spatial quality of pan-sharpened images (Wald *et al.*, 1997; Du *et al.*, 2007) can be summarised in terms of two properties:

- consistency—if the pan-sharpened image is downsampled to match the spatial resolution of the multispectral image, it should closely resemble the original multispectral image; and
- synthesis—the pan-sharpened image should resemble an image that would be acquired by an appropriate sensor with corresponding spectral and spatial resolutions (Amro *et al.*, 2011).

The ideal outcome of pan-sharpening is an image with enhanced spatial information from the panchromatic image that does not compromise spectral detail from the multispectral image. This is achieved by considering the physics of image acquisition and adapting methods appropriately (Thomas *et al.*, 2008).

6.2 Spatial and Temporal Blending

A number of methods have been proposed to merge a high temporal resolution dataset, such as MODIS, with higher spatial resolution imagery (such as Landsat TM/ETM+/OLI). Examples of such methods include:

- STARFM (Spatial and Temporal Adaptive Reflectance Fusion Model; Gao *et al*., 2006);
- STAARCH (Spatial Temporal Adaptive Algorithm for mapping Reflectance Change; Hilker *et al*., 2009);
- downscaling unmixing models (Zurita-Milla *et al*., 2009);
- STRUM (Spatial and Temporal Reflectance Unmixing Model; Gevaert and Garcia-Haro, 2015); and
- semi-physical BRDF spectral model (Roy *et al*., 2008).

These methods attempt to simulate image datasets with higher spatial and temporal resolutions, which may be informative for monitoring rapidly changing biophysical processes. Since the Terra/MODIS and Landsat sensors have equivalent orbital parameters and acquire imagery at similar times of the day, their images have similar viewing and illumination geometries (see Volume 1B—Section 3). These sensors also share similar spectral resolutions for their red and NIR bands (see Table 6.3). Given these similarities, several algorithms have been proposed to synthesise daily Landsat images using coincident Terra/MODIS datasets. A generic theoretical framework for such methods is described in Excursus 6.1.

Table 6.3 Landsat and Terra/MODIS characteristics

Characteristic	Landsat TM/ ETM+/OLI	Terra/MODIS
Equatorial crossing time	~10:00 am	~10:30 am
Altitude	705 km (L-8)	713 km
Red bandwidth (nm)	630–690	620–670
NIR bandwidth (nm)	780–900	841–876
Spatial resolution (red and NIR)	30 m	250 m (red/NIR)
Revisit frequency	16 days	≤ 1 day

Adapted from Emelyanova *et al.* (2012) Table 4

One such method is the Spatial and Temporal Adaptive Reflectance Fusion Model (STARFM) proposed by Gao *et al*. (2006), which uses the MODIS daily 500 m surface reflectance product (MOD91GHK; see Section 10) to effectively interpolate the Landsat time series. To ensure that both image datasets are spatially and radiometrically comparable, calibrated image products are used (see Section 3.1). This method is most simply described with reference to Figure 6.1, which shows how a higher resolution image at time T1 is processed with lower resolution imagery at times T1 and T0 to synthesise a higher resolution image at time T0 :

- step 1—within a moving window, pixels that are spectrally similar to the central pixel are identified in the fine resolution image to use as sample pixels;
- step 2—sample pixels are filtered;
- step 3—both fine and coarse resolution data are used to determine weights (darker shading indicating heavier weights) for each sample pixel based on the:
  - spectral difference between T1 Landsat and T1 MODIS surface reflectance values;
  - temporal difference between T1 and T0 MODIS surface reflectance values; and
  - spatial Euclidean difference between the sample pixel and the central pixel; then
- step 4—the weighted values are used to a predict a higher resolution surface reflectance value of the central pixel at time T1.

However, this sequence is applied to each spectral band separately, which can generate unrealistic spectra in the synthesised image (Gevaert and Garcia-Haro, 2015).

A significant advantage of blending methods based on unmixing is that they do not require the higher and lower resolution image datasets to have corresponding spectral bands (Gevaert and Garcia-Haro, 2015). This gives more flexibility on input datasets and allows inclusion of biophysical parameters and non-EO datasets. Such algorithms involve four steps:

- cluster higher resolution dataset to define end members;
- calculate fractions (abundances) of each end member in each lower resolution pixel;
- unmix lower resolution pixel; and
- assign reflectance spectra to higher resolution pixels (Gevaert and Garcia-Haro, 2015);

This approach delivers more reliable results for gap-filling and cloud masking, especially when the high resolution dataset is temporally sparse (Gevaert and Garcia-Haro, 2015). It is also computationally less expensive and creates synthesised images with more realistic spectra (see Figure 6.2). An approach that blends STARFM with the unmixing blending method is called STRUM, which computes simulated surface reflectance values that are more accurate than either single method, but requires corresponding spectral bands in both input datasets. Thus, for a pair of MODIS and Landsat images on the base date and a MODIS image on the prediction date, STRUM creates a synthesised Landsat image on the prediction date using these steps:

- cluster higher resolution dataset to define end members;
- calculate fractions (abundances) of each end member in each MODIS pixel;
- unmix the difference image between the two input MODIS images; and
- assign temporal change of the relevant endmember to each synthesised Landsat pixel (Gevaert and Garcia-Haro, 2015).

All blending methods are based on assumptions related to the rate of change in surface reflectance with time and the extent of spatial variance and autocorrelation within an image. Accordingly, different methods may generate more appropriate results for particular datasets. Since blending algorithms can generate errors in terms of changing spatial and temporal variance between the input images, their performance needs to be assessed in terms of accuracy and constraints. Emelyanova *et al.* (2013) compared four blending algorithms in two areas of NSW with contrasting land cover and inundation dynamics:

- LIM (Linear Interpolation Model; Emelyanova *et al.*, 2012);
- GEIFM (Global Empirical Image Fusion Model; Emelyanova *et al.*, 2012);
- STARFM; and
- ESTARFM (Enhanced STARFM; Zhu *et al.*, 2010).

The results of these analyses for two study sites are summarised in Figure 6.3. This study concluded that more sophisticated blending algorithms do not necessarily produce better results if the lower resolution input imagery does not sample the spatial variance of land cover changes adequately. It also observed that the site with the most dynamic spatial and temporal changes proved to be the most challenging for all algorithms.

Figure 6.1 STARFM approach

In this four step schematic, T1 is the base date for the input images and T0 is the image date being simulated at a higher resolution (or the prediction date). In step 1, within a moving window on finer resolution imagery, circles indicate pixels that are determined to be spectrally similar to the central pixel (marked with a cross). In step 2, these sample pixels are filtered. In step 3, both fine and coarse resolution data are used to determine sample weights, with darker shading indicating heavier weights. In step 4, the weighted values are used to compute the prediction value for the synthetic image.

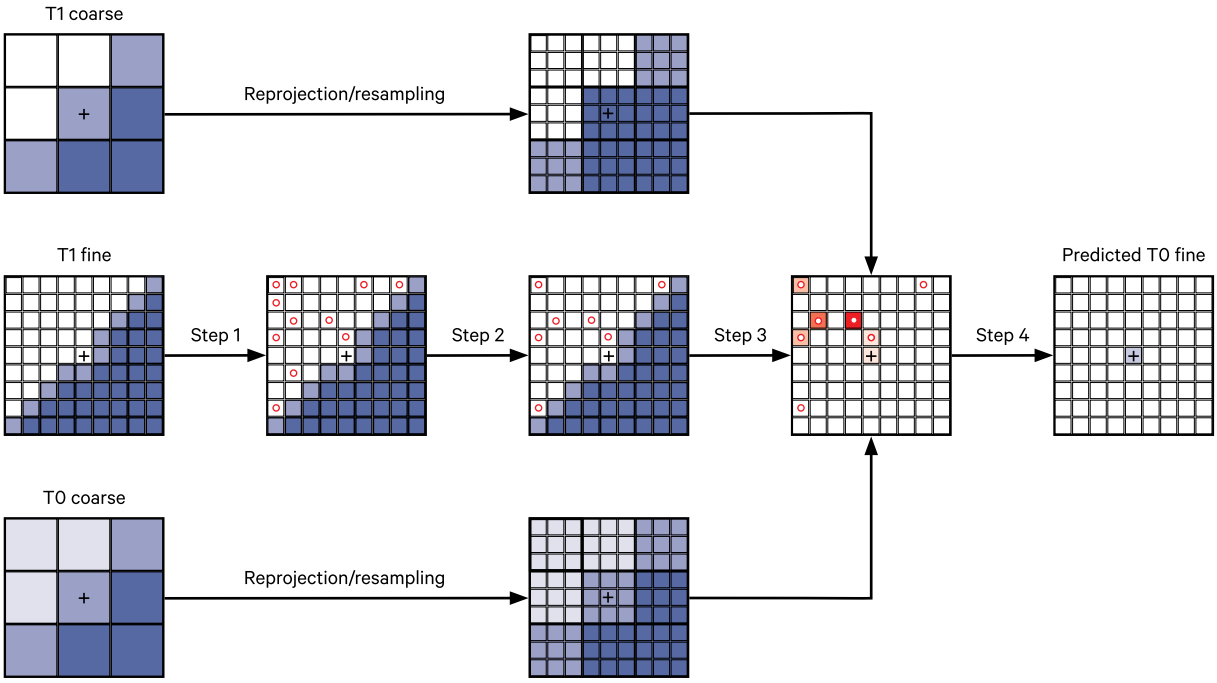

Adapted from Gao *et al.* (2006) Figure 1

Figure 6.2 Temporal profiles of blending algorithms

For a predominantly agricultural study area, three temporal profiles from blending MODIS and Landsat imagery are shown in terms of the Normalised Difference Vegetation Index (NDVI).

a. Based on all available Landsat images

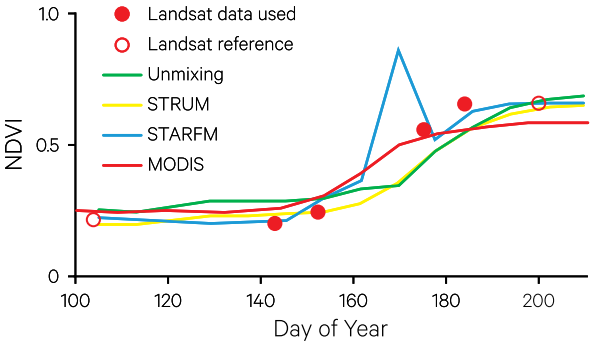

b. Based on first available Landsat image only

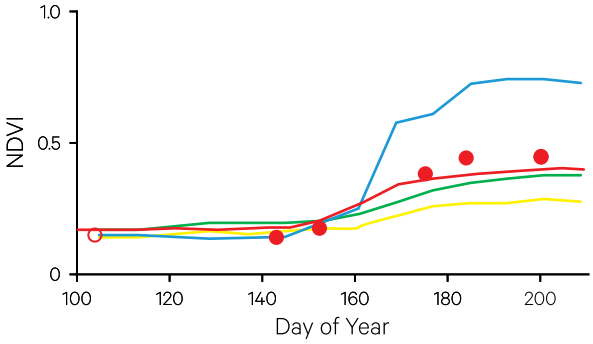

c. Based on last available Landsat image only

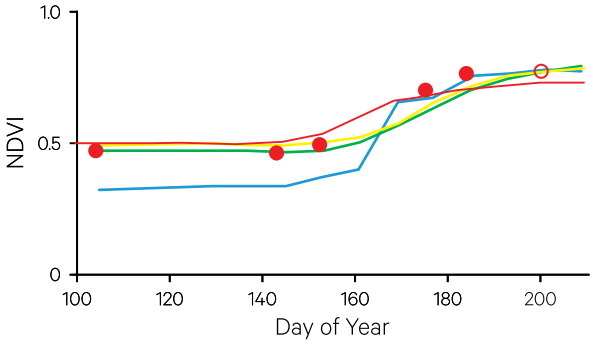

Source: Gevaert and Garcia-Haro (2015) Figure 6

Figure 6.3 Image blending algorithms

Observed Landsat data (bands 5, 4, 3 as RGB) compared with simulated Landsat-like images using four different blending algorithms.

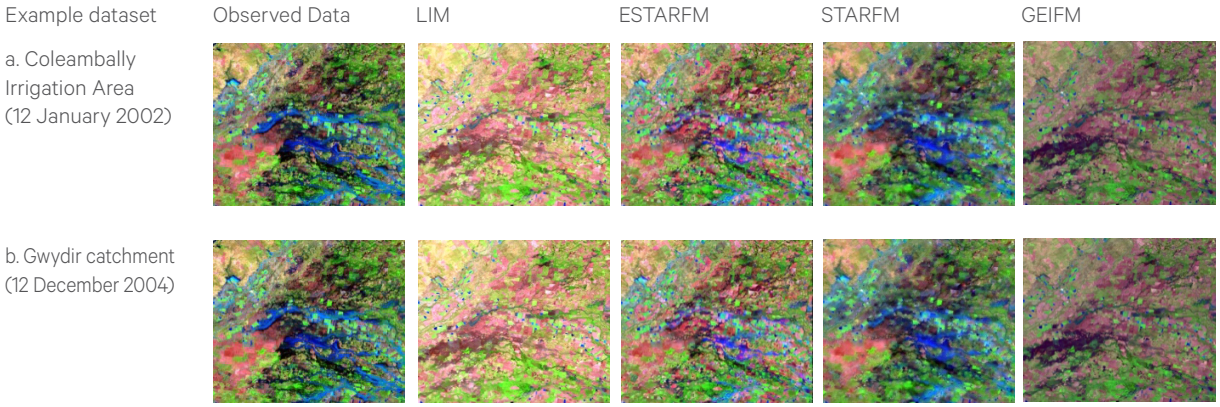

Source: Emelyanova *et al.* (2013) Figure 3

Excursus 6.1—Theoretical Framework for Image Blending

Source: Emelyanova *et al.* (2012)
Further Information: Gao *et al.* (2006)

This Excursus presents a generic framework for simulating higher spatial resolution imagery at required dates (see Figure 6.4a). The example below blends Landsat and MODIS images, however the framework is adaptable to other image types. In this case:

- Landsat (l) is an example of high spatial resolution / low temporal density imagery; and
- MODIS (M) is an example of low spatial resolution / high temporal density imagery.

For clarity, the notation used below for different image datasets, variables and operators is summarised in Table 6.4.

Table 6.4 Notation for blending framework

Term	Definition
t_n	Image acquisition date n
t_s	Date of simulated image
l	Observed high spatial resolution/low temporal density image
L	l upscaled to the coarse resolution $l_t(X,Y)$
(x,y)	Locations in l
$l_t(x,y)$	Time series of l
$l_t(X,Y)$	Upscaled reflectance values of l
$\lambda_s(x,y)$	Simulated high spatial resolution/high temporal density image
M	Low spatial resolution / high temporal density image
(X,Y)	Locations in M
$M_t(X,Y)$	Time series of M
$M_t(x,y)$	Downscaled reflectance values of M
Ψ	Maps reflectance values from $M_t(X,Y)$ to $l_t(x,y)$
ε	Error between the observed $l_t(x,y)$ and modelled $\Psi(M_t(X,Y))$ data due to instrument and/or model discrepancies
h_t	Transformation of reflectance values from a finer to a coarser resolution
f_t	differences in sensor systems acquiring l and M

Time series of Landsat and MODIS images for a particular band can be described by the spatial and temporal functions $l_t(x,y)$ and $M_t(X,Y)$ respectively, where (x,y) and (X,Y) respectively denote spatial locations of fine and coarse spatial resolution pixels for images observed at acquisition date t. Since these spatial locations represent sample and line numbers of the pixels within the images, the geographical locations (longitude and latitude) of the centres of fine and coarse pixels with same spatial locations within the images are not necessarily the same. Notation $M_t(x,y)$ represents reflectance values of the MODIS image downscaled to the Landsat resolution. The simulated Landsat-like data is denoted $\lambda_s(x,y)$ to distinguish it from the observed (or measured) Landsat reflectances, $l_t(x,y)$.

Assuming that Landsat and MODIS sensors have similar spectral characteristics for three visible spectral bands (blue, green and red, which are B1, B2 and B3 Landsat bands respectively) and three IR spectral bands (NIR infrared and two SWIR which are B4, B5 and B7 Landsat bands respectively), a relationship between Landsat and MODIS surface reflectances for a particular band can be performed by an operator Ψ which maps a MODIS reflectance value $M_t(X,Y)$ into a Landsat reflectance value $l_t(x,y)$:

$$l_t(x,y) = \Psi\,(M_t(X,Y)) + \varepsilon$$

where

- ε represents the error between the observed $l_t(x,y)$ and modelled $\Psi\,(M_t(X,Y))$ data due to instrument and/or model discrepancies.

The operator $\Psi : M \xrightarrow{f_t^{-1}} L \xrightarrow{h_t^{-1}} l$ provides a two-step mapping from:

- set M of the MODIS image reflectance values at the coarse resolution observed at acquisition date t $\{M_t(X,Y)\}$ to
- set L of the Landsat reflectance values upscaled to the coarse resolution $l_t(X,Y)$ to
- set l of the observed fine resolution Landsat reflectance values $\{\, l_t(x,y) \,\}$.

If h_t describes the transformation of reflectance values from a finer to a coarser resolution:

$$l_t(X,Y) = h_t\,(l_t(x,y))$$

and f_t accounts for the differences in sensor systems (such as orbit parameters, bandwidths and spectral response functions) between the concurrent Landsat and MODIS surface reflectance measurement, then:

$$M_t(X,Y) = f_t\,(l_t(X,Y))$$

and we can define the operator Ψ as a composition of the inversed scale and reflectance sensor conversion functions:

$$\Psi_t = H_t \circ F_t$$

where $H_t = h_t^{-1}$ and $F_t = f_t^{-1}$.

We assume that these inverse functions exist. Please note, this composition means a consecutive application of function F_t and then function H_t.

Therefore, a change in Landsat reflectances at pixel (x,y) over a time interval $[t_1, t_2]$ can be described as a change in the transformed MODIS reflectance values:

$$l_2(x,y) - l_1(x,y) = \Psi_2\,(M_2(X,Y)) - \Psi_1\,(M_1(X,Y))$$

While the spatial and spectral resolution relationships h_1 and f_1, respectively, can be modelled using the concurrent pair of observed Landsat and MODIS data recorded at time t_1, it is impossible to explicitly describe functions h_s and f_s because the problem is ill-posed due to the absence of Landsat measurements of spectral reflectances $l_s(x,y)$ for the date of simulation. However, we can substitute h_s and f_s by the models derived from the available data to generate Landsat-like reflectances for time t_s.

From the definition of f_t above, the function f_s models the inter-sensor reflectance transformation and ideally is dependent on the inter-sensor spectral characteristics only (that is, theoretically f_s is spatially and temporally independent). The relationship described by function f_1 can be used to estimate MODIS reflectances from the Landsat reflectances observed at time t_s, that is, $t_1 \approx t_s$. We describe the MODIS temporal reflectance changes during the time period $[t_1, t_s]$ by the function:

$$g_s : M_s(X,Y) = g_s\,M_1\,(X,Y)$$

which is intra-sensor and thus independent of spatial resolution, so:

$$M_s(x,y) = g_s\,(M_1\,(x,y))$$

The MODIS reflectance grid recorded at the simulation date t_s can then be downscaled by:

$$H_s\,(M_s(X,Y)) = M_s(x,y)$$
$$= g_s\,(M_1\,(x,y)) = g_s\,H_1\,(M_1\,(X,Y))$$

If g_s and h_1 are linear functions that obey the distributive law (Kolmogorov and Fomin, 1999):

$$\lambda_s(x,y) = l_1(x,y) + F_1\,(H_s\,(M_s(X,Y))$$
$$- H_1\,(M_1(X,Y)))$$

they can be used for simulating Landsat-like reflectances at time t_s from available measurements of Landsat and MODIS reflectances observed at time t_1 and MODIS data acquired at time t_s. After downscaling, this can be rewritten:

$$\lambda_s(x,y) = l_1\,(x,y) + F_1\,(M_s(X,Y) - M_1\,(X,Y))$$

This is a generic equation that describes Landsat-MODIS blending algorithms if the inter-sensor, spatial resolution and temporal relationships between Landsat and MODIS reflectances are assumed to be linear and have inverse functions (except for the temporal function as $t_1 < t_s < t_2$). A schematic of the generic blending process is shown in Figure 6.4b.

Figure 6.4 Generic overview of Landsat-MODIS blending.

The direction of information flow is represented by the arrows and the simulated image is indicated by the yellow line.

a. Simulation of a Landsat-like image at time t_S from two Landsat-MODIS image pairs (at times t_1 and t_2) and one MODIS image observed at t_S where $t_1 < t_S < t_2$.

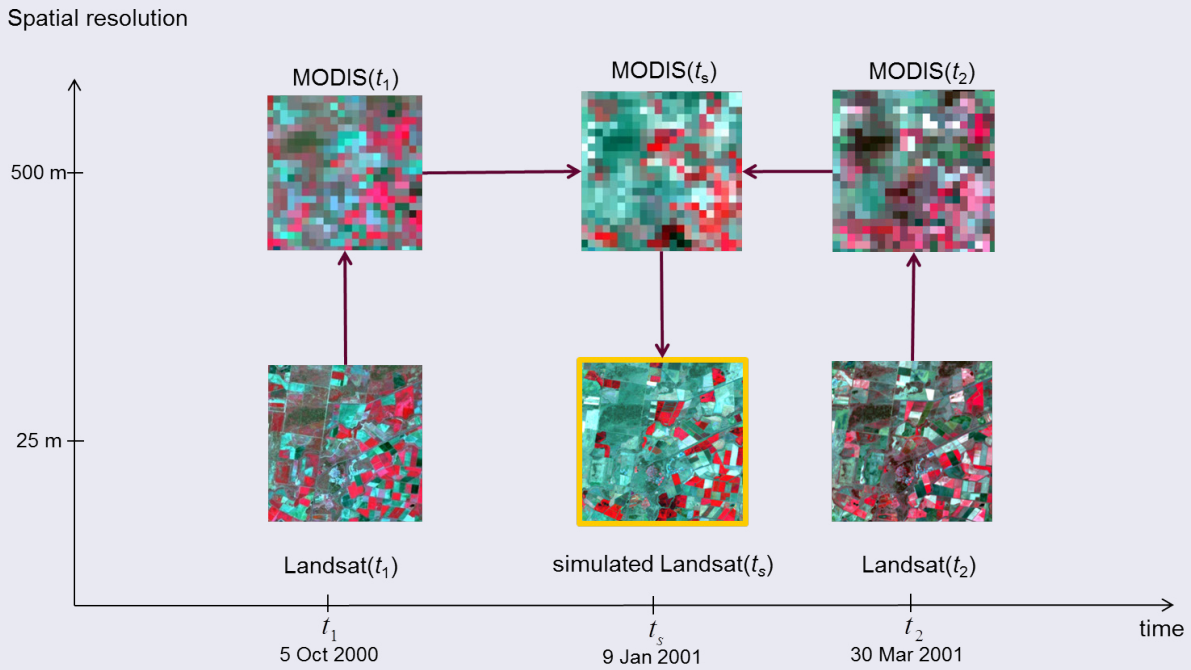

b. Schematic representation of the blending procedure, see Table 6.4 for the description of the notation. The outer black solid and dashed lines represent observed and calculated data, respectively, and $L_1(x,y)$ and $L_2(x,y)$ are spatially upscaled Landsat images associated with 5 October 2000 and 30 March 2001, respectively.

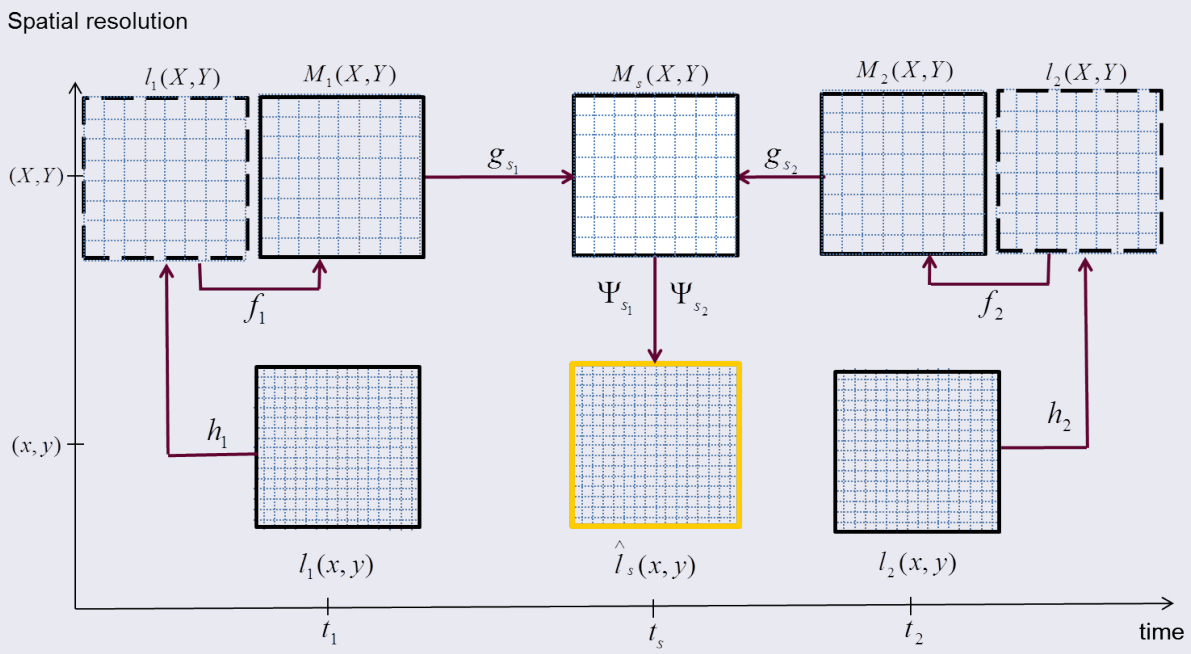

6.3 Further Information

Chang and Bai (2018)

Perracchione *et al*. (2018)

Zheng *et al*. (2018)

6.4 References

Amolins, K., Zhang, Y., and Dare, P. (2007). Wavelet based image fusion techniques—An introduction, review and comparison. *ISPRS Journal of Photogrammetry and Remote Sensing*, 62 (4), 249–263. *https://doi.org/10.1016/j.isprsjprs.2007.05.009*

Amro, I., Mateos, J., Vega, M., Molina, R., and Katsaggelos, A.K. (2011). A survey of classical methods and new trends in pansharpening of multispectral images. *EURASIP Journal on Advances in Signal Processing*, 2011:79.

Bates, R.H.T., and McDonnel, M.J. (1986). *Image Restoration and Reconstruction*. Clarendon Press, Oxford.

Burt, P.J., and Adelson, E.H. (1983). The Laplacian pyramid as a compact image code. *IEEE Transactions on Communications*, COM-3l(4), 532–540.

Crespo, J.L., Zorrilla, M., Bernardos, P., and Mora, E. (2007). A new image prediction model based on spatio- temporal techniques. *The Visual Computer*, 23(6), 419–431.

Candès, E.J., and Guo, F. (2002). New multiscale transforms, minimum total variation synthesis: applications to edge-preserving image reconstruction. *Signal Processing*, 82, 1519–1543.

Chang, N.-B., and Bai, K. (2018). *Multisensor Data Fusion and Machine Learning for Environmental Remote Sensing*. CRC Press, Boca Raton. ISBN 9781315154602

Choi, M., Kim, RY., Nam, MR., and Kim, H.O. (2005). Fusion of multi-spectral and panchromatic satellite images using the Curvelet transform. *IEEE Geoscience and Remote Sensing Letters*, 2(2), 136–140. *https://doi.org/10.1109/LGRS.2005.845313*

Donoho, M.N., and Vetterli, M. (2002). *Contourlets*. Academic Press, New York. ISSN 0890-5401

Dou, W., Chen, Y., Li, X., Sui, D.Z. (2007). A general framework for component substitution image fusion: An implementation using the fast image fusion method. *Computers and Geosciences*, 33, 219–228.

Du, Q., Younan, N.H., King, R., and Shah, V.P. (2007). On the Performance Evaluation of Pan-Sharpening Techniques. *IEEE Geoscience and Remote Sensing Letters*, 4(4), 518–522.

Emelyanova, I.V., McVicar, T.R., Van Niel, T.G., Li, L.T., and van Dijk, A.I.J.M. (2012). *On blending Landsat–MODIS surface reflectances in two landscapes with contrasting spectral, spatial and temporal dynamics*. WIRADA project 3.4: Technical report. Australia: CSIRO Water for a Healthy Country Flagship. *https://doi.org/10.4225/08/5852dc6879ab8*

Emelyanova I.V., McVicar, T.R., Van Niel, T.G., Li, L.T., and van Dijk, A.I.J.M. (2013). Assessing the accuracy of blending Landsat-MODIS surface reflectances in two landscapes with contrasting spatial and temporal dynamics: A framework for algorithm selection. *Remote Sensing of Environment*, 133, 193–209.

Fasbender, D., Radoux, J., Bogaert, P. (2008). Bayesian data fusion for adaptable image pansharpening. *IEEE Transactions on Geoscience and Remote Sensing*, 46, 1847–1857.

Fonseca, L., Namikawa, L., Castejon, E., Carvalho, L., Pinho, C., and Pagamisse, A. (2011). Image Fusion for Remote Sensing Applications. Ch 9 in *New Advances in Image Fusion*. (Ed: Zheng, Y.) InTechOpen.

Gao, F., Masek, J., Schwaller, M., and Hall, F. (2006). On the blending of the Landsat and MODIS surface reflectance: Predicting daily Landsat surface reflectance. *IEEE Transactions on Geoscience and Remote Sensing*, 44(8), 2207–2218. *https://doi.org/10.1109/TGRS.2006.872081*

Gevaert, C.M., and Carcía-Haro, F.J. (2015). A comparison of STARFM and an unmixing-based algorithm for Landsat and MODIS data fusion. *Remote Sensing of Environment* 156, 34–44. *http://dx.doi.org/10.1016/j.rse.2014.09.012*

Gonzalez, R.C., and Woods, R.E. (1992). *Digital Image Processing*. 3rd Edn, Pearson/Prentice Hall, Harlow.

González-Audícana, M., and Otazu, X. (2005). Comparison between Mallat's and the à trous discrete wavelet transform based algorithms for the fusion of multispectral and panchromatic images. *International Journal of Remote Sensing*, 26(3), 595–614. *https://www.tandfonline.com/doi/abs/10.1080/01431160512331314056*

Heinsch, F.A., Zhao, M., Running, S.W., Kimball, J.S., and Nemani, R.R. (2006). Evaluation of remote sensing based terrestrial productivity from MODIS using regional tower eddy flux network observations. *IEEE Transactions on Geoscience and Remote Sensing*, 44(7), 1908–1925.

Hilker, T., Wulder, M.A., Coops, N.C., Seitz, N., White, J.C., Gao, F., Masek, J.G., and Stenhouse, G. (2009). Generation of dense time series synthetic Landsat data through data blending with MODIS using a spatial and temporal adaptive reflectance fusion model. *Remote Sensing of Environment*, 113(9), 1988-1999.

Jiang, D., Zhuang, D., and Huang, Y. (2013). Investigation of Image Fusion for Remote Sensing. Ch 1 in *New Advances in Image Fusion*. (Ed: Zheng, Y.) InTechOpen.

Le Hégarat-Mascle, S., Richard, D., and Ottlé, C. (2003). Multi-scale data fusion using Dempster-Shafer evidence theory. *Integrated Computer-Aided Engineering*, 10(1), 9–22. *https://doi.org/10.3233/ICA-2003-10103*

Mallat, S.G. (1989). A theory for multiresolution signal decomposition: the wavelet representation. *IEEE Transactions on Pattern Analysis and Machine Intelligence*, 11, 674–693,

McVicar, T.R., Davies, P.J., Qinke, Y., and Zhang, G. (2002). An Introduction to Temporal-Geographic Information Systems (TGIS) for Assessing, Monitoring and Modelling Regional Water and Soil Processes. In *Regional water and soil assessment for managing sustainable agriculture in China and Australia*. (Eds: McVicar, T.R., Rui, L., Walker, J., Fitzpatrick, R.W., and Changming, L.). ACIAR Monograph 84, Canberra, pp. 205–223, *http://www.eoc.csiro.au/aciar/book/PDF/Monograph_84_Chapter_16.pdf*

Pajares, G., and de la Cruz, J.M. (2004). A wavelet-based image fusion tutorial. *Pattern Recognition*, 37 (9), 1855–1872. *https://doi.org/10.1016/j.patcog.2004.03.010*

Park, J., and Kang, M. (2004). Spatially adaptive multi-resolution multispectral image fusion. *International Journal of Remote Sensing*, 25(23), 5491–5508. *https://doi.org/10.1080/01431160412331270830*

Perracchione, E., Polato, M., Tran, D., Piazzon, F., Aiolli, F., De Marchi, S., Kollet, S., Montzka, C., Sperduti, A., Vianello, M. Putti, M. (2018). *Data Fusion guidelines*. GEOEssential Deliverable 1.6, ERA-PLANET. *http://www.geoessential.eu/wp-content/uploads/2019/01/GEOEssential-D_1.6_final.pdf*

Price, J.C. (1999). Combining multispectral data of differing spatial resolution. *IEEE Transactions on Geoscience and Remote Sensing*, 37(3), 1199–1203. *https://doi.org/10.1109/36.763272*

Ranchin, T., and Wald, L. (2000). Fusion of high spatial and spectral resolution images: the ARSIS concept and its implementation. *Photogrammetric Engineering and Remote Sensing*, 66(1), 49–61.

Renzullo, L.J., Barrett, D.J., Marks, A.S., Hill, M.J., and Guerschman, J.P. (2008). Multi-sensor model–data fusion for estimation of hydrologic and energy flux parameters. *Remote Sensing of Environment*, 112(4), 1306–1319.

Rogge, D.M., Rivard, B., Zhang, J., and Feng, J. (2006). Iterative spectral unmixing for optimizing per-pixel endmember sets. *IEEE Transactions on Geoscience and Remote Sensing*, 44(12), 3725–3736.

Roy, D.P., Ju, J., Lewis, P., Schaaf, C., Gao, F., Hansen, M., and Linquist, E. (2008). Multi-temporal MODIS–Landsat data fusion for relative radiometric normalization, gap filling, and prediction of Landsat data. *Remote Sensing of Environment*, 112(6), 3112–3130.

Shutao, L., Kwok, J.T., and Yaonan, W. (2002). Multifocus image fusion using artificial neural networks. *Pattern Recognition Letters*, 23, 985–997.

Thomas, C., Ranchin, T., Wald, L., and Chanussot, J. (2008). Synthesis of Multispectral Images to High Spatial Resolution: A Critical Review of Fusion Methods Based on Remote Sensing Physics. *IEEE Transactions on Geoscience and Remote Sensing*, 46(5), 1301–1312.

Tu, T.-M., Lee, Y.-C., Change, C.-P., and Huang, P.S. (2005). Adjustable intensity-hue-saturation and Brovey transform fusion technique for IKONOS/QuickBird imagery. *Optical Engineering*, 44(11), 116201.

Wald, L. (1998). Data fusion: a conceptual approach for an efficient exploitation of remote sensing images. *Proceedings of the 2nd International Conference on Fusion of Earth Data: Merging Point Measurements, Raster Maps and Remotely Sensed Images*. Sophia Antipolis, France. pp 17–24.

Wald, L. (1999). Some terms of reference in data fusion. *IEEE Transactions on Geoscience and Remote Sensing*, 37(3), 1190-1193.

Wald, L., Ranchin, T., and Mangolini, M. (1997). Fusion of satellite images of different spatial resolutions: Assessing the quality of resulting images. *Photogrammetric Engineering and Remote Sensing*, 63, 691–699.

Wu, H., Siegel, M., Stiefelhagen, R., Yang, J. (2002). Sensor Fusion Using Dempster-Shafer Theory. IEEE Instrumentation and Measurement Technology Conference, 21-23 May 2002, Anchorage, AK, USA.

Zhang, Y. (2004). Understanding Image Fusion. *Photogrammetric Engineering and Remote Sensing,* 70(6), 657–661.

Zheng, Y., Blasch, E., and Lu, Z. (2018). *Multispectral Image Fusion and Colorization*. SPIE Press. ISBN 9781510619067 (Ch 1: *https://spie.org/samples/PM285.pdf*)

Zhu, X.L., Chen, J., Gao, F., Chen, X.H., and Masek, J.G. (2010). An enhanced spatial and temporal adaptive reflectance fusion model for complex heterogeneous regions. *Remote Sensing of Environment*, 114(11), 2610–2623.

Zurita-Milla, R., Kaiser, G., Clevers, J.G.P.W., Schneider, W., and Schaepman, M.E. (2009). Downscaling time series of MERIS full resolution data to monitor vegetation seasonal dynamics. *Remote Sensing of Environment*, 113(9), 1874–1885.

7 Change Detection Methods

This Section considers bi-temporal methods for change detection, that is, detecting changes between two images acquired on different dates. Such methods compare an 'initial state' image (the first date) with a 'final state' image (the second date). Section 9 details time series ('temporal trajectory') methods, which isolate and analyse trends within a temporal sequence of multiple images.

The analysis of differences between pairs of EO images is relevant to a wide range of environmental applications, including assessment of:

- land cover changes in forests (Vogelmann, 1988), grasslands (Henebry, 1993), wetlands (Houhoulis and Michener, 2000; Munyati, 2000), and rangelands (Graetz *et al*., 1988);
- land use changes in agricultural (Manavalan *et al*., 1995) and urban areas (Jensen, 1983; Gupta and Munshi, 1985);
- defoliation (Muchoney and Haack, 1994), mortality (Macomber and Woodcock, 1994) and damage (Vogelmann and Rock, 1988; Vogelmann, 1990) in vegetated canopies;
- extent and severity of natural disasters, including fire (Jakubauskas *et al*., 1990; Garcia-Haro *et al*., 2001), flood (Zhou *et al*., 2000), drought (Peters *et al*., 2002) and landslides (Kimura and Yamaguchi, 2000); and
- glacial changes (Engeset *et al*., 2002).

Change detection processing has traditionally required that one image be rewritten to precisely match the geometry of another (see Section 3.1 and Volume 2B—Section 5). As detailed in Volume 1, each EO image acquisition observes the reflectance/emissions from features on the Earth's surface. While these observations can be calibrated for internal consistency and comparison with reference standards, and associated with feature characteristics, they cannot be directly inverted into those features (see Section 1.1). Thus, changes detected between images are only indicative of surface feature changes.

However, some surface feature changes occur as part of natural cycles and may not be relevant to the type of changes being investigated. Accordingly, bi-temporal change detection methods simply attempt to highlight those pixels whose values differ between the 'initial state' image and the 'final state' image. Additional information is required to identify the type of change and suggest causal factors.

Prior to applying change detection methods, it may also be appropriate to remove irrelevant portions of the images, such as water in a land-based study, or pixels outside of a specified management region (see Section 4.1 and Volume 2A—Section 10). Some change detection studies have also segmented imagery into regions to assess changes within groups of pixels rather than on a per-pixel basis (Desclée *et al*., 2006).

Most approaches to bi-temporal change detection comprise six fundamental stages, as summarised in Table 7.1). The results from these approaches can yield different levels of change information, such as:

- change or no change—locate the spatial distribution of differences;
- areal extent of change—use spatial distribution to compute the ground area of change;
- type of change—associate change patterns and extent with other information to determine the nature of change; and/or
- cause of change—correlate nature, area and distribution of change with other information to determine the reason(s) for changes.

Background image: Landsat-8 OLI over Lake Carnegie, WA, acquired on 8 July 2017 and displayed with bands 6, 5, 3 as RGB.
Source: Norman Mueller, Geoscience Australia

Table 7.1 Bi-temporal change detection stages

Stage	Description	Examples of Options
Image Selection	Select most appropriate image pair to highlight changes of interest	Anniversary dates
		Dates most relevant to change of interest
Pre-processing	Match geometries and radiance values of both images to a common base	Radiometric correction
		Geometric correction
		Spectral indices
Change Detection Method	Highlight pixels whose radiance values have changed between the two dates	Algebraic operations
		Linear transformations
		Classification approaches
Post-processing	Group changes into relevant categories	Thresholding to define change/no change
		Filtering to remove speckle
		Density slicing to define change classes
Labelling	Associate change categories with surface feature changes	Visual analysis
		Sample pixels
		GIS comparison
Accuracy Assessment	Determine accuracy of labelled change categories	Contingency table
		Kappa statistic

Adapted from Thonfeld *et al.* (2010)

For detected changes to be relevant to a particular purpose, it is paramount that an appropriate image pair is selected for analysis. Factors that impact this selection are considered in Section 2.2. Change detection approaches implicitly assume that the selected pair of images are comparable, and this generally involves several pre-processing steps as outlined in Sections 3.1 and 4 above.

Numerous authors have reviewed the wide range of image analysis methods that have been used to detect changes in EO imagery (including Lu *et al.*, 2003; Coppin *et al.*, 2004; Thonfeld *et al.*, 2010). In this section, we consider bi-temporal change detection methods in terms of three broad categories:

- algebraic operations between corresponding channels from each image—such as differencing or ratioing, (see Section 7.1);
- linear transformation of selected (or all) image channels from the two images—such as PCA, to highlight changes in fewer image dimensions (see Section 7.2); and
- classification of the two images, then per-pixel comparison of the resulting class allocations (see Section 7.3).

Various reviews of these methods suggest that no single approach can be recommended, but that different methods are appropriate for different cases (Lu *et al.*, 2003). As discussed in the introduction to Section 2, the analyst's underlying view of the landscape becomes evident when a change detection approach is selected: is the landscape (and the bi-temporal dataset(s) that observed it) an equilibrium state that changes or a dynamic system that is being observed? These concepts are further considered in Volumes 2E and 3. Post-processing of change detection results is discussed in Section 7.4 and approaches to accuracy assessment are introduced in Section 7.5 (see also Volume 2E).

7.1 Algebraic Operations

After suitable pre-processing, corresponding pairs of channels in the 'initial state' and 'final state' images can be subtracted or ratioed to highlight differences (see Sections 7.1.1 and 7.1.2 respectively). These operations can be computed for individual spectral bands or for spectral indices that highlight the most significant information in each image (see Volumes 2C and 3A). Results from these analyses indicate the location and extent of change, but do not generate detailed change matrices. Other algebraic operations that can be used to detect changes include channel regression (see Section 7.1.3) and Change Vector Analysis (see Section 7.1.4).

7.1.1 Channel subtraction

As detailed in Section 5.2 the differences between corresponding channels from two calibrated and registered image channels can be computed as their difference:

'change' image channel x = 'final state' image channel x – 'initial state' channel x

where

channel x represents the normalised reflectance measurements for a selected spectral attribute.

The resulting 'change' image is characterised by:

- those pixels whose reflectance values are brighter in the 'initial state' image forming one distribution peak (with values in 'change' image < 0); and
- those pixels whose reflectance values are brighter in the 'final state' image forming second distribution peak (with values in 'change' image > 0; see Figure 7.1).

Figure 7.1 Difference channel histogram

Change thresholds are equal to one standard deviation in this example. The data range of input images is assumed to be 0–255.

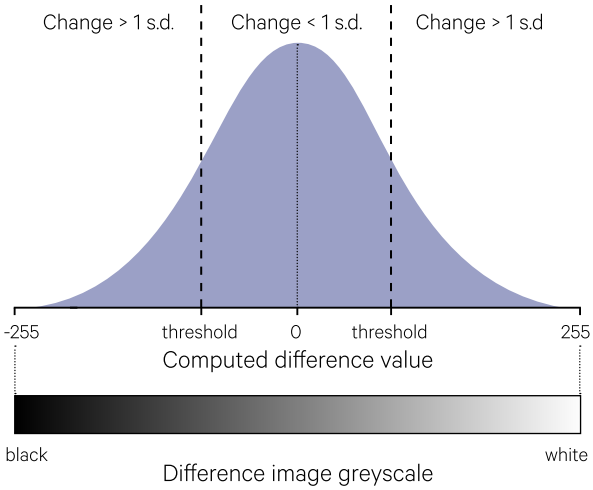

Before rescaling, those pixels with the same values in both images would have value zero in the 'change' image. An example of channel subtraction for a summer/winter pair of images in an agricultural district is shown in Figure 7.2.

Figure 7.2 Change detection based on differencing

This example is based on a summer-winter pair of Landsat-8 OLI images over the mixed agricultural district of Kerang in northern Victoria. A difference band is computed by subtracting the NIR band in the winter image from the NIR band in the summer image. In the difference band, unchanged values appear as mid-grey, pixels with higher values in the summer image appear brighter and pixels with higher values in the winter image appear darker.

a. Summer NIR band (7 January 2018)

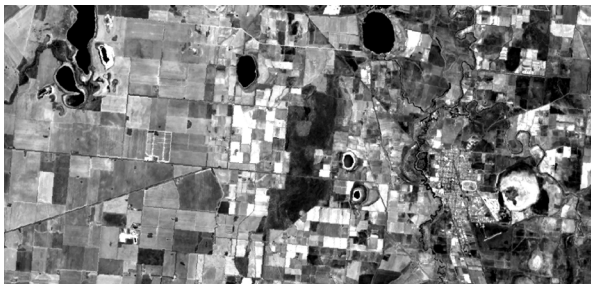

b. Winter NIR band (2 July 2018)

c. Difference of summer NIR band – winter NIR band

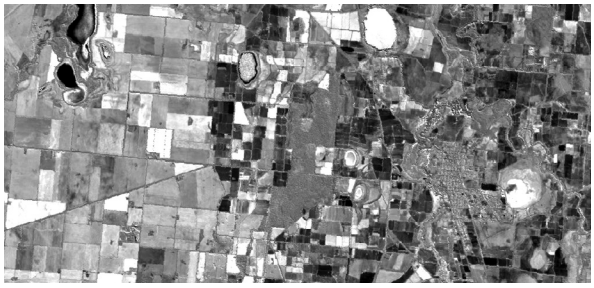

Source: Norman Mueller, Geoscience Australia

For example, to highlight changes associated with a fire event, the 'initial state' image would be acquired shortly before the fire and the 'final state' image would be acquired on an appropriate (smoke-free) date after the fire. If the image dates have been well selected, and no other major changes have occurred post-fire, the difference between these images would delineate the fire scar and thus provide information about the extent and severity of the fire.

Image differencing is computationally simple and offers a relatively straightforward summary of the distribution and extent of changes (see Section 5.1). Channel subtraction is the most commonly used method for bi-temporal change detection (Coppin *et al.*, 2004) and can be computed for individual spectral bands (albedo) or, more often, for derived spectral indices (Thonfeld *et al.*, 2010). Since the latter both emphasise the differences between relevant ground features and minimise the differences between images (see Volumes 2C and 3A), they are generally more efficient and robust for detecting image changes.

Various refinements of image differencing have been proposed to automate processing and/or to provide more robust results. For example, a moving window has been used to compute the minimum difference between a pixel in the 'initial state' image and the corresponding pixel values in its 3´3 neighbourhood in the 'final state' image, thereby compensating for imperfect geometric registration between the image pair (Castilla *et al.*, 2009).

7.1.2 Channel ratioing

Another relatively simple image processing option for comparing normalised image channels is to compute their ratio (see Volume 2C—Section 10):

$$\text{change image channel i} = \frac{\text{'final state' image channel i}}{\text{'initial state' image channel i}}$$

where

channel i represents normalised reflectance measurements for the same spectral attribute in both images.

This method produces a non-normal distribution so ratioed values are generally rescaled to permit further analyses (see Volume 2C—Section 2). Before the 'change' image results have been appropriate rescaled, its values will be:

- < 1 when reflectance values in the 'initial state' image are higher than in the 'final state' image;
- = 1 when reflectance values are the same in both images; and
- > 1 when reflectance values in the 'final state' image are higher than in the 'initial state' image (see Figure 7.3).

Channel ratioing reduces radiometric differences between images resulting from Sun position and topographic shading (see Volume 2C—Section 10). An example of channel ratioing for the same summer/winter pair of images shown in Figure 7.2 is given in Figure 7.4.

Figure 7.3 Ratio channel histogram

This stylised histogram assumes input image data is in the range 0–255 and uses non-linear scaling to represent the computed ratio values.

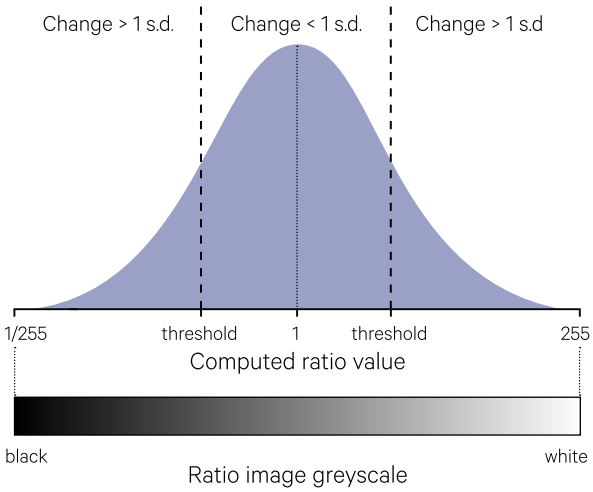

Figure 7.4 Change detection based on ratioing

This example is based on the same summer-winter pair of Landsat-8 OLI images over the mixed agricultural district of Kerang in northern Victoria that is used in Figure 7.2 above. To compute the ratio band, the NIR band in the summer image is divided by the NIR band in the winter image. In the ratio band, unchanged values appear as mid-grey, pixels with higher values in the summer image appear brighter and pixels with higher values in the winter image appear darker.

a. Summer NIR band (7 January 2018)

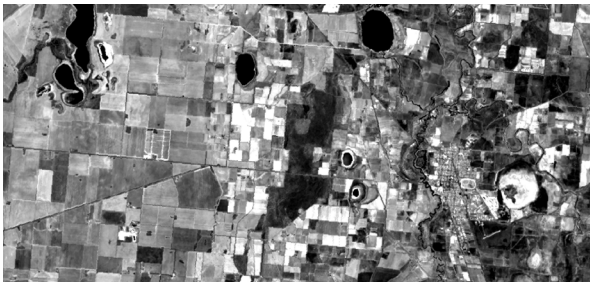

b. Winter NIR band (2 July 2018)

c. Difference of summer NIR band – winter NIR band

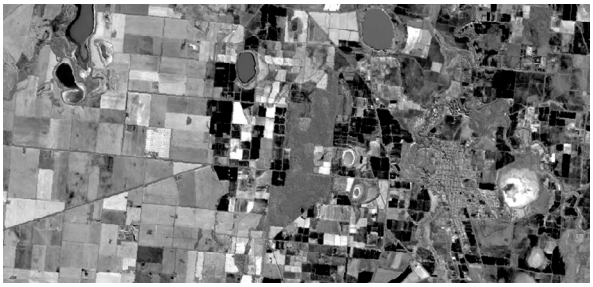

Source: Norman Mueller, Geoscience Australia

7.1.3 Channel regression

Regression techniques can be used to establish the relationship between pixels in the 'initial state' and 'final state' images for each pair of corresponding channels (see Volume 2A and Volume 2C—Section 7.2). In the context of change detection, the resulting regression relationship can be used to compute a theoretical 'final state' image from the 'initial state' image. The differences between the theoretical and actual 'final state' images highlight areas of change. This method also reduces radiometric differences between the two selected images resulting from atmospheric conditions, sensor variations and environmental factors.

A range of approaches can be used to determine appropriate regression parameters between channels including:

- Least squares regression (LS)—based on image statistics (see Volumes 2C and 2E);
- Pseudo-Invariant Feature (PIF)—based on the spectral values of features that are assumed to be invariant with time (Schott *et al.*, 1988);
- Radiometric Control Set (RCS)—based on the brightest and darkest features in the images (Hall *et al.*, 1991); and
- Automatic Scattergram-Controlled Regression (ASCR)—based on 'stable' clusters of land and water pixels (Elvidge *et al.*, 1995; Yang and Lo, 2000).

The ASCR method typically uses crossplots of NIR channels from the two images to identify stable clusters of land and water pixels then generates an initial regression line between the centres of the two clusters (see Figure 7.5). Thresholds can be placed either side of this regression line to demark 'no change', with adjacent regions representing positive and negative change.

Figure 7.5 Automatic Scattergram-Controlled Regression

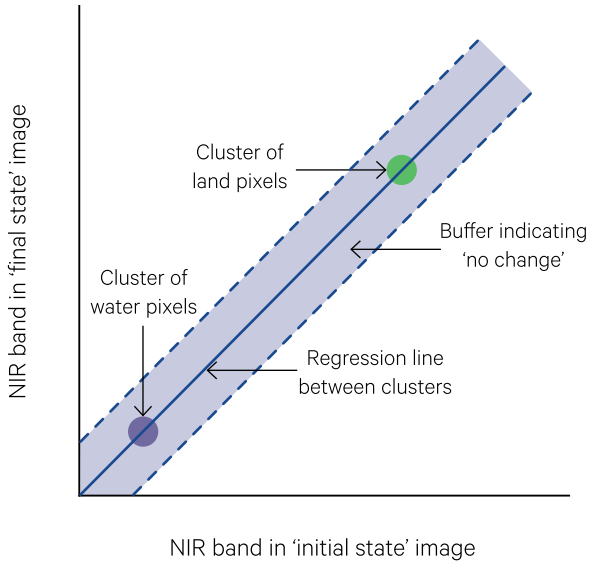

Adapted from: Yang and Lo (2000) Figure 1d

7.1.4 Change Vector Analysis

Change Vector Analysis (CVA) quantifies the per-pixel changes between a pair of bi-temporal images in terms of magnitude and direction (Malila, 1980). In the simplest implementation, two corresponding channels are selected from the 'initial state' and 'final' images then, for each pixel, the length and direction of the vector between these dates is determined (see Figure 7.6). These spectral change vector dimensions can also be computed for spectral indices and multi-channel datasets. The direction of the change vector is controlled by the type of change (see Figure 7.7), while the vector length is related to the severity of change (see Figure 7.8).

The greenness and brightness components from the Tasselled Cap transformation have typically been used with CVA to reduce data volume for processing (Kauth and Thomas, 1976; Crist and Cicone, 1984). In this transformation, brightness changes tend to be correlated with soil colour and moisture, while the greenness component tracks vegetation cover and vitality (see Volume 2C—Section 11). The total magnitude of change for each image pixel is computed as the Euclidean distance between the 'initial state' and 'final state' image values (see Figure 7.6 and Volume 2E). Changes in the direction of the brightness and greenness components can be grouped in quadrants to indicate four broad types of change (see Figure 7.7a). Possible land cover change classes corresponding to these four types of change direction are shown in Figure 7.7b. Similarly, changes in magnitude can be grouped into categories (see Figure 7.8a) and cross-tabulated against changes in direction to determine the extent of specific change classes (see Figure 7.8b). Thresholds can be defined to automatically determine the significance of detected changes (Chen *et al.*, 2003).

Figure 7.6 Change Vector Analysis (CVA)

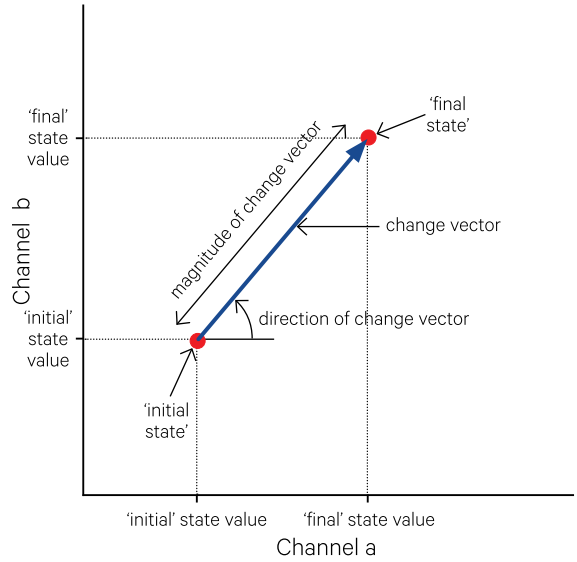

Adapted from Jensen (2016) Figure 12-35a

CVA has been used to delineate land cover changes (Lambin and Strahler, 1994a, 1994b; Kontoes, 2013), volcanic eruption damage (Kuzera *et al.*, 2005) and tsunami-related damage (Roemer *et al.*, 2010). Improved methods for computing CVA have been proposed by Chen *et al.* (2003), Carvalho *et al.* (2011) and Kontoes (2013).

Figure 7.7 Direction of change

a. Four potential directions of change between the 'initial state' image and the 'final state' image are shown using brightness and greenness axes. The 'initial state' values are shown as the central red dot and the change vector is shown as the blue arrow.

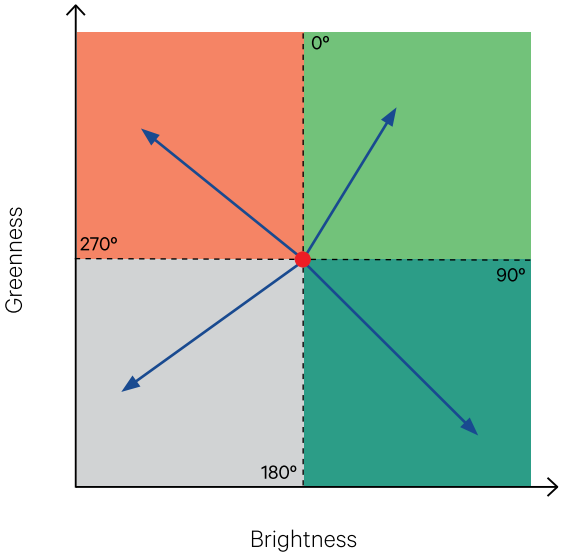

b. Interpretation of four potential change directions. These change classes were defined for a study to monitor land use/land cover dynamics in the Brazilian Amazon.

Change Angle (°)	Land Cover Change Class	Brightness Change	Greenness Change
0–89	Regeneration of woody vegetation	-	+
90–179	Deforestation	+	-
180–269	Conversion to pasture	+	+
270–359	Water or Fire Scar	-	-

Adapted from: a. Kuzera *et al.* (2005); b. Lorena *et al.* (2002)

Figure 7.8 Magnitude of change

a. The magnitude of change increases with distance from the 'initial stage' image values (shown as red dot below). Four magnitude categories (low, medium, high and extreme) are delineated in this example to indicate the change severity.

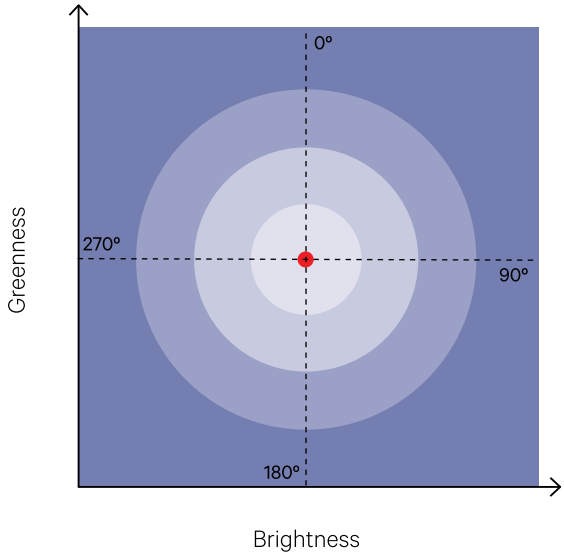

b. Land cover change classes defined in Figure 7.7a are cross-tabulated against the change severity categories delineated in Figure 7.8a to determine the extent of specific change classes.

Land Cover Change Class	Change Severity Categories			
	Low	Medium	High	Extreme
Regeneration of woody vegetation	*(area)*	*(area)*	*(area)*	*(area)*
Deforestation	*(area)*	*(area)*	*(area)*	*(area)*
Conversion to pasture	*(area)*	*(area)*	*(area)*	*(area)*
Water or Fire Scar	*(area)*	*(area)*	*(area)*	*(area)*

Adapted from Kuzera *et al.* (2005)

7.2 Linear Transformations

A wide range of linear transformations can be used to reduce data redundancy between image data channels, allowing relevant information to be represented in fewer channels (see Volume 2C—Sections 7, 8 and 9). Multiple images can also be compared using techniques such as:

- Principal Components Analysis (PCA; see Section 4.2.2 above and Volume 2C—Section 9);
- RGB to HSI Transformation (see Volume 2C—Section 8);
- Tasselled Cap or Kauth-Thomas Transformation (Kauth and Thomas, 1976; Crist and Cicone, 1984; see Volume 2C—Section 11);
- Multivariate Alternation Detection (MAD; Nielsen *et al*., 1998; see Volume 2C—Section 7.4); and
- Gram-Schmidt Orthogonalisation (Collins and Woodcock, 1994, 1996).

Such transformations may be applied separately to the individual images, then the resulting components compared, or applied to a merged dataset comprising channels from multiple images.

Principal Component Analysis (PCA) is reviewed in Section 4.2.2 above and detailed in Volumes 2C, 2E and 2X. The PCA transformation rotates the image data space to define uncorrelated channels, with the first component being aligned with the major axis of variance (see Figure 4.1 above). This results in a PC image in which covariance values are theoretically zero. The transformation is based on variance/covariance statistics from the image being processed, that is, its covariance or correlation matrix (Eklundh and Singh, 1993).

In terms of change detection, PCA can be applied to a merged set of geometrically-registered images. The rationale here is that the differences between the images will be highlighted in a small number of Principal Components (or PC channels). However, Fung and LeDrew (1987) suggest this approach has difficulties where major land cover changes have occurred since the transformations are not standardised between different images.

Alternatively, the two images (or selected channels thereof) are calibrated separately then combined into a single image. Transformations of the combined image are likely to highlight major changes as a single component (Richards, 1984; Ingebritsen and Lyon, 1985). Generally the higher order components of the merged image data are related to the brightness and greenness of surface features while the middle PCs are related to land cover changes. As with PCA of a single image, the lower PCs are insignificant in terms of the image variance they represent. Changes in specific features however may be summarised, and hence highlighted in a relative sense, in the lower PCs. An example of PCA applied to a merged two-date image is shown in Excursus 7.1.

Various authors have recommended the use of the image correlation matrix to produce standardised PCs (that is, with zero mean and unit variance; see Volume 2C—Section 9) since these minimise the effects due to atmospheric and illumination differences (Singh and Harrison, 1985; Elkundh and Singh, 1993; Fung and LeDrew, 1987). PCA for change detection should also be based on statistics derived from the whole image rather than apply only to a particular image feature (Fung and LeDrew, 1987).

PCA applied to a merged dataset is not the same as producing separate PC channels for each image then differencing them. Since PCA is necessarily scene-dependent, the components can represent different dimensions in different images. When the object of the exercise is to highlight changes, it is counter-productive to allow the pre-processing to mask differences. However, it is essential that image pairs be carefully registered geometrically (see Section 3.1.1.1) before applying PCA, as significant misregistration errors between a pair of images would increase the variation between channel pairs from different images and consequently inflate the covariance statistics.

Other linear transformations can be used to provide different representations of the image data. As detailed in Volume 2C—Section 11, the 'Tasselled Cap' transformation highlights stages of vegetation development and cover (Kauth and Thomas, 1976). MAD, based on canonical correlations analysis, sequentially extracts uncorrelated difference images to highlight changes (Nielsen and Conradsen, 1997). Unlike PCA, this transformation is invariant to linear and affine scaling, making it more relevant to change detection studies, especially when the MAF transformation is applied as post-processing (Nielsen *et al*., 1998; see Volume 2A—Section 7.4). The Gram-Schmidt Orthogonalisation produces multi-temporal analogues of brightness, greenness and wetness, plus a change component (Collins and Woodcock, 1994, 1996).

While capable of delivering good results, linear transformation methods are not readily transferable between datasets and tend to be used less frequently than arithmetic and classification methods for change detection (Thonfeld *et al*., 2010). Further, the results derived from these methods do not provide details of the type of change detected, and require thresholds to be defined to delineate the location and extent of changes.

Excursus 7.1—Change Detection using PCA

Source: Megan Lewis, University of Adelaide

Two Landsat MSS images of mallee vegetation, south of Renmark, SA, were selected to demonstrate change detection using PCA (see Figure 7.9). Land cover changes between these dates include scars from bushfires, clearing of native vegetation and changes in agricultural practices. The green, red and NIR bands from each image were combined into a single image then PCA was applied to the merged dataset.

The PCA matrix for the merged image indicates the contribution of each original band to each principal component (PC; see Table 7.2). Using the coefficients in the PCA matrix, we can deduce:

- PC1 represents the total brightness in both images as is typical of such analyses and essentially highlights the areas of no change;
- PC2 represents the differences between the corresponding bands in the two images so summarises all changes;
- PC4 represents the changes in contrast between vegetated areas in the Date 1 image and non-vegetated areas in the Date 2 image; and
- PC3, PC5 and PC6 represent less significant differences.

Table 7.2 PC transformation matrix

PC	Date 1 image bands			Date 2 image bands		
	Green	Red	NIR	Green	Red	NIR
1	0.390	0.602	0.469	0.207	0.346	0.321
2	0.218	0.355	0.301	-0.366	-0.622	-0.464
3	-0.309	-0.438	0.770	-0.096	-0.150	0.297
4	-0.116	-0.113	0.309	0.317	0.432	-0.046
5	0.825	--0.549	0.029	0.109	-0.059	-0.021
6	0.100	-0.070	0.016	-0.838	0.530	-0.046

The resulting PC channels are shown in Figure 7.10. In this case, the most significant PCs for change detection are:

- PC2—which summarises the changes in vegetation cover; and
- PC4—which highlights the areas that have lost vegetation between the two image dates.

Figure 7.9 Original images

Landsat MSS images of mallee vegetation, south of Renmark, SA, are displayed using NIR, red and green bands as RGB. In these images dark red indicates mallee vegetation, while the large aqua region in the date 2 image highlights a fire scar.

a. Date 1 image

b. Date 2 image

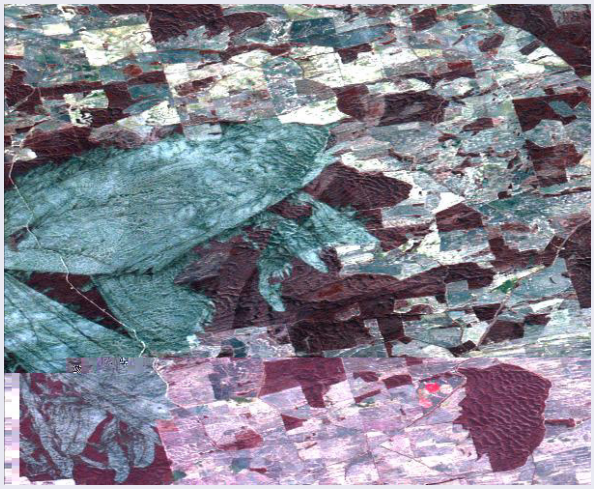

Figure 7.10 Principal components

Six principal component channels were derived for the merged image that contained the green, red and NIR bands of the images shown in Figure 7.9.

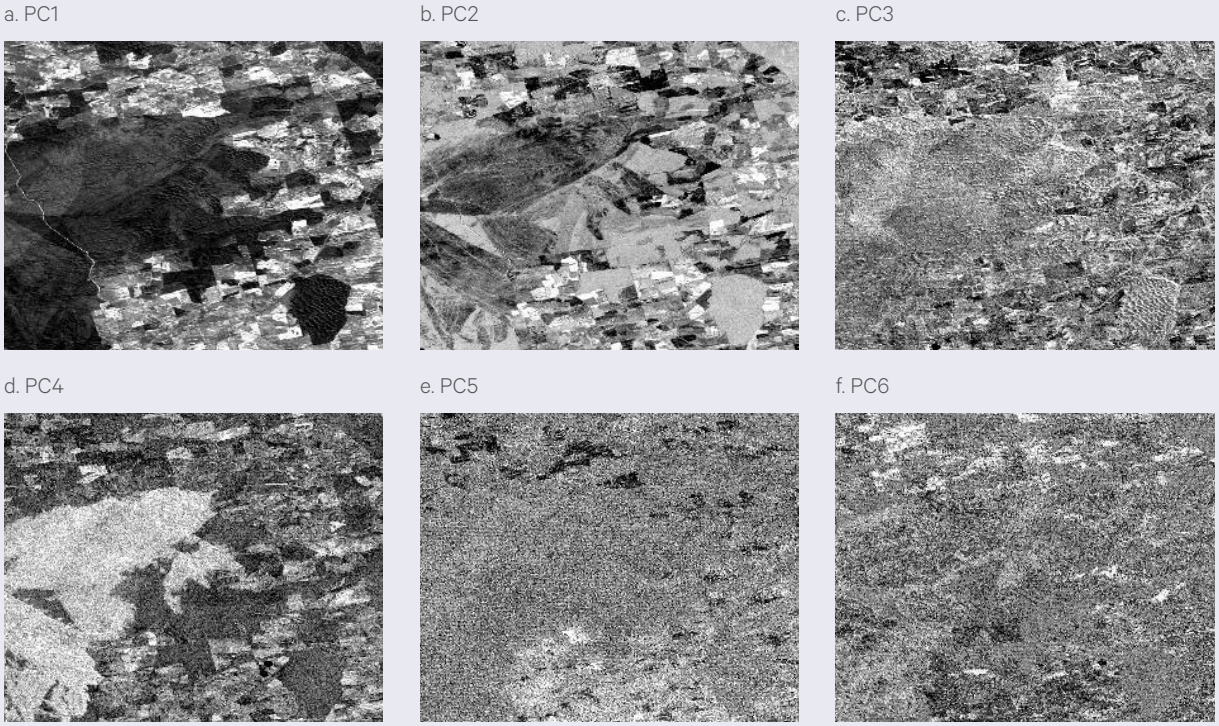

7.3 Classification Approaches

Classification can be used for change detection by:

- comparing separate classifications of the 'initial state' and 'final state' images (see Section 7.3.1);
- classifying a single composite image which contains corresponding channels from both the 'initial state' and 'final state' images (see Section 7.3.2); and
- classifying the differences between the bi-temporal images (see Section 7.1.1), which can either be based on the differences between corresponding pairs of original data bands, or between spectral indices derived from them (Sparks, 2005; see Volume 2C).

These approaches offer the opportunity to extract a complete matrix of change information as well as the location and area of each change class (Lu *et al.*, 2003). Data fusion methods have also been effective for integrating land cover change information from multiple classified images (Kiiveri and Campbell, 1992; Kiiveri and Caccetta, 1998 Kiiveri *et al.*, 2001; see Volume 2E). Image classification methods for EO imagery are summarised in Volume 2A—Section 9 and detailed in Volume 2E.

7.3.1 Comparing classifications

Rather than compare the reflectance values of the 'initial state' and 'final state' images directly, the changes between images can also be identified by first classifying each image separately and then comparing the classifications. This approach avoids standardising the two images to common radiometric values (Song *et al.*, 2001) and can be tailored to ignore irrelevant, transient changes. However, any pixel-based comparison between two images requires that both images be registered to a common geometric grid (Section 3.1 and Volume 2B).

This approach generally involves developing independent sets of classes in the two images that represent the categories of importance to a particular study. The resulting separate classifications can then be cross-compared using the sampling and analysis techniques detailed in Volume 2E.

Images can also be stratified before classification to reduce the possibility of misclassification (Xu and Young, 1990; see Section 4.1). Object-oriented methods distinguish bi-temporal changes for defined objects (often in conjunction with knowledge-based systems) rather than on a per-pixel basis (Hall and Hay, 2003; Desclée *et al*., 2006). The accuracy of any post-classification comparison exercise clearly depends on the accuracies of the two classifications being compared, and such comparisons invariably compound misclassification and misregistration errors.

Post-classification comparisons can produce summary statistics on the proportion of different land cover types that had changed between image dates (see Volume 2E). As described in Section 4.1.2, the classifications can be segmented using non-image boundaries (such as cadasta) to derive change statistics on the basis of some pre-defined regions. This method of change detection obviates the need for radiometric registration since each image is processed and interpreted individually. Provided sample points can be accurately located in each image (possibly using individual map-to-image registration models), geometric registration is not required either (see Volume 2B). However, two classifications and the comparison stage are time-consuming in terms of both computation and interpretation.

Singh (1989) considered post-classification comparison to be less accurate than difference or PC-based change detection methods and only slightly better than multi-date classification. A major problem with this approach is that the differences between classifications can be due to interpreter inconsistencies as well as image changes. To ensure compatibility between classifications, processing methodologies and labelling systems need to be as consistent as possible. Inaccuracies in either of the original classifications can also show as false changes in the post-classification comparison. Some authors have argued that the accuracy of change-mapping based on two classifications could equal the product of the accuracies of each classification (for example, if the original classifications were each deemed to be 80% accurate, the change analysis would be 64% accurate; Stow *et al*. 1980), though this will depend on the degree of spatial association between misclassified pixels in each image.

7.3.2 Classifying merged imagery

Some change detection studies have focussed on analysis of a merged image containing selected channels from the 'initial state' and 'final state' images, after appropriate pre-processing (see Section 3). Such analyses essentially assume that the statistics of changed patches of pixels will be significantly different from those that have not changed. To reduce the computational load of classifying a large number of channels, a subset or transformation, of channels is often used (see Section 4.2). Visual display of relevant channels from composite images can highlight prominent changes and isolate the most informative channels for subsequent analyses (see Volume 2A).

Classification methods based on this approach include 'multi-date clustering', 'spectral change pattern analysis' and 'spectral/temporal change classification'. The inherent heterogeneity of composite datasets is not well suited to segmentation and classification techniques, and the resulting classes have been difficult to label meaningfully (Coppin *et al*., 2004). Multi-temporal Spectral Mixture Analysis (MSMA) methods, however, have been reported as useful for detecting land cover changes (Adams *et al*., 1995; Roberts *et al*., 1998). Some other classification methods that have been used for bi-temporal change detection include artificial neural networks (Gopal and Woodcock, 1994), unsupervised change detection (Hame *et al*, 1998), and the Expectation-Maximisation algorithm (EM detection; Granville and Rasson, 1995; Bruzzone *et al*., 1999). These methods are reported to attain good accuracy, but involve greater processing complexity (see Volume 2E).

Given the diversity of possible land cover changes however, a large number of classes may be formed from multi-date classification. For example, in a given land cover type, pixels which have not changed should form one class and pixels which have changed will form one or more other classes depending on the types of change possible for that land cover. To avoid a complex interpretation task after classification, knowledge-based classifiers have been used to guide detection of class changes between images (see Volume 2E). Such solutions can be computationally intensive, however, and require prior knowledge of possible class changes. Singh (1989) observed that few authors reported accuracy testing of change detection methods, however his results showed multi-date classification to be the least accurate method of those described in this section.

7.4 Post-processing

Change detection results generally require some form of post-processing to assist interpretation. Commonly used methods include thresholding and labelling (see Section 7.4.1), filtering (see Section 7.4.2) and autocorrelation analysis (see Section 7.4.3).

7.4.1 Thresholding and labelling

Algebraic methods and linear transformations result in images that show regions of change and no change. The separation between these regions, however, requires thresholds to be defined, either by interactive testing (see Volume 2A—Section 9) or statistical measures (see Volume 2A—Section 8). Some thresholding techniques have also been proposed to determine thresholds automatically, based on attaining a pre-defined goal such as minimum noise (Bruzzone and Fernández Prieto, 2000a), minimum error (Bruzzone and Fernández Prieto, 2000b) or minimum 'cost' (Bruzzone and Fernández Prieto, 2000c). Obviously the accuracy of thresholds is as important as the accuracy of the change detection method in determining the value of the final product (Fung and LeDrew, 1988).

Once the thresholds have been selected to identify the areas of change and no change, some form of change labelling may be relevant to differentiate the change area in terms of change direction (positive or negative) and change severity (see Section 7.1.4). This is generally undertaken with reference to other datasets and can be implemented using density slicing (see Volume 2A—Section 9.2.1) or parallelepiped classification (see Volume 2A—Section 9.2.2). Image classification methods generally include a labelling stage, so implicitly involve this post-processing step as part of their processing sequence (see Volume 2E for details).

7.4.2 Filtering

A further post-processing method that may be relevant to some classified imagery is filtering to remove image speckle. Areas of change in difference images, for example, may be rendered more coherent using a modal filter. This technique is detailed in Volume 2C—Section 4.3 and Volume 2E. An image showing categorical changes could also be filtered using a modal, minimum or maximum filter, as appropriate for the data being processed (see Volume 2C—Sections 3 and 4).

7.4.3 Autocorrelation analysis

The Maximum Autocorrelation Factor (MAF) transformation can be used to highlight image regions where neighbouring pixels have similar values, or high spatial autocorrelation (see Volume 2C—Section 7.3). This process can be applied to difference images to highlight contiguous regions of change. For example, Nielsen *et al.* (1998) combined MAD and MAF transformations to retain spatial context in multi-temporal image analyses, and thus identify areas of spatially coherent change.

7.5 Accuracy Assessment

The accuracy of any change detection exercise needs to be determined before the results are used. As with any classification-style product, a range of statistical methods can be applied to verify the accuracy of the change categories.

Fundamentally, all accuracy assessment approaches compare the results from EO analyses with some reference dataset that is considered representative of the 'truth'. In terms of Earth surface features, ground 'truth' is generally derived from field sampling and/or visual analysis of higher resolution imagery. Relevant ground truth data for change detection implicitly requires two reference datasets: one to represent the 'initial state' image, and another to represent the 'final state' image. The differences between these two reference datasets are then assumed to indicate the type and extent of change in surface features.

Most accuracy assessment statistics are derived from an error matrix, which summarises the agreement between the EO results and the reference dataset for a set of sample pixels (Congalton and Plourde, 2002). For change detection studies, the error matrix tabulates the frequency with which sample pixels in the change image agree with the change indicated by the differences between the two reference datasets (Biging *et al.*, 1998, 1999). The most commonly derived statistics include overall accuracy, producer's accuracy, user's accuracy and Kappa coefficient (Congalton *et al.*, 1983; Hudson and Ramm, 1987; Congalton, 1991; Congalton and Green, 1999). Assessment methods tailored to change detection have also been proposed by Morisette and Khorram (2000) and Lowell (2001). Olofsson *et al.* (2014) recommend a set of good practice guidelines for assessing accuracy in change detection studies and estimating area of change. Accuracy assessment of EO analyses is considered in detail in Volume 2E.

7.6 Further Information

Land Cover Change:

CORINNE Land Cover (CLC): European Environment Agency (EEA) manages a hierarchical land cover inventory of Europe. This inventory defines 44 classes from EO imagery using a minimum mapping unit (MMU) of 25 ha. The original 1985 inventory (referenced as 1990) has been updated in 2000, 2006, 2012, and 2018, and is used for environmental modelling, agricultural monitoring and planning community infrastructure. Datasets and technical details can be downloaded from: *https://land.copernicus.eu/pan-european/corine-land-cover*

Global Vegetation Change:

NASA Land, Atmosphere Near real-time Capability for EOS (LANCE): *https://earthdata.nasa.gov/earth-observation-data/near-real-time*

7.7 References

Adams, J.B., Sabol, D., Kapos, V., Almeida Filho, R., Roberts, D.A., Smith, M.O., and Gillespie, A.R. (1995). Classification of Multispectral Images Based on Fractions Endmembers: Application to Land-Cover Change in the Brazilian Amazon. *Remote Sensing of Environment,* 52, 137–154.

Biging, G.S., Colby, D.R., and Congalton, R.G. (1998). Sampling systems for change detection accuracy assessment. In *Remote Sensing Change Detection—Environmental Monitoring Methods and Applications*. (Eds: Lunetta, R.S., and Elvidge, C.D.). Ann Arbor Press, Chelsea, MI. pp. 281–308.

Biging, G.S. Chrisman, N.R. Colby, D.R. Congalton, R.G. Dobson, J.E. Ferguson, R.L. Goodchild, M.F. Jensen, J.R. and Mace, T.H. (1999). *Accuracy assessment of remote sensing-detected change detection* Monograph Series. (Ed: Khorram, S.). American Society for Photogrammetry and Remote Sensing (ASPRS), Bethesda, MD, USA.

Bruzzone, L., and Fernandez Prieto, D. (2000a). An adaptive parcel-based technique for unsupervised change detection. *International Journal of Remote Sensing*, 21(4), 817–822, *https://doi.org/10.1080/014311600210614*

Bruzzone, L., and Fernández Prieto, D. (2000b). Automatic analysis of the difference image for unsupervised change detection. *IEEE Transactions on Geoscience and Remote Sensing*, 38(3), 1171–1182.

Bruzzone, L., and Fernández Prieto, D. (2000c). A minimum-cost thresholding technique for unsupervised change detection. *International Journal of Remote Sensing*, 21, 3539–3544.

Bruzzone, L., Fernández Prieto, D., and Serpico, S.B. (1999). A Neural-Statistical Approach to Multitemporal and Multisource Remote-Sensing Image Classification. *IEEE Transactions on Geoscience and Remote Sensing*, 37(3), 1350–1359.

Carvalho, O.A., Guimaraes, R.F., Gillespie, A.R., Silva, N.C., and Gomes, R.A.T. (2011). A new approach to Change Vector Analysis using distance and similarity measures. *Remote Sensing*, 3, 2473–2493.

Castilla, G., Guthrie, R.H., and Hay, G.J. (2009). The Land-cover Change Mapper (LCM) and its Application to Timber Harvest Monitoring in Western Canada. *Photogrammetric Engineering and Remote Sensing*, 75(8), 941–950.

Chen, J., Gong, P., He, C., Pu, R., and Shi, P. (2003). Land-Use/Land-Cover Change Detection using Improved Change Vector Analysis. *Photogrammetric Engineering and Remote Sensing*, 69(4), 369–379.

Collins, J.B., and Woodcock, C.E. (1994). Change detection using the Gramm–Schmidt transformation applied to mapping forest mortality. *Remote Sensing of Environment*, 50, 267–279.

Collins, J.B., and Woodcock, C.E. (1996). An assessment of several linear change detection techniques for mapping forest mortality using multitemporal Landsat TM data. *Remote Sensing of Environment*, 56, 66–77.

Congalton, R.G. (1991). A review of assessing the accuracy of classifications of remotely sensed data. *Remote Sensing of Environment*, 37, 35–46.

Congalton, R., and Green, K. (1999). Assessing the accuracy of remotely sensed data: Principles and practices. Lewis Publishers, New York.

Congalton, R.G., Oderwald, R.G. and Mead, R.A. (1983). Assessing Landsat classification accuracy using discrete multivariate analysis statistical techniques. *Photogrammetric Engineering and Remote Sensing,* 49, 1671–1678. [see also Erratum: *Photogrammetric Engineering and Remote Sensing,* 50, 1477.]

Congalton, R.G., and Plourde, L. (2002). Quality assurance and accuracy assessment of information derived from remotely sensed data In *Manual of Geospatial Science and Technology*. (Ed: Bossler, J.) Taylor and Francis, London. pp. 349–361.

Coppin, P., Jonckheere, I., Nackaerts, K., Muys, B., and Lambin, E. (2004). Digital change detection methods in ecosystem monitoring: A review. *International Journal of Remote Sensing*, 25(9), 1565–1596.

Crist, E.P., and Cicone, R.C. (1984). Application of the Tasselled Cap concept to simulated Thematic Mapper data. *Photogrammetric Engineering and Remote Sensing,* 50, 343–52.

Desclée, B., Bogaert, P., and Defourny, P. (2006). Forest change detection by statistical object-based method. *Remote Sensing of Environment*, 102, 1–11.

Eklundh, L., and Singh, A. (1993). A comparative analysis of standardized and unstandardized principal component analysis in remote sensing. *International Journal of Remote Sensing*, 14, 1359–1370.

Elvidge, C.D., Yuan, D., Werrackoon, R.D., and Lunetta, R.S. (1995). Relative radiometric normalisation of Landsat Multispectral Scanner (MSS) data using an automatic scattergram-controlled regression. *Photogrammetric Engineering and Remote Sensing*, 61(10), 1255–1260.

Engeset, R.V., Kohler, J., Melvold, K., and Lunden, B. (2002). Change detection and monitoring of glacier mass balance and facies using ERS SAR winter images over Svalbard. *International Journal of Remote Sensing*, 23, 2023–2050. *https://doi.org/10.1080/01431160110075550*

Fung, T., and LeDrew, E. (1987). Application of PCA for change detection. *Photogrammetric Engineering and Remote Sensing*, 53, 1649–1658.

Fung, T., and Ledrew, E. (1988). The determination of optimal threshold levels for change detection using various accuracy indices. *Photogrammetric Engineering and Remote Sensing*, 54, 1449–1454.

Garcia-Haro, F.J, Gilabert, M.A., and Melia, J. (2001). Monitoring fire-affected areas using Thematic Mapper data. *International Journal of Remote Sensing*, 22, 533–549.

Gopal, S., and Woodcock, C.E. (1994).Theory and methods for accuracy assessment of thematic maps using fuzzy sets. *Photogrammetric Engineering and Remote Sensing,* 60, 181–188.

Graetz, R.D, Pech, R.P and Davis, A.W. (1988). The assessment and monitoring of sparsely vegetated rangelands using calibrated Landsat data. *International Journal of Remote Sensing*, 8, 1201–1222.

Granville, V., and Rasson, J.P. (1995). Multivariate discriminant analysis and maximum penalized likelihood density estimation. *Journal of the Royal Statistical Society*, 57(3), 501–517.

Gupta, D.M., and Munshi, M.K. (1985). Urban change detection and land-use mapping of Delhi. *International Journal of Remote Sensing*, 6, 529–534.

Hall, O., and Hay, G.J. (2003). A Multiscale Object-Specific Approach to Digital Change Detection. *International Journal of Applied Earth Observation*, 4(4), 311–327. *https://doi.org/10.1016/S0303-2434(03)00010-2*

Hall, F.G., Strebel, D.E., Nickeson, J.E., and Goetz, S.J. (1991). Radiometric rectification: Towards a common radiometric response among multidate, multisensor images. *Remote Sensing of Environment*, 35, 11–27.

Hame, T., Heiler, I., and San Miguel-Ayanz, J. (1998). An unsupervised change detection and recognition system for forestry. *International Journal of Remote Sensing*, 19(6), 1079–1099, *https://doi.org/10.1080/014311698215612*

Henebry, G.M. (1993). Detecting change in grasslands using measures of spatial dependence with Landsat TM data. *Remote Sensing of Environment*, 46(2), 223–234. *https://doi.org/10.1016/0034-4257(93)90097-H*

Houhoulis, P.F., and Michener, W.K. (2000). Detecting wetland change: a rule-based approach using NWI and SPOT-XS data. *Photogrammetric Engineering and Remote Sensing*, 66, 205–211.

Hudson, W.D., and Ramm, C.W. (1987). Correct formulation of the Kappa coefficient of agreement. *Photogrammetric Engineering and Remote Sensing,* 53, 421–422.

Ingebritson, S.E., and Lyon, R.J.P. (1985). Principal components analysis of multitemporal image pairs. *International Journal of Remote Sensing*, 6, 687–696.

Jakubauskas, M.E, Kamlesh, P.L., and Mausel, P.W. (1990). Assessment of vegetation change in a fire altered forest landscape. *Photogrammetric Engineering and Remote Sensing*, 56, 371–377.

Jensen, J.R. (Ed). (1983). Urban/suburban land use analysis. In *Manual of Remote Sensing. Vol. 2.* 2nd Edn. American Society of Photogrammetry, pp. 1571–1666.

Jensen, J.R. (2016). *Introductory Digital Image Processing: A Remote Sensing Perspective*. 4th Edn. Pearson Education, Inc. ISBN 978-0-13-405816-0

Kauth, R.J., and Thomas, G.S. (1976). The Tasselled Cap—a graphic description of the spectral-temporal development of agricultural crops as seen by Landsat. *Proceedings of the Symposium on Machine Processing of Remotely Sensed Data*. Purdue University, West Lafayette, Indiana, 4B41–4B51.

Kiiveri, H., and Caccetta, P. (1998). Image Fusion with Conditional Probability Networks for Monitoring the Salinization of Farmland. *Digital Signal Processing*, 8(4), 225–230. *https://doi.org/10.1006/dspr.1998.0320*

Kliveri, H.T., and Campbell, N.A. (1992). Allocation of Remotely Sensed Data using Markov Models for Image Data and Pixel Labels. *Australian Journal of Statistics*, 34(3). *https://doi.org/10.1111/j.1467-842X.1992.tb01053.x*

Kiiveri, H., Caccetta, P., and Evans, F. (2001). Use of conditional probability networks for environmental monitoring. *International Journal of Remote Sensing*, 22(7), 1173–1190. *https://doi.org/10.1080/01431160151144305*

Kimura, H., and Yamaguchi, Y. (2000). Detection of landslide areas using satellite radar interferometry. *Photogrammetric Engineering and Remote Sensing*, 66, 337–343.

Kontoes, C.C. (2013). Operational Land Cover Change Detection using Change Vector Analysis. *International Journal of Remote Sensing*, 29(16), 4757–4779.

Kuzera, K., Rogan, J., and Eastman, R. (2005). Monitoring vegetation regeneration and deforestation using Change Vector Analysis: Mt. St. Helens Study Area. *ASPRS Annual Conference*, 7–11 March, Baltimore, Maryland.

Lambin, E.F., and Strahler, A.H. (1994a). Change-vector analysis in multitemporal space: a tool to detect and categorize land-cover change processes using high temporal resolution satellite data. *Remote Sensing of Environment*, 48, 231–244.

Lambin, E.F., and Strahler, A.H. (1994b). Indicators of land-cover change for change-vector analysis in multitemporal space at coarse spatial scales. *International Journal of Remote Sensing*, 15, 2099–2119.

Lorena, R.B., dos Santos, J. R., Shimabukuro, Y.E., Brown, I.F., and Kux, H.J.H. (2002). A change vector analysis techniques to monitor land use/land cover in SW Brazilian Amazon: ACRE state. In *PECORA–15 Integrating Remote Sensing at the Global, Regional and Local Scale*, Denver, Colorado, USA.

Lowell, K. (2001). An area-based accuracy assessment methodology for digital change maps. *International Journal of Remote Sensing*, 22, 3571–3596.

Lu, D., Mausel, P., Brondízio, E., and Moran, E. (2003). Change detection techniques. *International Journal of Remote Sensing*, 25(12), 2365–2407. *https://doi.org/10.1080/0143116031000139863*

Macomber, S.A., and Woodcock, C.E. (1994). Mapping and monitoring conifer mortality using remote sensing in Lake Tahoe Basin. *Remote Sensing of Environment*, 50(3), 255–266.

Malila, W.A. (1980). Change Vector Analysis: An Approach for Detecting Forest Changes with Landsat. *LARS Symposia*. Paper 385. *http://docs.lib.purdue.edu/lars_symp/385*

Manavalan, P., Kesavasamy, K., and Adiga, S (1995). Irrigated crops monitoring through seasons using digital change detection analysis of IRS-LISS 2 data. *International Journal of Remote Sensing*, 16(4), 633–340. *https://doi.org/10.1080/01431169508954430*

Morisette, J.T., and Khorram, S. (2000). Accuracy assessment curves for satellite-based change detection. *Photogrammetric Engineering and Remote Sensing*, 66(7), 875–880.

Muchoney, D.M., and Haack, B.N. (1994). Change detection for monitoring forest defoliation. *Photogrammetric Engineering and Remote Sensing*, 60(10), 1243–1251.

Munyati, C. (2000). Wetland change detection on the Kafue Flats, Zambia, by classification of a multitemporal remote sensing image dataset. *International Journal of Remote Sensing*, 21(9), 1787–1806, *https://doi.org/10.1080/014311600209742*

Nielsen, A.A., Conradsen, K., and Simpson. (1998). Multivariate Alternation Detection (MAD) and MAF Postprocessing in Multispectral Bitemporal Image Data: New Approaches to Change Detection Studies. *Remote Sensing of Environment*, 64, 1–19.

Nielsen, A.A., and Conradsen, K. (1997). *Multivariate alteration detection (MAD) in multispectral, bitemporal image data: a new approach to change detection studies*. Tech. Rep. 1997-11, IMM, Technical University of Denmark, Lynby.

Olofsson, P., Foody, G.M., Herold, M., Stehman, S.V., Woodcock, C.E., and Wulder, M.A. (2014). Good practices for estimating area and assessing accuracy of land change. *Remote Sensing of Environment*, 148, 42–57.

Peters, A.J., Walter-Shea, E.A., Lei, J., Vina, A., Hayes, M., and Svoboda, M.D. (2002). Drought monitoring with NDVI-based standardized vegetation index. *Photogrammetric Engineering and Remote Sensing*, 68, 71–76.

Richards, J.A. (1984). Thematic mapping from multitemporal image data using the PC transformation. *Remote Sensing of Environment,* 16, 35-46.

Roberts, D.A., Gardner, M., Church, R., Ustin, S., Scheer, G., and Green, R.O. (1998). Mapping chaparral in the Santa Monica mountains using multiple endmember spectral mixture models. *Remote Sensing of Environment*, 65, 267–279.

Roemer, H., Kaiser, G., Sterr, H., and Ludwig, R. (2010). Using remote sensing to assess tsunami-induced impacts on coastal forest ecosystems at the Andaman Sea coast of Thailand. Natural Hazards Earth Systems Science, 10, 729–745, *https://doi.org/10.5194/nhess-10-729-2010*

Schott, J.R., Salvaggio, C., and Volchok, W.J. (1988). Radiometric scene normalisation using pseudovarient features. *Remote Sensing of Environment*, 26, 1–6.

Singh, A. (1989). Digital change detection techniques using remotely-sensed data. *International Journal of Remote Sensing*, 10, 989–1003.

Singh, A., and Harrison, A. (1985). Standardised Principal Components. *International Journal of Remote Sensing*, 6, 883–896.

Song, C., Woodcock, C.E., Seto, K.C., Lenney, M.P., and Macomber, S.A. (2001). Classification and Change Detection Using Landsat TM Data: When and How to Correct Atmospheric Effects? *Remote Sensing of Environment,* 75, 230–244.

Sparks, T. (2005). Cotter Catchment Fire Recovery Mapping. *Proceedings of the SSC2005 Spatial Intelligence, Innovation and Praxis: The national biennial conference of the Spatial Sciences Institute*, Melbourne. ISBN 0-9581366-2-9

Stow, D.A., Tinney, L.R., and Estes, J.E. (1980). Revising land use/land cover change statistics from Landsat: A study of prime agricultural land. *Proceedings of 14th International Symposium on Remote Sensing of Environment*, ERIM, Ann Arbor, Michigan. pp 1227–1237.

Thonfeld, F., Hecheltjen, A., Braun, M., and Menz, G. (2010). From Algorithms to Processing Chains: A Review of Land Cover and Land Use Change Detection Methodologies. *Proceedings ESA Living Planet Symposium*. ESA SP-686. ESA, Bergen, Norway.

Vogelmann, J.E. (1988). Detection of forest change in the Green Mountains of Vermont using multi-spectral scanner data. *International Journal of Remote Sensing*, 9, 1187–1200.

Vogelmann, J.E. (1990). Comparison between two vegetation indices for measuring different types of forest damage in northeast United States. *International Journal of Remote Sensing*, 11, 2281–2297.

Vogelmann, J.E., and Rock, B.N. (1988). Assessing forest damage in high elevation coniferous forests in Vermont and New Hampshire using Thematic Mapper data. *Remote Sensing of Environment,* 24, 227–246.

Xu, H., and Young, J.A. (1990). Monitoring changes in land use through integration of remote sensing and GIS. *Proceedings IGARSS'90 Symposium*, University of Maryland, College Park, Maryland, pp. 957–960.

Yang, X., and Lo, C.P. (2000). Relative Radiometric Normalisation Performance for Change Detection from Multi-date Satellite Images. *Photogrammetric Engineering and Remote Sensing,* 66(8), 967–980.

Zhou, G., Luo, J., Yang, C., Li, B., and Wang, S. (2000). Flood monitoring using multitemporal AVHRR and RADARSET imagery. *Photogrammetric Engineering and Remote Sensing*, 66, 633–638.

Processing Time Series Datasets

In the context of EO data, a time series dataset refers to a set of calibrated images acquired at regular time intervals. Some of the commonly available EO time series datasets are listed in Section 2.1 above. EO-based time series datasets have been used to derive:

- various phenological parameters for a range of studies relating to ecosystem dynamics (see Volume 3A); and
- water-related metrics for inundation and marine condition studies (see Volume 3B).

Section 8 describes how time series datasets are derived from EO imagery. Some methods to condense time series datasets into composite images are described in Section 10, while Section 9 introduces some of the basic tools that are used to analyse image time series. The Digital Earth concept is described in Section 10, including the Australian implementation of Digital Earth Australia (DEA; see Section 11.2).

Contents

8 Time Series Analysis 87

9 Characterising Temporal Trends 101

10 Pixel-based Composites 111

11 Digital Earth 123

Background image on previous page: Annual Landsat-8 OLI pixel composite of Tasmania and southern Victoria for 2014 displayed using bands SWIR1, NIR and Green as RGB. **Source**: Norman Mueller, Geoscience Australia

8 Time Series Analysis

A time series comprises a sequence of consistent measurements repeated through time (see Volume 2A—Section 8.4). Such data indicate variations in the feature being measured, which may be useful to characterise its behaviour, highlight anomalies and forecast future states. Time series are commonly collected to systematically monitor the condition of various indicators. Examples of common time series datasets include economic variables, such as financial stock values, consumer spending or employment levels, and environmental variables, such as river flow, precipitation trends or atmospheric changes.

EO imagery offers a readily accessible form of time series data for monitoring changes in Earth surface features. The archived data from various satellite sensors are now available for several decades (see Table 2.2), providing a unique record of planet Earth. For a given sensor, the time series represents a sequence of consistent observations with near-global coverage. A pictorial representation of an image time series for Australia, for example, is illustrated in Figure 8.1. Such datasets enable Earth surface changes to be monitored through major variations in climatic conditions and significant changes in land use.

The temporal aspect of time series imagery greatly enhances the opportunity to differentiate Earth surface features, but also adds another dimension to data volume, processing and interpretation. Classification of single date imagery, for example, generally involves allocating pixels to classes based on their spectral similarity within a small number of image bands. Given the significant data volumes associated with EO time series data, a number of algorithms have been proposed to simplify the process of identifying and characterising major trends. Much effort has been directed into developing methods to produce robust time series from the voluminous archives of EO imagery (Viovy *et al.*, 1992; Roerink *et al.*, 2000; Jönsson and Eklundh, 2002; Zhang *et al.*, 2003; Chen *et al.*, 2004; Bradley *et al.*, 2007). More recently, Analysis Ready Data (ARD) have simplified the process of accessing image time series (see Section 3.2).

The basic characteristics of time series datasets are introduced in Volume 2A—Section 8.4. In the context of EO time series datasets, the following sub-sections consider:

- time series components and processing (see Section 8.1);
- the importance of understanding the dataset (see Section 8.2);
- methods to construct a data cube (see Section 8.3);
- detecting anomalies (see Section 8.4); and
- characterising data trends (see Section 9).

Background image: High resolution aerial image of Parliament House, Canberra., acquired on 25 April 2016. **Source:** © Nearmap.

Figure 8.1 Time series imagery of Australia

Successive EO images of Australia, acquired at regular intervals by the same sensor, provide a continental time series dataset.

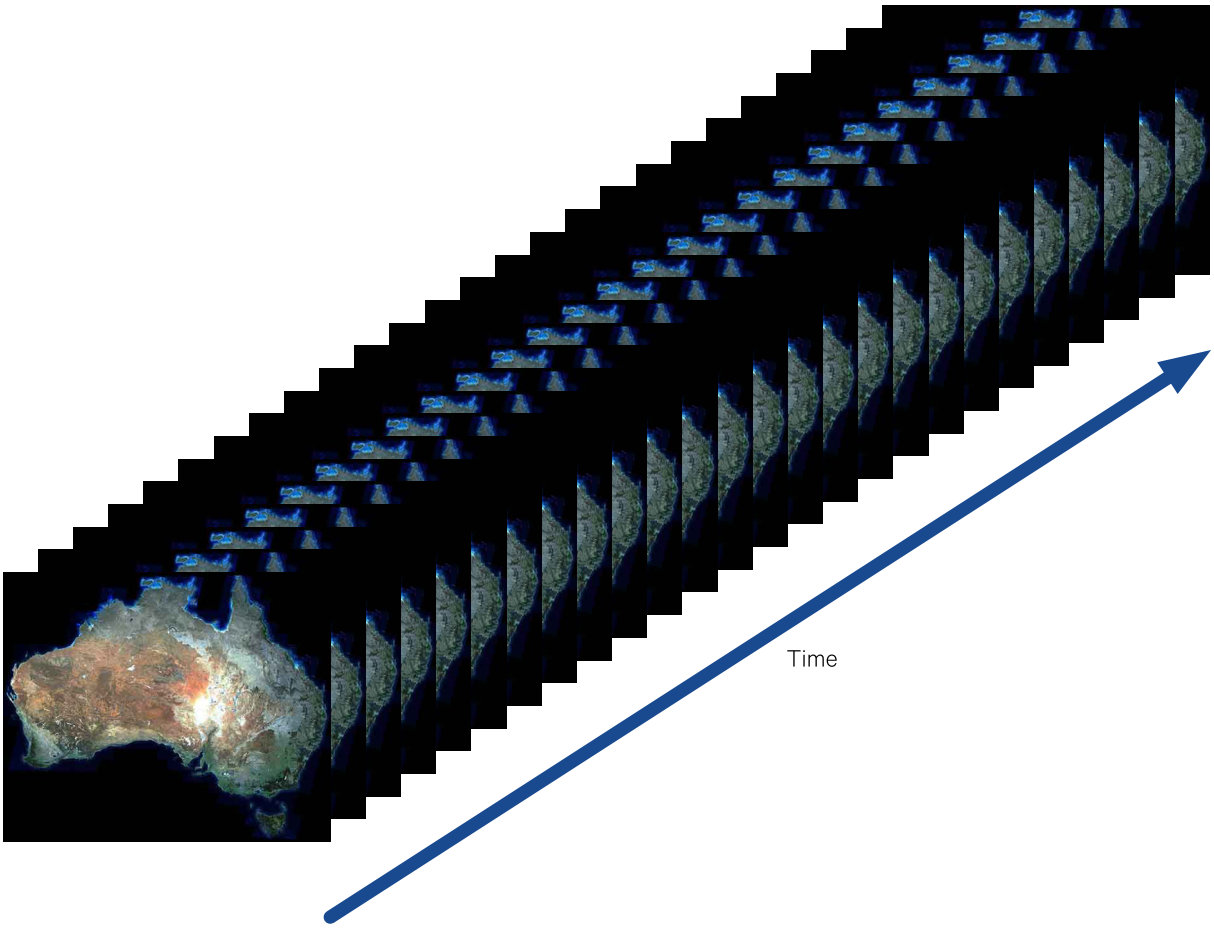

8.1 Time Series Components and Processing

The variations within a time series can be separated into three components:

- long term trends—slow changes with time;
- seasonal trends—correlated with calendar patterns or diurnal cycles; and
- irregular, ephemeral trends—random noise (see Figure 8.2).

These components combine to create the total time series, but their separation (where possible) enables analysis of individual components. In terms of Earth surface features, these three components correspond to gradual, seasonal and abrupt changes. Seasonal trends, in particular, are generally more stable and contain valuable information on the timing, direction and magnitude of systematic changes. For many Earth surface features, seasonal trends are directly related to phenology (see Volume 3A). Examples of MODIS-derived fPAR (fraction of Photosynthetically Active Radiation; see Excursus 8.1) timeseries for selected TERN Ozflux sites (see Volume 3A), which have contrasting vegetation and precipitation characteristics, are shown in Figure 8.3.

Most pre-processing methods for time series analysis aim to reduce data volume and remove outliers, and many approaches modify the spatial and temporal image resolutions during this process. The analysis of time series data involves three conceptual processes (see Table 8.1):

- represent image archive as a standardised data cube, that is, a three-dimensional matrix in which the spatial and temporal separation between adjacent pixels is consistent (see Section 8.3);
- identify and replace outlying values that are likely to have resulted from imaging artefacts. This stage ensures that all pixel values are comparable over space and time (see Section 8.4); and
- characterise seasonal and annual trends within the prepared data cube (see Section 9).

Figure 8.2 Components of time series variations

A 16-day NDVI time series of a pine plantation is decomposed into seasonal, trend and irregular components. Right hand bars show comparable data ranges. Seasonal amplitude range is around 0.1 NDVI.

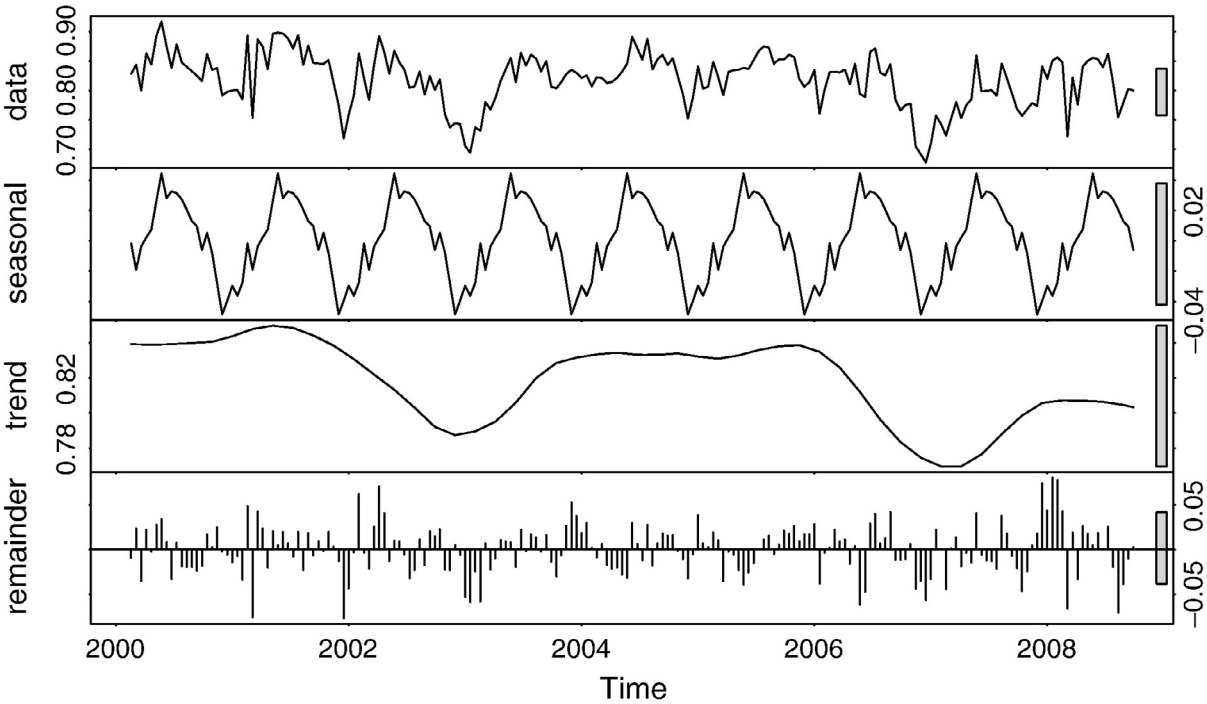

Source: Verbesselt *et al.* (2010) Figure 2

Table 8.1 Time series processing sequence

Stage	Options	Description
1. Create discrete data cube to reduce data volume	Reduce spectral density	Create spectral index
	Reduce temporal resolution	Create less frequent time steps between consecutive images by selecting 'best' pixel in time interval
	Reduce spatial resolution	Create larger pixel size
2. Identify and replace outliers	Compositing images acquired within selected time interval	Select 'best' pixel within time step
	Despiking of time series	Reset pixels with unusually high and low values to more likely levels using some filtering algorithm
3. Identify seasonal trends	Fit function to time series to model repeating patterns	See Table 9.2
	Break up time series into discrete stages based on rate of change	
	Analyse patterns within time series	

To steal ideas from one person is plagiarism but to steal from many is research.
(Wilson Mizner)

Figure 8.3 fPAR time series examples

These examples of MODIS-derived time series show fPAR (fraction of Photosynthetically Active Radiation) variations at selected TERN OzFlux sites.

a. Recovering mallee woodland at Calperum Station near Renmark, South Australia (mean annual precipitation: 240 mm)

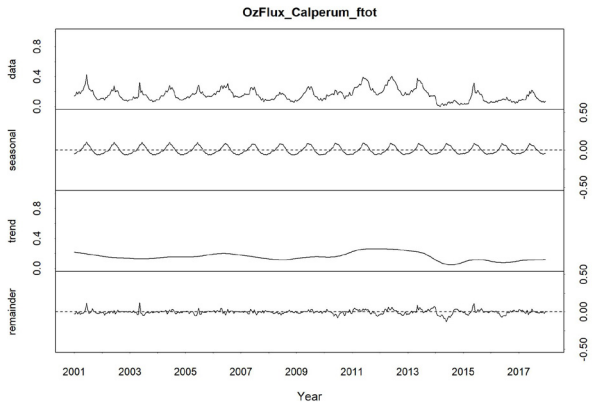

b. Semi-arid mulga at Pine Hill cattle station near Alice Springs, Northern Territory (mean annual rainfall: 306 mm)

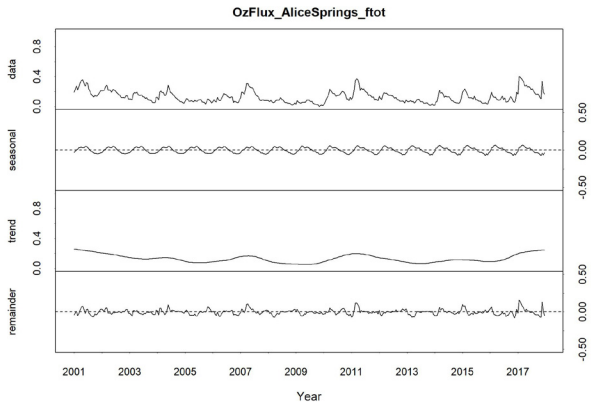

c. Predominantly Mitchell Grass in Sturt Plains, north of Tennant Creek, Northern Territory (mean annual precipitation: 640 mm)

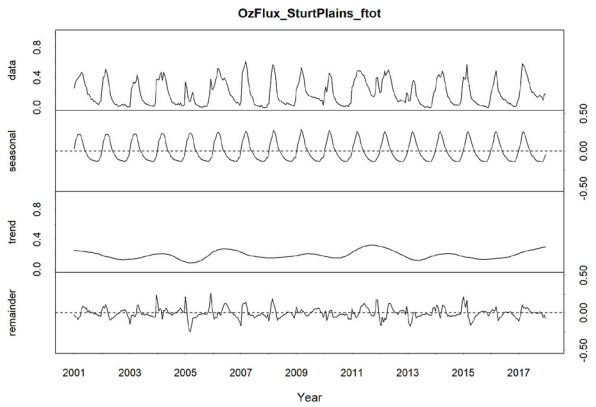

d. Uncleared woodland savanna in Douglas River Daly River Esplanade Conservation area, southwest of Pine Creek, Northern Territory (mean annual precipitation: 1170 mm)

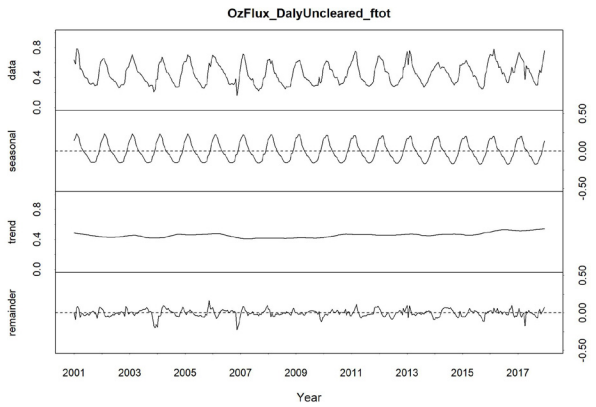

e. Irrigated cropping and pasture at Arcturus, near Emerald, central Queensland (mean annual precipitation: 572 mm)

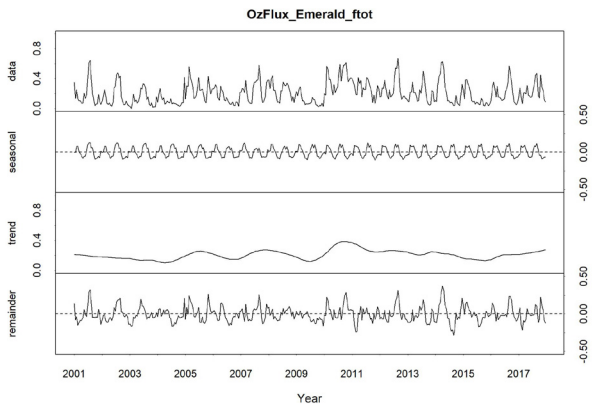

f. Dryland agriculture at Riggs Creek, near Shepparton, Victoria (mean annual precipitation: 650 mm)

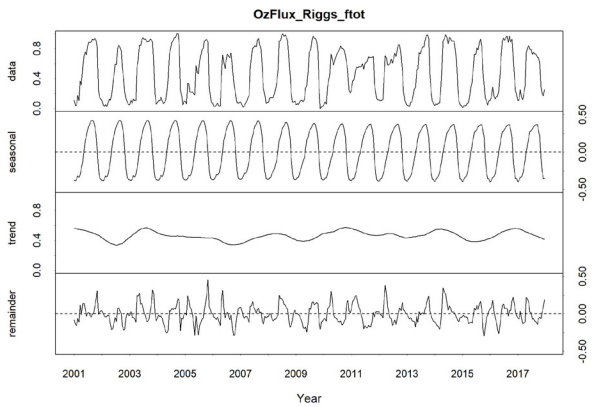

Source: Glenn Newnham and Randall Donohue (CSIRO). For details of TERN OzFlux sites, see: *http://www.ozflux.org.au/monitoringsites/*

8.2 Understanding the Data

While EO time series datasets offer great potential for monitoring and modelling surface features, they also contain significant challenges. Before considering some of the methods used to analyse these datasets, it is worth considering the conceptual problems inherent in this potential.

Firstly, many time series analysis methods have been developed for one-dimensional sequences of 'independent' observations. EO observations, however, are not independent. While the spacing of observations can be manipulated in both spatial and temporal dimensions, the time sequence associated with each pixel will generally be correlated with, if not dependent upon, the time sequences of nearby pixels. Thus, correlations exist in both the spatial and temporal dimensions.

Secondly, most time series analyses aim to differentiate different types of surface features, but it is the cumulative reflectance of all surface features within each imaged pixel that is measured by a remote sensor. In many cases, the surface features have different temporal characteristics, but only their combined reflectance is recorded at each time step. The resulting time series then potentially represents multiple temporal patterns—one for each of the surface features, and these features may be most appropriately sampled at different intervals. For example, annual plants such as grasses follow a clear annual cycle of relatively rapid greening and browning whereas evergreen trees change colour less dramatically between seasons. The time series for a pixel that covers both open trees and grass will be some combination of both cycles, and separating the cycles for each component is not necessarily a simple task, especially when those surface features have not been identified.

Thirdly, remote sensors are not perfect. They can and do record anomalous pixels, their measurements are thwarted by adverse atmospheric conditions and Sun positions, and, over time, their calibration systems can change so that measurements are not consistent (see Volume 1). Many of these problems are well defined and can be solved adequately, but long-term sensor drift remains a vexatious issue for time series datasets. This concern is exacerbated by the second problem mentioned above.

Thus, the trends in EO time series datasets result from the interactions between multiple factors relating to the:

- observed reflectance of Earth surface features as impacted by atmospheric conditions (see Volume 1B—Section 4);
- data resolution in all imaging dimensions (see Table 2.1 above and Volume 1B—Section 1) ; and
- sensor calibration (see Volume 1A—Section 13, Volume 1B—Section 2 and Volume 2A—Section 3).

In addition to the usual concerns about whether the image resolution is suitable to map a particular surface feature, the sampling rate, in conjunction with the actual timing of image planes, needs to be appropriate to the observable reflectance changes in the surface features (see Section 2.2). The analysis of such datasets effectively involves multiple unknowns:

- What is the contribution of the long term trend?
- What is the contribution of the seasonal pattern?
- What is the contribution of the error component?
- What is the relationship between the long term trend, the seasonal pattern and the error component—is it additive, multiplicative, or more complex?
- Is the time interval between image planes appropriate for the surface features being mapped?

In essence, EO time series datasets provide multidimensional data that are indirectly related to multidimensional surface features (see Section 1). Appropriate analysis approaches will recognise the inherent limitations of the data and minimise the number of unknowns (see Section 2.3). Some studies of EO time series data have tended to view the image archive as a series of discrete observations, such that the temporal sequence of values for each geometric pixel have been pre-processed and analysed independently as pixel trajectories. Given the intrinsic interrelationships between adjacent pixels in any EO image, there is some justification to question whether it is appropriate to analyse such datasets this way, especially for real time monitoring and/or short-term forecasting applications (White and Nemani, 2006).

While the fundamental goal of time series analysis of EO datasets may be an improved understanding of ecosystem dynamics, a successful outcome requires some initial familiarity with the relevant ecosystem(s). For example, the extent of serial correlation is related to the temporal resolution of the time series, that is, the time interval between image layers (or time slices). However, the extent of actual correlation between consecutive observations in a particular study will depend on the dynamics of the relevant ecosystem (Zoffoli *et al.*, 2008). In general, to characterise changes within a rapidly changing ecosystem, such as a grassland, would require a time series with higher temporal resolution than would be required to characterise changes in a more stable one, such as an old-growth forest.

The following preliminary analyses are recommended before time series datasets are analysed to derive trend information (Lhermitte *et al.*, 2011):

- mean time series—shows phenological cycle and differences over time;
- variance over time—shows temporal variability in amplitude and timing effects;
- serial correlation—shows the most appropriate temporal sampling interval for particular vegetation type (Alexandridis *et al.*, 2008);
- Principal Components Analysis (PCA; see Section 7.2 and Volume 2A—Section 9) and/or Fourier Transform (FT) components—significance of individual components needs to be understood; and
- noise estimation—must be able to distinguish signals from background noise.

8.3 Creating a Data Cube

It should be obvious that the primary dimension being analysed in time series studies is the temporal one. Accordingly, prior to that analysis, the image data needs to be standardised through time to ensure that data values are comparable in every sense. Many satellite sensors acquire imagery on a regular timetable, delivering observations that are theoretically consistent in space and time. When detecting trends in time series data, however, it is imperative that each temporal sequence of values for a given pixel be precisely:

- co-located, that is, represent the same ground area (see Section 3.1.1.1);
- comparable through time, that is, all pixel values in the dataset belong to a standardised distribution (see Section 3.1.1.2); and
- separated by equal time intervals.

The end result of a standardised time series dataset will be a three-dimensional data cube. For EO imagery, one dimension typically spans from north to south, a second spans from east to west, and the third spans from the first to the last image date (see Figure 8.1 above). Each two-dimensional image in the time series sequence can be viewed as an image plane, that is, a single image corresponding to a particular date. Where multiple image bands are included in a time series dataset, there are effectively multiple image planes for each date.

To convert the acquired image archive into a data cube requires that some of the intrinsic precision of the archive be sacrificed to increase consistency. Image resolution may need to be reduced in four dimensions:

- spectral—represent the image spectral extent in a single channel that is most appropriate for the study, such as a spectral index (see Volume 2C—Section 11);
- spatial—enlarge the original geometric pixel area to reduce data volume and/or improve locational accuracy (see Volume 2B);
- temporal—from a larger sequence of image acquisitions, select a smaller sequence of images separated by equal time intervals; and
- radiometric—represent the actual data range for the selected spectral channel in fewer bits.

These changes not only produce a consistent data cube, but also reduce the data volume that needs to be analysed. Given the inherently huge data volumes associated with EO time series datasets, this is a significant advantage, especially for global studies.

Reducing the spectral dimensionality of multispectral imagery is also advantageous for identifying ecologically significant factors in time series data. A common starting point for time series analyses of EO data is a spectral index, which summarises the changes in the most informative spectral channels for a particular surface feature (see Volume 2C—Section 11). For example, in terrestrial studies, an index that represents vegetation greenness, such as NDVI, is commonly used, particularly for phenological studies (see Excursus 8.1 and Volume 3A).

Excursus 8.1—Relative Calibration of Time Series Datasets

Source: Randall Donohue, CSIRO
Further Information: Donohue *et al.* (2007, 2008, 2009)
Calibrated fPAR dataset: *https://data.csiro.au/collections/#collection/CIcsiro:6084v1*

Some analyses have adopted a relative approach to calibrating EO time series datasets. For example, Donohue *et al.* (2008) developed an 'invariant-cover-triangle' method for relative calibration of AVHRR imagery over Australia. This method essentially standardises vegetation index values through time, and thus compensates for non-target variations in EO data, such as those resulting from atmospheric effects, sensor inconsistencies and changes in illumination geometry (see Section 3.1.1.2). As detailed below, the assumptions underlying this approach limit its application to regions with a wide range of bare soil types, which are spectrally distinct in the selected EO dataset.

Vegetation indices highlight the reflectance differences between surface features in order to differentiate levels of vegetation greenness (see Volume 2C—Section 11). When the spectral characteristics of surface features are plotted on a crossplot of red versus NIR reflectance, green vegetation forms a characteristic triangular shape, sometimes called the 'Tasselled Cap' (Kauth and Thomas, 1976). Bare soil typically plots in a line along the base of the vegetation triangle while vegetation plots above the soil line, with its greenness and cover determining distance from the line (see Figure 8.4).

Figure 8.4 Vegetation cover triangle

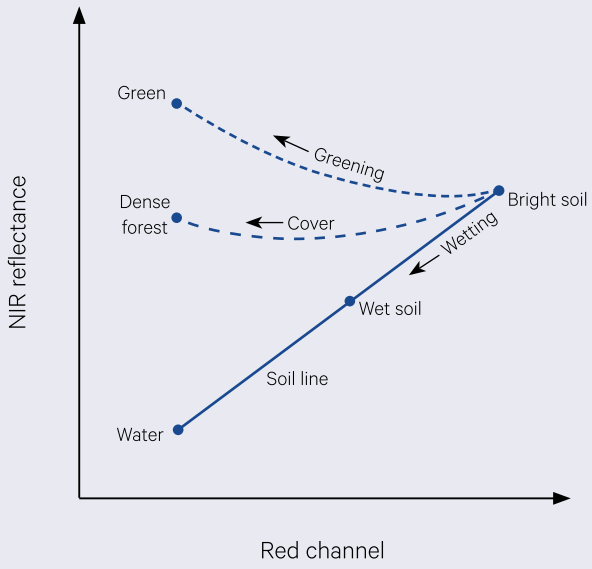

The invariant-cover-triangle approach assumes that the vegetation triangle does not vary in terms of red and NIR reflectances across all images. To achieve this, each image is modified so that its soil line has a slope of one and passes through the origin of the red/NIR crossplot, and the location of the dark value in the vegetation triangle is standardised as 2% of the red reflectance. These adjustments are consistent with the assumptions underlying the Normalised Difference Vegetation Index (NDVI). NDVI is then computed from the modified image values and converted to fraction of Photosynthetically Active Radiation (fPAR; see Volume 3A) for comparison with other biophysical parameters.

To illustrate the red/NIR reflectance ranges that are typical across Australia, six contrasting land cover types (based on the Interim Biogeographic Regionalisation for Australia (IBRA) 5.1; Environment Australia, 2000) are shown in Figure 8.5:

- dense, bright vegetation (1)—either closed forest (>70% cover) in summer or closed grasslands (cereal crops or improved pasture) in winter;
- bright soils with sparse vegetation in arid deserts (2)—open grasslands and shrublands with <30% cover;
- bright, bare surfaces (3)—typically dry salt lakes or winter snow;
- bare, dark surfaces (4)—water bodies or wet, bare soil;
- dense, dark vegetation (5)—open evergreen forests (30–70% cover) with dense, moist understoreys; and
- dark, moderately sparse vegetation on moderately dark soils (6)—woodlands (<30% cover), shrublands (<70% cover) or grasslands (<70% cover), plus improved pasture in southern regions during summer.

Figure 8.5 Land cover reflectances

AVHRR reflectance characteristics of six types of Australian land cover are shown in terms of their spectral characteristics and their spatial distribution. These land covers show equivalent reflectance characteristics in both summer and winter.

a. Summer: February 1996

Crossplot of red versus NIR reflectance

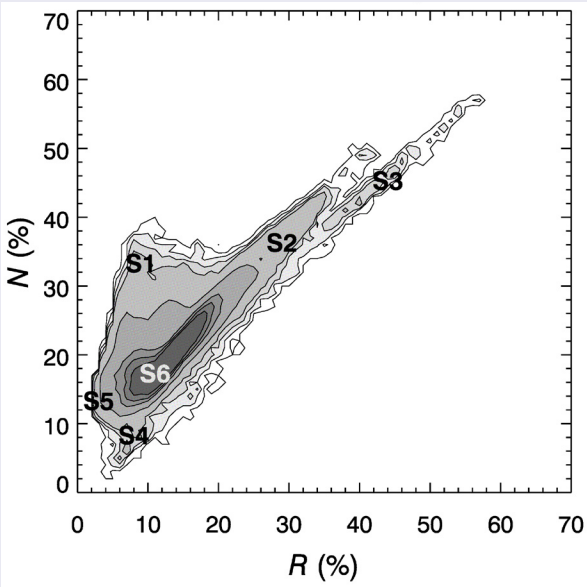

Spatial distribution of land cover types

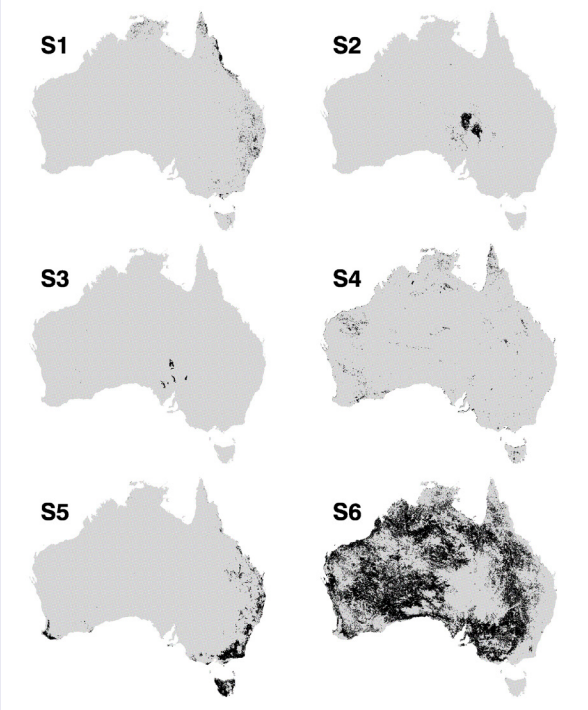

b. Winter: August 2003

Crossplot of red versus NIR reflectance

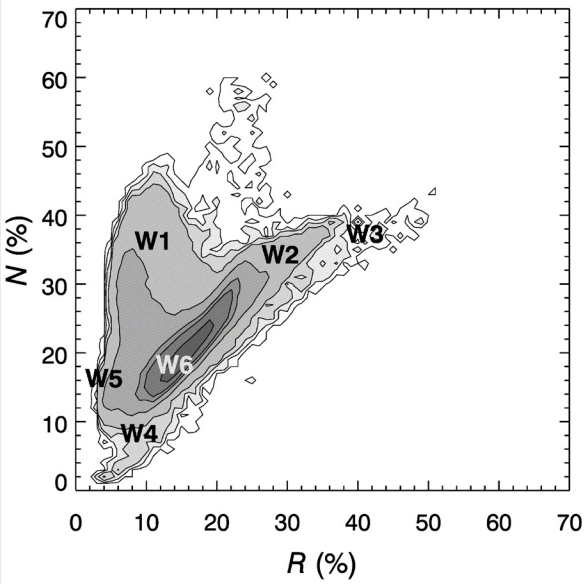

Spatial distribution of land cover types

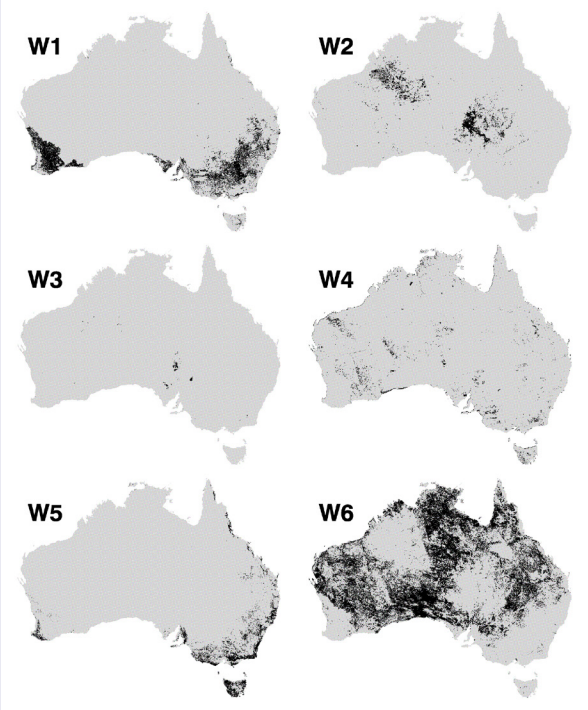

Source: Donohue *et al.* (2008) Figure 1 © Elsevier: Used with permission.

The 'cover invariant triangle' method was applied to a 25-year AVHRR image archive, derived from two different sources:

- PAL (Kidwell, 1998)—coarse resolution, fully calibrated, partially atmospherically corrected for 1981–1994; and
- CATS3.0 (King, 2003)—fine resolution, fully calibrated, non-atmospherically corrected for 1992–2004.

The resulting monthly fPAR dataset essentially harmonised these two datasets into a single time series, which was subsequently extended and used to model vegetation dynamics in Australia over two decades (Donohue *et al.* 2009; see Figure 8.6). The total fPAR time series was separated into two seasonally variable vegetation types:

- persistent—perennial vegetation that is actively photosynthesising all year; and
- recurrent—vegetation that grows in (annual) cycles of activity and dormancy (see Figure 8.7).

By comparing these three fPAR time series datasets with precipitation records for these years, this study demonstrated that during a period of increasing precipitation (7.2% between 1981–2006) across Australia, persistent vegetation increased by 21.3% while recurrent vegetation decreased by 7%. Site-based analyses showed that total cover increased even where precipitation decreased, with persistent vegetation being favoured over recurrent vegetation. The overall increase in vegetation cover was estimated as 7.8%, which may be attributable to the CO_2 fertilisation effect.

Figure 8.6 Seasonal trends 1981–2006

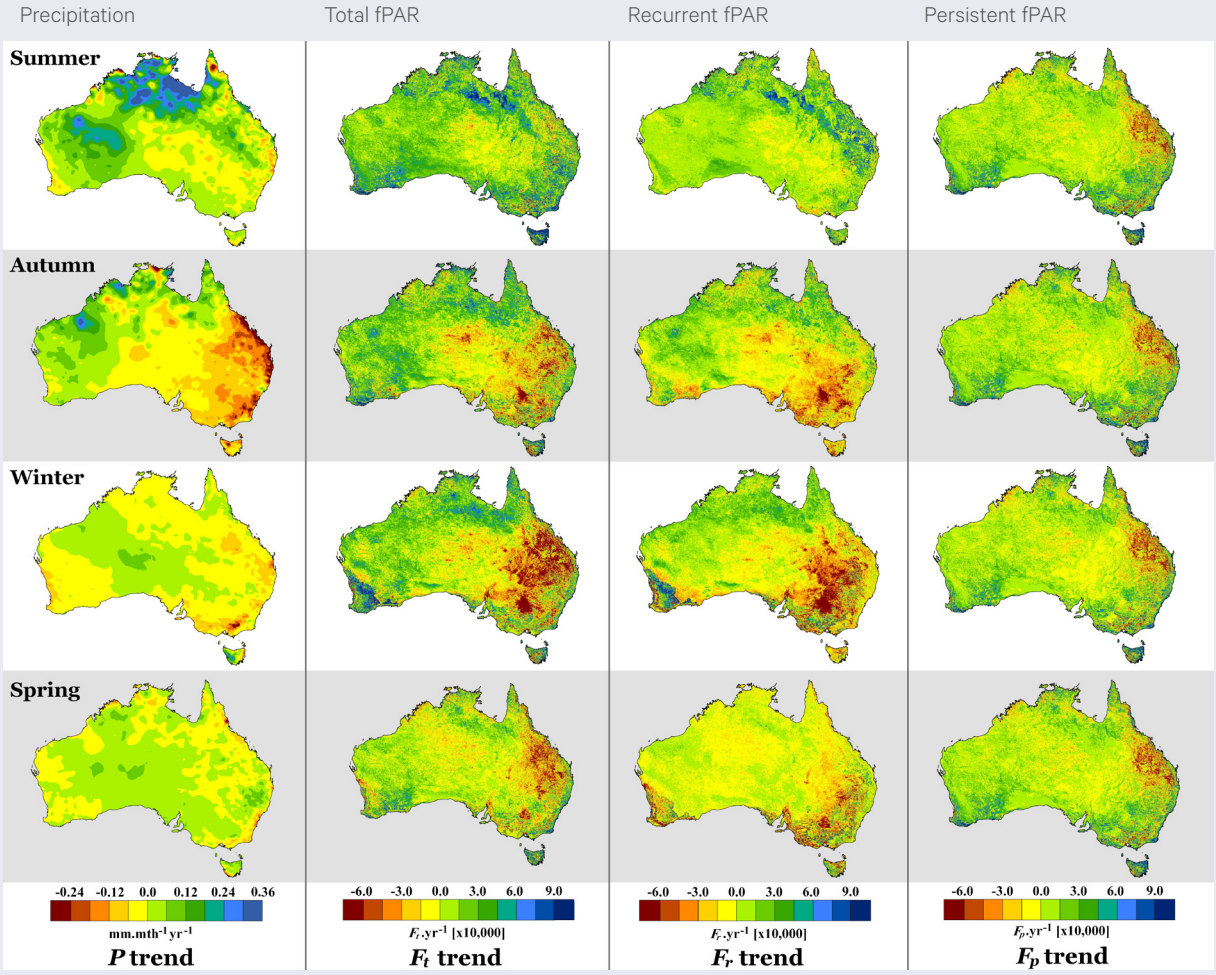

Source: Donohue *et al.* (2009) Figure 5 © Wiley: Used with permission.

Figure 8.7 fPAR decomposition

These graphs demonstrate the temporal decomposition of the total fPAR time series (black line) into persistent (dotted line) and recurrent (grey line) vegetation for three sites:

a. Coffs Harbour, coastal NSW, with grazed pastures and open *Eucalyptus* forest (50–80% cover);

b. Cowra, central NSW, with grazed pastures and winter crops; and

c. Longreach, central Queensland, with low open *Astrebla* tussock grassland (20–50% cover).

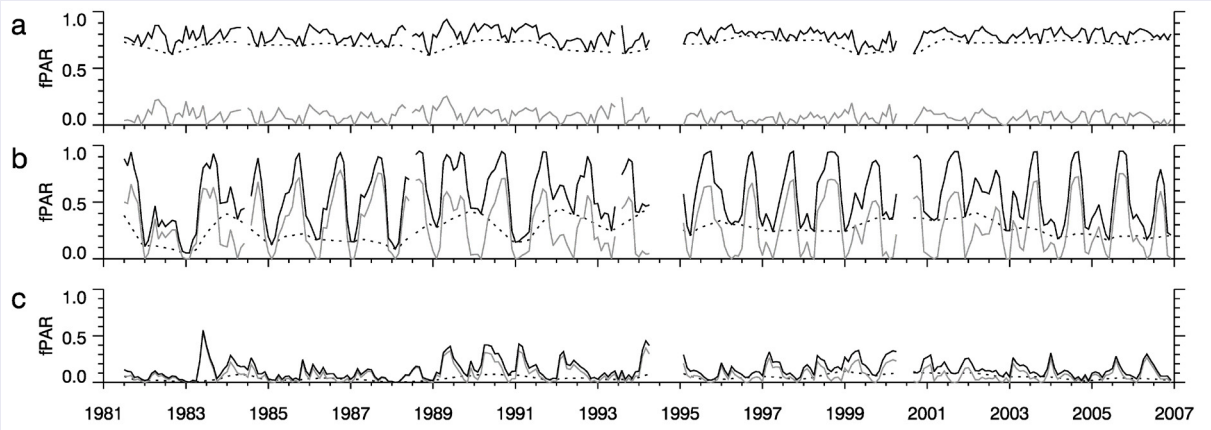

Source: Donohue *et al.* (2009) Figure 1 © Wiley: Used with permission.

Figure 8.8 Dynamic Time Warping (DTW)

a. Warping path matrix for two sequences

b. Resulting alignment

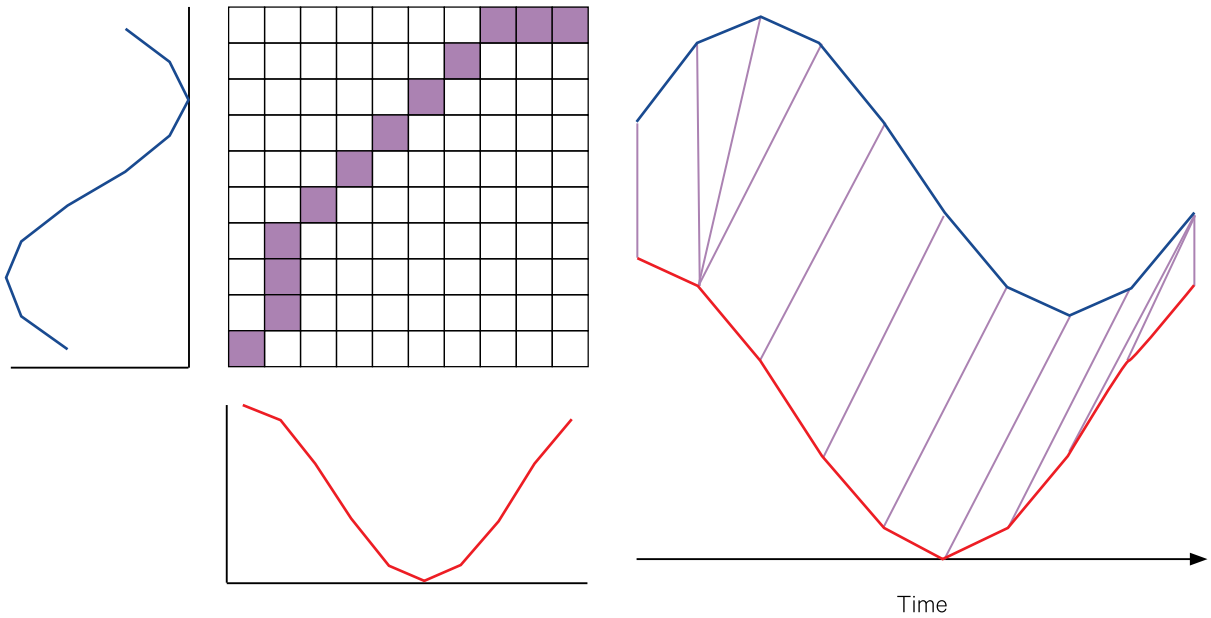

Source: Petitjean and Weber (2012b) Figure 3

To create equal time intervals between time series images, a composite image can be created from a number of acquisitions (see Section 10). While the goal of the compositing process is to convert a sequence of images into a manageable data cube, in which pixels have comparable values through regular time steps, it must be recognised that, by design, these products violate the criteria of equal time steps for each pixel.

An alternative approach to analysing EO time series datasets accepts irregular sampling in the temporal dimension and uses similarity measures such as Dynamic Time Warping (DTW) to 'match' seasonal trends (Petitjean *et al*., 2011, 2012a, 2012b; Petitjean and Weber, 2014). As illustrated in Figure 8.8, DTW analyses the trend information in image sequences to synchronise their patterns. Given that many surface features do not follow a strictly synchronous cycle for seasonal changes, this flexibility is appropriate for analysing EO time series, especially when coupled with irregular coverage due to atmospheric conditions.

The advent of ARD has resulted in the availability of regularised time series datasets for selected EO image sources, principally Landsat data (see Section 3.2). Data cubes have been created for several locations, including Australia (Lewis *et al*., 2016, 2017; see Section 11.2), USA (Dwyer *et al*., 2018) and Switzerland (Giuliani *et al*., 2017).

8.4 Detecting Anomalies

Apart from real changes in surface features, inter-annual variability in EO data can also result from data artefacts and atmospheric distortions, which confound trend detection methods. As introduced in Section 1, inconsistencies between image acquisitions can be introduced by instrumentation problems, changes in viewing and illumination geometry, surface anisotropy, and the presence of clouds, haze, and snow (see also Volume 1).

Outliers in images can be identified using a number of approaches. In EO imagery, outliers generally appear as unusually high values, but when spectral indices, such as NDVI, are used, they can manifest as unusually low values (see Volume 2C). Most outlier correction algorithms tend to consider each spatial pixel as a continuum of values in time. Given the statistical distribution underlying EO image acquisition, however, outlier analysis methods need to be appropriate to the data being processed (White and Nemani, 2006).

One of the difficulties in outlier detection in EO datasets is that cloud contamination does not occur as a random event, but will be related to seasonal cycles. This additional periodicity in the 'error' component confounds the assumption of stationarity, and requires careful consideration (see Volume 2E). Many cloud detection algorithms have been proposed and such artefacts should be identified in each image plane independently of the time series analysis (Zhu and Woodcock, 2012, 2014; Zhu *et al*., 2015). Some algorithms refer to a cloud mask to determine which pixels should be included in time series analyses (see Section 3.1.1.2).

Once outliers are identified, they are generally replaced with values interpolated from valid data pixels, rather than leave data gaps that complicate trend detection algorithms (see Volume 2C). This process also potentially introduces uncertainty into the dataset, as interpolation routines will be forced to rely on composite data trends before the seasonal and longer-term components have been separated.

In time series data, however, the concept of an outlying value can occur in the dimensions of both space and time. Whereas in a single image an outlying pixel value would be dramatically and inexplicably different to its spatially-adjacent neighbours, in a time series an outlying value can also occur in the temporal dimension, that is, the value of a pixel may differ markedly from its value at the preceding and succeeding time intervals. For example, the temporal consistency of the HLS ARD product (see Section 3.2) is analysed using a time series smoothness index, which effectively estimates the noise component (Claverie *et al*., 2018). In conjunction with a spatial filter to remove speckle, temporal outliers (often residual cloud pixels) are subsequently extracted using the Hampel (median) filter (Pearson, 2002), based on the simple ratio vegetation index (see Volume 2C). Other sources of noise in EO time series datasets could include long-term trends that are due to sensor shift over time (see Volume 1A—Section 13 and Volume 1B—Section 2) or the coincidence of geometric errors and outliers (see Volume 2A—Section 3 and Volume 2C).

8.5 Further Information

Data cubes:

Australia: *http://www.ga.gov.au/dea*

ESA Earth System Data Lab: *https://www.earthsystemdatalab.net*

8.6 References

Alexandridis, T.K., Gitas, I.Z., and Silleos, N.G. (2008). An estimation of the optimum temporal resolution for monitoring vegetation condition on a nationwide scale using MODIS/Terra data. *International Journal of Remote Sensing*, 29(12), 3589–3607.

Bradley, B.A., Jacob, R.W., Hermance, J.F., and Mustard, J.F. (2007). A curve fitting procedure to derive inter-annual phenologies from time series of noisy satellite NDVI data. *Remote Sensing of Environment*, 106(2), 137–145.

Chen, J.M., Jonsson, P., Tamura, M., Gu, Z. H., Matsushita, B., and Eklundh, L. (2004). A simple method for reconstructing a high-quality NDVI time-series data set based on the Savitzky–Golay filter. *Remote Sensing of Environment*, 91(3–4), 332–344.

Claverie, M., Ju, J., Masek, J.G., Dungan, J.L., Vermote, E.F., Roger, J.-C., Skakun, S.V., and Justice, C. (2018). The Harmonised Landsat and Sentinel-2 surface reflectance data set. *Remote Sensing of Environment*, 219, 145–161. *https://doi.org/10.1016/j.rse.2018.09.002*

Donohue, R.J., Roderick, M.L., and McVicar, T.R. (2007). *Correcting long-term AVHRR reflectance data using the vegetation cover triangle*. CSIRO Land and Water Science Report 26/07. Canberra: CSIRO Land and Water. *http://www.clw.csiro.au/publications/science/2007/sr26-07.pdf*

Donohue, R.J., Roderick, M.L., McVicar, T.R. (2008) Deriving consistent long-term vegetation information from AVHRR reflectance data using a cover-triangle-based framework. *Remote Sensing of Environment*, 112, 2938–2949. *https://doi.org/10.1016/j.rse.2008.02.008*

Donohue, R.J., McVicar, T.R., and Roderick, M.L. (2009). Climate-related trends in Australian vegetation cover as inferred from satellite observations, 1981–2006. *Global Change Biology*, 15, 1025–1039. *https://doi.org/10.1111/j.1365-2486.2008.01746.x*

Dwyer, J.L., Roy, D.P., Sauer, B., Jenkerson, C.B., Zhang, H.K., and Lymburner, L. (2018). Analysis Ready Data: Enabling Analysis of the Landsat Archive. *Remote Sensing*, 10, 1363. *https://doi.org/10.3390/rs10091363*

Environment Australia (2000). *Revision of the Interim Biogeographic Regionalisation for Australia (IBRA) and development of version 5.1*. Environment Australia, Canberra.

Giuliani, G., Chatenoux, B., De Bono, A., Rodila, D., Richard, J.-P., Allenbach, K., Dao, H., and Peduzzi, P. (2017). Building an Earth Observations Data Cube: lessons learned from the Swiss Data Cube (SDC) on generating Analysis Ready Data (ARD). *Big Earth Data*, 1(1–2), 100–117, *https://doi.org/10.1080/20964471.2017.1398903*

Jönsson, P., and Eklundh, L. (2002). Seasonality extraction by function fitting to time-series of satellite sensor data. *IEEE Transactions on Geoscience and Remote Sensing*, 40(8), 1824–1832.

Kauth, R.J., and Thomas, G.S. (1976). The Tasselled Cap—a graphic description of the spectral-temporal development of agricultural crops as seen by Landsat. *Proceedings of the Symposium on Machine Processing of Remotely Sensed Data*. Purdue University, West Lafayette, Indiana, 4B41–4B51.

Kidwell, K.B. (1998). *NOAA Polar Orbiter Data User's Guide (TIROS- N, NOAA-6, NOAA-7, NOAA-8, NOAA-9, NOAA-10, NOAA- 11, NOAA-12, NOAA-13 and NOAA-14)*. National Environmental Satellite Data and Information Service, NOAA, Suitland.

King, E.A. (2003). The Australian AVHRR Data Set at CSIRO/EOC: Origins, Processes, Holdings and Prospects. *CSIRO Earth Observation Centre Report 2003/04*. CSIRO Earth Observation Centre, Canberra. *http://www.eoc.csiro.au/tech_reps/2003/tr2003_04.pdf*

Lewis, A., Lymburner, L., Purss, M.B.J., Brooke, B., Evans, B., Ip, A., Dekker, A.G., Irons, J.R., Minchin, S., Mueller, N., Oliver, S., Roberts, D., Ryan, B., Thankappan, M., Woodcock, R., and Wyborn, L. (2016). Rapid, high-resolution detection of environmental change over continental scales from satellite data—the Earth Observation Data Cube. *International Journal of Digital Earth*, 9(1), 106–111. *https://doi.org/10.1080/17538947.2015.1111952*

Lewis, A., Oliver, S., Lymburner, L., Evans, B., Wyborn, L., Mueller, N., Raevksi, G., Hooke, J., Woodcock, R., Sixsmith, J., Wu, W., Tan, P., Li, F., Killough, B., Minchin, S., Roberts, D., Ayers, D., Bala, B., Dwyer, J., Dekker, A., Dhu, T., Hicks, A., Ip, A., Purss, M., Richards, C., Sagar, S., Trenham, C., Wang, P., and Wang, L.-W. (2017). The Australian geoscience data cube—Foundations and lessons learned. *Remote Sensing of Environment*, 202, 276–292. *https://doi.org/10.1016/j.rse.2017.03.015*

Lhermitte, S., Verbesselt, J., Verstraeten, W.W., and Coppin, P. (2011). A comparison of time series similarity measures for classification and change detection of ecosystem dynamics. *Remote Sensing of Environment*, 115, 3129–3152.

Pearson, R.K., (2002). Outliers in process modeling and identification. *IEEE Transactions on Control Systems Technology*, 10, 55–63. *https://doi.org/10.1109/87.974338*

Petitjean, F., Ketterlin, A. and Gançarski, P. (2011). A global averaging method for Dynamic Time Warping, with applications to clustering. *Pattern Recognition*, 44, 678–693.

Petitjean, F., Kurtz, C., Passat, N., and Gançarski, P. (2012a). Spatio-Temporal Reasoning for the Classification of Satellite Image Time Series. *Pattern Recognition Letters*, 33, 1805–1815. *https://doi.org/10.1016/j.patrec.2012.06.009*

Petitjean, F., Inglada, J., and Gançarski, P. (2012b). Satellite Image Time Series Analysis under Time Warping. *IEEE Transactions on Geoscience and Remote Sensing*, 50, 3081–3095. *https://doi.org/10.1109/TGRS.2011.2179050*

Petitjean, F., and Weber, J. (2014). Efficient satellite image time series analysis under time warping. *IEEE Transactions on Geoscience and Remote Sensing*, 11(6), 1143–1147. *https://doi.org/10.1109/LGRS.2013.2288358*

Roerink, G.J., Menenti, M., and Verhoef, W. (2000). Reconstructing cloudfree NDVI composites using Fourier analysis of time series. *International Journal of Remote Sensing*, 21(9), 1911–1917.

Verbesselt, J., Hyndman, R., Newnham, G., and Culvenor, D. (2010). Detecting trend and seasonal changes in satellite image time series. *Remote Sensing of Environment*, 114 (1), 106–115.

Viovy, N., Arinoa, O., and Belward, A.S. (1992). The Best Index Slope Extraction (BISE): A method for reducing noise in NDVI time-series. *International Journal of Remote Sensing*, 13(8), 1585–1590.

White, M.A., and Nemani, R.R. (2006). Real-time monitoring and short-term forecasting of land surface phenology. *Remote Sensing of Environment*, 104, 43–49. *https://doi.org/10.1016/j.rse.2006.04.014*

Zhang, X., Friedl, M., Schaaf, C., Strahler, A., Hodges, J., Gao, F., Reed, B., and Huete, A. (2003). Monitoring vegetation phenology using MODIS. *Remote Sensing of Environment*, 84(3), 471–475

Zhu, Z., and Woodcock, C.E. (2012). Object based cloud and cloud shadow detection in Landsat imagery. *Remote Sensing of Environment*, 118, 83–94. *https://doi.org/10.1016/j.rse.2011.10.028*

Zhu, Z., and Woodcock, C.E. (2014). Automated cloud, cloud shadow, and snow detection in multitemporal Landsat data: An algorithm designed specifically for monitoring land cover change. *Remote Sensing of Environment*, 152, 217–234. *https://doi.org/10.1016/j.rse.2014.06.012*

Zhu, Z., Wang, S., and Woodcock, C.E. (2015). Improvements and expansion of the Fmask algorithm: cloud, cloud shadow, and snow detection for Landsats 4–7, 8 and Sentinel 2 imags. *Remote Sensing of Environment*, 159, 269–277. *https://doi.org/10.1016/j.rse.2014.12.014*

Zoffoli, M.L., Kandus, P., Madanes, N., and Calvo, D.H. (2008). Seasonal and interannual analysis of wetlands in South America using NOAA-AVHRR NDVI time series: The case of the Parana Delta Region. *Landscape Ecology*, 23(7), 833–848.

9 Characterising Temporal Trends

Once we have a data cube with consistent values as described in Section 8, temporal trends in the data can be characterised. Various approaches are used to identify relevant cycles from time series of EO imagery. Some of these methods combine treatment of outliers with trend detection. The methods proposed to analyse EO time series datasets can be differentiated in terms of:

- image trajectory being processed (see Section 9.1):
  - individual pixels, for the whole sequence of time series or selected sub-sequence(s); or
  - groups of pixels, based on whole sequence or selected sub-sequence(s);
- processing of trajectory (see Section 9.2):
  - original data values (outliers removed);
  - smoothed data values;
  - sub-sampled data values;
  - transformed data values;
  - modelled data values; or
  - parameters extracted from original, smoothed, sub-sampled or transformed data values;
- comparison of processed trajectories (see Section 9.3):
  - classifying trajectories using similarity or distance metrics (see Volume 2E); or
  - clustering trajectories using hierarchical or partitioning algorithms (see Volume 2E).

Advanced processing methods for time series datasets include high-dimensional statistical analysis, visualisation (e.g. Small, 2012) and machine learning techniques (see Section 9.4). Applications of time series datasets are further detailed in Volume 3.

9.1 The Time Series Trajectory

The changing values of each pixel through time can be considered as its 'movement', which plots a trajectory. The temporal trajectories associated with Earth surface features can be characterised in terms of a number of discrete attributes, such as:

- baseline—background value of trajectory, without seasonal cycles;
- amplitude—difference between seasonal peak and baseline;
- timing—location of seasonal peak in time sequence;
- duration—length of seasonal cycle; and
- shape—rate of seasonal changes (see Figure 9.1).

Background image: International Space Station photograph of Albert and Leichhardt Rivers, Queensland, acquired on 21 June 2006 (ISS013-E39183).
Source: NASA. Retrieved from *https://eol.jsc.nasa.gov/searchphotos/photo.pl?mission=ISS013&roll=E&frame=39183*

Figure 9.1 Temporal trajectory attributes

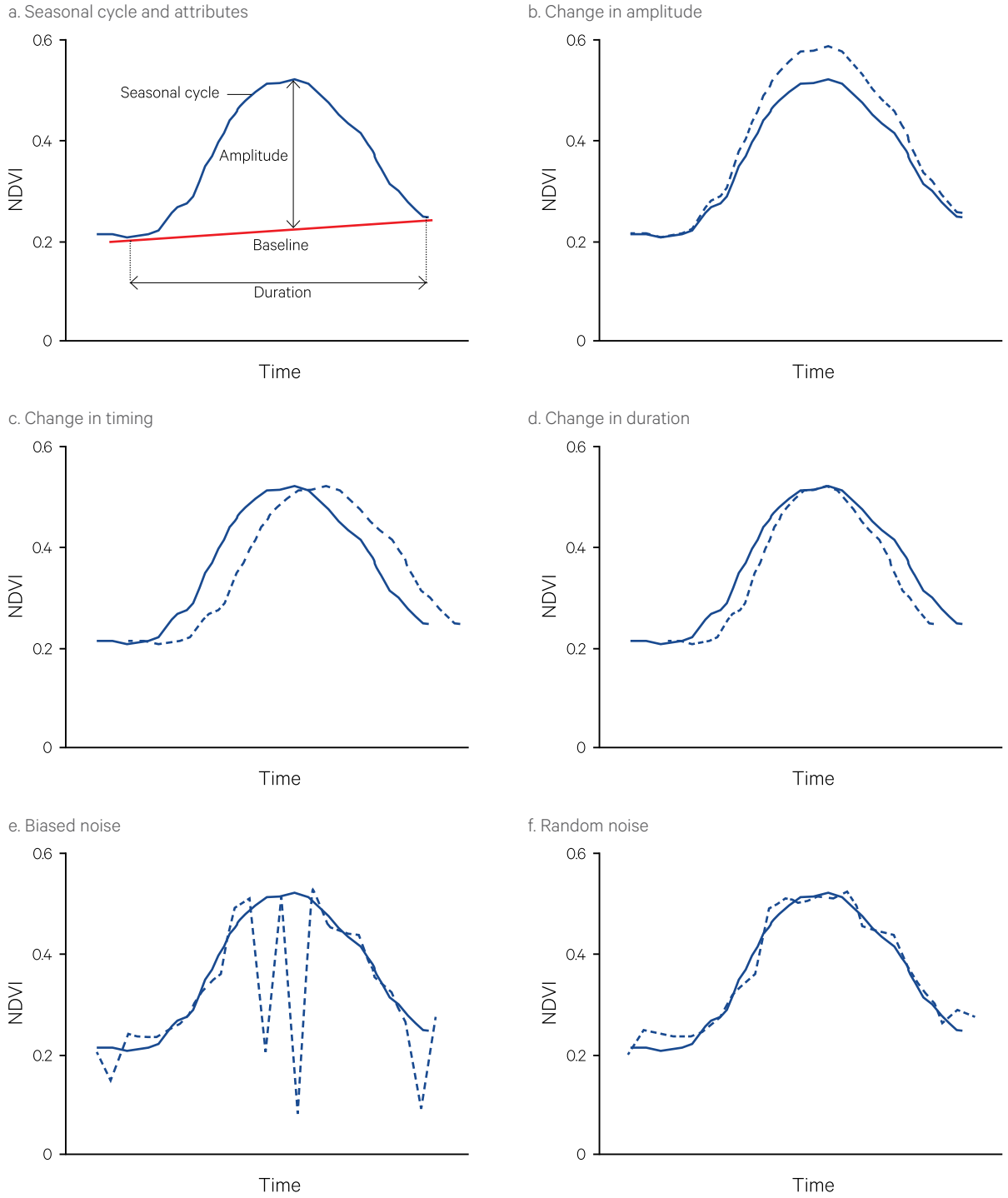

Adapted from Lhermitte *et al.* (2011) Figure 1

Time series that follow defined annual or seasonal cycles may be sub-divided into sub-sequences to allow tracking algorithms to focus on the most relevant changes. Within a sub-sequence, various metrics may be appropriate to help identify noise or cyclic patterns. In some situations, for example, while the shape of the seasonal change may be similar for two different locations, the baseline, amplitude and/or timing of the seasonal change may differ due to differences in temperature or precipitation between sites. Comparison of sub-sequences, either to detect noise or analyse trends, may highlight one or more of the following differences:

- rescaling of:
  - spectral values, that is, change in amplitude; and/or
  - time dimension, that is, change in season length; and/or
- shifting of:
  - spectral values, that is, change in baseline; and/or
  - time dimension, that it, change in timing (Lhermitte *et al*., 2011).

The relevance of these differences to interpreting EO imagery is summarised in Table 9.1.

Processing options can be applied to the trajectories of individual pixels or the time series of groups of pixels. In either case, the whole time series can be analysed or sub-sequences can be extracted based on some criteria. External datasets, such as climate data or land cover maps may be used to stratify the image time series into regions of phenologically and climatically similar pixels (White and Nemani, 2006; Bradley and Mustard, 2008; Petitjean *et al*., 2012a). Analysing trajectories for pixels groups rather than for individual pixels increases radiometric homogeneity and reduces data processing volumes (Petitjean and Weber, 2014). It also provides a more robust basis for forecasting trends and highlighting temporal changes within those groups (White and Nemani, 2006).

Table 9.1 Time series sub-sequence differences

Subsequence Attribute Change	Possible Reason for Difference in		
	Spectral Dimension	Temporal Dimension	Example
Shift Baseline	Change in background colour of soil or understorey vegetation		NDVI saturates in wetter regions with higher vegetation density (Geerken *et al*., 2005a; Heumann *et al*., 2007)
Rescale Amplitude	Change related to vegetation cover or condition		Vegetation changes could change height of NDVI curve (Eklundh and Olsson, 2003)
Shift Timing		Change in timing of peak growing season	Timing of growing season can change with timing of Spring rains (Reed *et al*., 1994; Hill and Donald, 2003; Wardlow *et al*., 2007)
Rescale Shape		Changes in length of growing season (Myneni et al., 1997)	
Change Shape		Major changes in land cover or use	

9.2 Analysing Trends

Some time series analysis methods are applied directly to EO datasets, but generally there is good reason to smooth, sub-sample, transform or model the data in some way prior to analysis. Transformation processes generally involve some form of data compression, which simplifies the time series, such as:

- Fourier decomposition—decompose time series into sum of sine waves;
- Piecewise approximations—represent time series as sequence of segments, possibly characterised by their slope;
- Singular value decomposition (SVD)—optimise dimensionality reduction; or
- Symbolic approximation—label each value range and represent as a sequence.

Various parameters can also be extracted from the time series and these parameters can be the basis for trend analysis. Alternatively, the trajectory can be sub-sampled or represented as a mathematical function (linear or non-linear). Relevant parameters could include the seasonal mean, minimum, maximum, variance, or integral, the duration of a growing season, the slope of a selected sub-sequence, or its variance within a specified time interval.

Table 9.2 Time series analysis methods

Method		Description	Case Study
Group	Example		
Step-wise Linear Regression	Weighted Least Squares	Piecewise linear regression approximates time series, weighted for local maxima within a moving window	Verbesselt *et al.* (2010a, 2010b)
Non-linear Functions	High-order Spline	Function fitted to time series data to model inter-annual phenology	Bradley *et al.* (2007); Bradley and Mustard, 2008); Hermance *et al.* (2007)
	Asymmetric Gaussian Function	Least squares fit to skewed Gaussian model	TIMESAT: Jönsson and Eklundh (2002; 2004);
	Savitsky-Golay Filter	Local polynomial least squares fit within a moving window	TIMESAT: Jönsson and Eklundh (2002; 2004); Hird and McDermid (2009)
	Asymmetric Double-Sigmoid Function	Inflection point of function fitted to NDVI related to deciduous greening onset	Soudani *et al.* (2008)
Step-wise Non-linear Regression	Series of piecewise logistic functions	Represent intra-annual vegetation dynamics, often based on four key transition dates for annual crops (see Volume 3A)	Zhang *et al.* (2003); Zhu *et al.* (2011)
Best Slope	Best Index Slope Extraction (BISE)	The NDVI change rate is used as a benchmark to discard outliers	White *et al.* (1997); Viovy *et al.* (1992)
Harmonic Analysis	Harmonic Analysis of Time Series (HANTS)	Iterative FFT to identify and remove cloud contaminated pixels, then replace with interpolated values from imagery acquired in close temporal proximity	Azzali and Menenti (1996)
	Fourier Function	Represent time series as set of sine/cosine curves	Olsson and Eklundh (1994); Jakubauskas *et al.* (2001, 2002)
	Discrete Fourier Transform (DFT)	First and second harmonics summarise amplitude and phase of annual and biannual cycles in AVHRR NDVI	Moody and Johnson (2001)
Affine Transformations for Data Reduction	Principal Components Analysis (PCA)	Standardised PCA of AVHRR imagery for Africa separate greenness, seasonal greenness changes, and variations related to sensor and climatic factors	Eastman and Fulk (1993)
	Minimum Noise Fraction (MNF)	Cascaded PCA transform with new components ordered by increasing signal-to-noise ratio using maximum autocorrelation factors	Nielsen (2011)

Data reduction transformations are relevant in this context to isolate the noise component as a single band, which can then be analysed or discarded (see Volume 2C). Some of the operations that might be used to process time series trajectories are summarised in Table 9.2. The Minimum Noise Fraction (MNF) transformation effectively orders image planes by data quality as estimated by their signal-to-noise ratio (Green *et al.*, 1988). The Maximum Autocorrelation Factor (MAF) procedure is often used to estimate the noise covariance matrix by assuming that the noise values are unlikely to be spatially correlated (Switzer and Green, 1984; Nielsen *et al.*, 1998). The transformed components then comprise a linear combination of spatially-correlated, orthogonal signal component(s) and an uncorrelated noise component. Once isolated, the noise component may be filtered then recombined with the signal and back-transformed to the original image space (see Volume 2C).

9.3 Comparing Trajectories

Once trajectories have been appropriately selected and prepared, they can be compared on the basis of some measure of separation and either classified into pre-defined groups or clustered in order of similarity (see Volume 2E). Clustering methods that are used with time series datasets are reviewed by Liao (2005). Distance functions can be:

- metric, that is based on positivity, symmetry and triangle inequality (see Volume 2E), such as Euclidean distance or correlation methods (see Volume 2E); or
- non-metric, such as Dynamic Time Warping (DTW) or Longest Common Sub-Sequence (LCSS).

Euclidean distance and DTW are compared in Figure 9.2. Non-metric distance functions, such as DTW, have particular advantages when time series datasets contain missing values or irregular time intervals (Petitjean *et al.*, 2012a, 2012b). Various relevant classification and clustering metrics, algorithms and approaches are detailed in Volume 2E.

Several time series similarity measures used with EO data were reviewed by Lhermitte *et al.* (2011) in terms of three categories, namely:

- direct use of the original time series data;
- indirect use via transformations extracted from the data; or
- indirect use via metrics derived from the data (see Table 9.3).

Their comparisons of different time series similarity measures stressed that both the time series characteristics and the ecosystem dynamics need to be understood before an analysis method is selected.

Figure 9.2 Time series distance measures

a. Euclidean Distance matches two datasets based on equal time intervals between observations.

b. Dynamic Time Warping allows two datasets to include missing values and irregular time intervals.

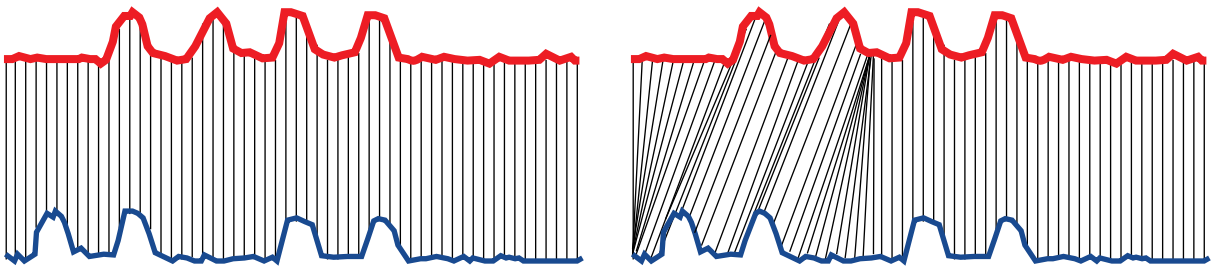

Adaped from: Mike Izbicki, Claremont McKenna College (*http://izbicki.me/blog/converting-images-into-time-series-for-data-mining*)

Table 9.3 Time series similarity measures

Data Used	Type of Approach	Example Approach	Features	Limitations	Example
Original Data	Distance measures	Minkowski distance	Easy to compute and interpret in vector analysis and land cover classification; quantifies difference between time series	Sensitive to rescaling/ shifting of amplitude and timing, and introduced noise	Bayarjargal *et al.* (2006); Viovy (2000); Loveland *et al.* (2000); Ehrlich and Lambin (1996); Bergen *et al.* (2005)
	Correlation measures	Pearson's cross-correlation coefficient	Accounts for temporal correlation	Insensitive to amplitude changes but sensitive to timing changes and noise	Geerken *et al.* (2005a, 2005b); Wang *et al.* (2009)
Transformed Data	Data Reduction	Principal Component Analysis	Higher order components capture most information; quantifies difference between time series	Sensitive to rescaling/ shifting of amplitude and timing, but not noise	Lobo and Maisongrande (2008)
	Harmonic or Frequency Analysis	Fourier Transform	Isolates periodic signals with specific frequency; quantifies difference between time series; derived metrics can quantify shape similarity (Evans and Geerken, 2006)	More sensitive to amplitude and timing rescaling and noise, but less sensitive to amplitude shifting	Azzali and Menenti (2000)
Indirect Metrics derived from original or transformed data	Growing Season Parameters related to photosynthetic activity	e.g. Beginning of Growing Season; End of Growing Season	Time series represented as simple statistics	Not inter-comparable	Reed *et al.* (1994); Zhang *et al.* (2003)
		Adapted Scale-Invariant Similarity Measures	Can be designed to user requirements	External knowledge required to interpret results	Defries *et al.* (1995); Borak *et al.* (2000); Hansen *et al.* (2003)

Adapted from Lhermitte *et al.* (2011)

9.4 Analytical Methods

While a wide range of analysis methods has been applied to EO time series datasets for many different environmental applications, hitherto there has been no definitive approach. For example, some of the integrated change detection approaches developed for multi-temporal Landsat imagery are summarised in Table 9.4. A greater emphasis on near real time products is anticipated in the future (Zhu *et al.*, 2017).

To date, most EO time series analyses have focussed on the temporal characteristics, especially for medium resolution datasets such as the Landsat archive (Zhu *et al.*, 2017). However, it is important when analysing EO time series datasets that the spatial dependence of pixels is considered in conjunction with the temporal dimension. Militino *et al.* (2018) consider this non-trivial problem, and discuss suitable approaches such as spatio-temporal stochastic models.

Table 9.4 Landsat-based change detection approaches

Name	Description	Method category	Applications
Landsat-based detection of Trends in Disturbance and Recovery (LandTrendr)	Segmentation methods are used to detect abrupt change in the Normailsed Burn Ration (NBR) value. Gradual changes are described by slope of segments between abrupt changes.	Segmentation	Forest disturbance and recovery (Kennedy *et al.*, 2010, 2012) Land cover change (Franklin *et al.*, 2015)
Vegetation Change Tracker (VCT)	Landsat images are normalised into a probability index called the integrated forest z-score (IFZ) then thresholding is used to detect disturbance.	Thresholding	Forest disturbance (Huang *et al.*, 2010) Wetland change (Kayastha *et al.*, 2012)
Breaks for Additive Season and Trend (BFAST Monitor)	The NDVI time series is decomposed in trend, season and noise components to detect gradual and abrupt changes	Statistical boundary method	Drought-related vegetation disturbance (Verbesselt *et al.*, 2012)
Continuous Change Detection and Classification (CCDC)	All spectral bands are used to detect changes in surface features.	Statistical boundary method	Land cover change (Zhu and Woodcock, 2014; Zhu et al., 2016)

Source: Zhu *et al.* (2017)

9.5 Further Information

TIMESAT: A software package for analysing time-series of satellite sensor data

Jönsson and Eklundh (2004)

Eklundh and Jönsson (2016)

https://www.nateko.lu.se/research/remote-sensing-and-earth-observation/lund-earth-observation-research-group/time-series-analysis-in-remote-sensing

http://web.nateko.lu.se/timesat/timesat.asp

LandTrendr: Temporal segmentation algorithms

Kennedy *et al.* (2010)

TimeSync: Time-series visualization and data collection tool

Cohen *et al.* (2010)

9.6 References

Azzali, S., and Menenti, M. (Eds) (1996). *Fourier analysis of temporal NDVI in the Southern African and American continents*. DLO Winand Staring Centre, Wageningen, The Netherlands. *http://edepot.wur.nl/363147*

Azzali, S., and Menenti, M. (2000). Mapping vegetation–soil–climate complexes in southern Africa using temporal Fourier analysis of NOAA-AVHRR NDVI data. *International Journal of Remote Sensing*, 21(5), 973–996.

Bayarjargal, Y., Karnieli, A., Bayasgalan, M., Khudulmur, S., Gandush, C., and Tucker, C.J. (2006). A comparative study of NOAA-AVHRR derived drought indices using change vector analysis. *International Journal of Remote Sensing*, 105(1), 9–22.

Bergen, K.M., Brown, D.G., Rutherford, J.F., and Gustafson, E.J. (2005). Change detection with heterogeneous data using ecoregional stratification, statistical summaries and a land allocation algorithm. *Remote Sensing of Environment*, 97(4), 434–446.

Borak, J.S., Lambin, E.F., and Strahler, A.H. (2000). The use of temporal metrics for land cover change detection at coarse spatial scales. *International Journal of Remote Sensing*, 21(6–7), 1415–1432.

Bradley, B.A., and Mustard, J.F. (2008). Comparison of phenology trends by land cover class: A case study in the Great Basin, USA. *Global Change Biology*, 14(2), 334–346.

Bradley, B.A., Jacob, R.W., Hermance, J.F., and Mustard, J.F. (2007). A curve fitting procedure to derive inter-annual phenologies from time series of noisy satellite NDVI data. *Remote Sensing of Environment*, 106(2), 137–145.

Cohen, W.B., Yang, Z., and Kennedy, R. (2010). Detecting trends in forest disturbance and recovery using yearly Landsat time series: 2. TimeSync—Tools for calibration and validation. *Remote Sensing of Environment*, 114, 2911–2924. *https://doi.org/10.1016/j.rse.2010.07.010*

Defries, R.S., Hansen, M.C., and Townshend, J.R.G. (1995). Global discrimination of land cover types from metrics derived from AVHRR path finder data. *Remote Sensing of Environment*, 54(3), 209–222.

Eastman, J.R., and Fulk, M. (1993). Long sequence time series evaluation using standardized principal components. *Photogrammetric Engineering and Remote Sensing*, 59(8), 1307–1312.

Ehrlich, D., and Lambin, E.F. (1996). Broad-scale land-cover classification and interannual climatic variability. *International Journal of Remote Sensing*, 17(5), 845–862.

Eklundh, L., and Olsson, L. (2003). Vegetation index trends for the African Sahel 1982–1999. *Geophysical Research Letters*, 30(8), 1430. *https://doi.org/10.1029/2002GL016772*

Eklundh, L. and Jönsson, P (2016). TIMESAT for processing time-series data from satellite sensors for land surface monitoring. In *Multitemporal Remote Sensing*, (Ed. Y. Ban) Springer International Publishing, pp. 177-194.

Franklin, S.E., Ahmed, O.S., Wulder, M.A., White, J.C., Hermosilla, T., and Coops, N.C. (2015). Large Area Mapping of Annual Land Cover Dynamics Using Multitemporal Change Detection and Classification of Landsat Time Series Data. *Canadian Journal of Remote Sensing*, 41, 293–314. *https://doi.org/10.1080/07038992.2015.1089401*

Geerken, R., Batikha, N., Celis, D., and Depauw, E. (2005a). Differentiation of rangeland vegetation and assessment of its status: Field investigations and MODIS and SPOT VEGETATION data analyses. *International Journal of Remote Sensing*, 26(20), 4499–4526.

Geerken, R., Zaitchik, B., and Evans, J.P. (2005b). Classifying rangeland vegetation type and fractional cover of semi-arid and arid vegetation covers from NDVI time-series. *International Journal of Remote Sensing*, 26(24), 5535–5554.

Green, A.A., Berman, M., Switzer, P., and Craig, M.D. (1988). A Transformation for Ordering Multispectral Data in Terms of Image Quality with Implications for Noise Removal. *IEEE Transactions on Geoscience and Remote Sensing*, 26(1), 65–74.

Hansen, M.C., DeFries, R.S., Townshend, J.R.G., Carroll, M., Dimiceli, C., and Sohlberg, R.A. (2003). Global percent tree cover at a spatial resolution of 500 meters: First results of the MODIS vegetation continuous elds algorithm. *Earth Interactions*, 7(10), 1–15.

Hermance, J.F., Jacob, R.W., Bradley, B.A., and Mustard, J.F. (2007). Extracting phenological signals from multiyear AVHRR NDVI time series: Framework for applying high-order annual splines with roughness damping. *IEEE Transactions on Geoscience and Remote Sensing*, 45(10), 3264–3276.

Heumann, B.W., Seaquist, J.W., Eklundh, L. and Jönsson, P. (2007). AVHRR Derived Phenological Change in the Sahel and Soudan, Africa, 1982-2005. *Remote Sensing of Environment*, 108, 385–392.

Hill, M.J., and Donald, G.E. (2003). Estimating spatio-temporal patterns of agricultural productivity in fragmented landscapes using AVHRR NDVI time series. *Remote Sensing of Environment*, 84(3), 367–384.

Hird, J.N., and McDermid, G.J. (2009). Noise reduction of NDVI time series: An empirical comparison of selected techniques. *Remote Sensing of Environment*, 113(1), 248–258.

Huang, C., Goward, S.N., Masek, J.G., Thomas, N., Zhu, Z., and Vogelmann, J.E. (2010). An automated approach for reconstructing recent forest disturbance history using dense Landsat time series stacks. *Remote Sensing of Environment*, 114, 183–198. *https://doi.org/10.1016/j.rse.2009.08.017*

Jakubauskas, M.E., Legates, D.R., and Kastens, J.H. (2001). Harmonic Analysis of Time-Series AVHRR NDVI Data. Photogrammetric Engineering and Remote Sensing, 67(4), 461–470.

Jakubauskas, M.E., Peterson, D.L., Kastens, J.H., and Legates, D.R. (2002). Time Series Remote Sensing of Landscape-Vegetation Interactions in the Southern Great Plains. *Photogrammetric Engineering and Remote Sensing*, 68(10), 1021–1030.

Jönsson, P., and Eklundh, L. (2002). Seasonality extraction by function fitting to time-series of satellite sensor data. *IEEE Transactions on Geoscience and Remote Sensing*, 40(8), 1824–1832.

Jönsson, P., and Eklundh, L. (2004). TIMESAT—a program for analysing time-series of satellite sensor data. *Computers and Geosciences*, 30, 833–845.

Kayastha, N., Thomas, V., Galbraith, J., and Banskota, A. (2012). Monitoring wetland change using inter-annual landsat time-series data. *Wetlands*, 32, 1149–1162. *https://doi.org/10.1007/s13157-012-0345-1*

Kennedy, R.E., Yang, Z., and Cohen, W.B. (2010). Detecting trends in forest disturbance and recovery using yearly Landsat time series: 1. LandTrendr—temporal segmentation algorithms. *Remote Sensing of Environment*, 114, 2897–2910. *https://doi.org/10.1016/j.rse.2010.07.008*

Kennedy, R.E., Yang, Z., Cohen, W.B., Pfaff, E., Braaten, J., and Nelson, P. (2012). Spatial and temporal patterns of forest disturbance and regrowth within the area of the Northwest Forest Plan. *Remote Sensing of Environment*, 122, 117–133. *https://doi.org/10.1016/j.rse.2011.09.024*

Liao, T. (2005). Clustering of time series data—A survey. *Pattern Recognition*, 38(11), 1857–1874.

Lobo, A., and Maisongrande, P. (2008). Searching for trends of change through exploratory data analysis of time series of remotely sensed images of SW Europe and NW Africa. *International Journal of Remote Sensing,* 29(17) 5237–5245.

Loveland, T.R., Reed, B.C., Brown, J.F., Ohlen, D.O., Zhu, Z., Yang, L., and Merchant, J.W. (2000). Development of a global land cover characteristics database and IGBP DISCover from 1 km AVHRR data. *International Journal of Remote Sensing*, 21(6–7), 1303–1330.

Lhermitte, S., Verbesselt, J., Verstraeten, W.W., and Coppin, P. (2011). A comparison of time series similarity measures for classification and change detection of ecosystem dynamics. *Remote Sensing of Environment*, 115, 3129–3152.

Militino, A.F., Ugarte, M.D., and Pérez-Goya, U. (2018). An Introduction to the Spatio-Temporal Analysis of Satellite Remote Sensing Data for Geostatisticians. Ch 13 in *Handbook of Mathematical Geosciences: Fifty Years of IAMG*. (Eds: Sagar, B.S.D., Cheng, Q., and Agterberg, F.). Springer Open. ISBN 978-3-319-78999-6 *https://link.springer.com/content/pdf/10.1007%2F978-3-319-78999-6.pdf*

Moody, A., and Johnson, D.M. (2001). Land-surface phenologies from AVHRR using the discrete Fourier transform. *Remote Sensing of Environment*, 75(3), 305–323.

Myneni, R.B., Keeling, C.D., Tucker, C.J., Asrar, G., and Nemani, R.R. (1997). Increased plant growth in the northern high latitudes from 1981 to 1991. *Nature*, 386(6626), 698–702.

Nielsen, A.A. (2011). Kernel Maximum Autocorrelation Factor and Minimum Noise Fraction Transformations. *IEEE Transactions on Geoscience and Remote Sensing,* 20(3), 612–624.

Nielsen, A.A., Conradsen, K., and Simpson, J.J. (1998). Multivariate Alteration Detection (MAD) and MAF Postprocessing in Multispectral, Bitemporal Image Data: New Approaches to Change Detection Studies. *Remote Sensing of Environment*, 64, 1–19.

Olsson, L., and Eklundh, L. (1994). Fourier Series for analysis of temporal sequences of satellite sensor imagery. *International Journal of Remote Sensing*, 15(18), 3735–3741. *https://doi.org/10.1080/01431169408954355*

Petitjean, F., Kurtz, C., Passat, N., and Gançarski, P. (2012a). Spatio-Temporal Reasoning for the Classification of Satellite Image Time Series. *Pattern Recognition Letters*, 33, 1805–1815. *https://doi.org/10.1016/j.patrec.2012.06.009*

Petitjean, F., Inglada, J., and Gançarski, P. (2012b). Satellite Image Time Series Analysis under Time Warping. *IEEE Transactions on Geoscience and Remote Sensing*, 50, 3081–3095. *https://doi.org/10.1109/TGRS.2011.2179050*

Petitjean, F., and Weber, J. (2014). Efficient satellite image time series analysis under time warping. *IEEE Transactions on Geoscience and Remote Sensing*, 11(6), 1143–1147. *https://doi.org/10.1109/LGRS.2013.2288358*

Reed, B.C., Brown, J.F., Vanderzee, D., Loveland, T.S., Merchant, J.W., and Ohlen, D.O. (1994). Measuring phenological variability from satellite imagery. *Journal of Vegetation Science*, 5(5), 703–714.

Small, C. (2012). Spatiotemporal dimensionality and Time-Space characterization of multitemporal imagery. *Remote Sensing of Environment*, 124, 793–809. *https://doi.org/10.1016/j.rse.2012.05.031*

Soudani, K., le Maire, G., Dufrene, E., Francois, C., Delpierre, N., Ulrich, E., and Cecchini, S. (2008). Evaluation of the onset of green-up in temperate deciduous broadleaf forests derived from Moderate Resolution Imaging Spectroradiometer (MODIS) data. *Remote Sensing of Environment*, 112(5), 2643–2655.

Switzer, P., and Green, A.A. (1984). Min/max autocorrelation factors for multivariate spatial imagery. *Tech. Report 6,* April 1984, Dept. Statistics, Stanford.

Verbesselt, J., Hyndman, R., Newnham, G., and Culvenor, D. (2010a). Detecting trend and seasonal changes in satellite image time series. *Remote Sensing of Environment*, 114 (1), 106–115.

Verbesselt, J., Hyndman, R., Zeileis, A., and Culvenor, D. (2010b). Phenological change detection while accounting for abrupt and gradual trends in satellite image time series. *Remote Sensing of Environment*, 114(12), 2970–2980.

Verbesselt, J., Zeileis, A., and Herold, M. (2012). Near real-time disturbance detection using satellite image time series. *Remote Sensing of Environment,* 123, 98–108. *https://doi.org/10.1016/j.rse.2012.02.022*

Viovy, N. (2000). Automatic Classification of Time Series (ACTS): A new clustering method for remote sensing time series. *International Journal of Remote Sensing*, 21 (6–7), 1537–1560.

Viovy, N., Arinoa, O., and Belward, A.S. (1992). The Best Index Slope Extraction (BISE): A method for reducing noise in NDVI time-series. *International Journal of Remote Sensing*, 13(8), 1585–1590.

Wang, L., Chen, J., Gong, P., Shimazaki, H., and Tamura, M. (2009). Land cover change detection with a cross-correlogram spectral matching algorithm. *International Journal of Remote Sensing*, 30(12), 3259–3273.

Wardlow, B. D., Egbert, S. L., and Kastens, J. H. (2007). Analysis of time-series MODIS 250 m vegetation index data for crop classification in the US Central Great Plains. *Remote Sensing of Environment*, 108(3), 290–310.

White, M.A., and Nemani, R.R. (2006). Real-time monitoring and short-term forecasting of land surface phenology. Remote Sensing of Environment, 104, 43–49. *https://doi.org/10.1016/j.rse.2006.04.014*

White, M.A., Thornton, P E., and Running, S.W. (1997). A continental phenology model for monitoring vegetation responses to interannual climatic variability. *Global Biogeochemical Cycles*, 11, 217–234.

Zhang, X., Friedl, M., Schaaf, C., Strahler, A., Hodges, J., Gao, F., Reed, B., and Huete, A. (2003). Monitoring vegetation phenology using MODIS. *Remote Sensing of Environment*, 84(3), 471–475.

Zhu, W., Tian, H., Xu, X., Pan, Y., Chen, G., and Lin, W. (2011). Extension of the growing season due to delayed autumn over mid and high latitudes in North America during 1982–2006. *Global Ecology and Biogeography*, 21(2), 260–271. *https://doi.org/10.1111/j.1466-8238.2011.00675.x*

Zhu, Z. (2017). Change detection using landsat time series: A review of frequencies, preprocessing, algorithms and applications. *ISPRS Journal of Photogrammetry and Remote Sensing*, 130, 370–384. *https://doi.org/10.1016/j.isprsjprs.2017.06.013*

Zhu, Z., and Woodcock, C.E. (2014). Continuous change detection and classification of land cover using all available Landsat data. *Remote Sensing of Environment*, 144, 152–171. *https://doi.org/10.1016/j.rse.2014.01.011*

Zhu, Z., Gallant, A.L., Woodcock, C.E., Pengra, B., Olofsson, P., Loveland, T.R., Jin, S., Dahal, D., Yang, L., and Auch, R.F. (2016). Optimizing selection of training and auxiliary data for operational land cover classification for the LCMAP initiative. *ISPRS Journal of Photogrammetry and Remote Sensing*, 122, 206–221. *https://doi.org/10.1016/j.isprsjprs.2016.11.004*

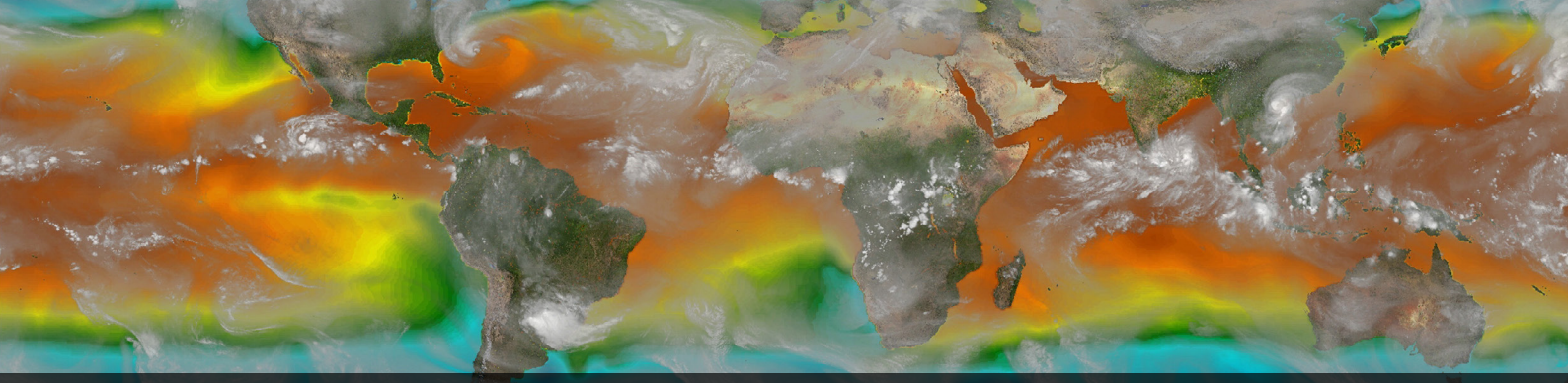

10 Pixel-based Composites

Fusion methods that merged image values from a pair of spatially-coincident images into a single image were described In Section 6. Below we will consider pixel-based methods for compositing multiple, spatially-coincident images from a time series dataset acquired by a particular sensor into a single image (see Section 10.1). Pixel-based composite images are also being generated using pixels acquired by two or more different sensors (see Section 10.2).

A pixel-based composite image comprises pixels that were acquired in multiple, overlapping images within a given time period. A number of satellite image products are now routinely available from various EO data suppliers that use compositing methods to provide a single, summary image representing that time period. Such pixel-based, composite images are useful for large area coverage, rapid assessment of surface condition and change, and long term monitoring of trends. Pixel-based composites enable all images—even those that are partially clouded—to be potentially included in analyses (Griffiths *et al*., 2019). They also tend to display better colour balance than is generally achievable from mosaicking of multiple image scenes (Roberts *et al*., 2017).

Compositing methods generally involve selecting the 'best' pixel from a set of images acquired over a specified time period, where 'best' is judged by some criteria, such cloud-free, optimum Sun angle, and/or proximity to regular time steps. The resulting composite image thus includes pixels acquired on different dates with potentially different atmospheric conditions and/or different imaging geometries. While these images are particularly useful for global and regional studies, the compositing process may introduce artefacts that need to be considered in subsequent processing (see Section 3.1.1.1). To compare composited data through time, especially for global monitoring, Tan *et al*. (2006) recommend consistency in the:

- geometry and frequency of sensor observations;
- methods used for compositing; and
- cloud frequency.

It is worth noting that different gridding algorithms are used across the range of MODIS composite products (Tan *et al*., 2006).

The values in composite images may be based on calibrated spectral reflectance values (see Section 3.1), or a selected spectral index that emphasises the trend in features of interest through time (see Section 4.2.1 or Volume 2C). Compositing methods reduce the impact of cloud, aerosols and differences in imaging geometry within a set of temporal images, and also signficantly reduce data volume, which is an important advantage when processing very large time series datasets. As such, they have been used to monitor meteorological conditions for several decades (Kohrs *et al*., 2014) and are increasingly useful for generating regional to global maps of land cover and land use (Cihlar, 2000; Hansen and Loveland, 2012; Griffiths *et al*., 2013).

Background image: Global composite image for 28 October 2012 (12:00 UTC) showing water vapour data (derived from geostationary satellite datasets and MODIS imagery) overlaid on sea surface temperature (Reynolds, 1988; Reynolds and Marsico, 1993). Land features are superimposed for context from NASA's 'Blue Marble' global image, which was mosaiked from MODIS imagery acquired during 2001 with topographic shading based on the GTOPO30 elevation dataset (see Section 13.4). **Source:** Kohrs *et al.* (2014) Figure 36

10.1 Single Sensor Datasets

Rapid EO imaging from the GOES geostationary satellites has been available since 1975 (Purdom and Menzel, 2016) and animations made from these images have provided ongoing insights into the drivers and mechanisms of weather events (Purdom, 1976). Composite images from polar orbiting satellites emerged early in the 1970s, with composites derived from geostationary satellite images appearing during the Global Weather Experiment (GWE)[3] at the end of that decade.

More recently, image composites for land-based studies have been generated from publicly-available, image archives for various satellite sensors with near-daily, global coverage, including:

- AVHRR (Holben 1986; Cihlar *et al*., 1994);
- MODIS (Roy, 2000; Justice *et al*., 2002; Ju *et al*., 2010);
- Landsat (White *et al*., 2014; Roberts *et al*., 2017; Griffiths *et al*., 2019); and
- Sentinel-2 (Griffiths *et al*., 2019).

Pixel compositing techniques were first proposed to create regularly-updated, cloud-free images of specific features at regional and global scales. Sensors with large area coverage and rapid revisit frequency, such as AVHRR and MODIS, were primarily used to create such composites, especially since these sensors were carried by multiple satellites and thus delivered a higher temporal density of images. Such sensors achieve large area coverage by using a wide scan angle, although this viewing geometry also presents challenges relating to pixel size and placement in the composited images (see Section 3.1.1.1). From these dense time series, frequent image composites have been generated on a routine basis, to provide daily, weekly and/or monthly coverages (see Table 10.1). These global composite products provide valuable input to a wide range of studies of the Earth's surface and its atmosphere, including weather forecasting, climate modelling, pollution monitoring, vegetation productivity, water usage, carbon cycling and oceanography (see Volume 3).

More recently, with the availability of free Landsat images, more detailed composites have been generated using increasingly sophisticated metrics and corrections (Woodcock *et al*., 2008; Zhu *et al*., 2019). The frequency of Landsat Images is most appropriate for seasonal, annual or epoch composites, based on either surface reflectance or a vegetation index (Roy *et al*., 2010; White *et al*., 2014).

Below we will review some of the most commonly used methods for generating pixel-based composites from imagery acquired by a single sensor. Features of these methods are introduced in terms of selecting the:

- time period for compositing (see Section 10.1.1); and the
- values of pixels included in the composite image (see Section 10.1.2).

10.1.1 Time period

Compositing techniques are applied to time series of calibrated image data to generate a single representative dataset (Wolfe *et al*., 1998). These techniques either apply to multiple orbits of imagery that were sensed on the same day, or multiple orbits sensed over several hours, days, weeks or months. A sequence of composite images can also be used to assess change on a seasonal or annual basis (White *et al*., 2014).

The goal of the image compositing process is to populate the final composite with the 'best available pixel' (BAP) values that are located within each grid cell. The sequence of images from which BAP values are selected can include overlap regions that occur between acquistion paths for satellite sensors. Given the increased overlap of satellite paths closer to the poles, higher latitude regions typically have a larger number of images available for compositing and would potentially be able to produce more frequent image composites (Long *et al*., 1999).

The time period selected for creating an image composite needs to be appropriate for the feature being investigated. For example, a wide range of time periods are used to composite the various land products derived from MODIS imagery (see Excursus 10.1). While some products, such as active fires, need to be up-to-date, land cover varies more slowly so can be described in annual, or longer, intervals (see Table 10.1). Meteorological products, such as brightness temperature, are typically composited within intervals less than one hour (Kohrs *et al*., 2014).

The selected time period also needs to make sense in terms of the revisit frequency of the selected sensor and seasonal cycles that might impact image utility. Basically, to achieve a useful composite, there needs to be a sufficient number of 'good' pixels in the set of candidate images acquired during the compositing period.

3 Originally known as the First Global Atmospheric Research Program (GARP) Experiment (FGGE)

Excursus 10.1—MODIS Composites

Source: *https://lpdaac.usgs.gov/dataset_discovery/modis*

MODIS (Moderate Resolution Imaging Spectroradiometer) is a sensor carried by the Terra and Aqua satellites. Its swath width of 2,330 km enables the full globe to be imaged each day or two in 36 spectral bands at 250 m, 500 m or 1 km pixel resolutions (see Volume 1). In addition to the raw image data, a range of image products are generated by USGS to simplify access to the MODIS archive.

Since 2000, up to four MODIS images have been acquired daily over most of the globe. A wide range of image composite products has been derived from the MODIS time series (see Table 10.1). The MOD13Q1 package, for example, summarises this archive into a series of composite images for two spectral indices (Normalised Difference Vegetation Index (NDVI) and Enhanced Vegetation Index (EVI); see Volumes 2C and 3A) by selecting the 'best' pixels from all MODIS Terra images that were acquired within a 16-day window, after correction for atmospheric and Sun angle effects. In this case, the 'best' pixels are determined using the criteria of high NDVI and close-to-zenith sensor view angle. Spatially adjacent pixels from a single image are used where possible. As a result of the compositing process, however, the MOD13Q1 images can contain pixels that have been imaged from different view angles. The impact of view angle differences within composite datasets has been the subject of recent and ongoing research in Australia (e.g. Gill *et al.*, 2009 and Bhardari *et al.*, 2011).

Table 10.1 MODIS land products

MODIS product codes denote the satellite that acquired the image data by the letters 'OD' for Terra, 'YD' for Aqua and 'CD' forTerra or Aqua. In the product codes listed in column 2 below, these codes should be substituted for 'xx'.

Product	Product code	Spatial resolution (m)	Composites available					
			Daily	4-day	8-day	16-day	Monthly	Annual
Reflectance	Mxx09/19	250/ 500/ 1000/ 5600	✓	×	✓	×	×	×
Temperature, Emissivity	Mxx11/21	1000/ 5600	✓	×	✓	×	✓	×
Land cover	Mxx12C1/Q1	500/ 5600	×	×	×	×	×	✓
Vegetation Indices (NDVI and EVI)	Mxx13	250/ 500/ 1000/ 5600	×	×	×	✓	✓	×
Thermal Anomalies and Fire	Mxx14	1000	✓	×	✓	×	×	×
Leaf Area Index (LAI) and Fraction of Photosynthetically Active Radiation (FPAR)	Mxx15A2H/3H	500	×	✓	✓	×	×	×
Evapotranspiration	Mxx16	500	×	×	✓	×	×	✓
Gross/Net Primary Productivity (GPP/NPP)	Mxx17A2H/3H	500	×	×	✓	×	×	✓
Radiance	Mxx18A1/2	5600	✓	×	×	×	×	×
Aerosol Optical Depth	Mxx19A2	1000	✓	×	×	×	×	×
Bidirectional Reflectance Distribution Function (BRDF) and Albedo	Mxx43	500	✓	×	×	×	×	×

Source: NASA MODIS Data Products: *https://modis.gsfc.nasa.gov/data/dataprod/index.php*

MODIS EVI was developed to be less sensitive to the colour of soil background, atmospheric path radiance and saturation in high biomass vegetation than NDVI (Huete *et al.*, 2002). Variations within vegetation index (VI) time series reflect both the seasonal growth phases (or phenology) and irregular perturbations, such as changes in plant health or the impact of fire. Bhardari *et al.* (2011) observed both amplitude and phase differences between the seasonal response cycles in NDVI and EVI time series, with EVI being characterised by an earlier response. Being computed from both blue and red reflectance data, it was proposed that EVI was impacted by both albedo and greenness. The suitability of NDVI and EVI composites for vegetation studies are further discussed in Volume 3A. MODIS vegetation index products have been correlated with a range of ecological parameters, including photosynthetic potential and ecosystem structure and function in Australian evergreen forests (Restrepo-Coupe *et al.*, 2016; see Volume 3A).

The Lands Processes Distributed Active Archive Centre (LP DAAC), a partnership between USGS and NASA, has processed, archived and freely distributed NASA global EO products for land applications since 1990. Some commonly used MODIS Land Products are summarised in Table 10.1. Other MODIS products include:

- Level-1 and atmosphere products—distributed by LAADS (L1 and Atmosphere Archive and Distribution System);
- cryosphere data products—distributed by NSIDC DAAC (National Snow and Ice Data Centre Distributed Active Archive Centre); and
- ocean colour and sea surface temperature products—distributed by the Ocean Color Web (see Section 10.3).

10.1.2 Composite values

For each pixel in the time series grid, the 'composite' value is either based on a 'rule' or a statistic (Roberts *et al.*, 2017). A rule-based approach defines criteria that select the 'best' value from those acquired in the nominated time period (see Section 10.1.1), whereas a statistics-based approach computes a summary statistics (such as the mean) from the multiple pixel observations available for each grid cell. The goal here is to produce a single image which contains the 'best selection of clear-sky pixels' available within the time series (Latifovic *et al.*, 2015) and, to avoid potential imaging artefacts, preferring those observations that were acquired with near-nadir viewing angle (Wolfe *et al.*, 1998). The compositing methods, however, may inadvertently bias selection of pixels towards those that are not necessarily representative, which can impact subsequent analyses (Park *et al.*, 2005).

10.1.2.1 Rule-based criteria

A range of rule-based criteria have been proposed over the past few decades to select the 'best' pixel to use as the composite value (see Table 10.2). One or more rules are applied individually, or in ordered sets, to the time series of pixel values in each grid cell, in order to select those pixel observations to use as the composite values.

Table 10.2 Popular criteria for selecting 'best' pixel

Factor	Criteria	Reason	Reference
Atmospheric conditions	Distance to cloud and cloud shadow	Avoid using pixels that are close to cloud or cloud shadow	Potapov *et al.* (2011) Griffiths *et al.* (2013)
	Atmospheric conditions	Avoid pixels acquired in hazy conditions	Masek *et al.* (2006)
Surface cover	Maximum greenness	Greenness values are lower for cloud, poor atmospheric conditions and off-nadir viewing angles, but can be problematic over water and non-vegetated, or sparsely-vegetated, surfaces	Cihlar *et al.* (1994) Roy *et al.* (2011)
	Maximum brightness temperature	Reduces limb darkening effects and useful for non-vegetated pixels	Kohrs *et al* (2014) Roy *et al.* (2011)
Sensor characteristics	Minimum scan angle	Selects pixels acquired closer to nadir viewing angle	Cihlar *et al.* (1994) Huete *et al.* (2002)
	Preferred sensor	Can avoid known imaging artefacts (such as Landsat-7 ETM+ SLC-off data)	White *et al.* (2014)
Timing	Preferred time or date	Favours pixels acquired closer to the middle of compositing period or in a particular season	White *et al.* (2014) Griffiths *et al.* (2013)

In conjunction with using Analysis Ready Data (ARD; see Section 3.2), most current, rule-based criteria include atmospheric corrections and cloud-masking (see Section 3.1.1.2), and define preferences for sensor characteristics and timing of image acquisition. For example, to generate annual BAP composites over Canada from the Landsat image time series, White *et al.* (2014) used rules that allocated scores for:

- proximity of image to target date-of-year (DOY; Griffiths *et al.*, 2013);
- distance from pixel to cloud or cloud shadow (Griffiths *et al.*, 2013);
- atmospheric opacity (Kaufman *et al.*, 1997; Masek *et al.*, 2006); and
- preferred sensor.

The sum of these scores was then used to select the best pixel value for each grid cell.

While many rule-based criteria for selecting the best pixel for image composites are based on spectral values (see Table 10.2), Tan *et al.* (2006) caution that such criteria can introduce bias, especially with spectral indices such as NDVI, potentially resulting in the preferential selection of vegetated pixels (Wolfe *et al.*, 1998). Some of the implications of gridding artefacts in MODIS image composites are introduced in Section 3.1.1.1 above, and such artefacts have also been reported to bias certain selection criteria, especially for data from sensors with wide scan angles (Tan *et al.*, 2006). Similarly, the maximum brightness temperature algorithm, developed to reduce limb darkening in geostationary images, results in a warm bias in the composited image due to parallax differences between overlapping input images (Kohrs *et al.*, 2014). When accurate cloud masking methods are available (such as Fmask: Zhu and Woodcock, 2012, 2014; Zhu *et al.*, 2015), spectrally independent criteria such as minimum view zenith angle (to select pixels closest to nadir) render least bias in the resulting image composite (Tan *et al.*, 2006).

10.1.2.2 Statistical criteria

A range of summary statistics can be generated from the available pixel observations to use as the composite value (Vancutsem *et al.*, 2015; Griffiths *et al.*, 2019). For example, Long *et al.* (1999) compared surface brightness temperature composites derived from SSM/I imagery, which were based on three statistics (mean, second-highest value, and a modified maximum average) with a hybrid compositing algorithm, and concluded that while each statistic offered both advantages and disadvantages in different situations, the hybrid algorithm combined the strengths of the best statistics (see Figure 10.1). Synthetic Landsat composites have also been derived by fitting harmonic models to all available data (Zhu *et al.*, 2015).

Figure 10.1 Brightness Temperature Composites from SSM/I

SSM/I 85 GHz vertical channel clear region spatial brightness temperature distributions are shown for four compositing statistics.

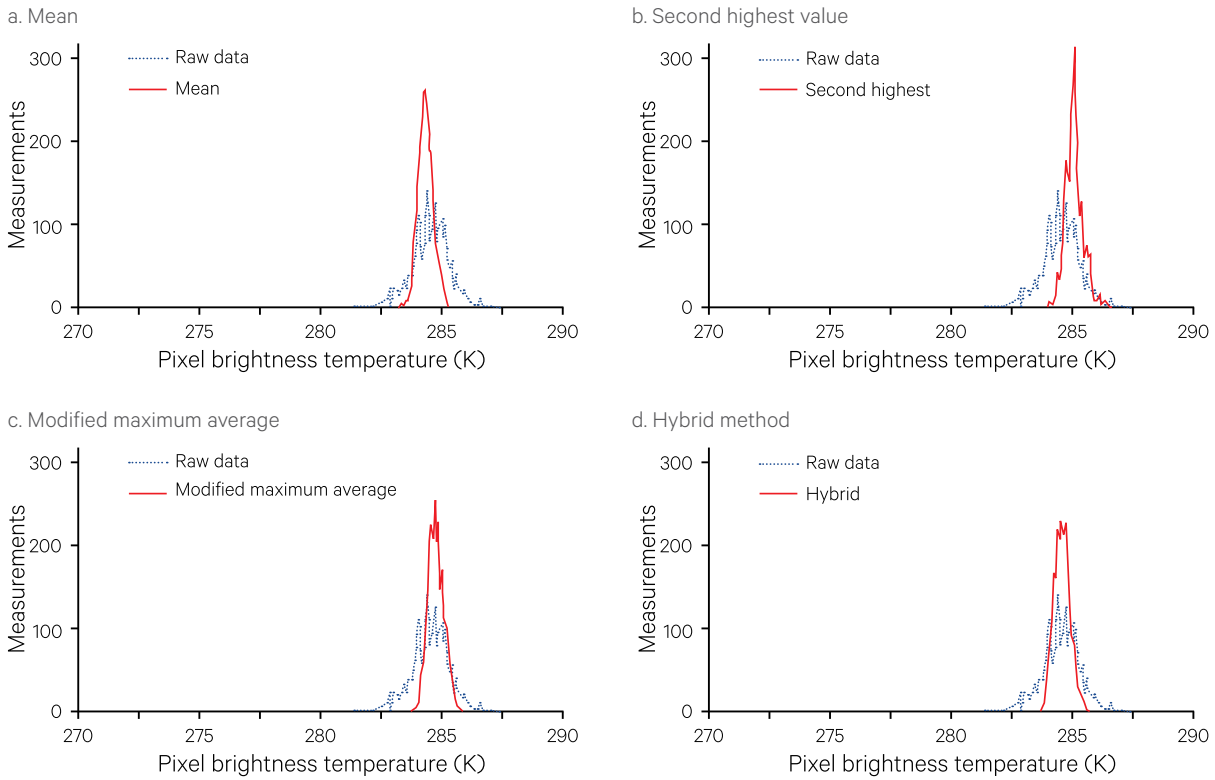

Source: Long *et al.* (1999) Figure 13

Figure 10.2 Workflow for Australian Landsat composite images

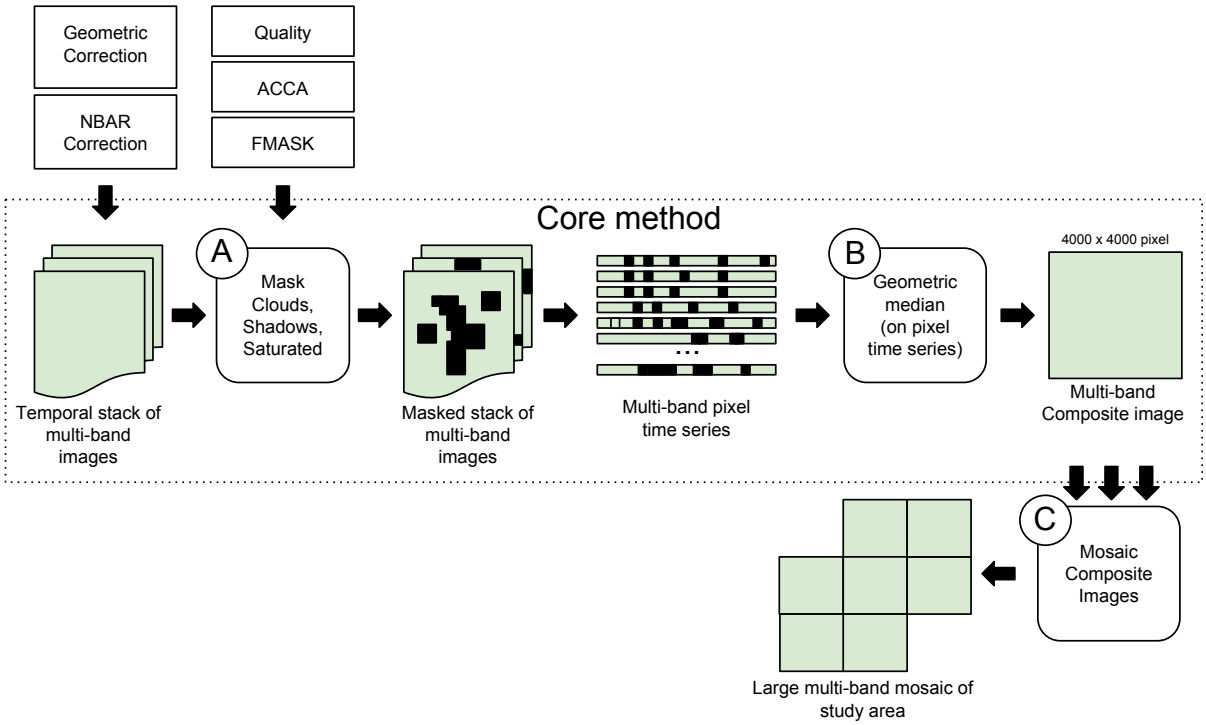

Source: Roberts *et al.* (2017) Figure 2

Using statistical criteria for multichannel imagery, however, requires consideration of the relationships between spectral bands. Although it is a simple process to compute such statistics for individual image bands, and the derived composite bands may recombine into a visually appealing colour composite image, the relationships between the resulting composite bands will not correctly represent those of the input images (Roberts *et al.*, 2017). This is particularly important where subsequent processing will be applied to the composite image. Examples of high-dimensional summary statistics that have been developed to avoid this problem include the:

- medoid (Flood, 2013), which calculates the median then selects the nearest actual observation to create a seasonal composite; and the
- geometric (or spatial) median (Roberts *et al.*, 2017), which is being used to generate annual continental composites from the Landsat archive for Australia (see Figure 10.2).

However, while statistics-based algorithms for compositing produce images that appear homogeneous, the pixel values in the composite image do not correspond with actual observations acquired by the sensor, which may undesirable for some applications.

10.1.2.3 Proxy values

A valid pixel value may be not available for a given grid cell within the images included in the compositing period, due to either missing or anomalous data. Missing data can result from sensor acquisition malfunction or cloud-masking, while anomalous data includes unexpected values, possibly caused by atmospheric haze, sunglint or sensor aberrations. Anomalous pixels may be identified by tracking the temporal trajectory of each pixel over time to highlight those values that fall outside of a pre-defined range (see Section 8.4).

In some compositing algorithms, a 'proxy' value may be assigned to missing and anomalous pixels. For pixels with 'stable' temporal trajectories, a suitable value may be determined using appropriate statistics derived from the pixel values in that trajectory. For example, the MODIS annual composite of Land Cover Dynamics (MCD12Q2 v006) product specifies each data gap is filled using a 'good quality' value of that cell in the preceding or subsequent year (USGS, 2019). However, for pixels deemed to be not temporally stable, the proxy value would be based on an understanding of change events in the trajectory of that pixel (see Section 9), and possibly the trajectories of neighbouring pixels, and it may be appropriate to derive the proxy from the pixel values near the missing grid cell location (White *et al.*, 2014). At higher latitudes with cloudy skies, however, this approach can still be problematic if 'good' data is persistently elusive over several years.

10.2 Multiple Sensor Datasets

Technological advances have enabled faster and more extensive multisensor composites from a greater range of meteorological datasets with higher resolutions in all imaging dimensions (see Table 2.1). Datasets are operationally sourced from both geostationary and polar orbiting satellites to create composites with continental, hemispheric, polar and global coverage. For example, GMGSI (Global Mosaic of Geostationary Satellite Imagery) remaps GOES, METEOSAT and Himawari-8 datasets to 8 km spatial resolution every three hours (NOAA, 2016).

Multisensor composites have been routinely produced over the Southern Ocean and Antarctic continent since 1992 (Lazzara *et al*., 2003; see University of Wisconsin entry in Section 10.3). With increasing computing power, advanced algorithms for mosaiking and compositing have been developed to select between the available co-located pixels (see Section 10.1.2). In the early 1990s, three hours of processing was required to create global composites from six satellite datasets at 20 km resolution, whereas by 2014, composites were generated every 15 minutes from 14 satellite datasets at 1 km resolution for five spectral bands (Kohrs *et al*., 2014). An overview of the compositing process in 2014 is shown in Figure 10.3.

Multisensor ARD products are introduced in Section 3.2. These advanced time series enable denser temporal coverage that is suitable for image compositing of medium resolution EO imagery. For example, the HLS dataset (Claverie *et al*., 2018; Skakun *et al*., 2018) derived from Sentinel-2 MSI and Landsat-8 OLI has been composited to create the M30 product. M30 delivers surface reflectance data in Landsat OLI spectral bands with 5 day temporal frequency at 30 m spatial resolution over the Sentinel-2 tiling system. Another compositing approach for the HLS dataset has been proposed by Griffiths *et al*. (2019) for crop and land cover mapping. This area of EO image processing is changing rapidly and will, no doubt, generate a range of streamlined products, delivered in near real time, in the coming years.

Figure 10.3 Flow chart for multisensor composites

The University of Wisconsin Space Science and Engineering Centre (SSEC) routinely generates multisensor composites from five satellite sensors: GOES-W (NOAA-15), GOES-E (NOAA-16), MSG (NOAA-19), FY2E (Metop B) and MTSAT. This diagram summarises the data flow from ingest on separate workstations for each satellite, through a series of tests to select the best pixels for each composite image.

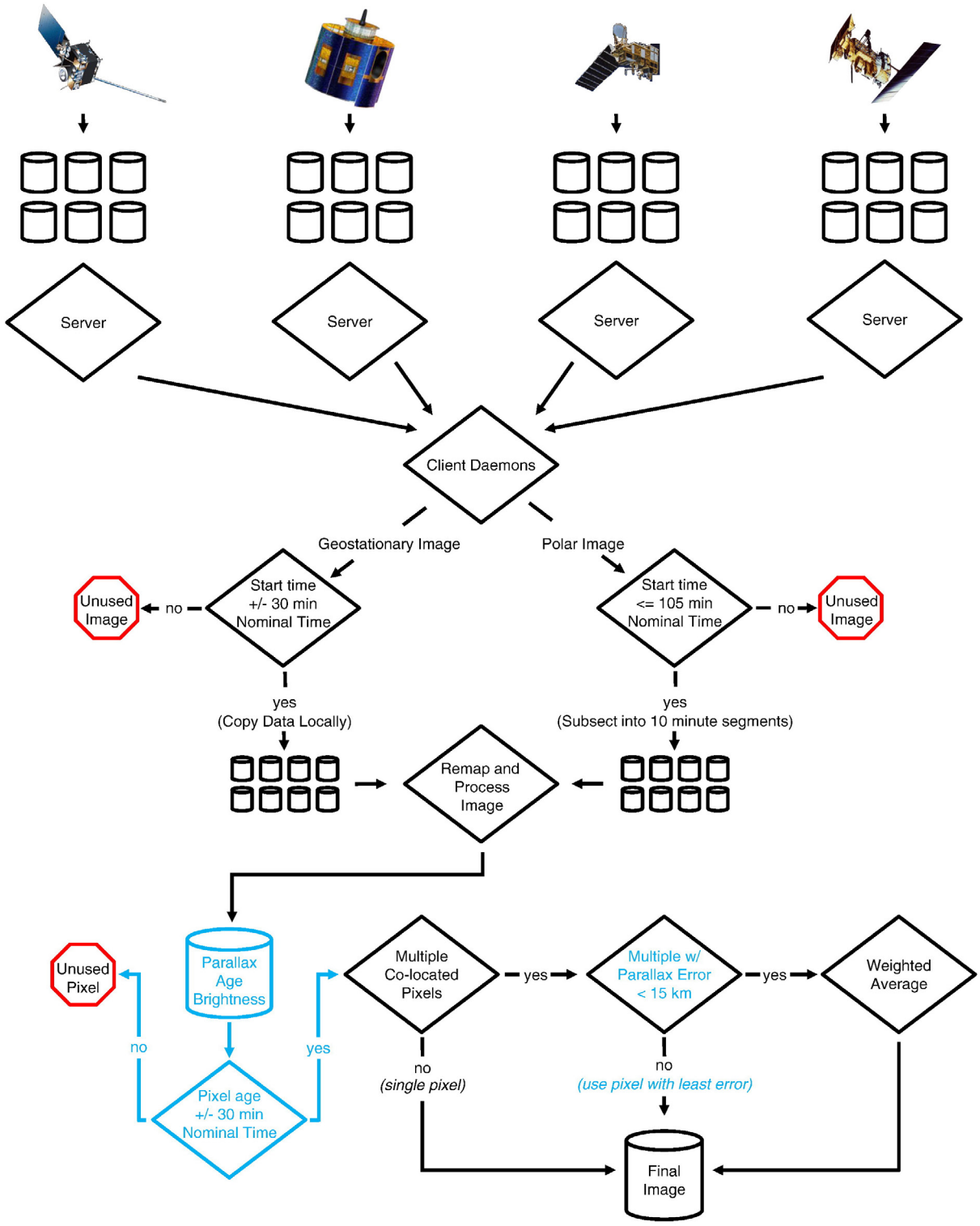

Source: Kohrs *et al.* (2014) Figure 22

10.3 Further Information

Image Products:

NOAA Composite Satellite Imagery: *https://www.ospo.noaa.gov/Products/imagery/composite.html*

MODIS: *https://modis.gsfc.nasa.gov/data/dataprod/*
Land: *https://lpdaac.usgs.gov/product_search/?collections=Combined+MODIS&collections=Terra+MODIS&collections=Aqua+MODIS&view=list*
Ocean Colour Web: *https://oceancolor.gsfc.nasa.gov*
Atmosphere: *https://ladsweb.modaps.eosdis.nasa.gov/search/order/1/MODIS:Terra,MODIS:Aqua*

ASTER: *https://asterweb.jpl.nasa.gov*

Landsat ARD:
Australia (DEA): *https://www.ga.gov.au/dea/products*
USA: *https://www.usgs.gov/land-resources/nli/landsat/us-landsat-analysis-ready-data?qt-science_support_page_related_con=0#qt-science_support_page_related_con*

Harmonised Landsat Sentinel-2 (HLS): *https://hls.gsfc.nasa.gov*

University of Wisconsin: *https://www.ssec.wisc.edu/data/composites/*

UN FAO Global Vegetation/Precipitation Indicators: *http://www.fao.org/giews/earthobservation/asis/index_2.jsp?lang=en*

ISS Image Composites: *https://eol.jsc.nasa.gov/Collections/Composites/*

10.4 References

Bhandari, S., Phinn, S., and Gill, T. (2011). Assessing viewing and illumination geometry effects on the MODIS vegetation index (MOD13Q1) time series: Implications for monitoring phenology and disturbances in forest communities in Queensland, Australia. *International Journal of Remote Sensing*, 32, 7513–7538.

Cihlar, J. (2000). Land cover mapping of large areas from satellites: status and research priorities. *International Journal of Remote Sensing*, 21(6), 1093–1114.

Cihlar, J., Manak, D., and D'Iorio, M. (1994). Evaluation of compositing algorithms for AVHRR data over land. *IEEE Transactions on Geoscience and Remote Sensing*, 32, 427–437.

Claverie, M., Ju, J., Masek, J.G., Dungan, J.L., Vermote, E.F., Roger, J.-C., Skakun, S.V., and Justice, C. (2018). The Harmonised Landsat and Sentinel-2 surface reflectance data set. *Remote Sensing of Environment*, 219, 145–161. *https://doi.org/10.1016/j.rse.2018.09.002*

Flood, N. (2013). Seasonal composite Landsat TM/ETM+ images using the medoid (a multi-dimensional median). *Remote Sensing*, 5(12), 6481–6500.

Gill, T.K., Phinn, S.R., Armston, J.D., and Pailthorpe, B.A. (2009) Estimating tree cover change in Australia: challenges of using the MODIS vegetation index product. *International Journal of Remote Sensing*, 30(6), 1547–1565, *https://doi.org/10.1080/01431160802509066*

Griffiths, P., van der Linden, S., Kuemmerle, T., and Hostert, P. (2013). A pixel based Landsat compositing algorithm for large area land cover mapping. *Journal of Selected Topics in Applied Earth Observations and Remote Sensing*, 6(5), 2088–2101.

Griffiths, P., Nendel, C., and Hostert, P. (2019). Intra-annual reflectance composites from Sentinel-2 and Landsat for national-scale crop and land cover mapping. *Remote Sensing of Environment*, 220, 135–151. *https://doi.org/10.1016/j.rse.2018.10.031*

Hansen, M.C.and Loveland, T.R. (2012). A review of large area monitoring of land cover change using Landsat data. *Remote Sensing of Environment*, 122, 66–74.

Holben, B. (1986). Characteristics of maximum value composite images from temporal AVHRR data. *International Journal of Remote Sensing*, 7, 1417–1434.

Huete, A., Didan, K., Miura, T., Rodriguez, E.P., Gao, X., and Ferreira, L.G. (2002). Overview of the radiometric and biophysical performance of the MODIS vegetation indices. *Remote Sensing of Environment*, 83, 195–213.

Ju, J., Roy, D.P., Shuai, Y., and Schaaf, C. (2010). Development of an approach for generation of temporally complete daily nadir MODIS reflectance time series. *Remote Sensing of Environment*, 114, 1–20. *https://doi.org/10.1016/j.rse.2009.05.022*

Justice, C.O., Townshend, J.R.G., Vermote, E.F., Masuoka, E., Wolfe, R.E., Saleous, N., Roy, D.P., and Morisette, J.T. (2002). An overview of MODIS land data processing and product status. *Remote Sensing of Environment,* 83, 3–15.

Kaufman, Y.J., Tanre, D., Remer, L.A., Vermote, E.F., Chu, A., and Holben, B.N. (1997). Operational remote sensing of tropospheric aerosol over the land from EOS MODIS. *Journal of Geophysical Research Atmosphere*, 102, 17051–17068

Kohrs, R.A., Lazzara, M.A., Robaidek, J.O., Santek, D.A., and Knuth, S.L. (2014). Global satellite composites—20 years of evolution. *Atmospheric Research*, 135–136, 8–34. *http://dx.doi.org/10.1016/j.atmosres.2013.07.023*

Latifovic, R., Pouliot, D., Sun, L., Schwarz, J., and Parkinson, W. (2015). *Moderate Resolution Time Series Data Management and Analysis: Automated Large Area Mosaicking and Quality Control*. Geomatics Canada, Open File 6, 25 p. *https://doi.org/10.4095/296204*

Lazzara, M.A., Keller, L.M., Stearns, C.R., Thorn, J.E., and Weidner, G.A. (2003). Antarctic Satellite Meteorology: Applications for Weather Forecasting. *Monthly Weather Review*, 131, 371–383. *https://journals.ametsoc.org/doi/pdf/10.1175/1520-0493%282003%29131%3C0371%3AASMAFW%3E2.0.CO%3B2*

Long, D.G., Remund, Q.P., and Daum, D.L. (1999). A Cloud-Removal Algorithm for SSM/I Data. *IEEE Transactions on Geoscience and Remote Sensing*, 37(1), 54–62.

Masek, J.G., Vermote, E.F., Saleous, N., Wolfe, R., Hall, F.G., Huemmrich, F., Gao, F., Kutler, J., and Lim, T.K. (2006). A Landsat surface reflectance data set for North America, 1990 2000. *IEEE Geoscience and Remote Sensing Letters*, 3 (1), 68–72.

NOAA (2016). Composite Satellite Imagery webpage. NOAA Office of Satellite and Product Operations webpage: *https://www.ospo.noaa.gov/Products/imagery/composite.html*

Park, S., Feddema, J.J., and Egbert, S.L. (2005). MODIS land surface temperature composite data and their relationships with climatic water budget factors in the central Great Plains. *International Journal of Remote Sensing*, 26(6), 1127–1144.

Potapov, P., Turubanova, S., and Hansen, M.C. (2011). Regional-scale boreal forest cover and change mapping using Landsat data composites for European Russia, *Remote Sensing of Environment*, 115(2), 548–561.

Purdom, J.F.W. (1976). Some Uses of High-Resolution GOES Imagery in the Mesoscale Forecasting of Convection and Its Behaviour. *Monthly Weather Review*, 104, 1474–1983. *https://journals.ametsoc.org/doi/pdf/10.1175/1520-0493%281976%29104%3C1474%3ASUOHRG%3E2.0.CO%3B2*

Purdom, J.F.W., and Menzel, W.P. (2016). Evolution of Satellite Observations in the United States and Their Use in Meteorology. Ch 5 in *Historical Essays on Meteorology, 1919–1995*. (Ed: Fleming, J.) American Meteorology Society. 617 pp.

Restrepo-Coupe, N., Huete, A., Davies, K., Cleverly, J., Beringer, J., Eamus, D., van Gorsel, E., Hutley, L.B., and Meyer, W. (2016). MODIS vegetation products as proxies of photosynthetic potential along a gradient of meteorologically and biologically driven ecosystem productivity, *Biogeosciences*, 13, 5587–5608, *https://doi.org/10.5194/bg-13-5587-2016*

Reynolds, R.W. (1988). A real-time global sea-surface temperature analysis. *Journal of Climate*, 1, 75–86.

Reynolds, R.W., and Marsico, D.C. (1993). An improved real-time global temperature analysis. *Journal of Climate*, 6, 114–119.

Roberts, D., Mueller, N., and McIntyre, A. (2017). High-dimensional Pixel Composites From Earth Observation Time Series. *IEEE Transactions on Geoscience and Remote Sensing*, 35(11), 6254–6264. *https://doi.org/10.1109/TGRS.2017.2723896*

Roy, D.P. (2000). The impact of misregistration upon composited wide field of view satellite data and implications for change detetcion. *IEEE Transactions on Geoscience and Remote Sensing*, 38, 2017–2032.

Roy, D.P., Ju, J., Kline, K., Scaramuzza, P.L., Kovalskyy, V., Hansen, M., Loveland, T.R., Vermote, E., Zhang, C. (2010). Web enabled Landsat Data (WELD): Landsat ETM+ composited mosaics of the conterminous United States. *Remote Sensing of Environment*, 114, 35–49. *http://qa4eo.org/docs/case-studies/NASA_WELD_115890_v2.pdf*

Roy, D., Ju, J., Kommareddy, I., Hansen, M., Vermote, E., Zhang, C., and Kommareddy. A. (2011). Web Enabled Landsat Data (WELD) Products—Algorithm Theoretical Basis Document, February, 2011. *https://globalmonitoring.sdstate.edu/projects/weld/WELD_ATBD.pdf*

Skakun, S., Ju, J., Claverie, M., Roger, J.-C., Vermote, E., Franch, B., Dungan, J.L., and Masek, J.G. (2018). Harmonized Landsat Sentinel-2 (HLS) Product User's Guide. Version 1.4. NASA. *https://hls.gsfc.nasa.gov/wp-content/uploads/2019/01/HLS.v1.4.UserGuide_draft_ver3.1.pdf*

Tan, B., Woodcock, C.E., Hu, J., Zhang, P., Ozdogan, M., Huang, D., Yang, W., Knyazikhin, Y., and Myneni, R.B. (2006). The impact of gridding artifacts on the local spatial properties of MODIS data: Implications for validation, compositing, and band-to-band registration across resolutions, *Remote Sensing of Environment*, 105, 98–114.

USGS (2019). *MCD12Q2 v002* webpage: *https://lpdaac.usgs.gov/products/mcd12q2v006/*

Vancutsem, C., Pekel, J.F., Bogaert, P., and Defourny, P. (2007). Mean compositing, an alternative strategy for producing temporal syntheses. Concepts and performance assessment for SPOT VEGETATION time series. *International Journal of Remote Sensing*, 28, 5123–5141. *https://doi.org/10.1080/01431160701253212*

White, J.C., Wulder, M.A., Hobart, G,W., Luther, J.E., Hermosilla, T., Griffiths, P., Coops, N.C., Hall, R.J., Hostert, P., Dyk, A., Guindon. L. (2014). Pixel-based image compositing for large-area dense time series applications and science. *Canadian Journal of Remote Sensing*, 40(3), 192–212. *http://dx.doi.org/10.1080/07038992.2014.945827*

Wolfe, R.E., Roy, D.P., and Vermote, E. (1998). MODIS Land Data Storage, Gridding, and Compositing Methodology: Level 2 Grid. *IEEE Transactions on Geoscience and Remote Sensing*, 36(4), 1324–1338.

Woodcock, C.E., Allen, R., Anderson, M., Belward, A., Bindschadler, R., Cohen, W., Gao, F., Goward, S.N., Helder, D., Helmer, E., Nemani, R., Oreopoulos, L., Schott, J., Thenkabail, P.S., Vermote, E.F., Vogelmann, J., Wulder, M.A., Wynne, R. (2008). Free access to Landsat imagery. *Science,* 320, 1011.

Zhu, Z., and Woodcock, C.E. (2012). Object-based cloud and cloud shadow detection in Landsat imagery. *Remote Sensing of Environment*, 118, 83–94. *https://doi.org/10.1016/j.rse.2011.10.028*

Zhu, Z., and Woodcock, C.E. (2014). Automated cloud, cloud shadow, and snow detection in multitemporal Landsat data: An algorithm designed specifically for monitoring land cover change. *Remote Sensing of Environment*, 152, 217–234. *https://doi.org/10.1016/j.rse.2014.06.012*

Zhu, Z., Wang, S., and Woodcock, C.E. (2015). Improvements and expansion of the Fmask algorithm: cloud, cloud shadow, and snow detection for Landsats 4–7, 8 and Sentinel 2 imags. *Remote Sensing of Environment*, 159, 269–277. *https://doi.org/10.1016/j.rse.2014.12.014*

Zhu, Z., Woodcock, C.E., Holden, C., and Yang, Z. (2015). Generating synthetic Landsat images based on all available Landsat data: Predicting Landsat surface reflectance at any given time. *Remote Sensing of Environment*, 162, 67–83. *https://doi.org/10.1016/j.rse.2015.02.009*

Zhu, Z., Wulder, M.A., Roy, D.P., Woodcock, C.E., Hansen, M.C., Radeloff, V.C., Healey, S.P., Schaaf, C., Hosteret, P., Strobl, P., Pekel, J.-F., Lymburner, L., Pahlevan, N., and Scambos, T.A. (2019). Benefits of the Free and Open Landsat Data Policy. *Remote Sensing of Environment*, 224, 382–385. *https://doi.org/10.1016/j.rse.2019.02.016*

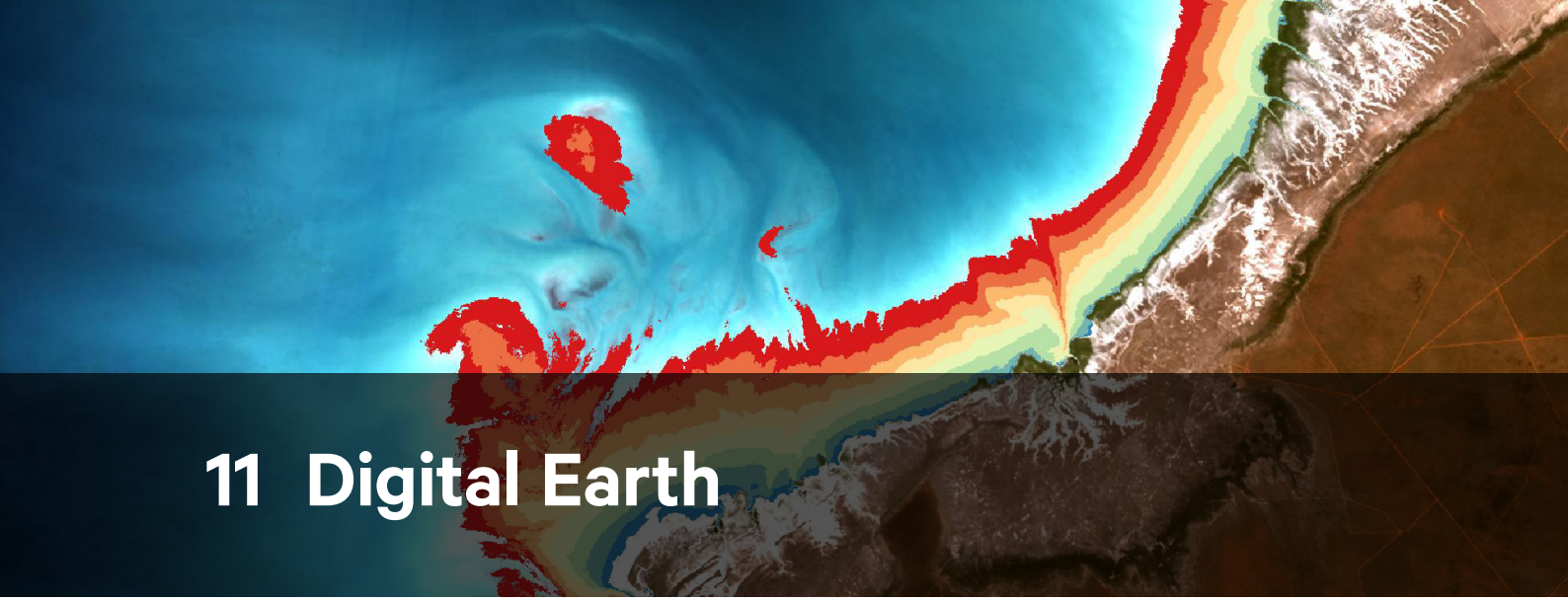

11 Digital Earth

11.1 The Concept

The term 'Digital Earth' (DE) was coined in 1998 as part of a vision for the digital future, in which all citizens of the world could freely interact with volumes of geo-referenced information presented on a virtual globe (Gore, 1998). While technological advances have changed the original vision of this concept, the value of real time access to current and historical information about environmental, economic and social conditions on our planet is unprecedented. Such information can now be derived from myriad data sources, including EO.

A succession of technological and global advances have enabled development of the DE (see Figure 11.1). To realise the goal of easy accessibility by ordinary citizens, a range of technical challenges needed to be negiotated, including visualisation techniques, intuitive user interfaces, global data standards, fast data transfer rates and efficient storage mechanisms, as well as selection of the most relevant and reliable sources of information. The integration of a diverse range of technological and organisational challenges has required collaboration and coordination at global levels between governments and private enterprises (Foresman, 2008; Craglia *et al*., 2012; Goodchild *et al*., 2012; Mattmann, 2013).

As the world's population and resource consumption both continue to grow, sustainable development is a major concern. Our finite resources of energy, food and water need to be shared equitably and efficiently. To support sustainable development around the globe, the DE framework needs to integrate data and models describing economic, social and environmental systems and conditions. In 2009–2010, the International Council for Science (ICSU) canvassed the views of over one thousand scientists to identify five priorities, or Grand Challenges facing research into global sus.tainability:

- developing the ***observation systems*** needed to manage global and regional environmental change;
- improving the usefulness of ***forecasts*** of future environmental conditions and their consequences for people;
- recognising key ***thresholds*** or non-linear changes to improve our ability to anticipate, recognise, avoid and adapt to abrupt global environmental change;
- determining what institutional, economic and behavioural ***responses*** can enable effective steps towards global sustainability; and
- encouraging ***innovation*** (coupled with sound mechanisms for evaluation) in developing technological, policy and social responses to achieve global sustainability (Craglia *et al*., 2012).

With greater awareness of pollution and environmental degradation, the DE provides an integrated platform for identifying key drivers of changes, and monitoring those changes at a range of spatial and temporal scales, with a view to minimising the adverse impacts of human civilisation on our planet into the future.

The ICSU also advocated the need for more effective communication of science to both citizens and policy makers, and emphasised the advantages of involving citizens in the scientific process of environmental monitoring (Craglia *et al*., 2012). One interesting outcome of DE is the two-way exchange of information with citizens. Not only are the Earth's residents able to download huge volumes of data for professional and personal use, but the geo-referenced observations and opinions of citizens can be uploaded to complement professional surveys related to natural disasters, environmental conditions, and a wide range of other concerns. This opportunity has particular relevance to EO for involving citizen scientists and crowdsourcing with ground truthing exercises in remote regions (see Section 12.4; also Volume 1A—Section 10.3 and Volume 3B).

Background image: Landsat-8 OLI image of Roebuck Bay, WA, overlaid with tidal regions defined by the Intertidal Extents Model (ITEM; see Volume 2A—Excursus 2.1). **Source:** Steven Sagar, Geoscience Australia

Figure 11.1 Technological and cultural advances enabling Digital Earth

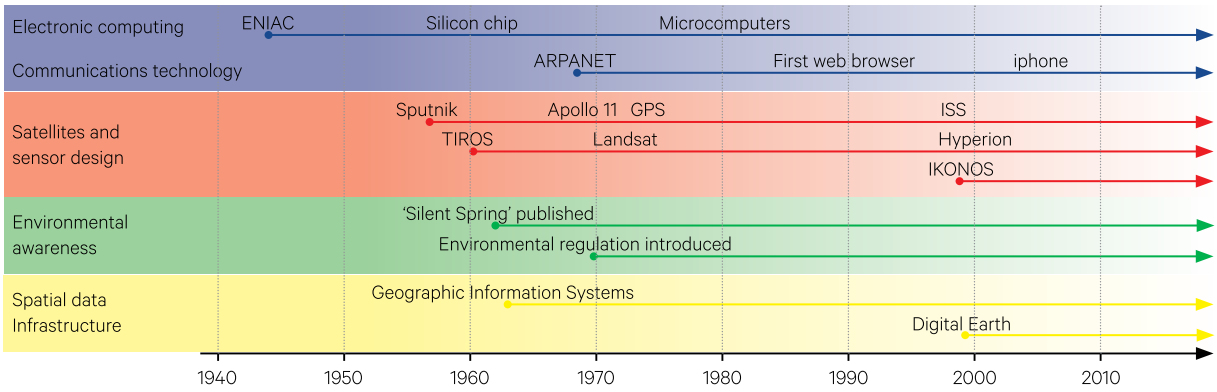

Adapted from Foresman (2008) Figure 1

As the array of sensors observing our planet—and our lives—increases (see Volume 1B—Section 10), so does the need for international cooperation, and better communication between data custodians and data users. The Sensor Web, including Volunteered Geographic Information (VGI) from citizens, has been likened to the DE nervous system—a mechanism to actively inform residents on Earth about current (and potential) events (De Longueville *et al.*, 2010). While the technological challenges of the sensor web increase with the volume of sensors, so do the expectations of users—data is expected to be reliable and relevant and its delivery is expected to be dynamic, interactive and engaging.

While originally envisioned as a virtual globe, and thus simplifying the interpretation of projected data (see Volume 2B), current realisations of the DE concept comprise a global network of data cubes (see Figure 11.2 and Section 8.3). The Australian implementation of a national data cube is introduced in Section 11.2.

Figure 11.2 Global network of data cubes

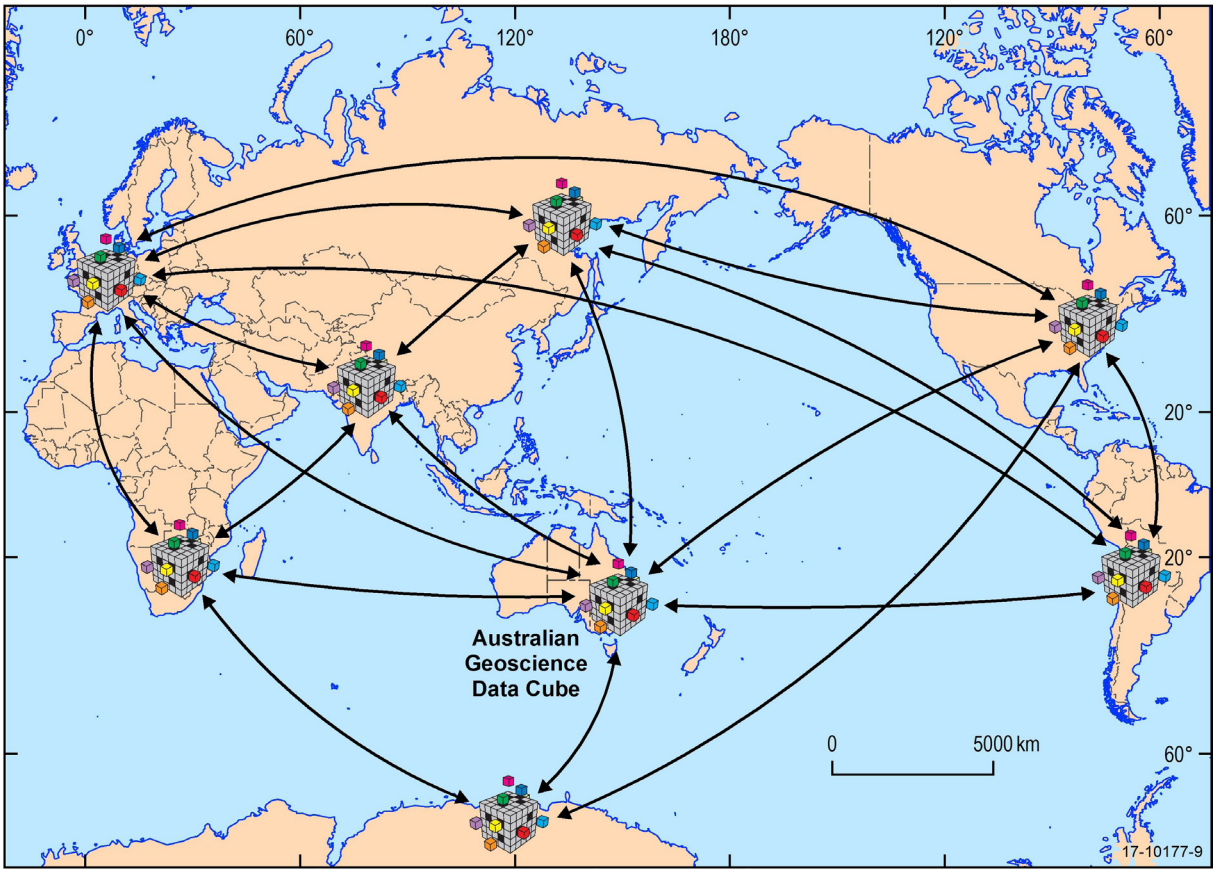

Source: Lewis *et al.* (2017) Figure 14

11.2 Digital Earth Australia

Originally called the Australian Geoscience Data Cube (AGDC) and rebadged as Digital Earth Australia (DEA) in 2016, this 'Big Data' infrastructure is a joint initiative between Geoscience Australia (GA), the National Computational Infrastructure (NCI) and CSIRO that 'aims to realise the full potential of Earth Observation data holdings for Australia' (Lewis *et al.*, 2017). The current Landsat archive managed by GA (dating from 1986), for example, comprises around 300,000 raw data images—or 10^{16} pixels of data. In addition to the raw data images, several continental-scale datasets have been derived from these Landsat images (see Section 14.1 and Volume 3), and Landsat is but one of many satellite series acquiring data over Australia (see Volume 1).

The existing archives of EO data clearly qualify the label of 'Big Data', having volume, velocity and variety (Laney, 2001), however, given the predicted increased volume of future sensors, particularly with higher revisit frequency, this data volume will increase significantly with time. As these volumes grow, so do the challenges for archiving and accessing the data efficiently. To meet these challenges, new methods of data analysis have been proposed that utilise the wealth of information contained within existing EO archives, including (Lewis *et al.*, 2017; Dhu *et al.*, 2017):

- detecting surface changes using time-series analysis techniques (Griffiths *et al.*, 2014; Kennedy *et al.*, 2010; Masek *et al.*, 2013; Zhu and Woodcock, 2014; see Section 9);
- systematically characterising land cover type(s) and climate indicators across multiple decades (Masek *et al.*, 2008; Mueller *et al.*, 2016; Sexton *et al.*, 2013; Hollman *et al.*, 2013; Kim *et al.*, 2015; see Volume 3A); and
- using 'best available pixel' composites, especially in cloudy locations (Hermosilla *et al.*, 2015; Thompson *et al.*, 2015; Zald *et al.*, 2016; see Section 10).

The DEA concept is illustrated in Figure 11.3 and comprises spatially and radiometrically consistent tiles. The original implementation was structured as regular, non-overlapping tiles of 4000´4000 pixels, with each tile spanning 1º by 1º, while in Version 2 the tile and pixel sizes are parameters that are set during data ingest. Version 2 also includes an indexing system for infrequently used data that directs processing functions to operate on the original data configuration, and thus avoids replication and associated problems of version control (Lewis *et al.*, 2016, 2017). The foundations for DEA products are summarised in Table 11.1.

Figure 11.3 DEA concept

Landsat scenes are reformatted as spatially-consistent tiles of data. While the spatial footprint of Landsat scenes changes over time, these tiles can maintain a constant footprint. This graphic shows four overlapping Landsat scenes over Brooks Island, Lake Eyre, acquired during 2009.

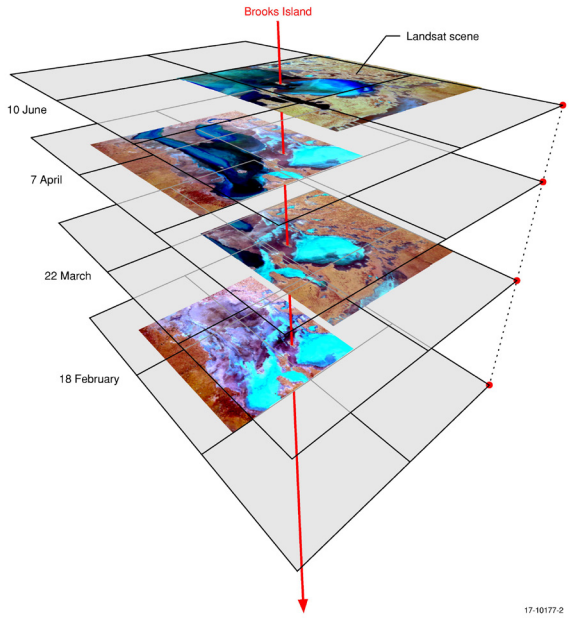

Source: Lewis *et al.* (2017) Figure 2

Digital Earth is a global initiative to construct a comprehensive virtual representation of the planet. It is a collaborative effort between Earth sciences, space sciences and information sciences to monitor and forecast natural and human phenomena. (International Society for Digital Earth)

Table 11.1 Foundations of DEA

Level 1	Level 2
Protocols to prepare data and manage archives	Accurate geometric alignment so that pixels are comparable in space (see Section 3.1.1.1 and Volume 2B)
	Accurate radiometric correction so that pixel values are comparable in time and space (see Figure 11.5 and Volume 2A—Section 3)
	Pixel quality flags to indicate known shortcomings in pixel values (see Volume 2A—Section 1.5)
	Tracking provenance and data and products
Software environment to manage and access data	Acquisition and inflow of data to 'analysis ready' level (see Section 3.2)
	Data cube infrastructure to index available data (see Section 8.3)
	Data and application platform to generate routine products and explore new products
	User interface and application layer to enable a variety of applications
High performance computing (HPC)/high performance data (HPD) environment to store and access enormous data volumes	Infrastructure based on National Environmental Research Data Interoperability Platform (NERDIP; Evans et al., 2015)
	NetCDF4/HDF5 data formats suitable for transdisciplinary access and high performance access Lewis et al. (2017)

Some of the operational products DEA has enabled include:

- Land Surface Reflectance—for Landsat imagery from 1987 to present (25 m spatial resolution with 16 day revisit time; see Excursus 11.1);
- Water Observations from Space (WOfS)—a web service displaying historical surface water observations for all of Australia, derived from Landsat imagery from 1987 to the present day (Mueller *et al*., 2016). WOfS aims is to allow a better understanding of:
  - where water is usually present;
  - where it is seldom observed; and
  - where inundation of the surface has been occasionally observed by satellite.

  This information is particularly valuable for flood modelling and assessment of environmental water flows (see Volume 1A—Excursus 5.1 and Volume 3B for details).
- Intertidal Extents Model (ITEM)—maps the extents and topography of Australia's intertidal mudflats, beaches and reefs, that is, the area exposed between high and low tide (Sagar *et al*., 2017, 2018). This information contributes to coastal management, habitat mapping and modelling applications (see Volume 2A—Excursus 2.1 for details).
- National Intertidal Digital Elevation Model (NIDEM)—provides intertidal elevation data for Australia's coastline, which is informative for mapping coastal habitats, coastal erosion and storm and flood mitigation efforts (see Figure 11.4);
- High and Low Tide Composites (HLTC)—visualise Australia's coasts, estuaries and reefs at low and high tide, without the influence of noise features such as clouds, breaking water and sunglint (Sagar *et al*., 2017). These datasets deliver a useful snapshot of Australia's coastline at different biophysical states.
- Fractional Cover (FC)—also derived from Landsat imagery from 1987 to the present day, this product maps the Australian landscape in terms of:
  - green (leaves, grass and growing crops);
  - brown (branches, dry grass or hay, and dead leaf litter); and
  - bare ground (soil or rock).

  This spatially detailed dataset monitors vegetation condition and extent through time, providing valuable insights for land managers (Scarth *et al*., 2010; Stewart *et al*., 2014; see Volume 3A); and
- Mangrove Dynamics—national maps of mangrove extent by canopy cover type have been generated annually from 1986 to 2016 for Australia (with 25 m spatial resolution; Lymburner *et al*., 2018).

Combinations of these products provide fascinating insights into the dynamics of land and water environments (see Volume 3).

Figure 11.4 National Intertidal Digital Elevation Model

Tidal flats of Roebuck Bay, WA, visualised in three dimensions.

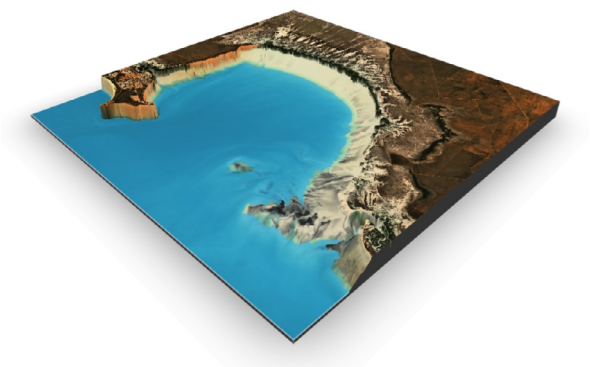

Excursus 11.1—GA Analysis Ready Data

Source: Lewis *et al.* (2017); GA (2015)

GA has acquired Landsat TM/ETM+ imagery over Australia for several decades and Landsat OLI imagery for several years. While this data has been used extensively for numerous land and coastal mapping studies, its utility for accurate monitoring of environmental resources has been limited by the processing methods that have been traditionally used to correct for the inherent geometric and radiometric distortions in EO imagery. To improve access to Australia's archive of Landsat TM/ETM+/OLI data, several collaborative projects have been undertaken (in conjunction with industry, government and academic partners), which have enabled implementation of a more integrated approach to image data correction. This approach is based on using physical models to correct for atmospheric effects, BRDF (Li *et al.*, 2010) and topographic shading (Li *et al.*, 2012) using DEM information (Li *et al.*, 2015) and has been applied to the complete Landsat archive to create the Land Surface Reflectance (LSR)[4] suite of products.

Across the Australian landmass and its coastal fringes, the LSR product suite provides standardised optical surface reflectance datasets, using robust physical models to correct for variations in image radiance values due to atmospheric properties, and Sun and sensor geometry. This suite of products aims to be available within a more general framework of nested grids with scalable cell sizes, for easy comparison between different products acquired by different sensors at varying spatial scales. The resulting stack of surface reflectance grids will effectively be consistent over space and time, and thus appropriate for identifying and quantifying environmental change.

The first product in this suite is the LSR25, a medium resolution (~25 m) grid based on the Landsat TM/ETM+/OLI archive and presents surface reflectance data in 25 m^2 grid cells. This product can be viewed as a data cube, with time as the third dimension (see Section 11.2). The surface reflectance data for each imaged date and time are stacked in chronological order, with Landsat TM/ETM+/OLI sources being interleaved as appropriate to their acquisition time. Interrogation of this data cube allows the time series for individual grid cells (as well as their heritage and data quality) to be extracted and compared.

To create a reliable data cube, all imagery in the time series need to be carefully calibrated to correct for radiometric and geometric distortions. The basic measurement in each LSR25 spectral band is Nadir BRDF Adjusted Reflectance (NBAR)—surface reflectance normalised for a nadir view with illumination at 45° elevation (Li *et al.*, 2010, 2012). The detailed procedures that are followed to create the LSR product are described below.

1. Geometric correction

Given that ancillary data sources are required for radiometric procedures (such as a digital surface model, atmospheric condition parameters, and BRDF parameters), geometric correction of imagery is a prerequisite to ensure that the ancillary data is correctly located in the image (Lewis *et al.*, 2017). This is most critical for terrain-illumination corrections and BRDF effect correction, which require sub-pixel locational accuracy (Li *et al.*, 2012, 2015).

The LSR25 product includes a Geometric Quality Assessment (GQA), which ranks pixels by an image matching algorithm. This information can be used to discard pixels with low spatial accuracy.

2. Radiometric correction

It has been traditionally assumed that Landsat imagery display negligible variation in Sun and sensor view angles, however these can vary significantly both within and between scenes, especially in different seasons and geographic regions (Li *et al.*, 2010, 2012). The LSR25 product delivers an estimate of surface reflectance from Landsat TM/ETM+/OLI/ data using physical rather than empirical models. This physical model couples BRDF and atmospheric correction models that can be applied to both flat and inclined surfaces (Li *et al.*, 2010, 2012; 2015), with the BRDF shape functions being derived from concurrent MODIS data (Lewis *et al.*, 2017). The resulting surface reflectance values are comparable both within individual images and between images acquired at different times and/or with different sensors (notwithstanding differences due to variations in spectral bandwidth between sensors). Accordingly, this product ensures that reflective value differences between imagery acquired at different times will be primarily due to on-ground changes in biophysical parameters rather than artefacts of the imaging environment (see Figure 11.5).

4 Formerly referenced as the Australian Reflectance Grid (ARG)

Figure 11.5 Radiometric correction of LSR25

Ancillary data inputs include digital surface model (1 arc second SRTM) to model elevation; concurrent MODIS imagery to derive BRDF shape function; aerosol data from Aeronet, AATSR, MISSR, MODIS and climatology sources; and field spectra collected at overpass times.

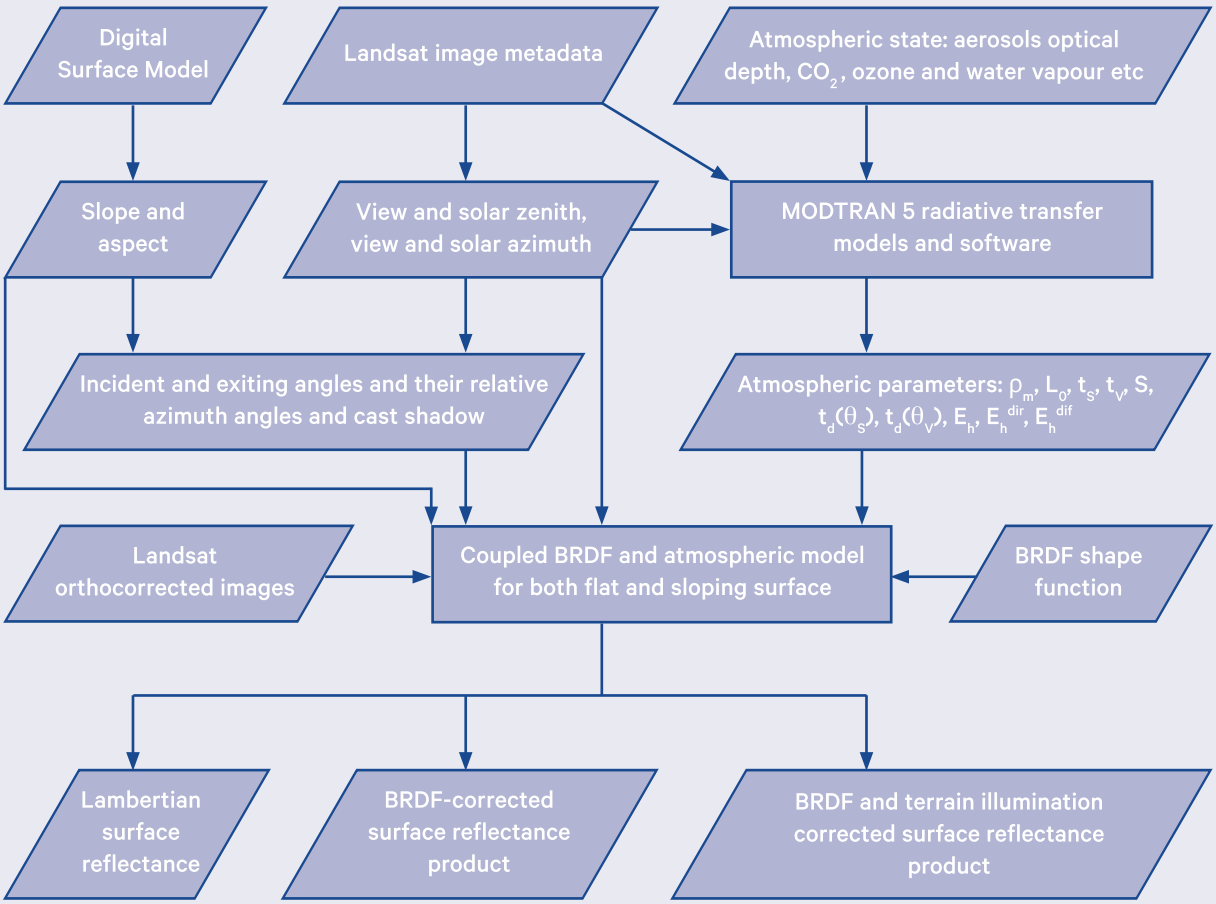

Source: Fuqin Li, Geoscience Australia

3. Pixel quality flags and metadata

To ensure that users understand the limitations of each pixel, quality flags are included in the LSR product. These are based on a series of tests applied during data preparation, including assessments of cloud, cloud shadow, topographic shadow, land/sea boundary, null values and sensor saturation (see Volume 2A—Section 1.5 for details). This approach allows all pixels in all available image scenes to be included in the product suite so that users can decide which pixels should be included in their analyses (Lewis *et al.*, 2017).

For complete transparency of EO products, the provenance of each pixel needs to be traceable back to its original observation values. The metadata included with the LSR products also assists dataset managers to determine when improvements in processing parameters, software or hardware warrants reprocessing of the archive or notifications to users. This includes maintaining hierarchical version numbers for software, ancillary data, and products, to indicate the significance of any changes.

11.3 Further Information

Digital Earth

International Society of Digital Earth (ISDE) (*www.digitalearth-isde.org*)

Global Spatial Data Infrastructure Association (*www.gsdi.org*),

International Council for Science and its Committee on Data for Science and Technology (*www.codata.org*),

Group on Earth Observations (GEO; and its geoportal, the GEO System of Systems (see Volume 1A—Section 1.5), *www.earthobservations.org*),

UN Committee of Experts on Global Geospatial Information Management (*ggim.un.org*),

Digital Earth Australia:

https://www.ga.gov.au/dea

11.4 References

Craglia, M., de Bie, K., Jackson, D., Pesaresi, M., Remetey-Fülöpp, G., Wang, C., Annoni, A., Bian, L., Campbel, F., Ehlers, M., van Genderen, J., Goodchild, M., Guo, H., Lewis, A., Simpson, R., Skidmore, A., and Woodgate, P. (2012). Digital Earth 2020: towards a vision for the next decade. *International Journal of Digital Earth*, 5, 4–21.

De Longueville, B., Annoni, A., Schade, S., Ostlander, N., and Whitmore, C. (2010). Digital Earth's nervous system for crisis events: real-time sensor Web enablement of volunteered geographic information. *International Journal of Digital Earth,* 3, 242–259.

Dhu, T., Dunn, B., Lewis, B., Lymburner, L., Mueller, N., Telfer, E., Lewis, A., McIntyre, A., Minchin, S., and Phillips, C. (2017) Digital earth Australia—unlocking new value from earth observation data. *Big Earth Data*, 1, (1–2), 64–74. *https://doi.org/10.1080/20964471.2017.1402490*

Evans, B., Wyborn, L., Pugh, T., Allen, C., Antony, J., Gohar, K., Porter, D., Smillie, J., Trenham, C., Wang, J., Ip, A., Bell, G. (2015). The NCI high performance computing and high performance data platform to support the analysis of petascale environ-mental data collections. In: *Environmental Software Systems. Infrastructures, Services and Applications* (Eds: Denzer, R., Argent, R.M., Schimak, G., Hrebicek, J.). IFIP Advances in Information and Communication Technology. Springer International Publishing, pp. 569–577.

Foresman, T.W. (2008). Evolution and implementation of the Digital Earth vision, technology and society, *International Journal of Digital Earth*, 1(1), 4–16, *https://doi.org/10.1080/17538940701782502*

GA (2015). *Australian Reflectance Grid (ARG25) Product Description V1.1*. Geoscience Australia, Canberra. *https://d28rz98at9flks.cloudfront.net/75062/Australian_Reflectance_Grid_ARG25_Product_Description_V1_1.PDF*

Goodchild, M.F., Guo, H., Annoni, A., Bian, L., de Bie, K., Campbell, F., Craglia, M., Ehlers, M., van Genderen, J., Jackson, D., Lewis, A.J., Pesaresi, M., Remetey-Fülöpp, G., Simpson, R., Skidmore, A., Wang, C., and Woodgate, P. (2012). Next-generation Digital Earth. *Proceedings of National Academy of Sciences of the USA*, 109 (28), 11088–11094.*https://doi.org/10.1073/pnas.1202383109*

Gore, A. (1998). *The Digital Earth: Understanding our planet in the 21st Century*. Speech given at the California Science Center, Los Angeles, on 31 January 1998. *http://www.crcsi.com.au/assets/Resources/c9fed807-0a8b-44ac-b167-690c32f6200a.pdf*

Griffiths, P., Kuemmerle, T., Baumann, M., Radeloff, V.C., Abrudan, I.V., Lieskovsky, J., Munteanu, C., Ostapowicz, K., and Hostert, P. (2014). Forest disturbances, forest recovery, and changes in forest types across the Carpathian ecoregion from 1985 to 2010based on Landsat image composites. *Remote Sensing of Environment*, 151, 72–88. *http://dx. doi.org/10.1016/j.rse.2013.04.022*

Hermosilla, T., Wulder, M.A., White, J.C., Coops, N.C., and Hobart, G.W. (2015). An integrated Landsat time series protocol for change detection and generation of annual gap-free surface reflectance composites. *Remote Sensing of Environment*, 158, 220–234. *https://doi.org/10.1016/j.rse.2014.11.005*

Hollmann, R., Merchant, C.J., Saunders, R., Downy, C., Buchwitz, M., Cazenave, A., Chuvieco, E., Defourny, P., de Leeuw, G., Forsberg, R., Holzer-Popp, T., Paul, F., Sandven, S., Sathyendranath, S., van Roozendael, M., and Wagner, W. (2013). The ESA climate change initiative: satellite data records for essential climate variables. *Bulletin of the American Meteorological Society*, 94, 1541–1552. *http://dx.doi.org/10.1175/BAMS-D-11-00254.1*

Kennedy, R.E., Yang, Z., and Cohen, W.B. (2010). Detecting trends in forest disturbance and recovery using yearly Landsat time series: 1. LandTrendr temporal segmentation algorithms. *Remote Sensing of Environment*, 114, 2897–2910. *https://doi.org/10.1016/j.rse.2010.07.008*

Kim, Y., Kimball, J.S., Robinson, D.A., and Derksen, C. (2015). New satellite climate data records indicate strong coupling between recent frozen season changes and snow cover over high northern latitudes. *Environmental Research Letters*, 10, 84004.

Laney, D. (2001). 3D data management: controlling data volume, velocity and variety. *META Group Research Note. 6: p. 70. https://blogs.gartner.com/doug-laney/files/2012/01/ad949-3D-Data-Management-Controlling-Data-Volume-Velocity-and-Variety.pdf*

Lewis, A., Lymburner, L., Purss, M.B.J., Brooke, B., Evans, B., Ip, A., Dekker, A.G., Irons, J.R., Minchin, S., Mueller, N., Oliver, S., Roberts, D., Ryan, B., Thankappan, M., Woodcock, R., and Wyborn, L. (2016). Rapid, high-resolution detection of environmental change over continental scales from satellite data—the Earth Observation Data Cube. *International Journal of Digital Earth*, 9(1), 106–111. *https://doi.org/10.1080/17538947.2015.1111952*

Lewis, A., Oliver, S., Lymburner, L., Evans, B., Wyborn, L., Mueller, N., Raevksi, G., Hooke, J., Woodcock, R., Sixsmith, J., Wu, W., Tan, P., Li, F., Killough, B., Minchin, S., Roberts, D., Ayers, D., Bala, B., Dwyer, J., Dekker, A., Dhu, T., Hicks, A., Ip, A., Purss, M., Richards, C., Sagar, S., Trenham, C., Wang, P., and Wang, L.-W. (2017). The Australian geoscience data cube—Foundations and lessons learned. *Remote Sensing of Environment*, 202, 276–292. *https://doi.org/10.1016/j.rse.2017.03.015*

Li, F., D.L.B. Jupp, S. Reddy, L. Lymburner, N. Mueller, P. Tan, and A. Islam (2010). An Evaluation of the Use of Atmospheric and BRDF Correction to Standardize Landsat Data. *IEEE Journal of Selected Topics in Applied Earth Observations and Remote Sensing*, 3(3), 257–270. *https://doi.org/10.1109/JSTARS.2010.2042281*

Li, F., Jupp, D.L.B., Thankappan, M., Lymburner, L., Mueller, N., Lewis, A., and Held, A. (2012). A physics-based atmospheric and BRDF correction for Landsat data over mountainous terrain. *Remote Sensing of Environment*, 124, 756–770. *https://doi.org/10.1016/j.rse.2012.06.018*

Li, F., Jupp, D.L.B., and Thankappan, M. (2015). Issues in the application of Digital Surface Model data to correct the terrain illumination effects in Landsat images, *International Journal of Digital Earth*, 8(3), 235–257. *https://doi.org/10.1080/17538947.2013.866701*

Li, F., Jupp, D.L.B., Paget, M., Briggs, P.R., Thankappan, M., Lewis, A., and Held, A. (2017). Improving BRDF normalisation for Landsat data using statistical relationships between MODIS BRDF shape and vegetation structure in the Australian continent. *Remote Sensing of Environment*, 195, 275–296. *http://dx.doi.org/10.1016/j.rse.2017.03.032*

Lymburner, L., Bunting, P., Lucas, R., Scarth, P., Alam, I., Phillips, C., Ticehurst, C. and Held, A. (2019). Mapping the multi-decadal mangrove dynamics of the Australian coastline. *Remote Sensing of Environment,* 111185. *https://doi.org/10.1016/j.rse.2019.05.004*

Masek, J.G., Huang, C., Wolfe, R., Cohen, W., Hall, F., Kutler, J., and Nelson, P. (2008). North American forest disturbance mapped from a decadal Landsat record. *Remote Sensing of Environment*, 112, 2914–2926. *http://dx.doi.org/10.1016/j.rse.2008.02.010*

Masek, J.G., Goward, S.N., Kennedy, R.E., Cohen, W.B., Moisen, G.G., Schleeweis, K., and Huang, C. (2013). United States Forest disturbance trends observed using Landsat time series. *Ecosystems*, 16, 1087–1104. *http://dx.doi.org/10.1007/s10021-013-9669-9*.

Mattmann, C.A. (2013). Computing: A vision for data science. *Nature*, 493:473–475. *http://dx.doi.org/10.1038/493473a*

Mueller, N., Lewis, A., Roberts, D., Ring, S., Melrose, R., Sixsmith, J., Lymburner, L., McIntyre, A., Tan, P., Curnow, S., and Ip, A. (2016). Water observations from space: mapping surface water from 25 years of Landsat imagery across Australia. *Remote Sensing of Environment*, 174, 341–352. *http://dx.doi.org/10.1016/j.rse.2015.11.003*

Sagar, S., Roberts, D., Bala, B., and Lymburner, L. (2017). Extracting the intertidal extent and topography of the Australian coastline from a 28 year time series of Landsat observations. *Remote Sensing of Environment,* 195, 153–169. *https://doi.org/10.1016/j.rse.2017.04.009*

Sagar, S., Phillips, C., Bala, B., Roberts, D., and Lymburner, L. (2018). Generating Continental Scale Pixel-Based Surface Reflectance Composites in Coastal Regions with the Use of a Multi-Resolution Tidal Model. *Remote Sensing*, 10, 480. *https://doi.org/10.3390/rs10030480*

Scarth, P., Roder, A., and Schmidt, M. (2010). Tracking grazing pressure and climate interaction—the role of Landsat fractional cover in time series analysis. *Proceedings of the 15th Australian Remote Sensing and Photogrammetry Conference*. 13-17 September, Alice Springs.

Sexton, J.O., Song, X.-P., Huang, C., Channan, S., Baker, M.E., and Townshend, J.R. (2013). Urban growth of the Washington, D.C.–Baltimore, MD metropolitan region from 1984 to 2010 by annual, Landsat-based estimates of impervious cover. *Remote Sensing of Environment*, 129, 42–53. *http://dx.doi.org/10.1016/j.rse.2012.10.025*

Stewart, J.B., Rickards, J.E., Randall, L.A., McPhee, R.K., and Paplinska, J.Z. (2014). *Ground cover monitoring for Australia: Final report July 2012 to June 2013*, ABARES Technical report 14.1, Australian Bureau of Agricultural and Resource Economics and Sciences, Canberra, May 2014.

Thompson, S.D., Nelson, T.A., White, J.C., and Wulder, M.A. (2015). Mapping dominant tree species over large forested areas using Landsat best-available-pixel image composites. *Canadian Journal of Remote Sensing*, 41, 203–218. *http://dx.doi.org/10.1080/07038992.2015.1065708*

Zald, H.S.J., Wulder, M.A., White, J.C., Hilker, T., Hermosilla, T., Hobart, G.W., and Coops, N.C. (2016). Integrating Landsat pixel composites and change metrics with lidar plots to predictively map forest structure and aboveground biomass in Saskatchewan. *Canadian Journal of Remote Sensing*, 176, 188–201. *http://dx.doi.org/10.1016/j.rse.2016.01.015*

Zhu, Z., and Woodcock, C.E. (2014). Continuous change detection and classification of land cover using all available Landsat data. *Remote Sensing of Environment*, 144, 152–171. *https://doi.org/10.1016/j.rse.2014.01.011*

Merging EO and Other Datasets

Ancillary datasets may be merged with EO imagery for a range of purposes and applications. Relevant attributes of ancillary data are introduced in Section 3.3 above. Assuming that any selected ancillary data sources are thematically appropriate to the EO dataset, the most critical aspects of scale for their integration are generally space and time.

Clearly, to compare two sets of data for a location they need to describe the exact same position on the ground. While the advent of portable GPS has simplified the process of accurately locating ground sites, locational accuracy alone does not ensure spatial compatibility between different sources of spatial data. If the characteristics of resolution, density and extent of the EO dataset cannot be related to those characteristics in the ancillary dataset then they will not integrate sensibly. For example, it is difficult to relate a pixel from an AVHRR image (1.1 km x 1.1 km) with point observations based on an area of 1 m x 1 m. The concept of a surface mosaic is introduced in Section 1.4 above, and the issue of scale is further discussed in Volume 2E.

In addition to spatial scale, the two datasets need to be coincident in time, at least in terms of relevant attributes of the surface features being identified. Timing of data acquisition can matter in terms of regular natural rhythms in target features, such as diurnal, seasonal and annual cycles. It is also relevant to variations in local conditions, such as changes in soil moisture, extent of cloud cover, and water surface conditions. The precise requirements for coincident timing will differ for different applications but, yet again, an understanding of the way the EO and ancillary datasets have been acquired is a prerequisite for credible results.

The following two sections present examples of ancillary datasets that may be integrated with EO data, including sample-based data, such as manual field sites, automatic sensors, spectral libraries and volunteered data (see Section 12), and gridded datasets, such as GIS, Digital Elevation Models (DEM) and meteorological records (see Section 13).

Contents

12 Sample-based Datasets 135

13 Gridded Datasets 149

Background image on previous page: Aerial imagery, acquired in March 2018 and centred on Collins Park, Forrest, ACT, overlaid with map information showing roads and cadastre in yellow. **Source:** Tony Sparks, Icon Water, based on ACT Government orthorectified imagery (MGA55 coordinates, GDA94 datum) acquired in 2018. The imagery was supplied by AAM (Ref. No.: 26121A) CC BY 4.0 and GIS data courtesy of ACT Office of the Surveyor-General and Land Information

12 Sample-based Datasets

The concept of scale is reviewed in Sections 1 and 2 above (see also Volume 1B—Section 1) and has particular significance when using ancillary datasets with EO imagery. In this context, scale is most relevant to the spatial and temporal dimensions. These spatial and temporal scales, however, may not be correlated, that is, the most appropriate scale for measuring a given attribute may not be the same as the best scale to either:

- estimate its values from population statistics (such as mean or variance) from a sample; or
- predict its values by computing the expected value at a particular location/time (Gallant *et al*., 2008).

The following sub-sections will review different types of ancillary data that are available in Australia. Some of the caveats for integration with EO datasets are also considered:

- manually-collected field site data (see Section 12.1);
- automatic sensors (see Section 12.2);
- spectral libraries (see Section 12.3); and
- volunteered data (see Section 12.4).

12.1 Manually-Collected Field Site Data

Recommended procedures and protocols for the manual collection of soil and vegetation information at Australian field sites are detailed in Hnatiuk *et al*. (2009) and McKenzie *et al*. (2008). Hnatiuk *et al*. (2009) defines 'attributes needed to describe systematically the site and soil conditions related to landform, vegetation, land surface, soil profile and substrate materials' as well as relevant terminology.

TERN Australia (2018) presents detailed information for the calibration and validation (Cal/Val) of terrestrial environmental variables derived from EO datasets and models, including best practice guidelines for collection of field datasets in the Australian environment for this purpose. This reference recommends standards for:

- collection and management of field data (see Trevithick, 2018), including ground biomass (Schaefer, 2018b), vegetation spectroscopy (Suarez *et al*., 2018; Chisholm and Hueni, 2018), ground cover (Stewart and Howorth, 2018), and terrestrial lidar (Calders *et al*., 2018);
- calibration of EO sensors (see Malthus, 2018); and
- calibration and/or validation of EO datasets and derived biophysical products (Soto-Berelov *et al*, 2018), including SAR (Mitchell and Thankappan, 2018), LAI (Schaefer *et al*., 2018), ground cover monitoring (Stewart *et al*., 2018), fractional cover (Scarth *et al*., 2018), persistent green vegetation fraction (Gill *et al*., 2018), phenology (Restrepo-Coupe *et al*., 2018), foliar chemistry (Youngentob, 2018), tree crown delineation (Cabello-Leblic, 2018), hyperspectral data (Broomhall *et al*., 2018), airborne lidar (Quadros and Keysers, 2018), and airborne imagery (Johansen *et al*., 2018).

Excursus 12.1 introduces an Australian system, the National Vegetation Information System (NVIS), that has been adopted by state and federal government agencies for collecting and classifying information related to vegetation type. This system is further detailed in Volume 3A. An EO-based system for mapping vegetation type in NSW, which is based on the NVIS framework, is called the NSW Stage Vegetation Type Map (SVTM). This product is described in Volume 3A.

Background image: Fisheye photograph of *Eucalyptus* canopy at TERN Warra Tall Eucalypt Supersite in Tasmania[5]. **Source:** Tim Wardlaw, University of Tasmania

5 *https://supersites.tern.org.au/supersites/wsbe*

Excursus 12.1—National Vegetation Information System

Source: Richard Thackway, Australian National University
Further Information: NVIS Technical Working Group (2017); NVIS (2019)

NVIS (National Vegetation Information System) is now accepted as the national method for compiling and translating State and Territory mapped vegetation data on the extent and distribution of vegetation types in Australia (see Volume 3A for details). Much of the vegetation information available in the national NVIS database was collected and classified using the CSIRO guidelines prior to 2003 (such as Specht, 1970; Walker and Hopkins, 1990). In those states and territories that used different attribute and mapping frameworks, the NVIS framework was used to reclassify and remap those datasets. Today all states and territories generate and supply vegetation mapping and attribute data to the Australian Government's NVIS database that is consistent with the NVIS framework (NVIS, 2019).

As well as providing a framework for translating and compiling available vegetation mapping, NVIS is a comprehensive system that:

- specifies guidelines for standardising the collection, compilation and monitoring of Australia's vegetation;
- stores data on the type and extent of native vegetation with grid cell resolution of 100 m × 100 m;
- holds standardised geographic and attribute data for native vegetation, non-native vegetation and non-vegetated cover types across Australia that complements and facilitates analysis and reporting; and
- provides, monitors and maintains the technical infrastructure to support these activities (NVIS, 2019).

The approach adopted for describing and classifying vegetation derives from Hnatiuk *et al.* (2009). This hierarchical approach can be used to classify native, agricultural and other vegetation on the basis of its:

- structure—both vertical and horizontal—growth form, height, cover and strata; and
- floristics—the dominant genera or species in different strata, plus characteristic plant species (Hnatiuk *et al.*, 2009).

Basically, at each mapped polygon or grid cell (native vegetation, non-native vegetation and non-vegetated) is described systematically (see Table 12.1). Initially the dominant stratum and, where present, the mid-stratum and/or ground stratum, are distinguished for specific locations. Key attributes of relevant strata are then measured at those locations and the NVIS framework is used to classify them. For any given location, the dominant stratum is generally determined by analysing available EO imagery prior to assessing the other levels by field survey. Additional levels may be included to describe broad florisitic subformations, and other associations if required for particular types of vegetation, such as wetlands or rainforests. Nomenclature and methods for using the NVIS classification system are detailed in Thackway *et al.* (2008), Hnatiuk *et al.* (2009) and NVIS Technical Working Group (2017).

Table 12.1 Information Hierarchy

Level 5 (association) is recommended as the minimum level of input for input data to NVIS. Hnatiuk *et al.* (2009) refer to Level 1 as Formation.

Level	Category	Description
1	Class	Dominant growth form for the structurally dominant stratum
2	Structural formation	Dominant growth form, cover and height for the structurally dominant stratum
3	Broad floristic formation	Dominant genus (or genera) plus growth form, cover and height for the structurally dominant stratum
4	Sub-formation	Dominant genus (or genera) plus growth form, cover and height for each of the three main strata. (Upper, Mid and Ground)
5	Assocation	Dominant growth form, height, cover and species (to a maximum of 3 species) for each of the three main strata. (Upper, Mid and Ground)
6	Sub-association	Dominant growth form, height, cover and species (to a maximum of 5 species) for each of the substrata

Source: NVIS Technical Working Group (2017)

To populate the national NVIS database, detailed mapped polygon or grid cell (native vegetation, non-native vegetation and non-vegetated) datasets from each State and Territory have been translated and compiled to conform to the NVIS framework. The national database is updated as new data becomes available. NVIS Version 5.1 products include:

- detailed data from state and territory custodians, which is appropriate for use at a regional scale; and
- for national scale analyses, 33 Major Vegetation Groups (MVG) and 85 Major Vegetation Subgroups (MVS) defined by generalising the detailed data and adding non-NVIS gap-fill data (NVIS, 2019).

For the national-scale (Version 5.1) products, analysis tools are also provided, such as raster uncertainty layers to indicate data quality. MVG and MVS represent the dominant native vegetation type in each grid cell. These maps are produced for both current (extant) vegetation and estimated (pre-European) vegetation (see Volume 3A). For example, the NVIS methodology has also been adopted within the workflows used to create the NSW State Vegetation Type Map (SVTM; see Volume 3A).

12.2 Automatic Sensors

A variety of unmanned sensors may be used to record biophysical data at defined field locations on or near the ground, either on a temporary or permanent basis. Examples of such sensors include cameras, acoustic recorders, meteorological sensors, water sensors, and flux towers (see Volume 1A). While webcam photography has been used for monitoring environmental conditons for some time, webcam networks are being established for continual monitoring of ecosystems (Tanis *et al*., 2018).

Two of the key integrated observation networks that have been established in Australia are the:

- Terrestrial Ecosystem Research Network (TERN; see Excursus 12.2); and the
- Integrated Marine Observing System (IMOS; see Excursus 12.3).

As introduced below, these networks deliver a range of biophysical parameters that can be used to calibrate and validate EO datasets.

Excursus 12.2—Terrestrial Ecosystem Research Network (TERN)

Source: *http://www.tern.org.au*

The Terrestrial Ecosystem Research Network (TERN) observes, measures and records critical terrestrial ecosystem parameters and conditions for Australia over time, from continental scale to field sites at hundreds of representative locations. This information is standardised, integrated and transformed into model-ready data, enabling researchers to discern and interpret changes in land ecosystems.

The goal of TERN is to provide open access for researchers to Australia's land-based ecosystem monitoring infrastructure, data and research tools. This involves using nationally-consistent and standardised ecosystem measures over time to observe and measure ecosystem change across the continent in three measurement themes:

- biodiversity—monitoring patterns of change and their drivers at scales from genes to ecosystems;
- carbon and water—monitoring carbon stocks/flows and water resources; and
- land and terrain—tracking key processes and monitoring soils and vegetation.

As Australia's land ecosystem observatory, TERN is structured around three scales of observation:

- Landscape assessment monitoring—mostly through EO techniques based on satellite data, with the use of airborne data from autonomous vehicles (UAVs). Modelling and synthesis activities are also undertaken to extrapolate and interpolate from observational data to produce modelled data products.
- Ecosystem surveillance monitoring—which enables detection and monitoring of biodiversity change across a wider spatial extent of environments. TERN uses an extensive network of monitoring plots distributed along environmental gradients and in key biomes (see Figure 12.1).
- Targeted ecosystem process monitoring—which gives a high level of detail at a small number of sites. This is done through intensive field stations or 'SuperSites' which combine instrumented or sensor measurements.

TERN delivers:

- Data—soil and vegetation measurements; gas, energy, and water exchange measurements; standardised EO datasets; and modelled data products about soil, climate, and landscape attributes;
- Tools—nationally consistent field methods for data collection and validation; vegetation and soil samples for physical analysis; data collection apps; and data publishing systems; and
- Infrastructure—supporting the discovery, access, and re-use of TERN data and other ecosystem data housed in our systems.

In particular, the EO products delivered via TERN include land cover dynamics and phenology, vegetation composition and diversity, fire dynamics and impacts, vegetation structural properties and biomass, field survey datasets, airborne datasets, corrected surface reflectance products and other environmental data such as solar radiation, rainfall, and water vapour pressure (see Excursus 14.1).

Figure 12.1 TERN sites

Field sites around Australia being monitored by TERN (current in September 2019).

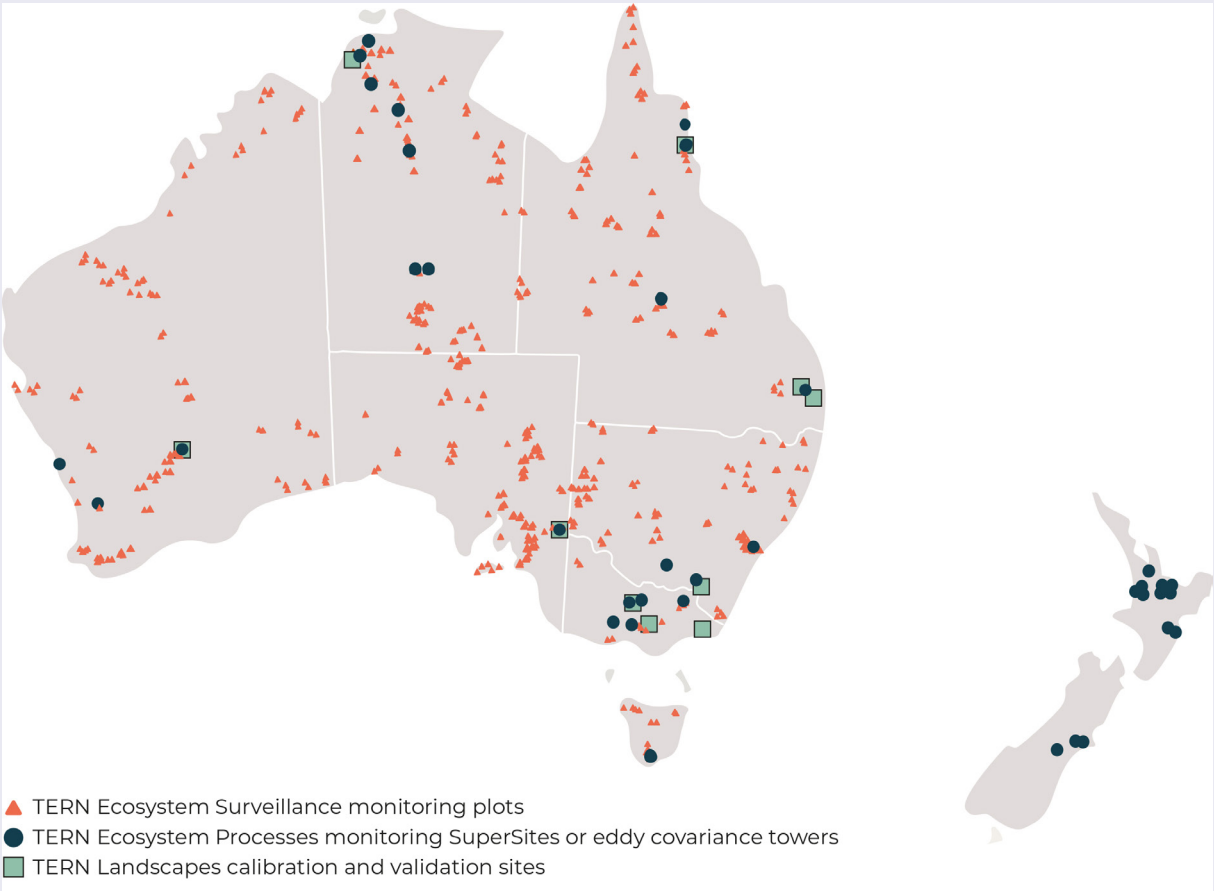

A site is a small area of land considered representative of the landform, vegetation, land surface and other land features associated with the soil observation. (Speight and McDonald, 2009)

Excursus 12.3—Integrated Marine Observing System (IMOS)

Source: *http://imos.org.au*

Since 2006, the Integrated Marine Observing System (IMOS) has been routinely operating a wide range of observing equipment throughout Australia's coastal and open oceans, making all of its data accessible to the marine and climate science community, other stakeholders and users, and international collaborators.

IMOS is a national collaborative research infrastructure, supported by Australian Government. It is operated by a consortium of institutions as an unincorporated joint venture, with the University of Tasmania as Lead Agent.

IMOS currently has a portfolio of Facilities that undertake systematic and sustained observing of Australia's marine environment, across scales (from open ocean, onto the continental shelf, and into the coast), and across disciplines (physics, biogeochemistry, and biology and ecosystems), including:

- Argo Floats—autonomous profiling floats that measure both temperature and salinity in the upper 2000 m of the ocean every 10 days;
- Ships of Opportunity—volunteer commercial and research vessels to collect data relating to physical, chemical and biological oceanography and ecology;
- Deep Water Moorings—located in Antarctica, sub-Antarctic, sub-tropical and tropical open waters around Australia, these moorings provide long-term information about temporal patterns in oceanographic and biological conditions;
- Ocean Gliders—autonomous underwater gliders that measure temperature, salinity, dissolved oxygen, chlorophyll and turbidity in sub-surface waters;
- Autonomous Underwater Vehicles—provide rapid and cost-effective high resolution, accurately georeferenced and targeted acoustic imagery of the seafloor;
- National Mooring Network—located around the Australian coastline (see Figure 12.2), this network delivers long term, time series observations from a range of instruments including Acoustic Doppler Current Profilers (ADCP), WetLabs Water Quality Meters (WQM), fluorometers, Conductivity-Temperature-Depth (CTD) with turbidity and Dissolved Oxygen (DO) sensors;
- Ocean Radar—map ocean surface currents over meso-scale areas with high spatial and temporal resolution;
- Animal Tracking—uses acoustic technology, CTD satellite trackers and bio-loggers to monitor coastal and oceanic movements of marine animals around Australia and Antarctica;
- Wireless Sensor Networks—provide real time, spatially dense measurements of biophysical environmental variables on the Great Barrier Reef;
- Satellite Remote Sensing—acquire and process EO imagery for sea surface temperature (SST), ocean colour, oceanic surface wave and sea surface altimetry applications;
- Marine Microbiome Initiative—monthly water samples collected around Australia will build a time series of microbial data; and
- New Technology Proving—capability allowing for the development and establishment of new technologies, methods, and approaches in collecting sustained ocean observations.

IMOS observations are turned into data that can be discovered, accessed, downloaded, used and reused in perpetuity by our data Facility, the Australian Ocean Data Network (AODN). All of the IMOS data is freely accessible via the AODN Portal: *http://portal.aodn.org.au*

Figure 12.2 IMOS National mooring network

Location of the national reference station and shelf moorings (red triangles), acidification moorings (CO_2 icon) and passive acoustic moorings (hydrophone icon) around the Australian continent.

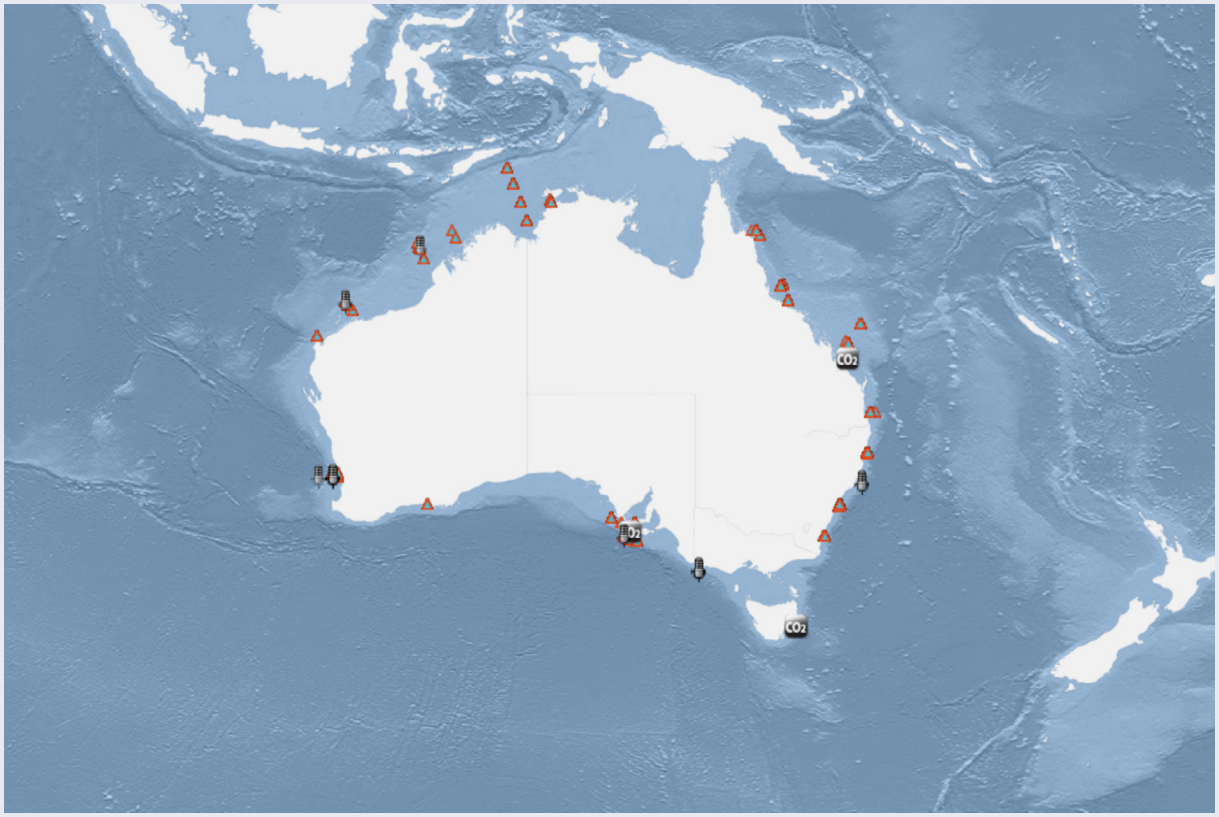

Know thy site.
(Ray Leuning)

12.3 Spectroscopy datasets

Spectroscopy datasets are commonly acquired in the field and/or laboratory to augment EO analyses. Some of the sensors that can be used to acquire spectroscopy data included spectrometers/ spectroradiometers, spectrophotometers, spectrographs or spectral analyzers (Chisholm and Hueni, 2018; see Volume 1A—Section 13). Recommended procedures for collecting spectral datasets for different applications in an Australian context are detailed in TERN Australia (2018).

Spectroscopy datasets have been used to calibrate data from EO sensors, validate EO analyses and/or investigate spectral reflectance characteristics of specific ground materials, such as particular plants or minerals (Chisholm and Hueni, 2018). A range of systems has been proposed to organise spectroscopy datasets, including:

- spectral libraries—static collections of reference spectra, such as the USGS spectral library or the ASTER spectral library;
- spectral databases—store spectral data in an organised manner, with appropriate metadata (Hueni *et al*., 2011); and
- spectral information systems (SIS)—provide tools to access and process spectral databases (Chisholm and Hueni, 2018).

Chisholm and Hueni (2018) describe the lifecycle of spectroscopy datasets in terms of six generic stages:

- planning of sampling experiments, including the definition of sampling protocols adhering to a metadata standard;
- actual data acquisition, where data are acquired according to predefined sampling protocols;
- ingestion of the acquired spectral data into the SIS;
- augmentation of the automatically generated metadata by manually or semi-automatically adding further metadata parameters to the spectral data collection;
- building further information by applying algorithms to spectral data and metadata; and
- retrieval of information for a particular purpose.

Unlike simple spectral libraries, SIS allow multiple reflectance measurements to be dynamically stored for a given target, with subsequent additional measurements being added over time and space. As with EO datasets, processing levels can be defined for spectroscopic data and its metadata (see Table 12.2), which enable the provenance of specific data to be traced and/or the most appropriate data for a particular task to be selected. SIS analysis tools are designed to use the full potential of combined metadata spaces (Wason and Wiley, 2000) and spectral spaces (Hueni *et al* 2012).

For example, SPECCHIO (Bojinski *et al*., 2003; Hueni *et al*., 2006, 2009) is an open source project that enables storage and analysis of spectral databases, including generating higher-level products and correcting spectral data for sampling equipment or sensor artefacts (Hueni *et al*., 2012). This Swiss product is freely available for ingesting, managing, and processing of spectral datasets (Hueni *et al*., 2009; SPECCHIO, 2019). The Australian Spectral Database, AUS-SPECCHIO (Chisholm and Hueni, 2018) will be hosted by Geoscience Australia in the near future (see Volume 3A).

Table 12.2 Spectral database processing levels

Level	Description
Raw	Raw, sensor generated files, stored as binary objects on a file system or in the database system. This forms the first tier of the DIKW hierarchy and allows regeneration of data/information at the following tiers (see Volume 1A—Section 1).
Level 0	Spectral measurements as digital number (DN), described by auto-generated metadata augmented by user-defined metadata parameters.
Level 1	Spectral measurements as radiances traceable to an international standard. Metadata as in level 0 but includes information related to the data calibration process.
Level 2	Spectral measurements as factors (reflectance factors, transmittance, absorbance), corrected for reference panel deficiencies where needed (non-ideal reflective and Lambertian properties). Metadata as in level 1 but includes information related to the data calibration process.
Higher level products	Products derived from the lower levels, similar to products generated in imaging spectrometer processing systems, such as estimated bio-geophysical properties.

Source: Chisholm and Hueni (2018) Table 14.2

12.4 Volunteered data

Data that has been volunteered by community members is becoming a valuable source of timely, local observations for a range of EO-based applications, including natural disaster management, faunal and floral surveys, compliance monitoring and assessment of water conditions. Volunteered data can be broadly divided into two categories:

- citizen science—collection of pre-defined measurements, photos and observations at identified locations, as part of a coordinated, scientific study; and
- crowdsourcing—*ad hoc* collection of potentially relevant observations.

The locational accuracy of volunteered information has improved with easy access to GPS technology in smart phones. Similarly, phone-based cameras allow volunteers to acquire and transmit local perspectives of various environmental events and conditions. The value of such information is further improved by independent time and date stamping.

Crowdsourcing can involve unplanned data collection by informal sensors. For example, as described in Volume 1B—Section 10, in California on 24 August 2014, fitness monitors tracked the time their wearers were woken by an earthquake. The resulting compilation of data by the manufacturer provided a map of the epicentre, based on the relationship between each wearer's location and the time they were woken from sleep (see Figure 12.3).

The key to acquiring consistently valuable data from volunteers is the same as for most other ancillary data sources: relevant timing, compatible spatial scaling and training of volunteers. One successful example of citizen scientists assisting EO studies is the global monitoring program 'EyeonWater'. The Australian implementation of this initiative is described in Excursus 12.4 (see Volume 3B—Section 11 for details).

Figure 12.3 Inadvertent map of distance to earthquake epicentre

Wearable devices assist seismic observations after a 6.0 earthquake occurred in Souther Napa Valley, California at 3:20 am on August 2014. As distance from the epicentre increased, fewer wearers of the Jawbone Up fitness monitor were woken from sleep.

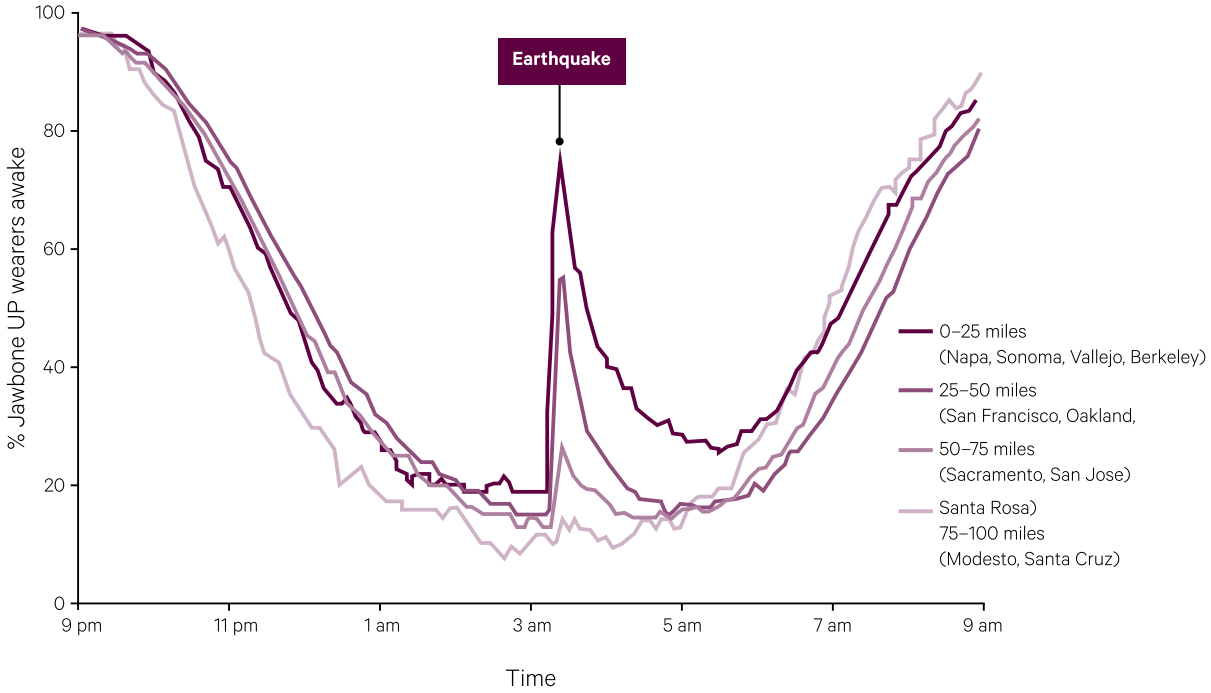

Adapted from Mandel (2014)

Excursus 12.4—EyeonWater Australia

Source: Janet Anstee, CSIRO
Further Information: *https://www.eyeonwater.org*

Another approach to EO of surface waters involves directly photographing the water surface and inferring water quality from image colour. A smartphone application, Eye on Water, which is used worldwide by different citizen science projects (Wernand *et al*. 2013; Novoa *et al*. 2015; Busch *et al*. 2016), has been adapted by CSIRO for Australian inland and coastal waters. The EyeonWater project was spawned from the European Union funded Citizens' Observatory for Coast and Ocean Optical Monitoring project (Citclops). As part of that project a smart phone app was developed to enable citizen scientists to easily add their own observations of water colour to the global database.

The EyeonWater Australia application was developed to assist validation of water colour from satellite imagery and to improve knowledge of aquatic systems, particularly in remote inland and coastal regions of Australia. Once installed on a smartphone, the app quantifies water colour. This involves guiding the citizen scientist through:

- reliably photographing the water surface; then
- comparing the water colour to the Forel-Ule colour scale (see Figure 12.4).

Figure 12.4 Using the EyeonWater Australia app

Part of the EyeonWater Australia project involves training students from the Bush Ranger program at the Broome Senior High School as citizen scientists to contribute water colour observations.

Source: a. Janet Anstee, CSIRO b. Broome Senior High School

Citizen scientists are needed for the project because water quality information is lacking in many places. As well as being part of a research project that is improving satellite-derived water quality products., community members gain a better understanding of water quality and its impact on our ecosystems. Scientists benefit from an increased number of observations, particularly in remote regions, as well as knowledge transfer from people who are well-connected to their localities.

The database currently stores all the water quality information that has been uploaded and this will help scientists determine seasonal influences on water quality and potentially determine the environmental drivers for detected changes (such as after a cyclone). Observations collated during 2017 and 2018 are shown in Figure 12.5. Over time, these observations will enable long-term monitoring of water colour, which otherwise would not be possible without expensive scientific surveys and water quality analyses.

Figure 12.5 EyeonWater Australian observations 2017–2018

Colours at sites relate to water colour on the Forel-Ule Scale (see Figure 12.4a and Volume 3B).

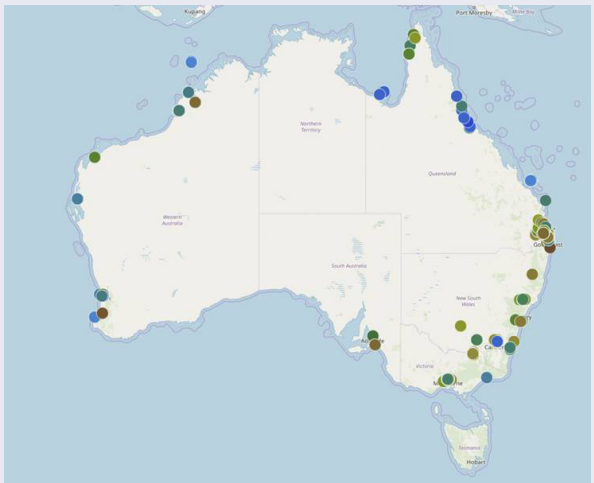

12.5 Further Information

Citizen Science:

EyeOnWater: *https://www.eyeonwater.org*

EyeOnWater Australia: *https://www.eyeonwater.org/apps/eyeonwater-australia*

Atlas of Living Australia: *https://www.ala.org.au*

Automatic Sensor Networks:

TERN: *http://www.tern.org.au*

TERN Ozflux: *http://www.ozflux.org.au*

IMOS: *http://imos.org.au*

Australian Phenocam Network: *https://phenocam.org.au/*

National Vegetation Information System (NVIS):

NVIS: *http://www.environment.gov.au/land/native-vegetation/national-vegetation-information-system*

Spectral Libraries and Databases:

National Spectral Database: planned for launch in 2020 by Geoscience Australia

Specchio: *https://specchio.ch*

USGS Spectroscopy Lab: *https://www.usgs.gov/labs/spec-lab*

USGS High Resolution Spectral Library: *https://www.usgs.gov/energy-and-minerals/mineral-resources-program/science/usgs-high-resolution-spectral-library?qt-science_center_objects=0#qt-science_center_objects*

12.6 References

Bojinski, S., Schaepman, M., Schlaepfer, D. and Itten, K. (2003). SPECCHIO: a spectrum database for remote sensing applications. *Computers and Geosciences*, 29, 27–38.

Broomhall, M., Johansen, K., and Wu, D. (2018). Quality assurance steps for TERN landscape assessment hyperspectral data. Ch 15 in *Effective Field Calibration and Validation Practices: A practical handbook for calibration and validation satellie and model-derived terrestrial environmental variables for research and management*. A TERN Landscape Assessment Initiative, NCRIS. ISBN: ISBN 978-0-646-94137-0. *https://www.tern.org.au/NEW-CalVal-handbook-for-remote-sensing-bgp4370.html*

Busch, J.A., Price, I., Jeansou, E., Zielinski, O., and van der Woerd, H.J. (2016). Citizens and satellites: Assessment of phytoplankton dynamics in a NW Mediterranean aquaculture zone. *International Journal of Applied Earth Observation Geoinformation,* 47, 40–49.

Cabello-Leblic, A. (2018). Tree crown delineation. Ch 11 in in *Effective Field Calibration and Validation Practices: A practical handbook for calibration and validation satellie and model-derived terrestrial environmental variables for research and management*. A TERN Landscape Assessment Initiative, NCRIS. ISBN: ISBN 978-0-646-94137-0. *https://www.tern.org.au/NEW-CalVal-handbook-for-remote-sensing-bgp4370.html*

Calders, K., Wilkes, P., Disney, M.I., Armston, J., Schaefer, M., and Woodgate, W. (2018). Terrestrial lidar for measuring above-ground biomass and forest structure. Ch 19 in *Effective Field Calibration and Validation Practices: A practical handbook for calibration and validation satellie and model-derived terrestrial environmental variables for research and management*. A TERN Landscape Assessment Initiative, NCRIS. ISBN: ISBN 978-0-646-94137-0. *https://www.tern.org.au/NEW-CalVal-handbook-for-remote-sensing-bgp4370.html*

Chisholm, L.A., and Hueni, A. (2018). The Spectroscopy Dataset Lifecycle: Best Practice for Exchange and Dissemination. Ch 14 in *Effective Field Calibration and Validation Practices: A practical handbook for calibration and validation satellie and model-derived terrestrial environmental variables for research and management*. A TERN Landscape Assessment Initiative, NCRIS. ISBN: ISBN 978-0-646-94137-0. *https://www.tern.org.au/NEW-CalVal-handbook-for-remote-sensing-bgp4370.html*

Gallant, J.C., McKenzie, N.J., and McBratney, A.B. (2008). Scale. Ch 3 in *Guidelines for Surveying Soil and Land Resources*. Australian Soil and Land Survey Handbook Series. (Eds: McKenzie, N.J., Grundy, M.J., Webster, R., and Ringrose-Voase, A.J.) CSIRO Publishing, Melbourne.

Gill, T., Johansen, K., Scarth, P., Armston, J., Trevithick, R., and Flood, N. (2018). Persistent green vegetation fraction. Ch 8 in *Effective Field Calibration and Validation Practices: A practical handbook for calibration and validation satellie and model-derived terrestrial environmental variables for research and management*. A TERN Landscape Assessment Initiative, NCRIS. ISBN: ISBN 978-0-646-94137-0. *https://www.tern.org.au/NEW-CalVal-handbook-for-remote-sensing-bgp4370.html*

Hnatiuk R.J., Thackway R. and Walker J. (2009). *Vegetation*. In: *Australian Soil and Land Survey: Field Handbook* (3rd Edition). (Eds National Committee on Soil and Terrain) pp. 73–125. CSIRO Publishing, Melbourne.

Hueni, A., and Tuohy, M. (2006). Spectroradiometer Data Structuring, Pre-Processing and Analysis—An IT Based Approach. *Journal of Spatial Science*, 51(2), 93–102.

Hueni, A., Nieke, J., Schopfer, J., Kneubühler, M., Itten, K. (2009). The spectral database SPECCHIO for improved long term usability and data sharing. *Computers and Geosciences*. *https://doi.org/10.1016/j.cageo.2008.03.015*

Hueni, A., Malthus, T., Kneubuehler, M. and Schaepman, M. (2011). Data Exchange between distributed Spectral Databases. *Computers and Geosciences*, 37: 861–873. *https://doi.org/10.1016/j.cageo.2010.12.009*.

Hueni, A., Chisholm, L., Suarez, L., Ong, C., Wyatt, M. (2012). Spectral information system development for Australia, in *Proceedings of the Geospatial Science Research Symposium 2*, RMIT, Melbourne, December 2012.

Johansen, K., Trevithick, R., Bradford, M., Hacker, J., McGrath, A., and Lieff, W. (2018). Australian examples of field and airborne TERN Landscape Assessment campaigns. Ch 17 in *Effective Field Calibration and Validation Practices: A practical handbook for calibration and validation satellie and model-derived terrestrial environmental variables for research and management*. A TERN Landscape Assessment Initiative, NCRIS. ISBN: ISBN 978-0-646-94137-0. *https://www.tern.org.au/NEW-CalVal-handbook-for-remote-sensing-bgp4370.html*

Malthus, T. (2018). Calibration of optical satellite and airborne sensors. Ch 4 in *Effective Field Calibration and Validation Practices: A practical handbook for calibration and validation satellie and model-derived terrestrial environmental variables for research and management*. A TERN Landscape Assessment Initiative, NCRIS. ISBN: ISBN 978-0-646-94137-0. *https://www.tern.org.au/NEW-CalVal-handbook-for-remote-sensing-bgp4370.html*

Mandel, E. (2014). *How the Napa earthquake affected bay area sleepers*. See *https://www.forbes.com/sites/dandiamond/2014/08/25/how-an-earthquake-will-mess-up-your-sleep-a-jawbone-chart/#7344fc2e3b3a*

McKenzie, N.J., Grundy, M.J., Webster, R., and Ringrose-Voase, A.J. (Eds) (2008). *Guildelines for Surveying Soil and Land Resources*. Australian Soil and Land Survey Handbook Series. CSIRO Publishing, Melbourne.

Mitchell, A., and Thankappan, M. (2018). Effective guidelines for calibration and validation of SAR data and derived biophysical products. Ch 5 in *Effective Field Calibration and Validation Practices: A practical handbook for calibration and validation satellie and model-derived terrestrial environmental variables for research and management*. A TERN Landscape Assessment Initiative, NCRIS. ISBN: ISBN 978-0-646-94137-0. *https://www.tern.org.au/NEW-CalVal-handbook-for-remote-sensing-bgp4370.html*

Novoa, S., Wernand, M.R., and van der Woerd, H.J. (2015). WACODI: A generic algorithm to derive the intrinsic color of natural waters from digital images. *Limnological and Oceanographic Methods*, 13, 697–711.

NVIS Technical Working Group (2017). *Australian Vegetation Attribute Manual: National Vegetation Information System, Version 7.0*. (Eds: Bolton, M.P., deLacey, C. and Bossard, K.B.). Department of the Environment and Energy, Canberra.

NVIS (2019). *NVIS data products* webpage: *http://www.environment.gov.au/land/native-vegetation/national-vegetation-information-system/data-products*

Quadros, N., and Keysers, J. (2018). Airborne lidar acquisition and validation. Ch 16 in *Effective Field Calibration and Validation Practices: A practical handbook for calibration and validation satellie and model-derived terrestrial environmental variables for research and management*. A TERN Landscape Assessment Initiative, NCRIS. ISBN: ISBN 978-0-646-94137-0. *https://www.tern.org.au/NEW-CalVal-handbook-for-remote-sensing-bgp4370.html*

Restrepo-Coupe, N., Huete, A., and Davies, K. (2018). Satellite phenology validation. Ch 9 in *Effective Field Calibration and Validation Practices: A practical handbook for calibration and validation satellie and model-derived terrestrial environmental variables for research and management*. A TERN Landscape Assessment Initiative, NCRIS. ISBN: ISBN 978-0-646-94137-0. *https://www.tern.org.au/NEW-CalVal-handbook-for-remote-sensing-bgp4370.html*

Scarth, P., Guerschman, J.P., Clarke, K., and Phinn, S. (2018). Validation of Australian Fractional Cover Products form MODIS and Landsat Data. Ch 7 in *Effective Field Calibration and Validation Practices: A practical handbook for calibration and validation satellie and model-derived terrestrial environmental variables for research and management*. A TERN Landscape Assessment Initiative, NCRIS. ISBN: ISBN 978-0-646-94137-0. *https://www.tern.org.au/NEW-CalVal-handbook-for-remote-sensing-bgp4370.html*

Schaefer, M.T., Farmer, E., Soto-Berelov, M., Woodgate, W., and Jones, S. (2018). Ch 6 in *Effective Field Calibration and Validation Practices: A practical handbook for calibration and validation satellie and model-derived terrestrial environmental variables for research and management*. A TERN Landscape Assessment Initiative, NCRIS. ISBN: ISBN 978-0-646-94137-0. *https://www.tern.org.au/NEW-CalVal-handbook-for-remote-sensing-bgp4370.html*

Schaefer, M.T. (2018). Measurement of above ground biomass. Ch 12 in *Effective Field Calibration and Validation Practices: A practical handbook for calibration and validation satellie and model-derived terrestrial environmental variables for research and management*. A TERN Landscape Assessment Initiative, NCRIS. ISBN: ISBN 978-0-646-94137-0. *https://www.tern.org.au/NEW-CalVal-handbook-for-remote-sensing-bgp4370.html*

Soto-Berelov, M., Jones, S., Farmer, E., and Woodgate, W. (2018). Review of validation standards of biophysical Earth Observation products. Ch 2 in *Effective Field Calibration and Validation Practices: A practical handbook for calibration and validation satellie and model-derived terrestrial environmental variables for research and management*. A TERN Landscape Assessment Initiative, NCRIS. ISBN: ISBN 978-0-646-94137-0. *https://www.tern.org.au/NEW-CalVal-handbook-for-remote-sensing-bgp4370.html*

SPECCHIO (2019). *SPECCHIO* website: *https://specchio.ch*

Specht, R.L. (1970). Vegetation. In *The Australian Environment* (4th Edn). (Ed: Leeper, G.W.). CSIRO, Melbourne.

Speight, J.G., and McDonald, R.C. (2009). *The Site Concept*. In: *Australian Soil and Land Survey: Field Handbook* (3rd Edn). (Eds National Committee on Soil and Terrain) pp. 73–125. CSIRO Publishing, Melbourne.

Stewart, J.B., and Howorth, J.E. (2018). A calibration and validation framework to support ground cover monitoring for Australia. Ch 18 in *Effective Field Calibration and Validation Practices: A practical handbook for calibration and validation satellie and model-derived terrestrial environmental variables for research and management*. A TERN Landscape Assessment Initiative, NCRIS. ISBN: ISBN 978-0-646-94137-0. *https://www.tern.org.au/NEW-CalVal-handbook-for-remote-sensing-bgp4370.html*

Suarez, L., Restrepo-Coupe, N., Hueni, A., and Chisholm, L.A. (2018). Vegetation spectroscopy. Ch 13 in *Effective Field Calibration and Validation Practices: A practical handbook for calibration and validation satellie and model-derived terrestrial environmental variables for research and management*. A TERN Landscape Assessment Initiative, NCRIS. ISBN: ISBN 978-0-646-94137-0. *https://www.tern.org.au/NEW-CalVal-handbook-for-remote-sensing-bgp4370.html*

Tanis, C.M., Peltoniemi, M., Linkosalmi, M., Aurela, M., Böttcher, K., Manninen, T., and Arslan, A.N. (2018). A System for Acquisition, Processing and Visualization of Image Time Series from Multiple Camera Networks. *Data*, 3, 23. *https://doi.org/10.3390/data3030023*

TERN Australia (2018). *Effective Field Calibration and Validation Practices: A practical handbook for calibration and validation satellie and model-derived terrestrial environmental variables for research and management*. A TERN Landscape Assessment Initiative, NCRIS. ISBN: ISBN 978-0-646-94137-0. *https://www.tern.org.au/NEW-CalVal-handbook-for-remote-sensing-bgp4370.html*

Thackway, R., Neldner, J., and Bolton, M. (2008). Vegetation. In: *Australian Soil and Land Survey Handbook Guidelines for Conducting Surveys* (2nd Edition). (Eds: McKenzie, N.J., Grundy, M.J., Webster, R., and. Ringrose-Voase, A.J.). CSIRO Publishing, Melbourne.

Trevithick, R. (2018). Field data collection and management for Earth Observation image validation. Ch 3 in *Effective Field Calibration and Validation Practices: A practical handbook for calibration and validation satellie and model-derived terrestrial environmental variables for research and management*. A TERN Landscape Assessment Initiative, NCRIS. ISBN: ISBN 978-0-646-94137-0. *https://www.tern.org.au/NEW-CalVal-handbook-for-remote-sensing-bgp4370.html*

Walker, J., and Hopkins, M.S. (1990). Vegetation. In *Australian Soil and Land Survey Handbook: Guidelines for Conducting Surveys*. (Eds: Gunn, R.H., Beattie, J.A., Reid, R.E., and van der Graaff, R.H.M.). Inkata Press, Melbourne. pp 58–86.

Wason, T.D., and Wiley, D. (2000). Structured Metadata Spaces. *Journal of Internet Cataloging*, 3(2/3), 263–277.

Wernand, M.R., van der Woerd, and H.J., Gieskes, W.W.C., (2013). Trends in ocean colour and chlorophyll concentration from 1889 to 2000, worldwide. *PLoS One*, 8, e63766.

Youngentob, K.N. (2018). Estimating foliar chemistry of individual tree crowns with imaging spectroscopy. Ch 10 in *Effective Field Calibration and Validation Practices: A practical handbook for calibration and validation satellie and model-derived terrestrial environmental variables for research and management*. A TERN Landscape Assessment Initiative, NCRIS. ISBN: ISBN 978-0-646-94137-0. *https://www.tern.org.au/NEW-CalVal-handbook-for-remote-sensing-bgp4370.html*

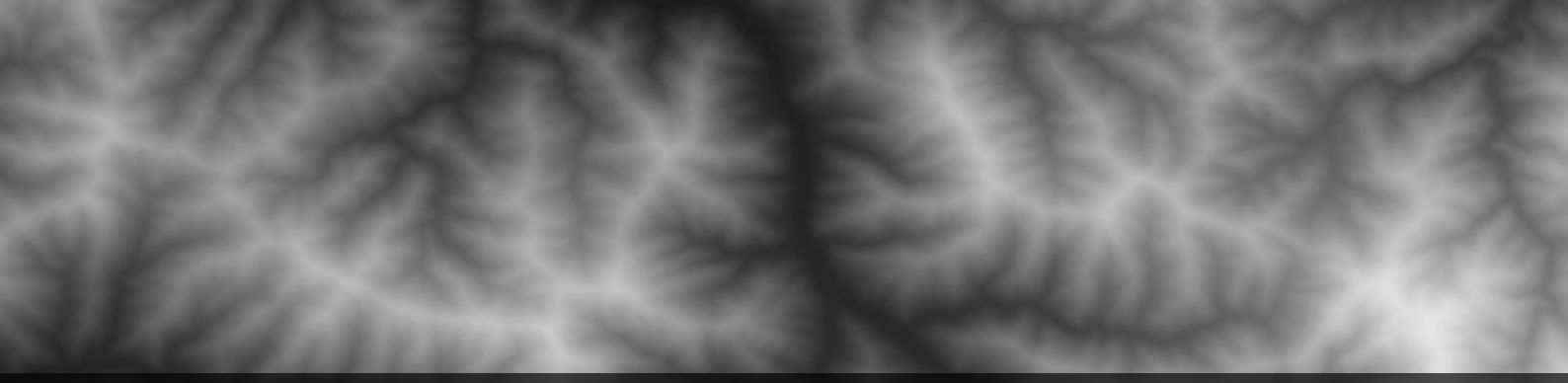

13 Gridded Datasets

This section considers three categories of gridded, spatial data that can be integrated with EO datasets:

- GIS attributes (see Section 13.1);
- digital elevation models (see Section 13.2); and
- meteorological records (see Section 13.3).

13.1 Geographic Information Systems

Geographic Information Systems (GIS) compile, access and interrogate spatial data in digital format. The unique characteristic of spatial data is the component that indicates location, either explicitly or implicitly. As introduced in Section 3.3.2, most digital geographic data is represented in either raster or vector format, but it is more appropriate to code some types of data (such as terrain heights, see Section 13.2) in a format known as Triangular Irregular Network (TIN).

The strength of GIS is their ability to store and analyse large volumes of spatial data for environmental, commercial and legislative purposes. Analyses typically include some of the raster operations described in Volumes 2A, 2B and 2C, such as combining attributes, neighbourhood operations, and segmentation/classification, plus specific vector-based analyses, such as proximity functions, network modelling, spatial prediction and terrain analysis (Bolstad, 2008). Spatial and spatio-temporal modelling tools are increasingly available in GIS.

A wide range of environmental and socio-economic attributes are now available as spatial coverages in Geographic Information Systems (GIS). For example, the online mapping tool, NationalMap, enables access to a growing range of geospatial datasets for Australia, many of which have been derived using EO data (see Excursus 13.1). As with other forms of ancillary data, to be sensibly integrated with EO datasets, GIS attributes need to be spatially accurate, geometrically coincident and temporally relevant (see Section 3.3 above and Volume 2B).

A GIS is a computer-based system to aid in the collection, maintenance, storage, analysis, output and distribution of spatial data and information.
(Bolstad, 2008)

Background image: Digital Elevation Model over alpine region in Victoria, displayed with black for lowest altitudes to white for highest altitudes. **Source:** Fuqin Li, Geoscience Australia

Excursus 13.1—NationalMap

Source: *https://nationalmap.gov.au/about.html*

NationalMap is an online map-based tool to allow easy access to geospatial data from Australian federal, state and territory government agencies. In this open architecture implementation, data is generally accessed directly from the custodians. It is intended for information purposes only. In March 2019, base maps for Australia included topography (Geoscience Australia), Bing maps (Microsoft), Natural Earth II (public domain), Black Marble (NASA), and Positron (Light) and Dark Matter (Carto). These underlays can be integrated with terrain information from Cesium Word Terrain (Cesium Ion) and geocoded information from G-NAF (PSMA geocoded national address file), Bing Maps (Microsoft) and the Gazetter of Australia.

The NationalMap tool enables multiple geospatial datasets to be integrated on a selected base map for a given location. Categories of national datasets, for example, include communications, elevation, environment, framework, groundwater, habitation, health, infrastructure, land, national boundaries, satellite imagery, social and economic, statistical boundaries, surface water and marine, terrain, transport, utility and vegetation. Resulting compilations can be downloaded and shared, or integrated with personal datasets, and data values for displayed locations can be queried.

National spatial websites that can be accessed via NationalMap include:

- AREMI (Australian Renewable Energy Mapping Infrastructure;
- NEII viewer (National Environmental Information Infrastructure);
- AURIN (Australian Urban Research Infrastructure Network); and
- SOE map (State of the Environment).

13.2 Digital Elevation Models

A digital elevation model (DEM; or digital terrain model, DTM) represents a terrain surface as a three-dimensional, digital model. A digital surface model (DSM), represents the height of the surface, including the heights of any objects that are above the terrain (see Figure 13.1). Traditionally, elevation has been recorded as topographic contours, that is, lines of uniform elevation that are orthogonal to the local slope (Bolstad, 2008), but other common formats for elevation data include a raster format of grid cells and a triangulated irregular network (TIN; see Section 3.3.2 and Figure 13.2). Most DEM used for resource assessment are now based on a raster format (Gallant and Hutchinson, 2008).

DEM have also been derived from 236 lidar surveys over Australia that were acquired between 2001 and 2015 (GA, 2019). Covering over 245,000 sq. km, these datasets have been merged into 5 m and 25 m grids, which focus on populated regions, coastal zones, and floodplains within the Murray-Darling Basin.

Figure 13.1 DTM versus DSM

A digital surface model (DSM) represents the heights of all objects on the terrain (shown as green) whereas a digital terrain model only represents the elevation of the terrain surface (shown as blue).

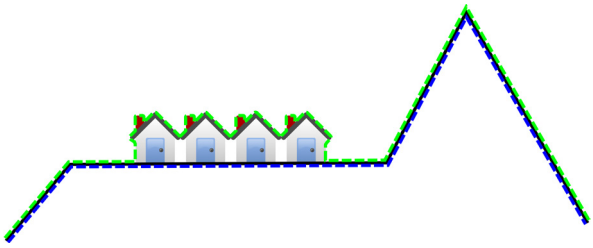

Adapted from: Wikimedia Commons (Arbeck). Retrieved from *https://commons.wikimedia.org/wiki/File:The_difference_between_Digital_Surface_Model_(DSM)_and_Digital_Terrain_Models_(DTM)_when_talking_about_Digital_Elevation_models_(DEM).svg*

Figure 13.2 Elevation data formats

a. Raster b. Vector c. Triangulated Irregular Network (TIN)

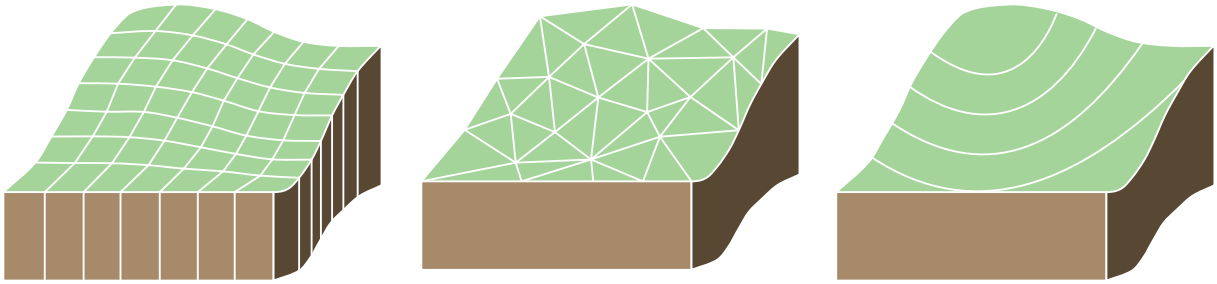

Since terrain height directly determines surface water distribution and biogeography (including human settlement), accurate mapping of elevation is essential for many environmental and demographic analyses. In addition to elevation, several terrain variables have been identified, which quantify information about landform (see Table 13.1). By summarising the relationship between landform and other landscape attributes, such as soil type and vegetation (Gallant and Hutchinson, 2008), these terrain variables have become important for a range of activities related to landscape planning and resource management including stratifying sampling sites (Hewitt *et al.*, 2008), providing explanatory variables in soil-landscape models (McKenzie *et al.*, 2000), and visualising landscapes (Gallant and Hutchinson, 2008).

Table 13.1 Terrain variables

Group	Variable	Description	Importance
Exposure	Height	Elevation above base	Temperature, vegetation, visibility
	Slope	Change in elevation relative to change in horizontal distance	Water flow, flooding, erosion, transport cost, construction suitability, geology, insolation, soil depth
	Aspect	Downhill direction of steepest slope	Insolation, temperature, vegetation, soil characteristics and moisture, hazards
Curvature	Profile curvature	Curvature parallel to slope direction	Erosion, water flow acceleration
	Plan curvature	Curvature perpendicular to slope direction	Water flow convergence, soil water, erosion
Hydrologic functions	Flow direction	Direction of flow of excess surface water	Water runoff, erosion
	Flow length	Longest upstream flow path to a point	Sediment and erosion rates
	Upslope area	Watershed area above a point	Soil moisture, volume and timing of water runoff, pollution or erosion hazards
	Upslope length	Mean upstream flow path length to a point	Sediment and erosion rates
Landscape aesthetics	Landscape position	Location of site within context of surrounding landscape	Spatial prediction of landscape patterns
	Visiblilty	Site obstruction from given viewpoints	Utility location, viewshed preservation
	Viewshed	Collection of areas visible from a point	Utility location,
Non-terrain	Topographic wetness index	Ratio of specific catchment area to slope	Measure of relative soil wetness
	Stream power index	Product of specific catchment area to slope	Measure of ability of surface flow to transport sediment
	Shortwave radiation	Solar radiation reaching land surface	Insolation, Sun shading

Source: Bolstad (2008) Table 11-1 and Gallant and Hutchinson (2008)

As the word 'model' implies, a DEM only offers an approximate 'representation' of the actual surface, and does not attempt to mimic all local variations in terrain height or necessarily represent the actual elevation at specific locations (Gallant and Hutchinson, 2008). Construction of a reliable DEM requires consideration of numerous constraints relating to drainage, scaling, and interpolation, as well as addressing any underlying data errors. The ANUDEM software suite, for example, computes DEM for a range of scales with logical shape and drainage structure. This software has been used to develop the national DEM-9S and improve DEM products derived from the Shuttle Radar Topography Mission (SRTM; ANU/GA, 2008).

The national DEM available for Australia are listed in Table 13.2. Versions of the SRTM DEM include:

- DSM (3-second DEM only): ground surface topography plus features above the ground, such as vegetation and man-made structures;
- DEM: ground surface topography with vegetation features removed;
- DEM-S: ground surface topography with vegetation features removed and smoothed to improve surface shape and reduce noise; and
- DEM-H (1-second DEM only): hydrologically-enforced version of DEM-S.

The Australian Hydrological Geospatial Fabric is a specialised GIS based on the 1-second DEM, which defines logical hydrological features in the Australian landscape (see Excursus 13.2).

Table 13.2 Australian DEM

Name	Spatial resolution (m)	Based on
GEODATA 9-second DEM and D8 Flow Direction Grid 2008 (DEM-9S) v3	250	Elevation data at 1:100,000 and 1:250,000 cartographic scales
SRTM 3-second DEM v1.0	90	Shuttle Radar Topographic Mission, 2000
SRTM, 1-second DEM v10	30	Shuttle Radar Topographic Mission, 2000
Lidar 25 m grid	25	236 Lidar surveys between 2001 and 2015
Lidar 5 m grid	5	236 Lidar surveys between 2001 and 2015

Source: GA (2019)

Excursus 13.2—Australian Hydrological Geospatial Fabric

Source: BoM (2019a)
Further Information: *http://www.bom.gov.au/water/geofabric/documents/Geofabric_Info_Sheet_online.pdf*
http://www.bom.gov.au/water/geofabric/documentation.shtml

A collaborative development between the Bureau of Meteorology (BoM), Geoscience Australia (GA), ANU[6] and CSIRO[7] has produced the Australian Hydrological Geospatial Fabric (Geofabric). This specialised GIS registers the spatial relationships between important hydrological features such as rivers, water bodies, aquifers and monitoring points (BoM, 2019a). The spatial dimensions of these hydrofeatures indicate how they are connected, and how water is stored, transported and used through the landscape.

The Geofabric comprises six product datasets:

- (1) Hydrology Reporting Regions—define drainage divisions and river regions across Australia, for consistent reporting by governments and other organisations;
- (2) Hydrology Reporting Catchments—building blocks of reporting regions, providing increased detail for smaller rivers, including a simplfied stream network;
- (3) Surface Catchments—define the base level of catchments for stream segments, sinks and coastal draining areas. Universities, governments and consultants use these to identify contributing catchment areas;
- (4) Surface Network—provides a detailed, fully-connected and directed stream network. This enables stream flow paths to be traced, then linked to Surface Catchments;
- (5) Surface Cartography—allows surface water features, such as dams, canals and bridges, to be visualised. This context is useful for water managers and emergency services, for example, to anticipate how downstream communities may be affected by floods; and
- (6) Groundwater Cartography—shows groundwater resources and their features, such as aquifer boundaries, salinity, and rocks and sediments at different levels below the surface (see Figure 13.3).

The Geofabric is based on a set of contracted nodes (points), which represent important hydrological features in the landscape. These points have a permanent identifier included in all versions of the Geofabric, and provide a persistent framework through space and time. A subset of the contracted nodes is used to create a simplified node-link network with associated contracted catchments. Phase 2 of the Geofabric is based on 1:250,000 scale map features and the 9-second DEM. Phase 3 (released in 2019) is based on 1-second DEM and finer-scaled map features. The ANUDEM software (see Section 13.2) was used in development of data for the Geofabric.

Figure 13.3 Geofabric datasets

The Geofabric comprises six dataset products: (1) Hydrology Reporting Regions; (2) Hydrology Reporting Catchments; (3) Surface Catchments; (4) Surface Network; (5) Surface Cartography; (6) Groundwater Cartography.

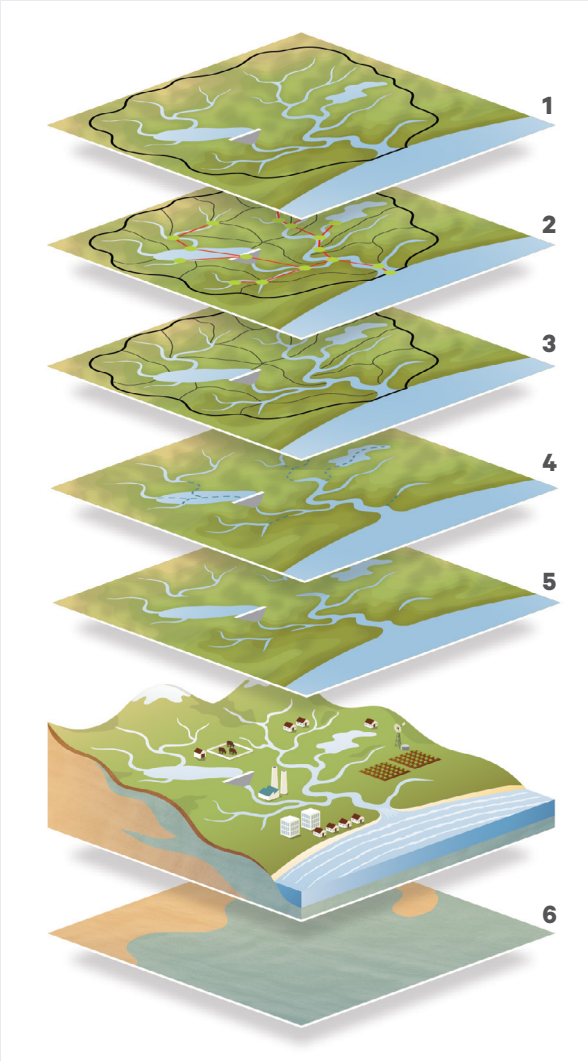

Source: BoM (2015)

6 Australian National University Fenner School of Environment and Society
7 CSIRO Water for a Healthy Country Flagship

13.3 Meteorological Records

Meteorological records are another source of ancillary data that may be analysed in conjunction with EO datasets. Instrumental weather records in Australia started within months of the First Fleet and continued in various locations using available equipment and expertise. Standardised equipment was gradually introduced by the Bureau of Meteorology since 1908 to create the current Australian network of 752 temperature recording sites, nearly 6,000 rain gauges and 610 automatic weather stations (AWS; BoM, 2019b). The AWS observe air temperature, humidity, wind speed, wind direction and precipitation every 30 minutes (Isaac *et al*., 2017).

These meteorological records have been calibrated and validated over time and space to ensure their accuracy and consistency, and spatially interpolated to create continuous, climate datasets. Some of the climate datasets now available for Australia include:

- Australian Climate Observations Reference Network (ACORN-SAT version 2)—Surface Air Temperature 1910–2018 (BoM, 2019c);
- daily and monthly estimates of precipitation, maximum daily temperature, minimum daily temperature and vapour pressure humidity (9 am and 3 pm) on a 0.05° grid (Jones *et al*., 2009) derived from the national climate databank, Australian Data Archive for Meteorology (ADAM; CLIMARC, 2020);
- Australian Water Availability Project (AWAP; Raupach *et al*., 2008); and
- daily and monthly observations and statistics for rainfall, temperature and solar exposure at weather stations (BoM, 2019c).

Figure 13.4 GPCC average precipitation 1982–2010

Precipitation units are shown in m/a.

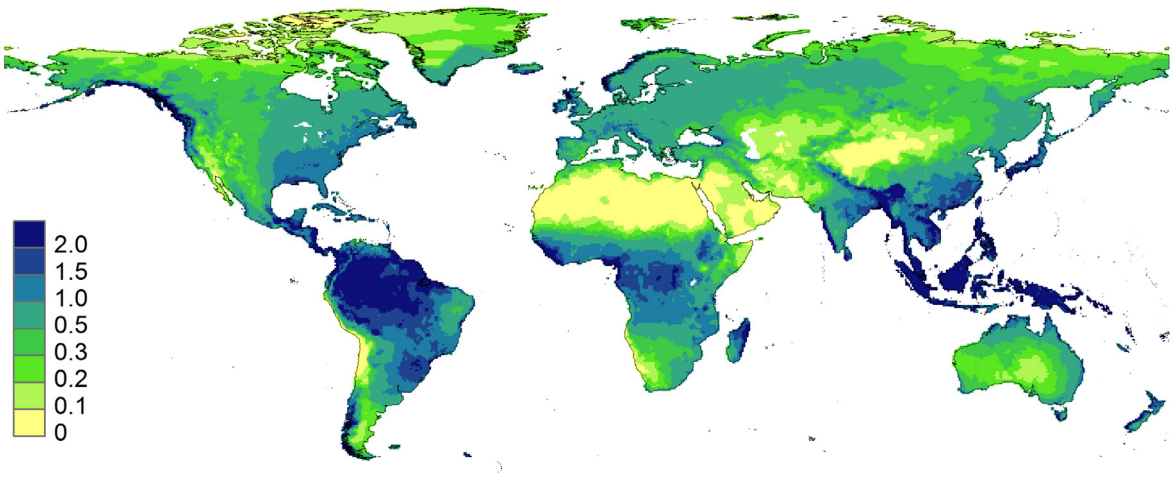

Source: Donohue *et al.* (2013) Figure 1 © Wiley: Used with permission. Data source: Rudolf *et al.* (2010)

Some of the geostatistical techniques used to generate climate analyses for Australia are reviewed by Seaman and Hutchinson (1985) and Jones and Trewin (2000). For example, an anomaly-based approach, which decomposes each meteorological variable into its long-term average and an associated 'anomaly', was used by Jones *et al*. (2009) to create the 0.05° gridded datasets. While such datasets appear to provide continuous coverage, the spatial interpolation methods can generate data for large areas at considerable distance from a real weather station. Use of such data requires that consideration be given to the underlying observations, which may mean that data cells with significant temporal discontinuities generally need to be excluded from time series analyses. For example, when examining climate-related trends in Australian vegetation cover using EO imagery, Donohue *et al*. (2009) extracted site-based measures of montly precipitation and pan evaporation from the Monthly Australian Data Archive for Meteorology (MADAM) database (BoM, 2006) but only included sites with near-complete records, where complete was defined as:

- at least 25 days of data each month;
- at least 9 complete months of data each year; and
- at least 20 complete years of data for each station included (see Excursus 8.1).

Similarly, as part of an EO-based study to assess the impact of CO_2 fertilisation on global vegetation, Donohue *et al*. (2013) sourced global precipitation data from the Global Precipitation Climatology Centre (GPCC) Full Data Reanalysis Version 6 dataset (Rudolf *et al*., 2010; see Figure 13.4). This spatially interpolated dataset spanned 29 years but included data-poor regions. Spurious cells were excluded by defining a buffer around those with less than one rainfall station for 90% of included months. The remaining data stations are shown in Figure 13.5.

Figure 13.5 GPCC buffer mask

Blue cells indicate the locations where near-continuous temporal coverage exists for the data shown in Figure 13.4.

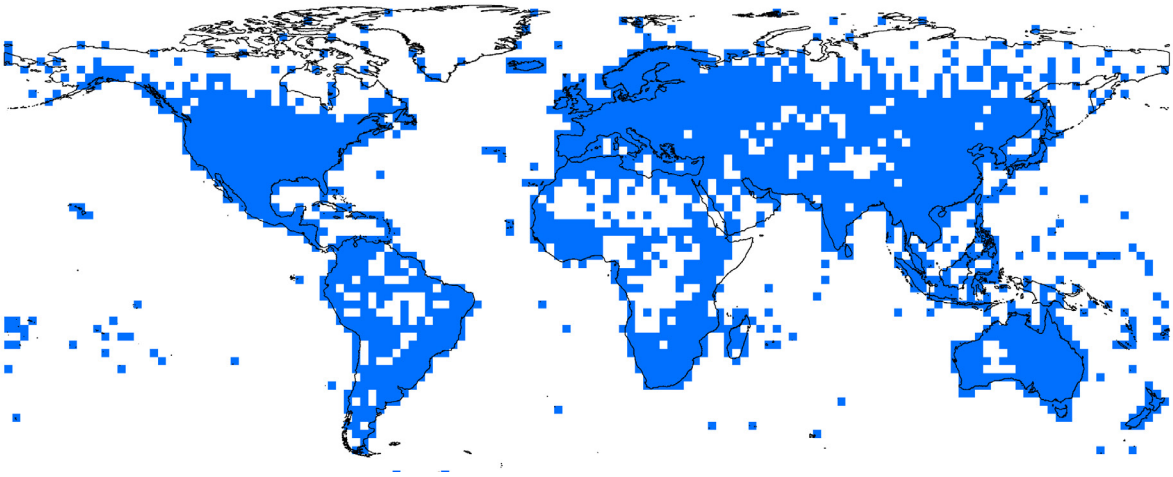

Source: Donohue *et al.* (2013) Figure 2 © Wiley: Used with permission. Data source: Rudolf *et al.* (2010)

13.4 Further Information

Geographic Information Systems:

NationalMap: *https://nationalmap.gov.au/about.html*

Digital Elevation Models:

GA (2019)

CHARIM (Caribbean Handbook on Risk Information Management): *http://www.charim.net/datamanagement/32*

Australian Spatial Data Directory:

A national metadata hub for searching other national, state and territory directories to facilitate the discovery of published geospatial datasets throughout Australia:
http://www.nccarf.jcu.edu.au/terrestrialbiodiversity/index.php/41-general/272-australian-spatial-data-directory.html
https://www.australia.gov.au/information-and-services/business-and-industry/science-and-technology/spatial-information

Geoscience Australia:

Digital Elevation Data: *https://www.ga.gov.au/scientific-topics/national-location-information/digital-elevation-data*

Bureau of Meteorology:

National Environmental Information Infrastructure (NEII): *http://www.neii.gov.au/*

Climate online: *http://www.bom.gov.au/climate/data/*

Other climate data: *http://www.bom.gov.au/climate/data-services/*

Australian Landscape Water Balance: *http://www.bom.gov.au/water/landscape/#/sm/Actual/day/-28.4/130.4/3/Point////2019/8/11/*

Weather Stations: *http://www.bom.gov.au/climate/data/stations/about-weather-station-data.shtml*

CSIRO:

Soil and Landscape Grid of Australia: *http://www.clw.csiro.au/aclep/soilandlandscapegrid/About-FactSheet.html*

Global Meteorological Data:

Global Precipitation Climatology Centre (GPCC) Full Data Reanalysis Version 6: Rudolf *et al.* (2010)

Global vapor pressure deficit (based on European Centre for Medium-Range Weather Forecasts' ERA-interim reanalysis monthly near-surface ddew point and near-surface air temperature products: Dee *et al.* (2011)

Global DEM:

Intermap:
NEXTMap Elevation Data Suite: *https://www.intermap.com/nextmap*
Airbus Defence and Space: *https://www.intelligence-airbusds.com/elevation-models/*

NASA:
ASTER GDEM2: *https://asterweb.jpl.nasa.gov/gdem.asp*

USGS:
GTOPO30: *https://www.usgs.gov/centers/eros/science/usgs-eros-archive-digital-elevation-global-30-arc-second-elevation-gtopo30?qt-science_center_objects=0#qt-science_center_objects*
SRTM: *https://www.usgs.gov/centers/eros/science/usgs-eros-archive-digital-elevation-srtm-mission-summary?qt-science_center_objects=0#qt-science_center_objects*

JAXA:
ALOS World 3D: *https://www.eorc.jaxa.jp/ALOS/en/aw3d/index_e.htm*

13.5 References

ANU/GA (2008). *GEODATA 9 Second DEM and D8 Digital Elevation Model and Flow Direction Grid, User Guide*. Geoscience Australia.

Bolstad, P. (2008). *GIS Fundamentals: A First Text on Geographic Information Systems*. 3rd Edn. Elder Press, White Bear Lake, Minnesota. ISBN 978-0-9717647-2-9

BoM (2006). *Climate data: Australia CD-ROM*, Version 2.2, December 2006. Australian Government Bureau of Meteorology.

BoM (2015). *Australian Hydrological Geospatial Fabric factsheet*. Bureau of Meteorology, Melbourne. *http://www.bom.gov.au/water/geofabric/documents/Geofabric_Info_Sheet_online.pdf*

BoM (2019a). Bureau of Meteorology website. *About the Geofabric* webpage: *http://www.bom.gov.au/water/geofabric/about.shtml*

BoM (2019b). Bureau of Meteorology website. *Climate Data Online* webpage: *http://www.bom.gov.au/climate/data/*

BoM (2019c). Bureau of Meteorology website. *Long-term temperature record* webpage: *http://www.bom.gov.au/climate/data/acorn-sat/*

CLIMARC (2000). *Australian Data Archive for Meteorology. A draft document prepared for Cli-Manage 2000*. Bureau of Meteorology, Melbourne.

Dee, D.P., Uppala, S.M., Simmons, A.J., Berrisford, P., Poli, P., Kobayashi, S., Andrae, U., Balmaseda, M.A., Balsamo, G., Bauer, P., Bechtold, P., Beljaars, A.C.M., van de Berg, L., Bidlot, J., Bormann, N., Delsol, C., Dragani, R., Fuentes, M., Geer, A.J., Haimberger, L., Healy, S.B., Hersbach, H., Hólm, E.V., Isaksen, L., Kållberg, P., Köhler, M., Matricardi, M., McNally, A.P., Monge-Sanz, B.M., Morcrette, J.J., Park, B.K., Peubey, C., de Rosnay, P., Tavolato, C., Thépaut, J.N., and Vitart, F. (2011). The ERA-Interim reanalysis: configuration and performance of the data assimilation system. *Quarterly Journal of the Royal Meteorological Society*, 137(656), 553–597. *https://doi.org/10.1002/qj.828*.

Donohue, R.J., McVicar, T.R., and Roderick, M.L. (2009). Climate-related trends in Australian vegetation cover as inferred from satellite observations, 1981–2006, *Global Change Biology*, 15(4), 1025–1039, *https://doi.org/10.1111/j.1365-2486.2008.01746.x*.

Donohue, R.J., Roderick, M.L., McVicar, T.R., and Farquhar, G.D. (2013). Impact of CO_2 fertilisation on maximum foliage cover across the globe's warm, arid environments. *Geophysical Research Letters*, 40, 1–5. *https://doi.org/10.1002/grl.50563*

GA (2019). Geoscience Australian website, *Digital Elevation Data* webpage: *http://www.ga.gov.au/scientific-topics/national-location-information/digital-elevation-data*

Gallant, J.C., and Hutchinson, M.F. (2008). Digital terrain analysis. Ch. 6 in *Guildelines for Surveying Soil and Land Resources*. Australian Soil and Land Survey Handbook Series. (Eds: McKenzie, N.J., Grundy, M.J., Webster, R., and Ringrose-Voase, A.J.) CSIRO Publishing, Melbourne.

Hewitt, A.E., McKenzie, N.J., Grundy, M.J., and Slater, B.K. (2008). Qualitative Survey. Ch 18 in *Guildelines for Surveying Soil and Land Resources*. Australian Soil and Land Survey Handbook Series. (Eds: McKenzie, N.J., Grundy, M.J., Webster, R., and Ringrose-Voase, A.J.) CSIRO Publishing, Melbourne.

Isaac, P., Cleverly, J., McHugh, I., van Gorsel, E., Ewenz, C., and Beringer, J. (2017). OzFlux data: network integration from collection to curation, *Biogeosciences*, 14, 2903–2928, *https://doi.org/10.5194/bg-14-2903-2017*

Jones, D.A., and Trewin, B.C. (2000). On the description of monthly temperature anomalies over Australia. *Australian Meteorological Magazine*, 49, 261–76.

Jones, D.A., Wang, W., and Fawcett, R. (2009). High-quality spatial climate data-sets for Australia. *Australian Meteorological and Oceanographic Journal*, 58(4), 233–248.

McKenzie, N.J., Gessler, P.E., Ryan, P.J., and O'Connell, D. (2000). The role of terrain analysis in soil mapping. In *Terrain Analysis: Principles and Applications*. (Eds: Wilson, J.P., and. Gallant, J.C.). Wiley, New York.

Raupach, M.R., Briggs, P.R., Haverd, V., King, E.A., Paget, M., and Trudinger, C.M. (2008). *Australian Water Availability Project*. CSIRO Marine and Atmospheric Research Component. Final Report for Phase 3. Available from CSIRO, Canberra, Australia.

Rudolf, B., Becker, A., Schneider, U., Meyer-Christoffer, A.,and Ziese, M. (2010). *GPCC Status Report*. 7 pp, Global Precipitation Climatology Centre.

Seaman, R.S., and Hutchinson, M.F. (1985). Comparative real data tests of some objective analysis methods by withholding observations. *Australian Meteorological Magazine*, 33, 37–46.

Speight, J.G., and McDonald, R.C. (2009). *The Site Concept*. In: *Australian Soil and Land Survey: Field Handbook* (3rd Edn). (Eds: National Committee on Soil and Terrain) pp. 73–125. CSIRO Publishing, Melbourne.

Integrated Solutions

Environmental conditions are notoriously difficult to measure, let alone monitor, and considerable ecological research has not produced standard, dependable methods for measuring environmental 'condition'. However, parameters that are believed to be indicative of particular conditions can be measured (see Figure 1.1). Repeated measurements over time have been used to model the 'normal' cycles for selected environmental attributes and such structure models are now being used operationally to 'calibrate' EO-based measurements to highlight significant surface changes.

These final sections present examples of integrating EO information products with environmental process models to deliver current, regional and continental scale information about the Australian environment. As introduced in Section 1.4, EO analyses are generally part of a 'bigger picture', involving other datasets and producing pre-defined and reproducible metrics for a specific application. Once reliable datasets are available, the next step in making EO data accessible for a wide range of applications is the generation of information products that reliably condense the relevant information contained within EO datasets into attributes that directly relate to measurable surface features (see Section 14.1).

Information products can then be integrated into specific environmental monitoring and modelling applications, such as environmental accounting (see Section 14.2.1), compliance monitoring (see Section 14.2.2) and modelling of ecosystem dynamics (see Section 14.3). A wider range of application areas reliant on EO datasets are detailed in Volume 3.

Contents

14 Mapping, Monitoring and Modelling 161

Background image on previous page: The High Tide – Low Tide (HTLC) low tide composite mosaic showing the Kimberley Coastline and Montgomery Reef, Western Australia at low tide, with the overlaid InterTidal Elevation Model (ITEM v2.0) products illustrating the topography of the exposed intertidal mudflats and reefs in the region (see Section 11.2). **Source:** Stephen Sagar, Geoscience Australia

14 Mapping, Monitoring and Modelling

EO provides an opportunity to obtain regular, objective observations of energy levels being reflected or emitted by the Earth's surface (see Volume 1). Provided that sensor calibrations are reasonably accurate, the corrected measurements can usually be considered consistent within a given image and comparable between images (see Volumes 2A and 2B), with variations in atmospheric and illumination conditions over time being accounted for by suitable measurement models (see Figure 1.1 and Section 3). The importance of data provenance for EO imagery was introduced in Section 2.2 above and Volume 2A—Section 2.1. This is especially important when processing multiple images or time series datasets. Relevant caveats and processing methodogies for time series datasets are described in Sections 8 to 10 above.

Analysis of a single, calibated EO image enables mapping of surface features. This inventory approach describes surface characteristics at one point in time. A variety of image processing techniques can be applied to a single image to map specific surface features, including spectral indices (see Volume 2C), classification (see Volume 2E) and sub-pixel analyses (see Volume 3A). Some of the EO-based mapping products that are now routinely produced for Australia are introduced in Section 14.1.

The change detection methods described in Section 7 offer a mechanism for highlighting significantly different pixels in a pair of bi-temporal images. However, by definition, monitoring involves regularly-repeated measurements—this is not simply a case of detecting the changes that have occurred between two points in time. Change detection can be seen as one stage of monitoring only. To be effective, changes need to be monitored regularly and for a sufficient time period, which is greater than known natural cycles. Time series datasets offer the potential to achieve regular environmental monitoring. Section 14.2 considers some of the challenges for environmental monitoring using EO datasets, then provides two examples of environmental monitoring approaches in Australia: environmental accounting (see Section 14.2.1) and compliance monitoring (see Section 14.2.2). Environmental monitoring is further discussed in Volume 3 in the context of specific application areas.

Finally the integration of EO datasets with environmental modelling applications is introduced in Section 14.3.

14.1 Mapping

A range of image processing techniques have been used to map specific features on the Earth's surface using EO image datasets (see Volumes 2A, 2C and 2E). In particular, satellite-derived imagery offers a unique perspective for regional and global mapping. Potential mapping applications include:

- vegetation type, condition and structure (see Volume 3A); and
- water colour, temperature, extent and quality (see Volume 3B).

The distinction between EO data and information products was introduced in Volume 2A—Section 2.1 and reviewed in Section 2.4 above. In the context of Table 1.1, EO data products can be seen as examples of 'measurements' rather than observations, and information products represent application-specific attributes. For these relationships to hold, however, requires that the generation of both data and information products follows well-defined and validated procedures (see Section 2.5).

Background image: Fractional cover image derived from Landsat-8 OLI image over Three Rivers Station, near Kumarina in Western Australia. Fractional cover splits the landscape into fractions of green (leaves, grass, and growing crops), brown (branches, dry grass or hay, and dead leaf litter), and bare ground (soil or rock) and is used to monitor vegetation extent and grazing pressure (see Figure 2.3 and Volume 3A) **Source:** Norman Mueller, Geoscience Australia

Excursus 14.1—TERN Continental Products

Source: *https://www.tern.org.au/*
Further Information: *https://portal.tern.org.au/#/8063c731; https://maps.tern.org.au/#/*

TERN is Australia's land-based ecosystem observatory, delivering a wide range of data streams for environmental research and management (see Excursus 12.2). This critical research infrastructure enables Australians to track, understand and respond to changes in ecosystems—both through time and across the breadth of the continent, by providing ready access—for community members, policy-makers, industry leaders and scientists—to national information about the ecosystems on which our livelihoods, lifestyles and identity depends.

The TERN Data Discovery portal is a national data delivery service and expert network that provides a range of EO information about Australian environments. The major products include:

- time-series of key environmental variables—derived from AVHRR, MODIS, Landsat, and SPOT imagery;
- high-resolution airborne imagery and field datasets for particular sites; and
- essential ground calibration and validation datasets for airborne and satellite image data.

Products listed in Table 14.1 demonstrate the range of validated EO-based continental products that TERN has delivered over the past 10 years to address landscape monitoring, change and diversity. The list of products that TERN develops with its partners and delivers through the TERN Portal changes over time due to changing priorities and the availability of source EO or validation data.

Table 14.1 TERN EO-based continental products

Product	Derived from	Spatial Resolution	Temporal Resolution	Temporal Extent
Normalised Difference Vegetation Index	AVHRR (NOAA)	1 km/ 5 km	10 day composite/ 1 month composite	1992–2014
Fraction of Photosynthetically Active Radiation	AVHRR (NOAA)	1 km/ 5 km/ 8 km	1 month composite	1995–2011 (1/5 km) 1981–2011 (8 km)
Grassland curing	MODIS (Terra/Aqua)	500 m	8 day composite	2000+
Enhanced Vegetation Index (EVI) and Land Surface Temperature (spatially and temporally integrated)	MOD13A1/ MOD11A2	500 m	8 day composite	2000–2014
Leaf Area Index (LAI) and Fraction of Photosynthetically Active Radiation (FPAR)	MOD15A2(c5)	1000 m	8 day composite	2000+
Gross Primary Productivity (GPP)	MOD17A2(c5)	1000 m	8 day composite	2000+
Fractional Cover (FC)	MCD43A4	500 m	8 day composite / 1 month composite	2000+
Normalised Difference Vegetation Index (NDVI) and Enhanced Vegetation Index (EVI)	MOD13Q1(c5)	250 m	16 day composite	2000+
Land Condition Index (LCI)	MCD43A4	500 m	16 day composite	2000–2011
Fraction of Photosynthetic Radiation absorbed by Chlorophyll	MOD13C2	5 km	1 month composite	2000–2014
Ecosystem Disturbance Index	MOD13A1/ MYD11A2	500 m	12 month composite	2000–2013
Phenology	MOD13C1 EVI	5 km	12 month composite	2000–2015
Land Cover Type	MCD12Q1(c5.1)	500 m	12 month composite	2001+
Land Cover Dynamics	MCD12Q2(c5)	500 m	2 year composite	2001+
Seasonal Fractional Cover	Landsat TM/ETM+/ OLI	30 m	Seasonal composite	1986+
Persistent Green-Vegetation Fraction and Wooded Mask	Landsat TM/ETM+	30 m	Single product	2000–2010
Vegetation Height and Structure	GLAS (ICESat), PALSAR, Landsat	30 m	Single product	2003–2009

An increasing number of EO information products are becoming available for a wide variety of applications. For example, some of the continental-scale, information products that have been derived from EO imagery over Australia by TERN are listed in Excursus 14.1. A comparable set of information products relevant to water applications are available from the Australian Ocean Data Network (AODN; see Section 14.4). Examples of other information products are detailed in Volume 3.

14.2 Monitoring

Monitoring generally implies continuous, or regular, checks or measurements on some condition or attribute. The dynamics, that is the extent and type of change, of the condition indicate its stability, and possibly its independence relative to other known conditions. To interpret monitoring information sensibly requires that the normal amplitude and frequency of variation for the condition are known. Extraordinary changes can then be identified when the monitored measurements indicate a greater or lesser variation than expected for a given time interval. The emphasis here is on continuous measurements with some expectation of the range of values which would result from a 'normal' situation. Abnormalities are then identified by their deviation from the presumed norm.

Environmental monitoring is concerned with observing and quantifying changes in the environment. Topical environmental issues concerned with monitoring change include deforestation, pollution levels, sedimentation in water bodies, urban development, and the severity and extent of natural disasters, such as fire, flood, subsidence, volcanic activity and storms. The relationship between the environmental parameter (or attribute) domain and the image data (or observation) domain is summarised in Figure 1.1. Starting with a physical parameter, such as water depth, a structure model relates the parameter space to a measurement space, such as reflectance in a given wavelength range. A measurement model then relates the measurement space to the image data space, namely pixels, channels and calibrated values (see Section 3.1).

Effective monitoring using EO data must rely on this framework of models, which relates image values to physical, independently-measurable parameters. A variety of physically-based models are being developed in a diverse range of applications that offer a potential basis for using EO to monitor environmental change (see Section 14.3 and Volume 3). Traditional image analysis techniques that highlight changes over ad hoc time periods can offer constructive information pertaining to environmental changes but should not be viewed as monitoring.

Multi-temporal EO datasets provide valuable information for monitoring a wide range of environmental attributes. As detailed in Section 2.1.2, extensive archives are now available for several satellite sensors, including AVHRR, Landsat, MODIS and SPOT-Vegetation. These repositories offer a unique set of observations to explore phenological and other cyclic changes in biosphere properties (see Section 14.2.1). Environmental legislation has also prompted monitoring the status of specific natural resources, such as native vegetation, inland water quality and carbon sequestration (see Section 14.2.2 and Volume 3).

Finally, detecting reflectance changes between two image dates is not the same as identifying the changes on the ground, and is at least one step removed from linking actual changes to causal agents. Some detected changes may be more significant than others, both depending on management objectives and the severity of change. Additional information is generally required to differentiate between short-term, cyclic changes resulting from natural events, and longer-term changes resulting from anthropogenic activities or climatic variations.

14.2.1 Environmental Accounting

Environmental accounting broadly refers to tracking relevant environmental attributes to monitor the condition of natural resources. In order to manage these resources sustainably, environmental accounts need to be detailed, frequent and comprehensive. In common with the more traditional forms of accounting, environmental accounts essentially aim to 'track the transfer of value through time, between locations, and between owners (including households, businesses, and governments)' (BoM, 2013). By contrast, ecosystem accounting is defined as an '*integrated statistical framework for organising biophysical data, measuring ecosystem services, tracking changes in ecosystem assets and linking this information to economic and other human activity.*' (UN, 2014).

Environmental accounting is promoted in Australia and around the world as a way of providing regular information on changes in the state of the environment to support policy development and decision-making. (Vardon et al., 2018)

Sustainability, by definition, involves preserving the capital base. To make informed decisions, policy makers need more comprehensive information about Australia's natural capital base upon which to judge the sustainability of the systems they manage and the best mix of economic, social, human and environmental policies. (BoM, 2013)

There is a growing awareness that economic growth and living standards directly depend on environmental assets, such as land, soil, minerals, rivers, oceans and biodiversity (DEE, 2018). Accordingly, sustainable management of these resources is essential for the future livelihood of all socio-economic sectors of our community. Environmental-economic accounting aims to understand both the condition of the environment and its relationship with the economy. It can be used to define and demonstrate the relationships between different economic sectors and specific environmental resources, and increasingly underpins the development and implementation of government policy and legislation (see Section 14.2.2). EO data, which is spatially explicit with global coverage and standardized over space and time, provides a unique input for environmental accounting.

For example, ABS generates an annual set of environment-economic accounts in accordance with the System of Environmental-Economic Accounting (SEEA[8]; an international statistical standard that is consistent with the System of National Accounts). From 2002/03 to 2015/16, Australia's consumption of water and energy, emissions of greenhouse gases and generation of waste are compared with the value of economic production and change in population in Figure 14.1. These comparisons confirm that, since 2006/07, the economy has grown faster than both population and the selected environmental consumption measures, which indicates that resources are being used efficiently.

An introduction to environmental accounting in Australia is presented in BoM (2013). While ground measurements are an essential part of environmental accounting, they are not sufficient to capture the regional and continental perspective. EO imagery, however, with contiguous, calibrated observations, provides a unique view of the Earth (see Volume 1). When integrated with ground measurements and biophysical models, EO datasets can be used to monitor a wide range of environmental attributes, such as vegetation cover and condition, water resources, carbon cycling, and natural disasters.

One example of environmental accounting is the Australian model-data fusion system, OzWALD (see Excursus 14.2). This system assimilates various EO datasets into a water balance model (a variant of AWRA-L; Van Dijk, 2010; Frost *et al.*, 2016) to estimate vegetation properties and energy, water and carbon balance parameters across Australia. OzWALD is used to generate annual updates on the condition, change and trajectory of the Australian environment (ANU, 2019).

Figure 14.1 Australian environmental-economic account for agriculture

Selected socio-economic and environmental measures for Australia are shown from 2006/07 to 2015/16.

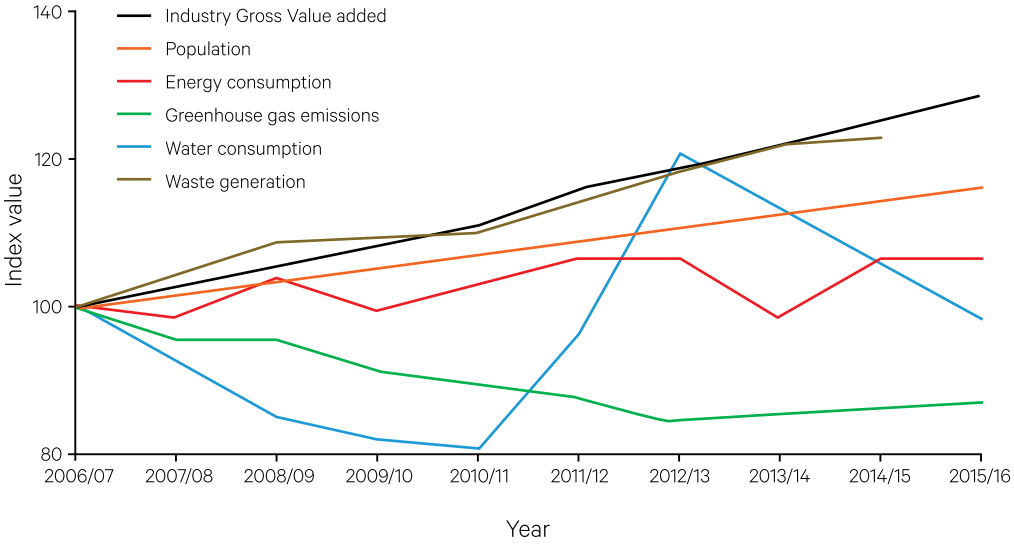

Source: ABS (2018)

8 The SEEA defines a flexible accounting framework that outlines methods to account for ecosystems in non-monetary terms (BoM, 2013).

Excursus 14.2—OzWALD

Source: Albert van Dijk, Australian National University
Further Information: van Dijk *et al.* (2017); van Dijk and Rahman (2019); *www.ausenv.online*

The Australian Water and Landscape Dynamics (OzWALD) system is a modular, data production workflow that is implemented using a combination of MatLab and Python scripts and libraries and executed on the National Computational Infrastructure (NCI)[9]. The system is largely automated with processing requirements amounting to around 30,000 processor-hours on the NCI's High Performance Computing Infrastructure. The volume of input data processed by OzWALD totals over 30 TB daily, which is condensed into annual summaries that total around 1 GB.

Development of OzWALD followed a review of national environmental reporting and accounting in Australia by van Dijk *et al.* (2014) which concluded 'Despite strong demand for information [and] considerable effort and investment, nation-wide environmental data collection and analysis remains a substantially unmet challenge'. Subsequent research demonstrated that environmental data, which is already being collected in Australia, can be usefully synthesised, interpreted and reported as an annual summary provided the technical challenges of routine data processing, web-based data access and effective communication of results are addressed.

The OzWALD system currently comprises five basic components as detailed below. Its statistical summaries can be visualised for selected time periods and regions via the Australia's Environment Explorer (AEE) and are reported in annual factsheets called Australia's Environment.

Data acquisition

Data from several gridded climate and satellite sources, most of which are stored in the NCI, are integrated in OzWALD, including:

- satellite-derived imagery produced by NASA:
  - surface reflectance and albedo (MCD43A4.006 and MCD43A3.006; Schaaf and Wang, 2015);
  - vegetation leaf area index (LAI, MCD15A3H.006; Myneni *et al.*, 2015); and
  - land surface temperature (LST, MYD11A1.006; Wan *et al.*, 2015);
- estimates of the fractions of bare soil, photosynthetic vegetation and non-photosynthetic vegetation derived from MCD43A4.006 (Guerschman and Hill, 2018) and produced by CSIRO;
- Landsat-based water presence mapping data (Water Observations from Space (WoFS; see Volume 1A—Excursus 5.1); Mueller *et al.*, 2016) available from Digital Earth Australia (DEA; see Section 11.2);
- precipitation and short-wave incoming radiation produced as part of the Australian Gridded Climate Data (AGDC; Jones et al., 2009) by Bureau of Meteorology (BoM); and
- hourly temperature, humidity, pressure and wind speed produced by the European Centre for Medium-range Weather Forecasting (ERA5, ECMWF; Copernicus Climate Change Service, 2017). These data are available and accessible to NCI users, while most can also be accessed via NCI THREDDS[10].

In addition, the following data are downloaded as a scheduled daily process or on demand:

- satellite-derived rainfall estimates (IMERG, Huffman *et al.*, 2015) from NASA[11];
- satellite-detected fire occurrence and intensity from the Sentinel Hotspots system (Geoscience Australia, 2014)[12]; and
- fire carbon emission estimates (Kaiser *et al.*, 2012) from ECMWF[13].

The stability, reliability, latency and continuity of data services are important factors that constrain workflow outcomes. For example, replacing MODIS Collection 5 with Collection 6 introduced a series of technical challenges.

Data reformatting

All original (raster and vector) data are resampled and reformatted to a single gridded standard in geographic coordinates and stored in NetCDF file format (see Volume 2A—Section 1.6). Data are temporally aggregated to a minimum daily resolution where necessary.

9 *www.nci.org.au*
10 *http://dapds00.nci.org.au/thredds/*
11 *https://pmm.nasa.gov/data-access/downloads/gpm*
12 *https://sentinel.ga.gov.au/*
13 *https://apps.ecmwf.int/datasets/data/cams-gfas/*

Data fusion and downscaling

Data fusion, blending of like data into a single consistent best-estimate data set, is applied to produce observation-based estimates of:

- precipitation—the AGCD and IMERG data grids are merged to estimate daily accumulated rainfall. Since the AGCD are derived by interpolating point data from weather stations, they are more accurate than the IMERG estimates where gauge density is greater than 1 /~500 km2 but become gradually less accurate at lower densities (Renzullo *et al.*, 2011). To select the most accurate rainfall estimates, an inverse-distance weighting scheme is used to blend the AGCD and IMERG datasets; and
- surface water extent—an internally-consistent data set of surface feature type (at 500-m and 8-day resolution) is derived from the fractions of surface water, snow, bare soil and living and dead vegetation, as well as LAI and albedo using the Water And Landscape Dynamics Multi-Observation Reanalysis and Filtering (WALDMORF) algorithm. This process involves various checks and balances, including data fusion methods (see Section 6.2), interpolation of missing values (see Volume 2A), and detecting outliers (see Volume 2E).

Climate data is downscaled to 500 m spatial resolution using the DEM-H product to enforce topographic and elevation consistency (Gallant *et al.*, 2011; see Section 13.2). Thus far, downscaling has been applied to terrain illumination from incoming shortwave radiation, air temperature, and vapour pressure.

Model-data assimilation

Biophysical modelling is used to estimate environmental variables for which spatial data are not directly available, such as root zone soil moisture, streamflow generation, and carbon uptake by the vegetation. The OzWALD model evolved from AWRA-L v0.5 (Van Dijk, 2010), which formed the core of BoM's operational daily landscape water balance modelling system (Frost *et al.*, 2016), the associated spatial information service[14], and the AWRA Community Modelling System[15]. The workflow steps in this multi-layer model are summarised in Table 14.2. Workflows for both the spin-up and final models comprise:

- retrieving and transforming climate forcing and satellite-derived surface properties;
- updating model parameters using satellite dataset with a simple nudging scheme;
- evolving model states one day forward using a daily time step model; then
- concatenating and storing the requested data.

Table 14.2 OzWALD model components

Module	Workflow description
HPC job generation	deploy workflow for specified model domains
Model workflow management	set up system environment
	initialise static model parameters and model states
	optional spin-up model run for a specified period to produce 'hot' initial states if needed
	produce and store the requested variables
Post-processing	collate and store outputs into annual national grids

Statistical summary

The daily or 8-daily, continental, 500-m resolution data files produced as described above are published through NCI THREDDS. For many users these results may be challenging to interpret, so temporal and regional summary statistics are calculated in a final post-processing step as these are what users are most likely to visualise through web applications:

- Annual summary maps—most commonly minimum, maximum and average and/or accumulated daily values are calculated for the year, and these are stored at the original spatial data resolution in gridded NETCDF format.
- Regional-average annual time series—annual summary maps are intersected with different region definitions derived from thematic vector maps. Because of their small data volume, these summary data are stored as CSV files on an external web server.
- Regional-average sub-annual time series—are calculated at the original temporal and stored as NetCDF files on NCI THREDDS with the two spatial dimensions being replaced by the region identifier.
- Annual regional summaries by broad land use type—as computed for the regional-average annual time-series maps described above with further stratifying by broad land-use type, and as cumulative spatial sums rather than averages where appropriate. The land-use classes are an amalgamation of the many classes in the 50 m resolution Catchment-scale Land Use Data (ABARES, 2017) into 20 broad classes. The resulting data are quite comparable to that used to construct environmental accounts.

14 *http://www.bom.gov.au/water/landscape/*
15 *https://github.com/awracms/awra_cms*

Visualisation and Analysis

OzWALD statistical summaries can be visualised via the Australia's Environment Explorer (AEE) website[16]. This interactive facility enables users to explore environmental changes by region, location or land use type which are presented as maps and charts (see Figure 14.2). Data can be queried for a particular location, or as the average across a predefined region, where region can be defined as:

- political and administrative units (states and territories, local government areas, federal electorates, natural resource management regions, national parks, Ramsar wetlands);
- biophysical units (bioregions, river regions and drainage divisions); and
- statistical accounting regions.

Regional summary data can be directly downloaded via the AEE website or edited online using the plotly visualization app (*http://plot.ly/*). The original and summary gridded time series can be accessed and downloaded from the NCI Data Collection, which provides an API to the data. All data is available under a Creative Commons license (CC BY 3.0 AU). Sub-annual and annual data produced by OzWALD are also available through the ANU-TERN Landscape Data Visualiser (*http://maps.tern.org.au*), a web app designed to help researchers and other interested users to visualise and explore data collected or produced by the Terrestrial Ecosystem Research Network (see Excursus 12.2) or ANU-WALD. Unlike the AEE, this website provides tools to visualise sub-annual gridded data, and to compare different datasets (such as flux tower measurements and gridded data) for a location of interest (see Volume 3A).

Regional and national Environmental Condition Scores (ECS) are also produced for seven variables by ranking annual values of each variable within the time series since the year 2000 (see Figure 14.3). Interpretation of the ECS component scores confirms the scientific consensus that environmental condition is directly dependent on water availability for most of Australia, which partially mitigates its limitations.

Figure 14.2 Australia's Environment Explorer

This example screenshot from Australia's Environment Explorer shows national persistent vegetation cover (see Volume 3A).

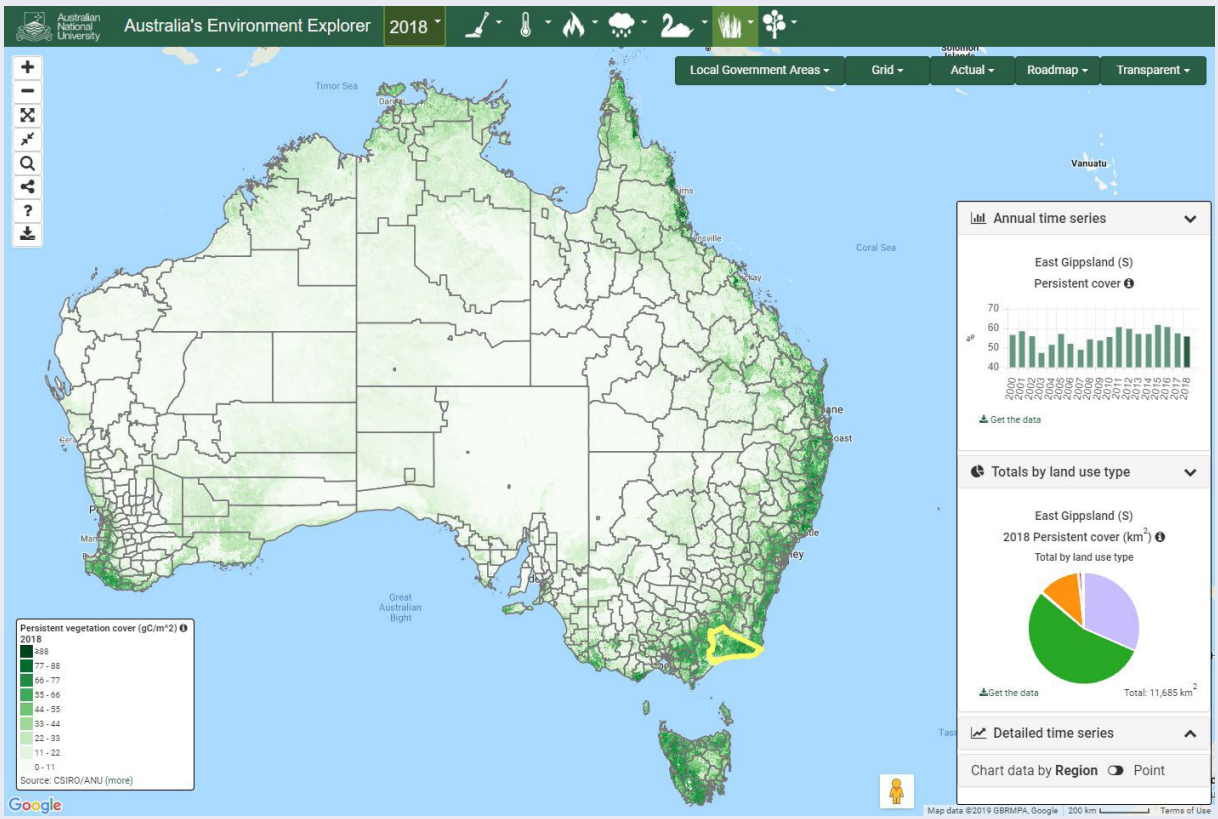

16 *www.ausenv.online*

Figure 14.3 2018 OzWALD summary for ACT

a. Annual environmental condition scores have been computed since 2000 as the average of seven components.

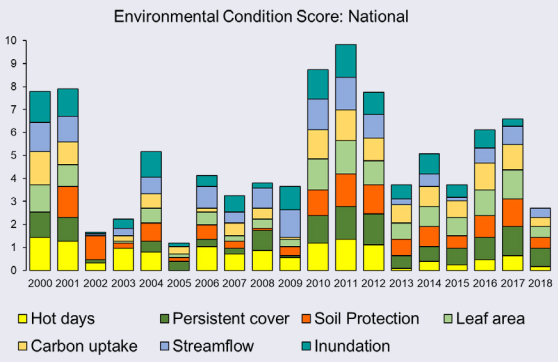

b. National map showing overall change from 2017 to 2018

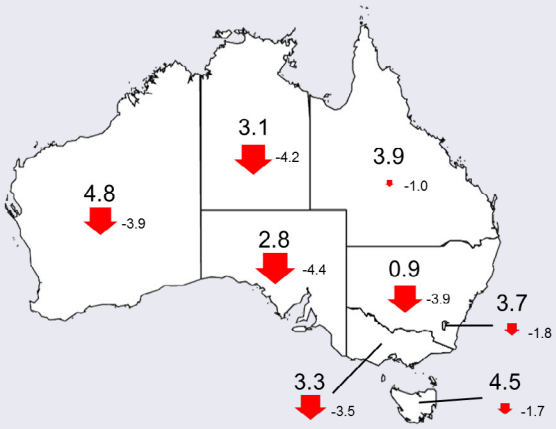

Source: van Dijk and Rahman (2019) Figure 3

Australia's Environment Report

The Australia's Environment (AE) report[17], which synthesises information from other sources and interprets specific events and temporal trends in global or non-spatial data (including ABS, BoM, IMOS, TERN, and Atlas of Living Australia, and the WMO), is produced annually. This provides additional opportunities to interpret information and report on time series representing smaller or unspecified areas within Australia, specific events and their impacts, different parts of the environment, and the global context.

Status Overview

The OzWALD system and AEE demonstrate that it is feasible to produce useful, observation-based annual environmental reports. Insights from this research and development include the:

- challenges to operational workflows presented by an unstable, and continually evolving, spatial data services environment;
- efficiencies provided by the rapid development of open source and cloud technologies;
- necessity of regular, detailed and accurate land cover and land use mapping to achieve successful environmental accounting;
- opportunities for environmental reporting enabled by the abundance of past, current and future satellite mission datasets; and
- ongoing difficulties in obtaining regular and reliable biodiversity data.

The goal of OzWALD is to continue—and as much as possible improve—the annual, environmental modelling and reporting process until a similar service is available from another source.

17 *http://wald.anu.edu.au/australias-environment/*

Problems cannot be solved with the same mind set that created them.
(Albert Einstein)

14.2.2 Compliance Monitoring

The responsibility for a range of regulatory functions under legislation rests with various government departments and agencies at federal, state and local levels. In order to achieve the specific objectives of each piece of legislation, regulated communities need to comply with defined rules or standards, which are frequently presented in terms of conditions associated with approvals, permits or licences (DEE, 2016). Compliance monitoring describes the bureaucratic process of ensuring that the community obligations to legislation are met.

An increasing volume of legislation relates to environmental protection in some form. For example, at a federal level, compliance monitoring activities are undertaken under the legal frameworks of four pieces of legislation:

- Environment Protection and Biodiversity Conservation Act 1999 (Parts 7, 9, and 10)—protects and manages Australia's land and marine biodiversity, threatened species, ecosystems, environment and heritage;
- Environment Protection (Sea Dumping) Act 1981—regulates the dumping of waste at sea, incineration at sea, and the placement of artificial reefs;
- Fuel Quality Standards Act 2000— places obligations on the fuel industry to ensure that supplied fuel meets strict environmental and human health requirements; and
- Ozone Protection and Synthetic Greenhouse Gas Management Act (1989)—helps to ensure that Australia meets its legal obligations under the Montreal Protocol (1989) and the United Nations Framework Convention on Climate Change.

Given the extent of Australia's land and maritime resources, EO-based datasets are playing an increasing role in compliance monitoring. For example, several Australian state governments have implemented legislation to protect natural biodiversity and restrict clearing of native vegetation. Regulation of these activities requires a benchmark from which changes in vegetation—and by inference, biodiversity—can be assessed. The benchmark that has been adopted for Australia is the estimated condition of vegetation in 1750, prior to European settlement (see Volume 3A).

To ensure that land owners are complying with these legislation, sophisticated systems based on EO datasets have been developed by several state governments. An overview of the well-established SLATS (State-wide Landcover and Trees Study) system used in Queensland and NSW is presented in Excursus 14.3.

Compliance monitoring ensures that the regulated community undertakes actions that are in accordance with the respective legislation. By ensuring that the regulated community does this, impacts to the environment and human health can be managed and minimised.
(DEE, 2016)

Excursus 14.3—SLATS: Monitoring Woody Vegetation Clearing

Source: Tim Danaher, NSW Department of Planning, Industry and Environment and Dan Tindall, Queenland Department of Environment and Science
Further Information: SLATS Queensland: *https://www.qld.gov.au/environment/land/management/mapping/statewide-monitoring/slats*
SLATS NSW: *https://www.environment.nsw.gov.au/topics/animals-and-plants/native-vegetation/reports-and-resources*

Background

Vegetation types within Australia are diverse due to many factors including climate, geology, soils, presence or absence of fire, and land management practices (see Volume 3A). Historic patterns of development and land management have altered, and in some cases degraded, many of these landscapes through land clearing, altered fire regimes and other land management activities, such as grazing.

In the past 20-30 years, there has been greater recognition of the legal and environmental responsibilities of state governments and the community to balance the production and conservation interests in these often fragile landscapes. This includes allowing appropriate clearing of vegetation but avoiding further degradation of these systems. The debate about how to achieve that balance is often polarised by different stakeholder interests and may be informed by data that is either incomplete or has limited spatial extent. Objective information about land cover changes, which is both spatially and temporally comprehensive, is needed to:

- inform policy decisions;
- support legislation regulation and compliance; and
- assist landholders and non-government organizations with managing these lands.

Satellite imagery, particularly imagery derived from systematic acquisition programs such as Landsat, provides an opportunity to monitor land cover change in an objective, repeatable and comprehensive way.

In 1995, the Queensland Government established a monitoring initiative known as the Statewide Landcover and Trees Study (SLATS) to provide monitoring of vegetation based on Landsat TM/ETM+/OLI satellite imagery across the entire state. The Landsat imagery delivered a suitable spatial resolution and extent for informing policy and regulatory compliance under relevant legislation, as well as restoration and other land management actions across the state. With a spatial resolution of 30 m, this imagery enabled the reliable delineation of woody vegetation changes greater than 1 ha, and direct calibration, validation, and interpretation of those changes in the field. The SLATS continues to monitor land cover change in Queensland annually.

The NSW government has also used the SLATS method for monitoring vegetation since 2006. The data generated by SLATS in Queensland and NSW has provided the foundation for a number of changes to vegetation and biodiversity management legislation and other land management and monitoring programs. This has included, for example, globally significant programs relating to the management of the Great Barrier Reef (see Volume 3B) and the Murray-Darling Basin (see Volume 3A).

In recent years, with the advent of higher resolution satellite missions (such as SPOT-5 and the European Space Agency's Sentinel-2A and -2B as part of their Copernicus programme), the SLATS methodology has been adapted to make use of these higher spatial resolution sensors. Firstly, NSW changed to using higher resolution 5 m resolution SPOT-5 imagery in 2009 and more recently Queensland and NSW have both transitioned to 10 m resolution Sentinel-2 imagery.

SLATS model

The primary objective of the SLATS methodology is to map the location and extent of woody vegetation clearing that results from anthropogenic (human-induced) removal of vegetation across an entire Australian state. The reduction in woody vegetation cover due to clearing needs to be mapped at time intervals of no longer than 1-2 years. Longer periods may miss some clearing events, since regrowth (which can have significant canopy density) and additional pasture or other herbaceous vegetation may establish within the intervening period, making it difficult to reliably detect and map changes in woody vegetation.

SLATS monitors woody vegetation clearing using a combination of automated and manual mapping techniques, primarily based on medium resolution satellite imagery acquired from the Landsat, SPOT-5 and Sentinel-2 satellites. The manual editing stage is supported by ancillary data sources, including higher resolution satellite imagery, and is an essential component for ensuring an accurate account of woody vegetation clearing across each state.

The SLATS methodology relies on efficient data management and processing systems that have been purpose-built on open source software foundations.

These systems enable largely automated processing of satellite imagery workflows in a high performance computing environment. Data management and software version control systems enable data provenance tracking and code management, and ensure efficiency and traceability in all stages of the mapping and analysis processes. A schematic overview of the SLATS methodology is shown in Figure 14.4 and an example of a clearing event mapped by SLATS is shown in Figure 14.5. The key processing and analysis steps can be summarised as follows:

1. Satellite imagery is acquired, then corrected for sensor calibration, atmospheric, topographic effects and Sun and sensor viewing angles (Flood *et al.*, 2013; see Section 3.1). The most cloud-free images from the dry season period are selected for each year (see Figure 14.5a and Figure 14.5b).
2. A woody vegetation clearing index is calculated to detect areas of change that represent possible clearing of woody vegetation. This model has been calibrated using historic mapping of cleared areas (Scarth *et al.*, 2008; Danaher *et al.*, 2011). It highlights most of the possible clearing and omits areas that are almost certain not to represent clearing (see Figure 14.5c and Figure 14.5d).
3. This initial clearing index is visually inspected, and manually edited by trained remote sensing scientists to confirm areas that have been cleared and omit areas that have not been cleared. The reason for the extensive manual editing is because naturally occurring events can affect vegetation in ways that appear similar to woody vegetation clearing in terms of the spectral and temporal responses observed by the satellite sensor (and used to calculate the clearing index). For example, damage by storms, fire and drought can all cause a reduction in canopy health or cover that can appear similar to a clearing event, and are often detected by the automated clearing index as possible clearing. This manual process makes use of any additional information available to aid decisions.

   During the manual editing step, each change area is allocated an appropriate class that indicates the replacement land cover or land use. The assignment or coding of these classes is primarily based on visual interpretation, with reference to ancillary data sources. In areas where there are many different forms of land use, it can be difficult to interpret the final replacement class and therefore this classification is indicative only. Broadly these classes distinguish clearing for pasture, agriculture, forestry, infrastructure and natural causes. There is a specific set of more detailed classes that varies for each jurisdiction.
4. Senior remote sensing scientists review the manual editing, so that mapped clearing has been visually checked and independently verified by another scientist. Further edits and quality control checks are undertaken to finalise the woody vegetation clearing mapping.
5. The mapping is compiled, and a statewide mosaic (see Volume 2B) of woody vegetation clearing is created.
6. Since the time period between annual images varies (depending on the availability of cloud-free satellite images), the mapping is converted to an annualised clearing rate to enable inter-annual comparisons.

Figure 14.4 Schematic representation of SLATS processing steps

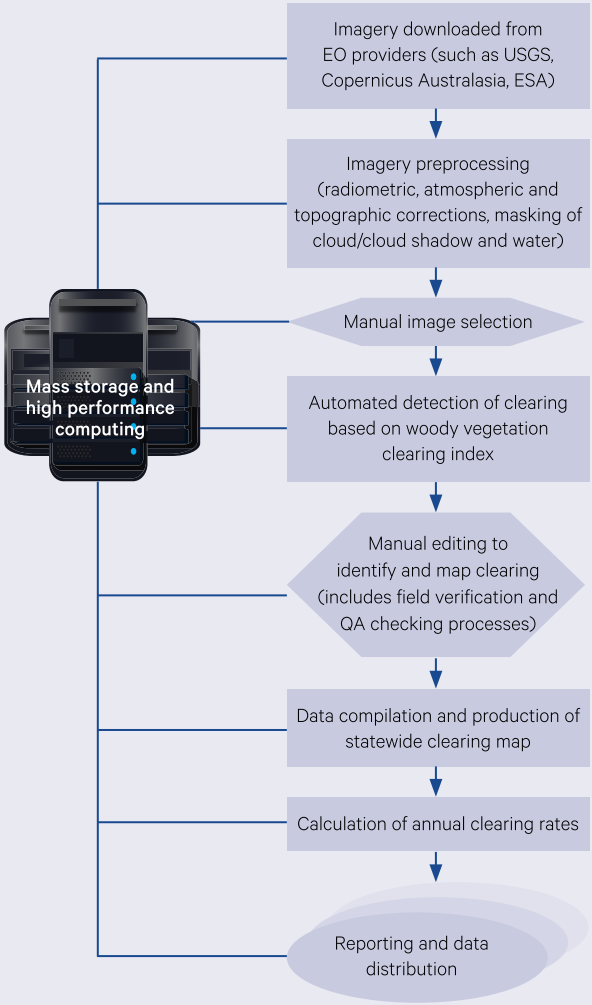

Figure 14.5 Example of SLATS change index and likelihood images

Two SPOT-5 images in the central tablelands of NSW were acquired on 18 April 2011 and 8 July 2012, before and after woody vegetation clearing. These images were used to create a change index image, in which the white areas are likely to indicate clearing. The change index image can be thresholded to create a change likelihood image. In this example, red highlights areas that are most likely to have been cleared, grey levels from dark grey to white are progressively less likely to have been cleared and yellow areas have not been cleared.

a. SPOT-5 image acquired before woody vegetation clearing

b. SPOT-5 image acquired after woody vegetation clearing

c. SLATS change index image

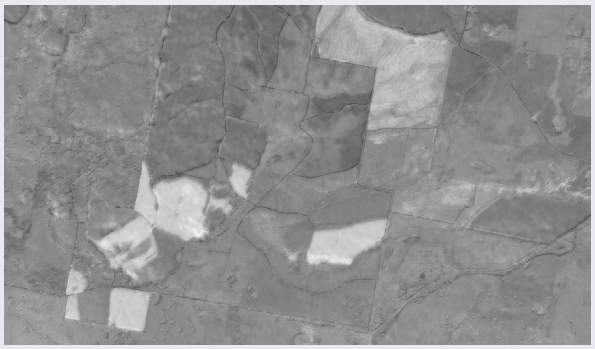

d. SLATS change likelihood image

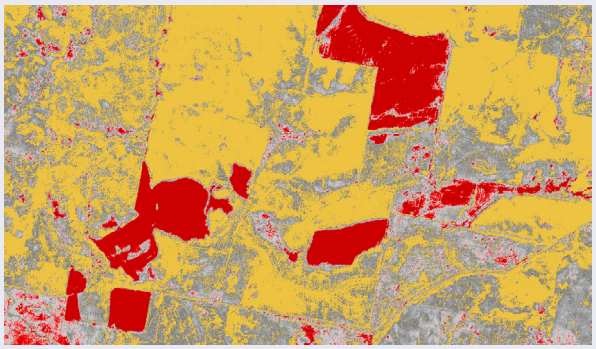

SLATS products and use

The SLATS information on vegetation change is generally published on an annual basis as a report with accompanying spreadsheets showing woody vegetation change by different regions, such as catchments, natural resource management regions, tenure etc. Additionally, the vegetation clearing data are analysed and compared with permits and development approvals to identify potential compliance issues that may require further investigation, and also to inform policy effectiveness and implementation of the legislation and regulatory frameworks. An example of a SLATS reporting outcome is shown in Figure 14.6 below.The SLATS change data is also used to update other forms of regulatory mapping, such as the Queensland Regional Ecosystems mapping or the NSW Native Vegetation Regulatory maps.

After annual reports are released the spatial vegetation change data is also released as open data and can be used by other practitioners and researchers for purposes such as biodiversity and land management, informing carbon and greenhouse gas emissions monitoring and sequestration programs, or for understanding the ecological impacts of vegetation change.

Figure 14.6 Example of SLATS reporting outcome

Annualised woody vegetation clearing rates in Queensland between 1988 and 2018 as reported by SLATS. In Queensland, the clearing rates are further analysed by a remnant and non-remnant vegetation status. This provides one indicator of the effectiveness of the vegetation management legislation in achieving its purpose, which includes conserving regional ecosystems.

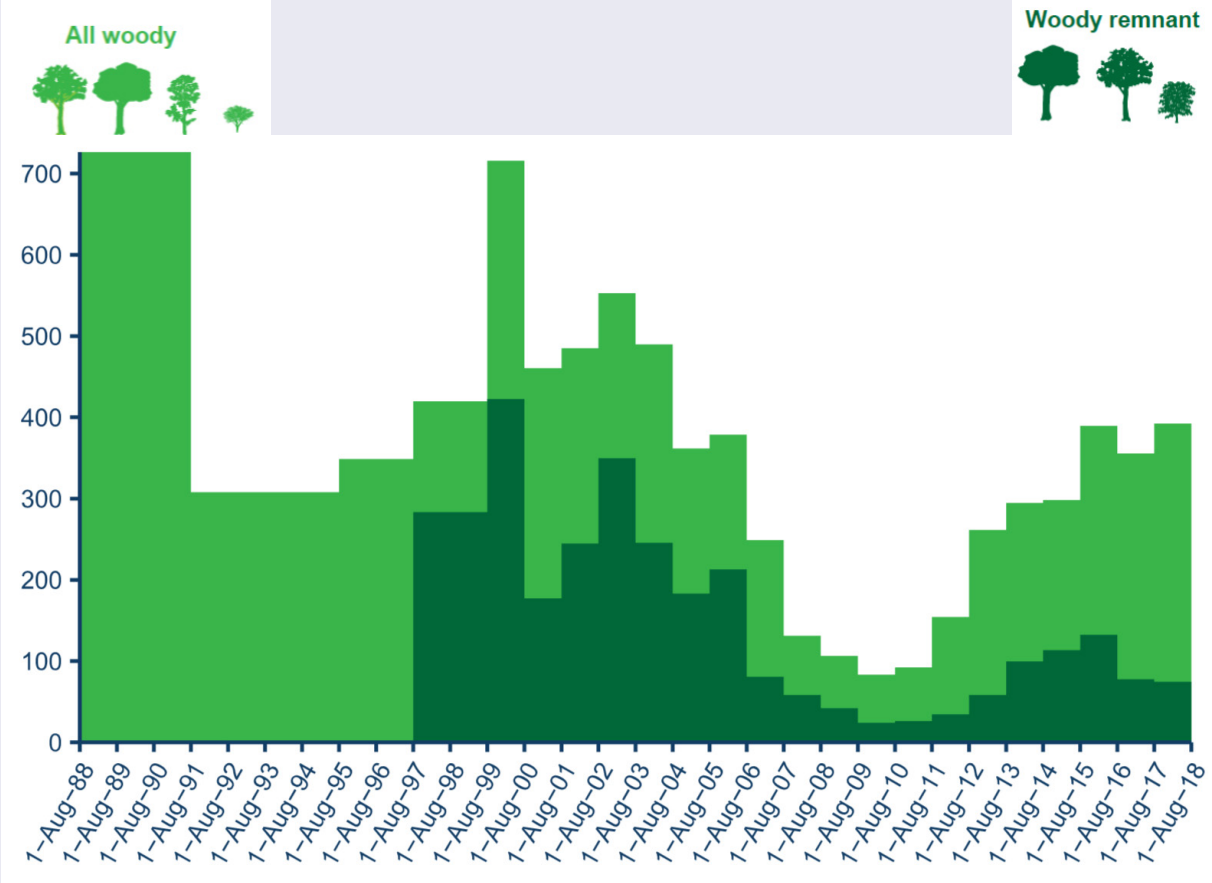

Applying SLATS in near real time

As governments have become more accustomed to the use of satellite imagery to inform monitoring programs, there has been increased interest in its ability to be used for regular monitoring for proactive compliance and regulatory actions relating to the management of various natural resources, such as vegetation and water. This interest, and the ability to develop methods for regular monitoring, has also been facilitated by free and open data policies, such as those of the Landsat and Copernicus programmes, coupled with significant developments in high performance computing capabilities.

In relatively recent developments, both Queensland and NSW have adapted the SLATS model to build proactive compliance programs that detect recent clearing activity on weekly to fortnightly time scales. Queensland's system was originally developed using Landsat, but more recently both states have adopted Sentinel-2 satellite imagery, due to its higher spatial resolution and temporal frequency. The adaptation of an annual monitoring program to a more regular and frequent time step is not without its challenges:

- imagery and data management systems need be revised to track and manage the increased and regular data and workflows;
- the vegetation change algorithm can be less effective, or suffer significant commission errors, in wetter or cloudier periods, due to landscape green-up, inadequate cloud masking or inundation; and
- a more regular flow of information can overload available resources to address any potential compliance issues.

In order to manage for these challenges, the systems which have been developed in Queensland and NSW apply a number of imagery and spatial filters (such as cloud cover thresholds, regulatory mapping filters) and a manual checking component, which is still essential to confirm clearing events. However the manual checking component is aimed at identifying or detecting clearing events, rather than mapping them, as is the case in the annual SLATS monitoring programs.

These programs are being successfully implemented in both states, and are aimed at early intervention compliance action, thus raising public awareness with regards to vegetation management responsibilities, and reducing the amount of serious, significant clearing cases due to the ability to use timely intervention methods that deter further planned clearing from occurring. In Queensland, for example, it is estimated that this system has accounted for approximately 90–95% of all of the potential compliance actions that would previously have resulted from an analysis of the annual SLATS data, with the advantage that action has been taken within weeks to months (sometimes within days) of the clearing activity, rather than a year or more later as previously occurred.

Collaborative research program and complementary products

Ongoing maintenance of, and improvements to, the SLATS methods are undertaken collaboratively through the Joint Remote Sensing Research Program (JRSRP). This research includes:

- building and maintaining a software environment to enable efficient processing and data management tools for large archives of satellite imagery;
- pre-processing corrections including methods for image calibration, radiometric correction and change analysis;
- transitioning the SLATS methods to work with different medium resolution imagery sources such as SPOT-5 and Sentinel-2; and
- developing related systems such as the continuous early detection of vegetation clearing events using Sentinel-2 imagery.

This long-standing collaboration has enabled sharing of capacity and scientific processes and extended the benefits of the SLATS model for the Queensland and NSW governments, and their partners in other jurisdictions. These benefits include the progressive development of SLATS, and other complementary EO products, which have been built on its processes and systems. These products include:

- fractional cover (Guerschman *et al.*, 2015; Scarth *et al.*, 2010);
- foliage projective cover and woody extent data (Armston *et al.*, 2009; Kitchen *et al.*, 2010);
- fire scar and fire severity mapping (Goodwin and Collett, 2014);
- crop monitoring (Pringle *et al.*, 2018; Schmidt *et al.*, 2016); and
- biomass mapping (Scarth *et al.*, 2019).

Current and future developments for SLATS include improving woody extent mapping using computer vision approaches (Flood *et al.*, 2019) and developing regrowth and biomass monitoring approaches using Landsat and Sentinel time series, radar (such as ALOS-2) and spaceborne lidar.

Accounts are a structured, systematic way of organising data into information for a clearly defined decision-making purpose. They track flows and stores of value (stocks) over a set period of time. Accounts present comparable information in a systematic fashion, using standard definitions based on a sound conceptual framework. They encourage the development of comprehensive and consistent data and provide a platform for producing a range of accounting reports and analyses.
(BoM, 2013)

14.3 Modelling

People don't understand the Earth, but they want to, so they build a model, and then they have two things they don't understand.
(Gerard Roe in 'The Whale and the Supercomputer' by C. Wohlforth)

A complex range of dynamic environmental attributes constitute planet Earth (see Volume 1A—Section 3). The structure, composition, biology and energy of Earth continue to change in variable time frames. The processes that drive these changes are the focus of modelling activities. By identifying the driving forces and the mechanisms involved in environmental processes, we can start to understand their interrelationships and rate of change, then predict the likely result of variations in current conditions. For example, EO-based models for climate and weather are the backbone of current weather forecasting systems (see Volume 1A—Section 16). Similarly, modelling indicators of photosynthetic activity derived from EO datasets now underpin a wide range of environmental and agricultural activities (see Volume 3A).

EO-based modelling was introduced in Volume 1A—Section 1.4.3 and some types of models that are used with EO datasets were described in Volume 2A—Section 2. In the context of EO, forward models are used to compute the likely EO values from known environmental attributes, whereas inverse models use the EO attributes to compute the likely environmental attributes. Broad categories of models between EO values and environmental attributes include:

- empirical or analytical, which are based on simple relationships such as regression analysis;
- semi-empirical or semi-analytical, which use prior knowledge to determine the relationship; and
- physics-based, which rely on their known physical relationship(s).

Modelling of carbon, water and energy fluxes between the Earth's surface and the atmosphere is increasingly important for hydrological and climate studies. Such models can focus on particular spatial scales then, with appropriate prerequisites and constraints, be scaled up to increasingly larger scenarios (Nemani *et al*., 2009; Pasetto *et al*., 2018). The extensive spatial and temporal coverage of many EO datasets offer particular advantages for multi-scale modelling (see Section 1.4). In this section, we will consider one Australian example of modelling ecosystem dynamics based on EO datasets; further examples are detailed in Volume 3.

The greatest enemy of knowledge is not ignorance, it is the illusion of knowledge.
(Stephen Hawking)

Excursus 14.4—eReefs

Source: Mark Baird, CSIRO
Further Information: *https://ereefs.org.au/ereefs*

Despite being one of the world's best managed reef systems, Australia's iconic Great Barrier Reef (GBR) has, with other reefs worldwide, suffered a decline in coral cover. In order to understand the factors that are influencing this decline, and to inform management strategies, a sophisticated information system, eReefs, has been developed to deliver past and near real time observations, modelling and analysis (Steven *et al.*, 2019). The eReefs information system is built upon an integrated system of data, catchment and marine models, visualisation, reporting and decision support tools that span the entire GBR area.

The eReefs marine models includes a range of process models that simulate hydrodynamic state (Herzfeld *et al.*, 2016), sediment transport (Margvelashvili *et al.*, 2018), water quality (Baird *et al.*, 2016), carbon chemistry (Mongin *et al.*, 2016) and basal ecology (Skerratt *et al*, 2019; Baird *et al.*, 2018) of the GBR lagoon and reef matrix. This collaborative project[18], started in 2012, is viewed as the first step in building a comprehensive coastal information system for Australia.

Simulations of the eReefs models enable the effectiveness of current management strategies to be assessed and provide valuable insights for regulatory authorities on a range of emergent and potential reef management challenges (Brodie *et al.*, 2017). The eReefs Platform integrates EO tools with near real time models to quantify significant coastal management issues, including:

- regional, three-dimensional hydrodynamic and biogeochemical models to map, monitor and forecast coastal water quality (such as sediment and nutrient loads) and ecological responses for the GBR region in relation to agricultural and land management activities in adjoining catchments (see Figure 14.7). In conjunction with EO and meteorological observations, these nested models consider land use, catchment flows, circulation of mesoscale oceanographic processes, and sediment transport to simulate their impact on reef health in a range of timeframes; and
- operational hydrodynamic coastal ocean forecasting based on meteorological data to analyse, predict and archive data relating to currents, temperature, salinity, and sea level within the waters of the GBR region, plus river tracer concentrations from major rivers. This information has relevance to a number of marine management activities, including ship routing, port management, modelling plumes, monitoring spills, fishing, recreation, and search and rescue operations.

The temporal and spatial scales involved with processes and observations in the GBR are illustrated in Figure 14.8. EO datasets, from both satellite and aerial platforms, are relevant to a range of these scales, in both space and time, and are used in conjunction with a variety of data from other sensors to derive essential inputs to eReefs models. One strength of the biogeochemical modelling is the assimilation of remotely sensed ocean colour data. The eReefs model became the first published biogeochemical model to use EO reflectance (at multiple wavelengths) as the model variable for which the mismatch drives the assimilation procedure (Jones *et al.*, 2016). The use of EO reflectance required the development of a complex optical model in eReefs, and replaced the use of ocean colour algorithms in other biogeochemical data assimilation systems. In coastal waters where ocean colour algorithms have large errors, this was a breakthrough.

18 Collaborators include the Science Industry Endowment Fund, CSIRO, The Australian Institute of Marine Science, the Bureau of Meteorology, and the Great Barrier Reef Foundation, with support from BHP Billiton Mitsubishi Alliance and the Australian and Queensland governments, and observations obtained through IMOS.

Figure 14.7 eReefs modelling framework

a. Conceptual model of GBR shelf ecosystem

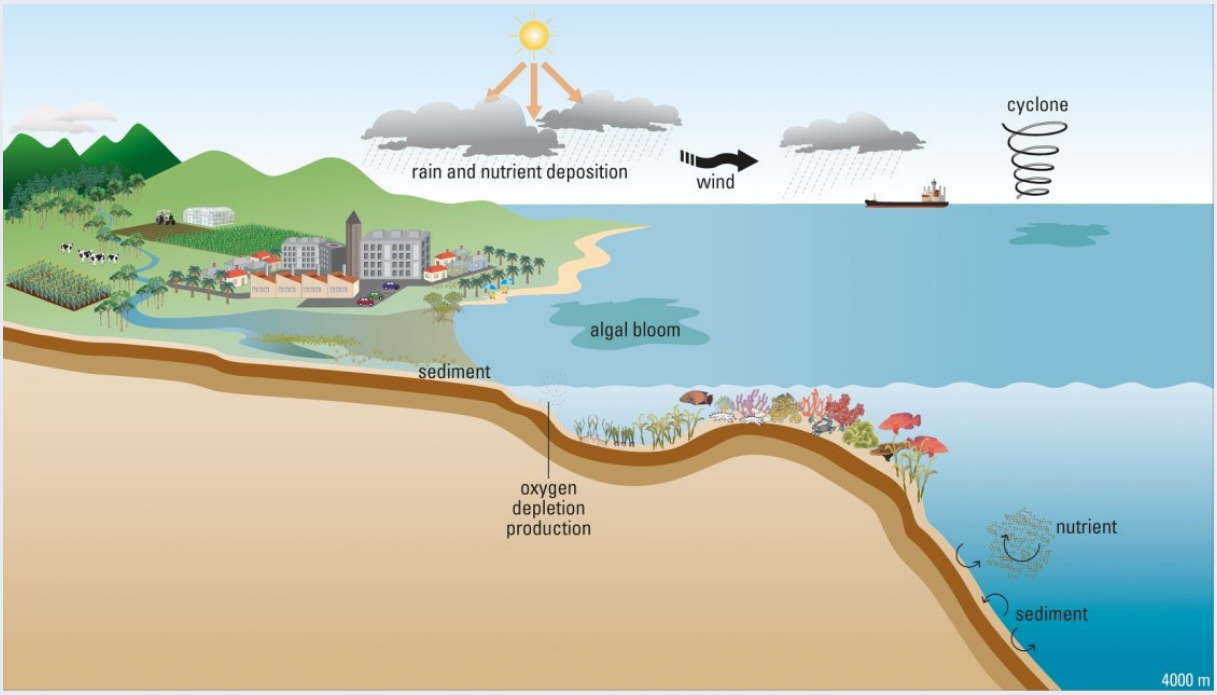

Source: Herzfeld *et al.* (2016) Figure 4.7.3 (page 155). Retrieved from *http://www.marine.csiro.au/cem/gbr4/eReefs_Marine_Modelling.pdf*

Figure 14.8 Temporal and spatial scales of GBR processes and observations

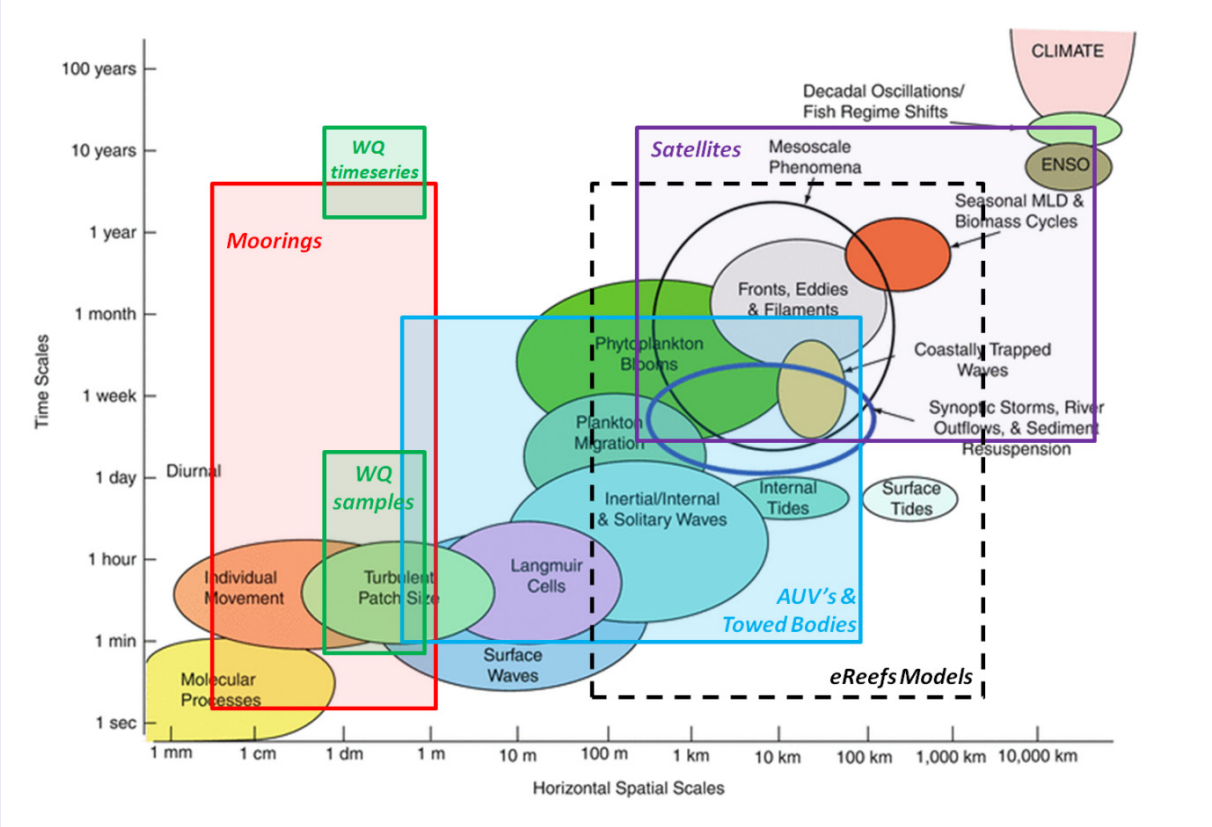

Source: Herzfeld *et al.* (2016) Figure 5.5.7 (page 354). Retrieved from *http://www.marine.csiro.au/cem/gbr4/eReefs_Marine_Modelling.pdf*

Figure 14.9 eReefs model interactions

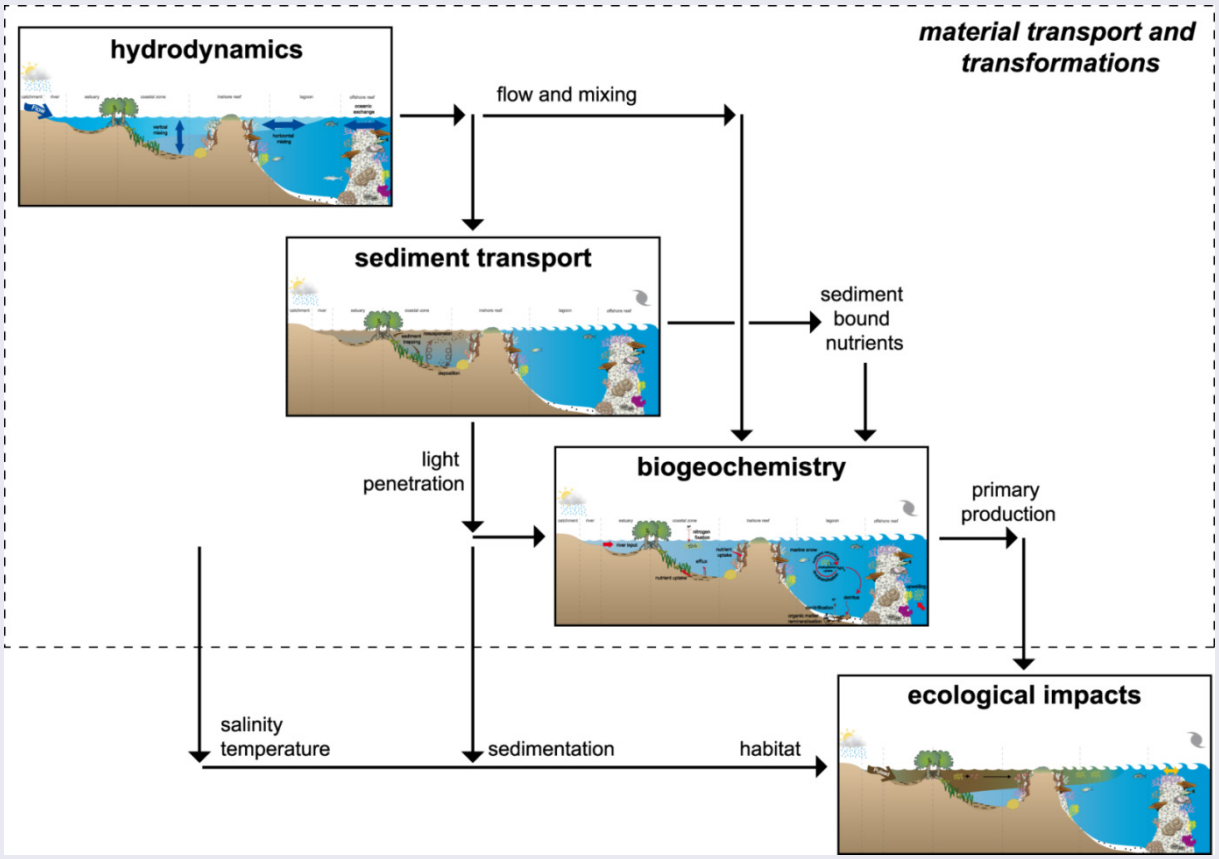

Source: Webster *et al.* (2008) Figure 1.1-2. Retrieved from *https://ereefs.org.au/ereefs/platform/regional-hydrodynamic-sediment-and-wq-modeling*

The three major process-based marine models described above that underpin eReefs to determine ecological impacts (see Figure 14.9) are:

- hydrodynamic model—predict physical state of the GBR regional system based on meteorological data and models;
- sediment transport model—predict movement of suspended fine sediments and biogeochemical variables; and
- biogeochemical model—simulates water column and benthic production, water quality and nutrient cycling; with supporting models that account for water optics and wave action.

Model results have been calibrated and validated against independent observations, and model uncertainty estimated (Skerratt *et al.*, 2016). Model outputs can be accessed as raw data, viewed online as animated loops of key variables, or interactively explored in web applications. This integrated modelling approach enables early detection and precise location of potential problems, such as infestations of crown of thorns starfish, hotspots for coral bleaching, and decreasing oxygen levels.

Some of the reef management challenges that can be simulated and predicted by eReefs include the impact of:

- ocean acidity on coral calcification;
- catchment-based activities that reduce water quality and undermine reef health;
- combined effect of extreme light and temperature on coral bleaching;
- extreme weather events and floods on marine systems; and
- activities of water users, including shipping, fishing and dredging, on reefal ecosystems.

The eReefs project has now been providing near real time and past reconstructions of since the beginning of 2016, and is expected to be an ongoing tool to support researchers and managers in understanding the fragile GBR environment and enhancing reef health for future generations.

14.4 Further Information

Global Data Products:

United Nations Environment Programme (UNEP) Environmental Data Explorer: *http://geodata.grid.unep.ch*

LandScan Population Distribution Model: *https://landscan.ornl.gov*

Global EO Images and Image Products:

Global Vegetation Index: *https://www.ospo.noaa.gov/Products/land/gvi/*

Nighttime 'city lights' DMSP OLS: *https://ngdc.noaa.gov/eog/dmsp/downloadV4composites.html*

NASA Visible Earth: *http://visibleearth.nasa.gov*

NASA Ocean Colour: *https://oceandata.sci.gsfc.nasa.gov*

USGS Earth Explorer: *https://earthexplorer.usgs.gov*

USGS Global Visualisation Viewer (GLOVIS): *https://glovis.usgs.gov*

USGS EROS Archive for AVHRR Data and Products: *https://www.usgs.gov/centers/eros/science/usgs-eros-archive-advanced-very-high-resolution-radiometer-avhrr?qt-science_center_objects=0#qt-science_center_objects*

Environmental Accounting Framework:

System of Environmental-Economic Accounting (SEEA): *https://seea.un.org/*

Australian EO Information Products:

Terrestrial Ecosystem Research Network (TERN): *https://www.tern.org.au/*

TERN-ANU Landscape Data Visualiser: *https://maps.tern.org.au*

Australian Ocean Data Network (AODN): This interoperable online network of marine and climate data resources includes data that covers a wide range of parameters in different ocean environments collected from ocean-going ships, autonomous vehicles, moorings and other platforms: *https://portal.aodn.org.au*

OzWALD:

Australia's Environment: *http://wald.anu.science/data_services/data/continuous-and-comprehensive-national-environmental-reporting-australias-environment/*

Australia's Environmental Explorer: *www.ausenv.online*

State of Environment:

SOE 2016: *https://www.environment.gov.au/science/soe*

State-based Environmental Monitoring:

Statewide Landcover and Trees Study (SLATS , Queensland): *https://www.qld.gov.au/environment/land/management/mapping/statewide-monitoring/slats*

Ground cover monitoring (Queensland): *https://www.qld.gov.au/environment/land/management/mapping/statewide-monitoring/groundcover*

SLATS NSW: *https://www.environment.nsw.gov.au/topics/animals-and-plants/native-vegetation/reports-and-resources*

Habitat Hectares (Victoria): *https://www.environment.vic.gov.au/native-vegetation/native-vegetation/biodiversity-information-and-site-assessment*

Spatial data for Victoria: *https://www2.delwp.vic.gov.au/maps?_ga=2.6531511.420315026.1549698228-873342548.1549698228*

eReefs:

https://ereefs.org.au/ereefs

14.5 References

ABS (2018). *Australian Environmental-Economic Accounts, 2018*, webpage: *http://www.abs.gov.au/ausstats/abs@.nsf/mf/4655.0*

ABARES (2017). *Catchment Scale Land Use of Australia—Update September 2017*. ABARES, Canberra.

Armston, J.D., Denham, R.J., Danaher, T.J., Scarth, P.F., and Moffiet, T. (2009). Prediction and validation of foliage projective cover from Landsat-5TM and Landsat-7TM ETM+ imagery for Queensland, Australia. *Journal of Applied Remote Sensing*, 3(1), 033540-033567.

ANU (2019). Australian National University, *Australia's Environment in 2018* webpage: *http://wald.anu.science/australias-environment/*

Baird, M.E., Cherukuru, N., Jones, E., Margvelashvili, N., Mongin, M., Oubelkheir, K., Ralph, P.J., Rizwi, F., Robson, B.J., Schroeder, T., Skerratt, J., Steven, A.D.L., and Wild-Allen, K.A. (2016). Remote-sensing reflectance and true colour produced by a coupled hydrodynamic, optical, sediment, biogeochemical model of the Great Barrier Reef, Australia: comparison with satellite data. *Environmental Modelling Software*, 78, 79–96.

Baird, M.E., Mongin, M., Rizwi, F., Bay, L.K., Cantin, N.E., Soja-Wozniak, M., and Skerratt, J. (2018). A mechanistic model of coral bleaching due to temperature-mediated light-driven reactive oxygen build-up in zooxanthellae. *Ecological Modelling*, 386, 20–37.

Brodie, J., Baird, M. Mongin, M., Skerratt, J., Robillot, C., and Waterhouse, J. (2017). Pollutant target setting for the Great Barrier Reef: Using the eReefs framework. In *MODSIM2017, 22nd International Congress on Modelling and Simulation*. (Eds: Syme, G., Hatton, T., MacDonald, D., Fulton, B. and Piantadosi, J.) Modelling and Simulation Society of Australia and New Zealand, December 2017, pp. 1913-1919. ISBN: 978-0-9872143-7-9. *https://www.mssanz.org.au/modsim2017/L22/brodie.pdf*

BoM (2013). *Guide to environmental accounting in Australia, Environmental Information Programme Publication Series no. 3,* Bureau of Meteorology, Canberra, Australia.

Copernicus Climate Change Service (2017). ERA5: Fifth generation of ECMWF atmospheric reanalyses of the global climate. In: *Copernicus Climate Change Service Climate Data Store (CDS)*, (Ed: ECMWF) *https://cds.climate.copernicus.eu/cdsapp#!/home*.

Danaher, T., Scarth, P., Armston, J., Collett, L., Kitchen, J., and Gillingham, S. (2011). Remote Sensing of Tree-Grass Systems: The Eastern Australian Woodlands. In *Ecosystem Function in Savannas: Measurement and Modelling at Landscape to Global Scales*. (Eds: Hill, M.J., and Hanan, N.P.) CRC Press, Boca Raton, pp. 175–194.

DEE (2016). *Environment Protection and Biodiversity Conservation Act 1999 (Parts 7, 9 and 10), Environment Protection (Sea Dumping) Act 1981, Fuel Quality Standards Act 2000 and Ozone Protection and Synthetic Greenhouse Gas Management Act 1989 Compliance Monitoring Program 2016–2017*. Department of Environment and Energy, Canberra.

DEE (2018). Department of Environment and Energy. *Environmental-economic accounting* webpage: *https://www.environment.gov.au/science/environmental-economic-accounting*

Flood, N., Danaher, T., Gill, T., and Gillingham, S. (2013). An Operational Scheme for Deriving Standardised Surface Reflectance from Landsat TM/ETM+ and SPOT HRG Imagery for Eastern Australia. *Remote Sensing*, 5, 83–109.

Frost, A.J., Ramchurn, A. and Smith, A.B. (2016). *The Bureau's Operational AWRA Landscape (AWRA-L) Model*. Bureau of Meteorology, Melbourne.

Gallant, J.C., Wilson, N., Dowling, T., Read, A., and Inskeep, C. (2011). *1 second SRTM Derived Digital Elevation Models User Guide*. Geoscience Australia, Canberra. *www.ga.gov.au/topographic-mapping/digital-elevation-data.html*

Geoscience Australia (2014). *Sentinel Hotspots Product Description Document V1.2*, code D2014-145826, Geocat Reference 70869.

Goodwin, N.R., and Collett, L.J. (2014). Development of an automated method for mapping fire history captured in Landsat TM and ETM+ time series across Queensland, Australia. *Remote Sensing of Environment*, 148, 206–221.

Guerschman, J.P., and Hill, M.J. (2018). Calibration and validation of the Australian fractional cover product for MODIS collection 6. *Remote Sensing Letters*, 9(7), 696–705.

Guerschman, J., Scarth, P., McVicar, T., Renzullo, L., Malthus, T., Stewart, J., Rickards, J., and Trevithick, R. (2015). Assessing the effects of site heterogeneity and soil properties when unmixing photosynthetic vegetation, non-photosynthetic vegetation and bare soil fractions from Landsat and MODIS data. *Remote Sensing of Environment*, 161, 12–26.

Herzfeld, M., Andrewartha, J., Baird, M., Brinkman, R., Furnas, M., Gillibrand, P., Hener, M., Joehnk, K.D., Jones, E., McKinnon, D., Margevlashvili, N., Mongin, M., Oke, P., Rizwi, F., Robson, B., Seaton, S., Skerratt, J., Tonin, H. and Wild-Allen, K. (2016). *eReefs Marine Modelling: Final Report*. CSIRO, Hobart, Tasmania.

Huffman, G.J., Bolvin, D.T., Braithwaite, D., Hsu, K., Joyce, R., Kidd, C., Nelkin, E.J., and Xie, P. (2015). *NASA global precipitation measurement (GPM) integrated multi-satellite retrievals for GPM (IMERG)*. Algorithm theoretical basis document, version, 4: 30.

Jones, D., Wang, W. and Fawcett, R. (2009). High-quality spatial climate data-sets for Australia. *Australian Meteorological and Oceanographic Journal*, 58, 233–248.

Jones, E., Baird, M., Mongin, M., Parslow, J., Skerratt, J., Lovell, J., Margvelashvili, J.N., Matear, R., Wild-Allen, K., Robson, B., Rizwi, F., Oke, P., King, E., Schroeder, T., Steven, A., and J. Taylor, J. (2016). Use of remote-sensing reflectance to constrain a data assimilating marine biogeochemical model of the Great Barrier Reef. *Biogeosciences*, 13, 6441–6469.

Kaiser, J.W. Heil, A., Andreae, M.O., Benedetti, A., Chubarova, N., Jones, L., Morcrette, J.-J., Razinger, M., Schultz, M.G., Suttie, M., and van der Werf, G.R. (2012). Biomass burning emissions estimated with a global fire assimilation system based on observed fire radiative power. *Biogeosciences*, 9(1), 527–554.

Kitchen, J., Armston, J., Clark, A., Danaher, T., and Scarth, P. (2010). Operational use of annual Landsat-5 TM and Landsat-7 ETM+ image time-series for mapping wooded extent and foliage projective cover in north-eastern Australia. In *Proceedings of the 15th Australasian Remote Sensing and Photogrammetry Conference,* Alice Springs, Australia.

Margvelashvili, N.M., Andrewartha, J., Baird, M. Herzfeld, M.,Jones, E., Mongin, M., Rizwi, F., Robson, B., Skerratt, J., Wild-Allen, K., and Steven, A. (2018). Simulated fate of catchment-derived sediment on the Great Barrier Reef shelf. *Marine Pollution Bulletin*, 135, 954–962.

Mongin, M., Baird, M.E., Tilbrook, B., Matear, R.J., Lenton, A., Herzfeld, M., Wild-Allen, K.A., Skerratt, J. Margvelashvili, N., Robson, B.J., Duarte, C.M., Gustafsson, M.S.M., Ralph, P.J., Steven, A.D.L. (2016). The exposure of the Great Barrier Reef to ocean acidification. *Nature Communications*, 7, 10732.

Mueller, N., Lewis, A., Roberts, D., Rign, S., Melrose, R., Sixsmith, J., Lymburner, L., McIntyre, A., Tan, P., Curnow, S., and Ip, A. (2016). Water observations from space: Mapping surface water from 25 years of Landsat imagery across Australia. *Remote Sensing of Environment*, 174, 341–352.

Myneni, R., Knyazikhin, Y., and Park, T. (2015). *MCD15A3H MODIS/Terra+Aqua Leaf Area Index/FPAR 4-day L4 Global 500m SIN Grid V006. 2015*. NASA EOSDIS Land Processes DAAC. *https://doi.org/10.5067/MODIS/MCD15A3H.006*.

Nemani, R, Hasimoto, H., Votava, P., Melton, F., Wang, W., Michaelis, A., Mutch, L., MIlesi, C., Hiatt, S., and White, M. (2009). Monitoring and forecasting ecosystem dynamics using the Terrestrial Observation and Prediction System (TOPS). *Remote Sensing of Environment*, 113, 1497–1509. *https://doi.org/10.1016/j.rse.2008.06.017*

Pasetto, D., Arenas-Castro, S., Bustamante, J., Casagrandi, R., Chrysoulakis, N., Cord, A.F., Dittrich, A., Domingo-Marimon, C., El Serafy, G., Karnieli, A., Kordelas, G.A., Manakos, I., Mari, L., Monteiro, A., Palazzi, E., Poursanidis, D., Rinaldo, A., Terzago, S., Ziemba, A., and Ziv, G. (2018). Integration of satellite remote sensing data in ecosystem modelling at local scales: Practices and trends. *Methods in Ecology and Evolution*, 2018:9, 1810–1821. *https://doi.org/10.1111/2041-210X.13018*

Pringle, M.J., Schmidt, M., and Tindall, D.R. (2018). Multi-decade, multi-sensor time-series modelling based on geostatistical concepts to predict broad groups of crops. *Remote Sensing of Environment*, 216, 183–200. *https://doi.org/10.1016/j.rse.2018.06.046*

Renzullo, L.J. Chappell, A., Raupach, T., Dyce, P., Li, M., and Shao, Q. (2011). An Assessment of Statistically Blended Satellite-Gauge Precipitation Data for Daily Rainfall Analysis in Australia, *34th International Symposium of Remote Sensing of Environment*. 10–15 April, Sydney.

Scarth, P., Gillingham, S., and Muir, J. (2008). Assimilation of spectral information and temporal history into a statewide woody cover change classification. *Proceedings of the 14th Australasian Remote Sensing and Photogrammetry Conference*, Darwin, Australia.

Scarth, P., Roder, A., and Schmidt, M. (2010). Tracking grazing pressure and climate interaction – the role of Landsat fractional cover in time series analysis. *Proceedings of the 15th Australasian Remote Sensing and Photogrammetry Conference*, Alice Springs, Australia, pp. 13–17.

Scarth, P., Armston, J., Lucas, R., and Bunting, P. (2019). A structural classification of Australian vegetation using ICESat/GLAS, ALOS PALSAR, and landsat sensor data. *Remote Sensing*, 11, 147. *https://doi.org/10.3390/rs11020147*

Schaaf, C., and Wang, Z., (2015). MCD43A4 MODIS/Terra+Aqua BRDF/Albedo Nadir BRDF Adjusted RefDaily L3 Global-500m V006. NASA EOSDIS Land Processes DAAC. *https://doi.org/10.5067/MODIS/MCD43A4.006*

Schmidt, M., Pringle, M., Devadas, R., Denham, J., and Tindall, D. (2016). A framework for large-area mapping of past and present cropping activity using seasonal Landsat images and time series metrics. *Remote Sensing*, 8(9), 312. *https://doi.org/10.3390/rs8040312*.

Skerratt, J.H., Mongin, M., Wild-Allen, K.A., Baird, M.E., Robson, B.J., Schaffelke, B., Soja-Wozniak, M., Margvelashvili, N., Davies, C.H., Richardson, A.J., Steven, A.D.L. (2019). Simulated nutrient and plankton dynamics in the Great Barrier Reef (2011-2016). *Journal of Marine Systems*, 192, 51–74.

Steven., A.D.L., Baird, M.E., Brinkman, R., Car, N.J., Cox, S.J., Herzfeld, M., Hodge, J., Jones, E., King, E., Margvelashvili, N., Robillot, C., Robson, B., Schroeder, T., Skerratt, J., Tuteja, N., Wild-Allen, K., and Yu, J. (2019). eReefs: An operational information system for managing the Great Barrier Reef. *Journal of Operational Oceanography*, 12:sup2, S12–S28. *https://doi.org/10.1080/1755876X.2019.1650589*.

UN (2014). *System of Environmental-Economic Accounting 2012: Experimental Ecosystem Accounting,* European Commission, Organisation for Economic Co-Operation and Development, United Nations and World Bank. eISBN: 978-92-1-056285-0. *https://unstats.un.org/unsd/envaccounting/seearev/eea_final_en.pdf*

van Dijk, A.I.J.M. (2010). *AWRA Technical Report 3. Landscape Model (version 0.5) Technical Description*. WIRADA/CSIRO Water for a Healthy Country Flagship, Canberra.

van Dijk, A., Mount, R., Gibbons, P., Vardon, M. and Canadell, P. (2014). Environmental reporting and accounting in Australia: Progress, prospects and research priorities. *Science of The Total Environment*, 473–474, 338–349.

van Dijk, A., Summers, D., Renzullo, L., and Yebra, M. (2017). *OzWALD Gridded Environmental Data for Australia. v2*. CSIRO. Data Collection. *https://doi.org/10.4225/08/5a3c52da083b8*

van Dijk, A., and Rahman, J. (2019). Synthesising multiple observations into annual environmental condition reports: the OzWALD system and Australia's Environment Explorer. *MODSIM2019*, Canberra.

Vardon, M., Ovington, J., Juskevics, V., Purcell, J., and Eigenraam, M. (2018). Down Payments on National Environmental Accounts. Ch 14 in *Land Use in Australia: Past, Present and Future*. (Ed: Thackway, R.) ANU eVIEW, Canberra. ISBN: 9781921934421

Wan, Z., Hook, S. and Hulley, G. (2015). *MYD11A1 MODIS/Aqua Land Surface Temperature/Emissivity Daily L3 Global 1km SIN Grid V006*. NASA EOSDIS Land Processes DAAC.

Webster, I.T., Atminskin, I., Bostock, H., Brooke, B., Douglas, G., Ford, P., Hancock, G., Herzfeld, M.J., Leeming, R., Lemckert, C., Margvelashvili, N., Noble, B., Oubelkheir, K., Radke, L., Revill, A., Robson, B.J., Ryan, D., Schacht, C., Smith, C., Smith, J., Vicente-Beckett, V. and Wild-Allen, K. (2006). *The Fitzroy Contaminants Project - A study of the nutrient and fine-sediment dynamics of the Fitzroy Estuary and Keppel Bay*, CRC for Coastal Zone, Estuary and Waterway Managment.

crc•si

CSIRO

Australian Government
Geoscience Australia

bushfire&natural
HAZARDSCRC